



UNIVERSITAT<sub>DE</sub>  
BARCELONA

**Novel antimicrobial peptides  
for therapeutic applications: design, synthesis,  
characterization, and evaluation of their  
biological and biophysical activity**

Rosario Segovia Laserna



Aquesta tesi doctoral està subjecta a la llicència **Reconeixement 4.0. Espanya de Creative Commons.**

Esta tesis doctoral está sujeta a la licencia **Reconocimiento 4.0. España de Creative Commons.**

This doctoral thesis is licensed under the **Creative Commons Attribution 4.0. Spain License.**

**Novel antimicrobial peptides for therapeutic applications: design, synthesis, characterization, and evaluation of their biological and biophysical activity**

Rosario Segovia Laserna

**Program of doctorate in Organic Chemistry**  
Department of Inorganic and Organic Chemistry  
Section of Organic Chemistry  
Faculty of Chemistry  
University of Barcelona

**Francesc Rabanal Anglada**  
Department of Inorganic and Organic  
Chemistry  
Section of Organic Chemistry  
Faculty of Chemistry  
University of Barcelona

**Yolanda Cajal Visa**  
Department of Pharmacy,  
Pharmaceutical Technology and  
Physical Chemistry  
Faculty of Pharmacy and Food Sciences  
University of Barcelona



“A scientist in his laboratory is not a mere technician: he is also a child confronting natural phenomena that impress him as though they were fairy tales.”

**Marie Curie**



Quan al febrer del 2015 vaig arribar per primer cop al laboratori per començar el meu TFG, mai hauria imaginat que aquell espai es convertiria en la meua segona casa per gairebé 7 anys més. Però aquells pocs mesos d'últim any de carrera hem van despertar un gran interès pel món de la recerca i dels antibiòtics, i això va ser en gran part gràcies al Dr. Francesc Rabanal i la Dra. Yolanda Cajal, que em van donar la gran oportunitat de treballar en el seu projecte. Així que des d'aquí volia agrair-los una vegada més tot el que he après d'ells, el seu constant suport i la confiança que han dipositat en mi tots aquests anys.

També voldria agrair a la Dra. Àngels Manresa i la Dra. Ana Maria Marquès la seva col·laboració en aquesta tesi, elles em van ensenyar tot el que sé del apassionant món de la microbiologia. Sens dubte ha estat una tasca molt interessant i molt molt important de la tesi que no hauria estat possible sense que elles m'acollissin als seus laboratoris.

I would also like to thank Dr. Anne Ulrich for giving me the incredible opportunity to join their group for four months, it was wonderful to live in Karlsruhe and work in her group. Thank you also to Dr. Erik Strandberg because I learned a lot working under his supervision. Finally, I would like to also thank Dr. Parvesh Wadhvani and the PepSy Lab, as well as Dr. Jochen Bürck and the CD Team, for their great support in my investigation.

De manera molt important m'agradaria també recordar a totes les persones que han passat pel grup 10P en aquests anys. L'Ariadna Grau que em va ensenyar durant els meus primers dies al laboratori, la Judith Solé, la Maria i tots els estudiants que han passat pel laboratori i que a la vegada que aprenien de mi, m'ensenyaven ells també moltíssimes coses, especialment la Irene, Matilde, l'Aina o la Júlia Ibañez. I com oblidar-me de les últimes integrants del grup... Júlia, Marina, se que deixo el laboratori en molt bones mans! I en concret a tu Marina, gràcies per les eternes hores al fluorímetre experimentant els "amargos caminos de la química", per tants riures i plors juntes. Gràcies per tot el suport que em vas donar en els moments més difícils, ja t'ho he dits molts cops, però sens dubte tu ets la persona que m'emporto de tota aquesta locura d'etapa. I per suposat no m'oblido de la meua altra pole dancer, la Marina Pérez, que sempre ha estat allà amb els seus somriures per alegrar-nos a tots. I a la resta dels companys i amics del departament Stuart, Fernanda, Héctor, Macarena, Miquel, Sergi, Alejandro, Javi, Ari gràcies per totes les

experiències que hem viscut junts en aquests anys, les festes, acampades, dinars, cafès, etc. ha estat un plaer!

I fora del departament, però encara dins de la química no puc oblidar-me de mencionar a la Judit, Anna, Jandri i Cucu. Ens vam conèixer gairebé el primer dia de carrera i 11 anys després aquí seguim, cadascú en una punta del món fent la seva química, però mantenint el contacte i l'amistat que ens va unir durant la carrera.

Y qué decir de Ana, que ya no se ni cuánto tiempo llevamos siendo amigas ¡y ahora compañeras de pisito! Nuestra soñada independencia coincidió con mi etapa final de la tesis y por unas cosas o por otras no ha sido como imaginábamos, pero no la cambiaría por nada. Porque, aunque nos veíamos poco, siempre sabía que te tenía allí, en la habitación de al lado, por si te necesitaba. Ahora que esta tesis ya no absorberá un 80 % de mis días recuperemos el tiempo perdido.

Y, por último, las personas más importantes de mi vida, mi familia. Mama, papa, Lorena, gracias, gracias y gracias por todo lo que habéis hecho por mi durante toda mi vida, por haberme apoyado tanto y por recordarme siempre lo orgullosos que estáis de mí, sé que os lo digo muy poco, pero ¡os quiero muchísimo! I a tu Ignasi que dir-te si ja ho saps tot... Vas aparèixer a la meva vida fa poquet, vas posar tot del revés i em vas fer sentir coses que mai havia sentit. Aquesta tesis és 50 % teva, perquè aguantar-me se que no ha estat gens fàcil i tu sempre has estat al meu costat, aguantant la meva ansietat durant la recta final, tu has cuidat de mi en moments en que jo mateixa m'oblidava de fer-ho, sempre disposat a ajudar, a llegir-te la tesis, a parlar durant hores de química o a treure'm a fer una volta o una birreta per que em donés l'aire. Mai tindrè suficients paraules per agrair-te el que has fet, t'estimo moltíssim!!!

## INDEX

GENERAL INTRODUCTION .....	1
a. The antibiotic era .....	3
b. Bacterial resistance .....	4
c. Antimicrobial peptides .....	7
c.1. Antimicrobial peptides structure .....	7
c.2. Antimicrobial peptides mechanism of action .....	8
c.2.1. Bacterial membranes.....	9
c.2.2. Proposed mechanisms of action.....	9
d. Resistance .....	13
d.1. Extracellular proteins .....	13
d.2. Biofilms.....	13
d.3. Surface modification .....	14
d.4. Cytoplasmic membrane alteration.....	14
d.5. Efflux pumps .....	14
d.6. Modulation of AMP gens expression.....	15
e. Antimicrobial peptides as therapeutic agents.....	15
f. Antimicrobial peptide synthesis .....	18
f.1. Brief history of chemical peptide synthesis .....	18
f.2. Fundamentals on solid phase peptide synthesis.....	20
GENERAL OBJECTIVES .....	29
CHAPTER 1: Development of new polymyxin B-based drugs .....	33
1.1. Introduction.....	35
1.1.1. Drug development process .....	35
1.1.1.1. Drug discovery .....	35
1.1.1.2. Preclinical research.....	36



1.1.1.3. Clinical trials .....	37
1.1.1.4. Drug approval .....	37
1.1.1.5. Scale-up of the manufacturing process.....	38
1.1.1.6. FDA Post-Market Safety Monitoring .....	38
1.1.2. Polymyxins.....	38
1.1.2.1. Mode of action.....	41
1.1.2.2. Toxicity.....	43
1.1.2.3. Resistance .....	44
1.1.2.4. Synthetic preparation of polymyxins.....	44
1.1.2.5. Design of new polymyxins .....	46
1.1.2.6. State of the art in new polymyxins development .....	48
1.1.3. General considerations about the techniques employed in this chapter.....	52
1.1.3.1. Solid phase peptide synthesis .....	52
1.1.3.2. Antimicrobial activity assays .....	55
1.1.3.3. Hemolysis assay .....	57
1.1.3.4. Transmission electron microscopy .....	57
1.1.3.5. Biophysical studies .....	58
1.2. Objectives of chapter 1 .....	67
1.3. Design of novel polymyxin analogues.....	67
1.3.1. Depsipeptide polymyxin analogues .....	69
1.3.2. Cysteine analogues .....	70
1.3.3. Hydroxamic acid analogues .....	72
1.3.4. Thiiothreonine analogues .....	73
1.4. Synthesis of polymyxin analogues .....	74
1.4.1. Novel acydolitic methodology for the total synthesis of polymyxin B <sub>3</sub> and other relevant peptides.....	74

1.4.1.1. Synthesis and cyclization of polymyxin B <sub>3</sub> .....	75
1.4.1.2. Bn-type protecting groups removal .....	77
1.4.1.3. Other applications for the novel acidolytic methodology .....	80
1.4.2. Synthesis of depsipeptide analogues .....	84
1.4.3. Synthesis of cysteine analogues .....	84
1.4.4. Hydroxamic acid analogues synthesis.....	86
1.4.5. Synthesis of thiothreonine analogues .....	88
1.4.6. Scale-up and optimization of the synthesis of thiothreonine analogues .....	88
1.4.6.1. Compound 27 .....	88
1.4.6.2. Compound 25 .....	92
1.5. Peptide characterization .....	93
1.5.1. Complete ionic characterization of peptide salts.....	93
1.5.1.1. CHNS elemental analysis .....	93
1.5.1.2. Chloride determination by titration .....	94
1.5.1.3. Electrospray ionization mass spectrometry .....	95
1.6. Antimicrobial activity .....	100
1.6.1. Polymyxin B <sub>3</sub> .....	101
1.6.2. Depsipeptide analogues.....	101
1.6.3. Cysteine analogues.....	102
1.6.4. Second series of cysteine analogues.....	103
1.6.5. Hydroxamic acid analogues .....	104
1.6.6. Thiothreonine analogues .....	105
1.6.7. Summary .....	106
1.7. Evaluation of the mechanism of action.....	107
1.7.1. Cysteine analogues .....	107
1.7.1.1 Hemolysis .....	107

1.7.1.2. Transmission Electron Microscopy .....	110
1.7.1.3. Biophysical evaluation of the mechanism of action .....	112
1.7.2. Thiiothreonine analogues .....	122
1.7.2.1. Hemolysis .....	122
1.7.2.2. Transmission electron microscopy .....	123
1.7.2.3. Biophysical assays with liposomes.....	123
1.7.2.3. Proposed mechanism of action for thiiothreonine analogues .....	131
1.8. Hit validation .....	132
1.8.1. Antimicrobial activity against resistant bacteria .....	132
1.8.2. In vivo nephrotoxicity assay .....	133
1.8.2.1. First in vivo nephrotoxicity assay.....	133
1.8.2.2. Second in vivo study .....	135
1.8.3. Study of polymyxin analogues metabolization .....	138
1.8.4. In vivo efficacy study .....	141
1.9. Conclusions.....	142
CHAPTER 2: Length dependent activity of $\alpha$ -helical antimicrobial peptides based on BP100 .....	145
2.1. Introduction .....	147
2.1.1. Peptidyl-glycine-leucine-carboxamide and its derivative MSI-103.....	147
2.1.2. Melittin, cecropin A and its derivative BP100.....	149
2.1.3. General considerations about the techniques used in this chapter .....	151
2.1.3.1. Antimicrobial activity.....	151
2.1.3.2. Hemolysis .....	151
2.1.3.3. Biophysical evaluation of the mechanism of action .....	152
2.2. Objectives of chapter 2 .....	160
2.3. Peptide design .....	161
2.4. Synthesis, purification, and characterization of BPKIA analogues.....	163

2.5. Antimicrobial activity .....	163
2.6. Hemolysis .....	164
2.7. Biophysical evaluation of the mechanism of action .....	166
2.7.1. Circular dichroism spectroscopy .....	166
2.7.2. Peptide binding study .....	168
2.7.3. Leakage of aqueous contents.....	170
2.7.4. Solid state NMR .....	172
2.7.5. Proposed mechanism of action.....	176
2.8. Conclusions.....	177
GENERAL CONCLUSIONS .....	179
EXPERIMENTAL SECTION.....	183
3.1. Experimental section of chapter 1 .....	185
3.1.1. Materials.....	185
3.1.1.1. Solvents .....	185
3.1.1.2. Reagents .....	185
3.1.1.3. Other material .....	187
3.1.1.4. Instrumentation.....	187
3.1.2. Methods.....	188
3.1.2.1 Analytical methods .....	188
3.1.2.2. Solid phase peptide synthesis .....	190
3.1.2.3. Antimicrobial activity.....	195
3.1.2.4. Hemolysis .....	196
3.1.2.5. Transmission electron microscopy .....	196
3.1.2.6. Biophysical experiments .....	197
3.1.3. Synthetic procedures .....	200
3.1.3.1. Amino acids protection.....	200

3.1.3.2. Synthesis of PxB <sub>3</sub> .....	202
3.1.3.3. Synthesis of dusquetide and RR4 .....	203
3.1.3.4. Synthesis of depsipeptide polymyxin analogues .....	204
3.1.3.5. Synthesis of cysteine analogues .....	206
3.1.3.6. Synthesis of hydroxamic acid analogues .....	209
3.1.3.7. Synthesis of thiothreonine analogues .....	211
3.1.3.8. Optimized synthesis of thiothreonine analogues .....	213
3.2. Materials and methods of chapter 2 .....	214
3.2.1. Materials .....	214
3.2.1.1. Solvents .....	214
3.2.1.2. Reagents .....	214
3.2.1.3. Other material .....	215
3.2.1.4. Instruments .....	215
3.2.2. Methods .....	215
3.2.2.1. Antimicrobial activity .....	215
3.2.2.2. Hemolysis .....	216
3.2.2.3. Circular dichroism spectroscopy .....	217
3.2.2.4. Peptide binding study .....	219
3.2.2.5. Vesicle leakage assay .....	220
3.2.2.6. Solid-state NMR .....	220
REFERENCES .....	223
APPENDIX .....	243
Appendix I: Abbreviations and acronyms .....	245
Appendix II: Amino acids used in this thesis .....	248
Appendix III: Special amino acids used in this thesis .....	250
Appendix IV: Protecting groups .....	251

Appendix V: Solid supports.....	252
Appendix VI: Coupling reagents and additives.....	253
Appendix VII: Synthesized peptides .....	254
Appendix VIII: Phospholipids .....	263
Appendix IX: ESI-HR MS study of the ionic composition of PxB <sub>3</sub> .....	264
Appendix X: Antibiotic susceptibility profiles of all tested microorganisms .....	272



## **ABOUT THE STRUCTURE OF THIS WORK**

This work is divided into the following sections:

First, there is a general introduction to the current pipeline of antibiotics and then, general objectives of the thesis are presented.

The first chapter consists of the design and synthesis of new polymyxin analogues devoid of toxic side effects, the scale-up and synthesis optimization of the best analogues previously synthesized along with the evaluation of their biologic and biophysical activity including *in vitro* and *in vivo* experiments.

The second chapter encloses the experimentation realized in a PhD research stay of 4 months in Dr. Anne S. Ulrich's group in the Karlsruhe Institute of Technology (KIT) (Germany). It describes the biological and biophysical assays performed in BP100 analogues in order to evaluate the length-dependent activity of this antimicrobial peptide and its mechanism of action.

Finally, the general conclusions and the experimental section are presented.





# **GENERAL INTRODUCTION**



## a. The antibiotic era

Antibiotics are among the most successful form of chemotherapy in the history of medicine. They are chemical compounds, generally produced by microorganisms, used to treat bacterial infections either by killing the bacteria (bactericidal effect) or by the inhibition of bacterial growth (bacteriostatic effect).

Antibiotics were used a long time before the advent of modern medicine, in fact, there are evidences of their use by some of the earliest civilizations such as the ancient Egypt, China, Greece or Rome, where a variety of molds and plant extracts were topically applied for the treatment of wounds and burns.<sup>1,2</sup> Even some modern antibiotics may have been available in ancient times, this is the case of tetracycline, whose traces were detected in human skeletons from ancient Sudanese Nubia dating back to 350 - 550 CE.<sup>3,4</sup>

During the 19<sup>th</sup> century, several observations of antagonisms between micro-organisms were described, but no antimicrobial molecule was isolated until 1909, when Paul Ehrlich discovered an arsenic-based chemical active against *Treponema pallidum*, the etiologic agent of syphilis.<sup>5,6</sup> In 1911 this antibiotic was marketed and frequently prescribed under the name Salvarsan, substituted afterwards by the less toxic Neosalvarsan.<sup>7</sup>

In the mid-1930s, following Ehrlich's lead, Gerhard Domagk discovered the antimicrobial effect of sulfonamides,<sup>8</sup> firstly synthesized by Paul Gelmo in 1908.<sup>9</sup> The molecule was commercialized by the name Prontosil and it was the first synthetic compound for the treatment of streptococcal infections, resulting in a sharp decrease in mortality from diseases as meningitis, childbed fever and pneumonia.

Meanwhile, Alexander Fleming accidentally discovered penicillin in 1928, a compound produced by *Penicillium notatum* highly active against *Staphylococcus* bacteria. However, it took over a decade, until Howard Florey and Ernst Chain published the penicillin purification protocol in 1940,<sup>10</sup> which led to the penicillin mass production and distribution in 1945. In addition, in those years, Dorothy Crowfoot Hodgkin determined its structure.<sup>11</sup>

Despite these discoveries, the word 'antibiotic' was not introduced until 1947 by Selman Waksman.<sup>12</sup> He isolated several important antibiotic and antifungals, such as streptomycin,<sup>13</sup> which was the first effective treatment for tuberculosis.

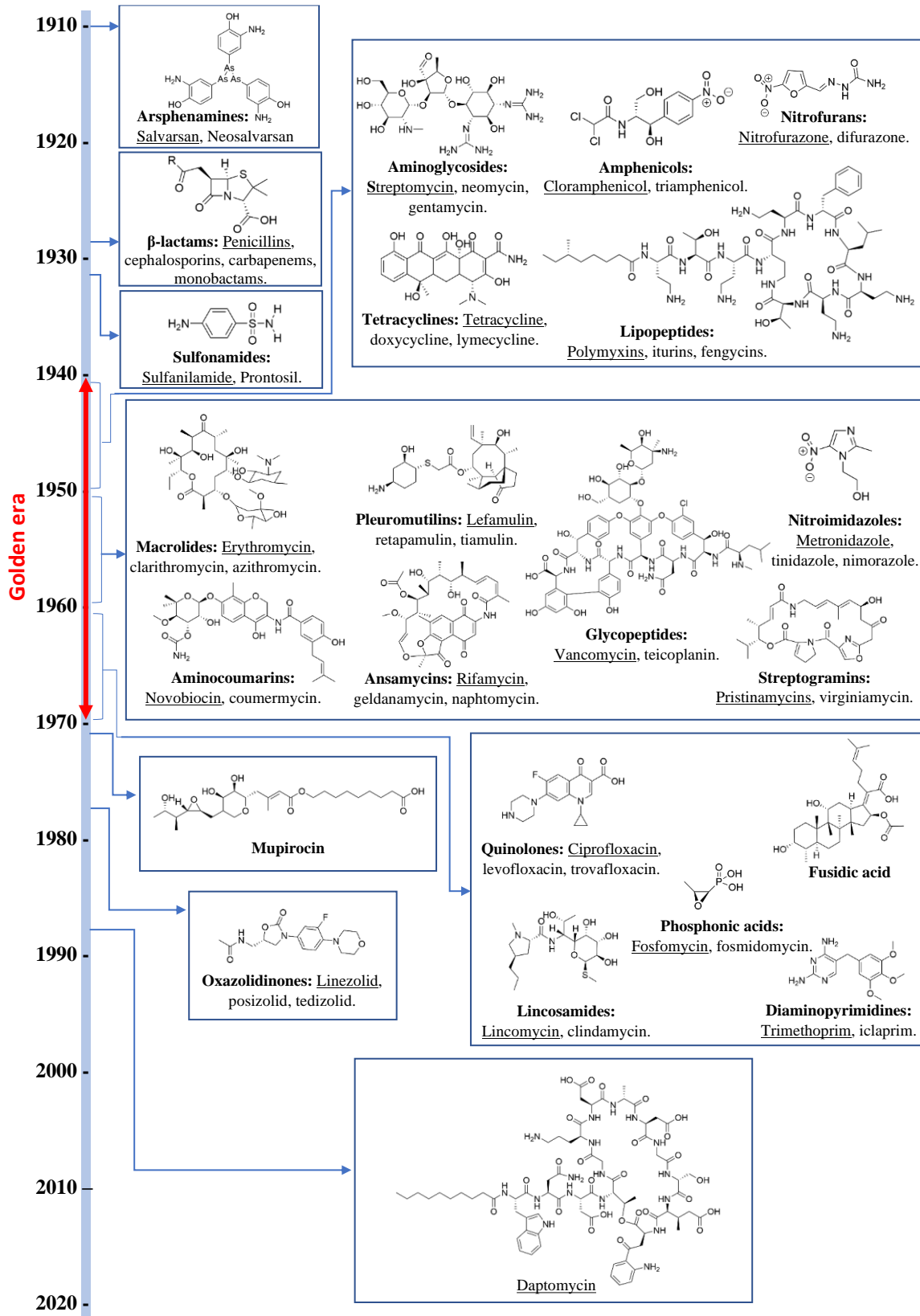
After this great kick-start, the period between the 1940s and 1970s is commonly named as ‘Golden Age’ of antibiotics, because about 20 new classes were discovered and introduced in the market (Figure 1). Unfortunately, from that moment, few new antibiotic classes have been discovered, among them oxazolidinones<sup>14,15</sup> and the lipodepsipeptide daptomicin<sup>16</sup> are particularly relevant.

## **b. Bacterial resistance**

The emergence of bacteria with acquired resistance has been reported since the introduction of penicillin in the 1940s<sup>17</sup> and after decades of exorbitant antibiotic misuse and overuse in human medicine, agriculture and livestock industry,<sup>18–20</sup> multidrug resistant bacteria (MDR) have increased alarmingly in all parts of the world. Antibiotic resistance consists in the loss of the drug’s ability to effectively inhibit bacterial growth and, as a result, common infections such as pneumonia, tuberculosis, or gonorrhoea, are becoming harder, and sometimes impossible, to treat. In fact, according to the World Health Organization (WHO), antibiotic resistance causes 700.000 deaths annually, and this number is anticipated to rise to 10 million worldwide by 2050<sup>21</sup> if no action is taken.

In this context, the Infectious Disease Society of America (IDSA) highlighted *Enterococcus faecium*, *Staphylococcus aureus*, *Klebsiella pneumoniae*, *Acinetobacter baumannii*, *Pseudomonas aeruginosa*, and *Enterobacter* (ESKAPE pathogens) as the most alarming species due to their growing multidrug resistance and virulence.<sup>22</sup> Subsequently, the WHO published in 2017 a list of the 12 most problematic pathogens, divided into 3 groups according to their urgency (Table 1).

Furthermore, the Coronavirus Disease 2019 (COVID-19) pandemic has had an impact on the problem of antibiotic resistance. This disease, caused by the virus SARS-CoV-2, generally consists of febrile respiratory illness that may progress to secondary bacterial infections, such as pneumonia, that can be more invasive than the initial viral infection. In this scenario, several studies suggest that an over prescription of antibiotics have occurred across the globe since February 2020, largely tied to the limited understanding and experience in managing COVID-19 patients, which derived in empiric antibacterial therapies, usually before a bacterial infection was even confirmed.<sup>23–25</sup>



**Figure 1:** Timeline of the discovery of antibiotic classes in clinical use. Molecules shown (name underlined) are a representative example of each class. Figure adapted from ref.<sup>26</sup>

**Table 1:** WHO priority pathogens list for research and development of new antibiotics.<sup>27</sup> Mycobacteria (including *Mycobacterium tuberculosis*, the cause of human tuberculosis) was not subjected to review as it is already a globally established priority for which innovative new treatments are urgently needed.

<b>Priority 1: CRITICAL</b>
<i>Acinetobacter baumannii</i>
<i>Pseudomonas aeruginosa</i>
Enterobacteriaceae <sup>a</sup>
<b>Priority 2: HIGH</b>
<i>Enterococcus faecium</i>
<i>Staphylococcus aureus</i>
<i>Helicobacter pylori</i>
<i>Campylobacter spp.</i>
<i>Salmonella spp.</i>
<i>Neisseria gonorrhoeae</i>
<b>Priority 3: MEDIUM</b>
<i>Streptococcus pneumoniae</i>
<i>Haemophilus influenzae</i>
<i>Shigella spp.</i>

<sup>a</sup>Enterobacteriaceae include: *Klebsiella pneumoniae*, *Escherichia coli*, *Enterobacter spp.*, *Serratia spp.*, *Proteus spp.*, and *Providencia spp.*, *Morganella spp.*

Alerted by this crisis, leading health authorities including the WHO,<sup>28</sup> IDSA,<sup>29</sup> the European Centre for Disease and Control (ECDC)<sup>30</sup> or the European Commission through the Innovative Medicines Initiative (IMI)<sup>31</sup> have promoted various initiatives to stimulate the research in this field. As a result, the current clinical antibacterial pipeline contains nearly 50 antibiotics and there are almost 300 diverse antibacterial agents in pre-clinical stage.<sup>32</sup> However, these compounds are still under development and they need to be proven effective and safe, and unfortunately, they do not address the problem of extensively or pan-drug-resistant Gram-negative bacteria.

Nowadays research is focused on the development of new drugs highly active against resistant bacteria, which present low propensity to develop resistance. In this context, antimicrobial peptides (AMPs) have been considered as promising candidates in the next generation of antibiotics due to their particular mechanism of action where the main target is the bacterial membrane.

### c. Antimicrobial peptides

Antimicrobial peptides (AMPs) are a diverse class of peptides with a broad activity spectrum against bacteria, fungi, virus, parasites and even cancer cells.<sup>33-37</sup> In addition to the direct killing of microorganisms, AMPs, also known as host defense peptides (HDPs), are involved in several aspects of the innate immunity, being them able to modulate the inflammatory responses of the body when it recognizes possible harmful pathogens.<sup>38</sup>

AMPs have been discovered in most species, from bacteria to mammals,<sup>39-41</sup> and they were firstly reported in 1922, when Alexander Fleming extracted an enzyme named lysozyme from human fluids, active against a small number of non-harmful bacteria.<sup>42</sup> Later, nisin<sup>43</sup> and gramicidin<sup>44</sup> were discovered from bacterial sources in 1928 and 1939 respectively. Nowadays up to 3250 AMPs have been discovered or synthesized and they are listed in the Antimicrobial Peptide Database (<https://aps.unmc.edu/>), a database created and regularly updated by researchers of the University of Nebraska (UNMC) (last time accessed October 2021).

#### c.1. Antimicrobial peptides structure

Notwithstanding the great diversity of AMPs in nature, they share some characteristic features such as they are generally short (between 10 - 100 amino acids) and amphiphilic, with around 50 % of hydrophobic residues. Furthermore, they are usually positively charged (ranging from +2 to +11). These features promote the interactions with negatively charged bacterial membranes, whereas mammalian cells have a high level of cholesterol and zwitterionic phospholipids putting human cells out of the range of AMPs and increasing their selectivity toward bacteria.<sup>45</sup> However, there are some AMPs which present negative charge, such as daptomycin or dermcidin.

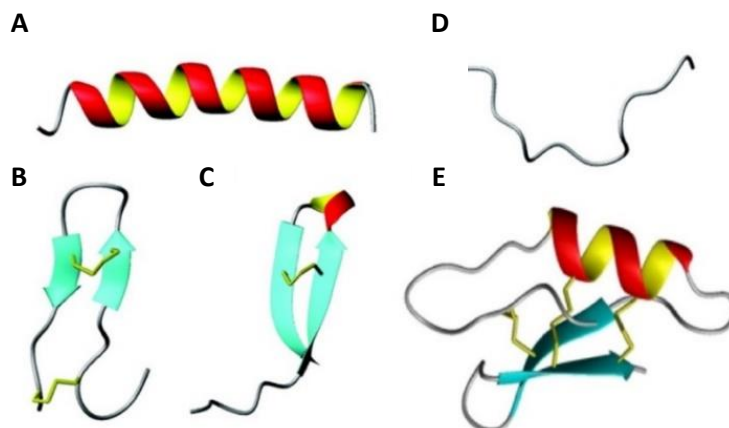
Based on their secondary structure, AMPs are commonly classified into four large classes as follows (Figure 2):<sup>46,47</sup>

- $\alpha$ -helical AMPs: Short and linear peptides, easily accessible to chemical synthesis, which are generally unstructured in aqueous solutions, but highly susceptible to form  $\alpha$ -helical structures in contact with biological membranes. Magainin, melittin, or human cathelicidin LL-37 are some examples of this category.



- $\beta$ -sheet AMPs: Cysteine containing peptides that contain at least two antiparallel  $\beta$ -sheet, they are highly ordered in solution due to their rigid structures stabilized by two or more disulfide bonds. The best-studied  $\beta$ -sheet AMPs are defensins, molecules produced by cells in the course of innate host defense.
- Loop structures: Rather small group of peptides that is stabilized by one disulfide, amide or isopeptide bond, often in the C-terminal part. For instance, thanatin, which is isolated from the spined soldier bug, presents this structure.
- Extended peptides: Peptides which lack secondary structure and are often enriched for specific amino acids such as arginine, proline or tryptophan, such as the tryptophan-rich indolicin or diaminobutíric-rich polymyxin.

However, there are many AMPs that do not fit particularly into any group above mentioned, but rather present a mixed structure combining different domains, for instance, this is the case of luciferin and plectasin, which present  $\alpha$ -helical and a  $\beta$ -sheet structure like domain (Figure 2E).



**Figure 2:** Structural classes of antimicrobial peptides: A)  $\alpha$ -helical magainin-2; B)  $\beta$ -sheet polyphemusin; C) looped thanatin; D) extended indolicin; E) mixed structure of plectasin. Disulfide linkages are indicated by yellow bonds. Figure taken from ref.<sup>48</sup>

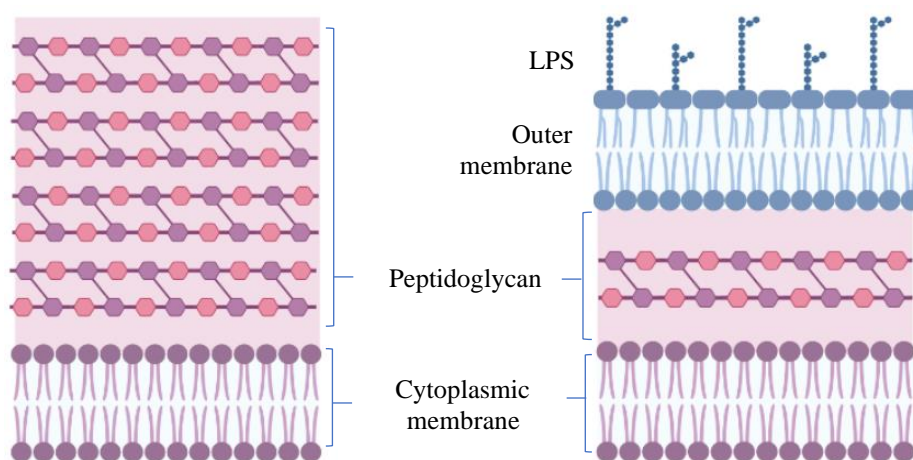
## c.2. Antimicrobial peptides mechanism of action

As previously introduced, the growing interest in AMPs lies in their particular mechanism of action against bacteria, which is commonly attributed to cytoplasmic membrane disruption.<sup>49,50</sup> However, new evidence points to additional intracellular mechanisms that target DNA/RNA/protein synthesis, protein folding, enzymatic activity or cell wall synthesis.<sup>51,52</sup> Therefore, even though the action mechanism of AMPs has not been

completely understood yet, there is evidence that bacterial membranes are their first target, even for intracellular mechanisms, where peptide must translocate across the membrane to reach the cell interior.

### c.2.1. Bacterial membranes

Bacteria cell envelope is a complex multi-layered structure that protects the organisms from hostile environments. Depending on membrane composition, is possible to classify bacteria into two large groups, Gram-positive and Gram-negative organisms (Figure 3). Both bacteria have similar inner or cytoplasmic membrane, a fluid bilayer composed of zwitterionic and anionic phospholipids that enclose the contents of the bacterial cell. However, the outer cell envelopes are significantly different, Gram-positive cytoplasmic membrane is surrounded by a thick layer of cross-linked peptidoglycan functionalized with anionic glycopolymers called teichoic acids. Gram-negative organisms present a more complex structure composed of a thinner peptidoglycan cell wall, which itself is surrounded by an asymmetric outer membrane containing lipopolysaccharide (LPS) molecules in its external side, bridged and stabilized with cations such as  $\text{Ca}^{2+}$  or  $\text{Mg}^{2+}$ .



**Figure 3:** Cell envelope composition of Gram-positive (left), Gram-negative (right) bacteria.

### c.2.2. Proposed mechanisms of action

In order to effectively exert their activity against Gram-positive bacteria, AMPs only need to diffuse across nanosized pores in the peptidoglycan envelope first, and then, interact with the cytoplasmic membrane, whereas Gram-negative bacteria present an extra outer membrane barrier to cross. Given the complex structure of LPS, the detailed mechanism of action has not been well understood, but self-promoted uptake hypothesis<sup>46,53,54</sup> shades

some light into the peptide translocation across the outer membrane. According to this hypothesis, the polar domain of the peptide interacts electrostatically with the highly anionic LPS surface, meanwhile the lipophilic face is inserted into the lipid tails of the LPS. These electrostatic and/or hydrophobic interactions destabilize the close packing of the outer membrane and compromise its permeability, and as a consequence, the membrane is weakened, and the peptide is then proposed to diffuse inward to the periplasmic space.

Having crossed the outer membrane and/or diffused across the peptidoglycan layer, the peptides approach the cytoplasmic membrane. Model studies have shown that, at low peptide/lipid ratios, AMPs first interact electrostatically with the negative charges of lipid head groups, adopting a parallel orientation toward the membrane. Thereafter, as the peptide/lipid ratio increases, different outcomes have been proposed, such as pore formation, membrane disruption or peptide translocation<sup>47,55</sup> (Figure 4):

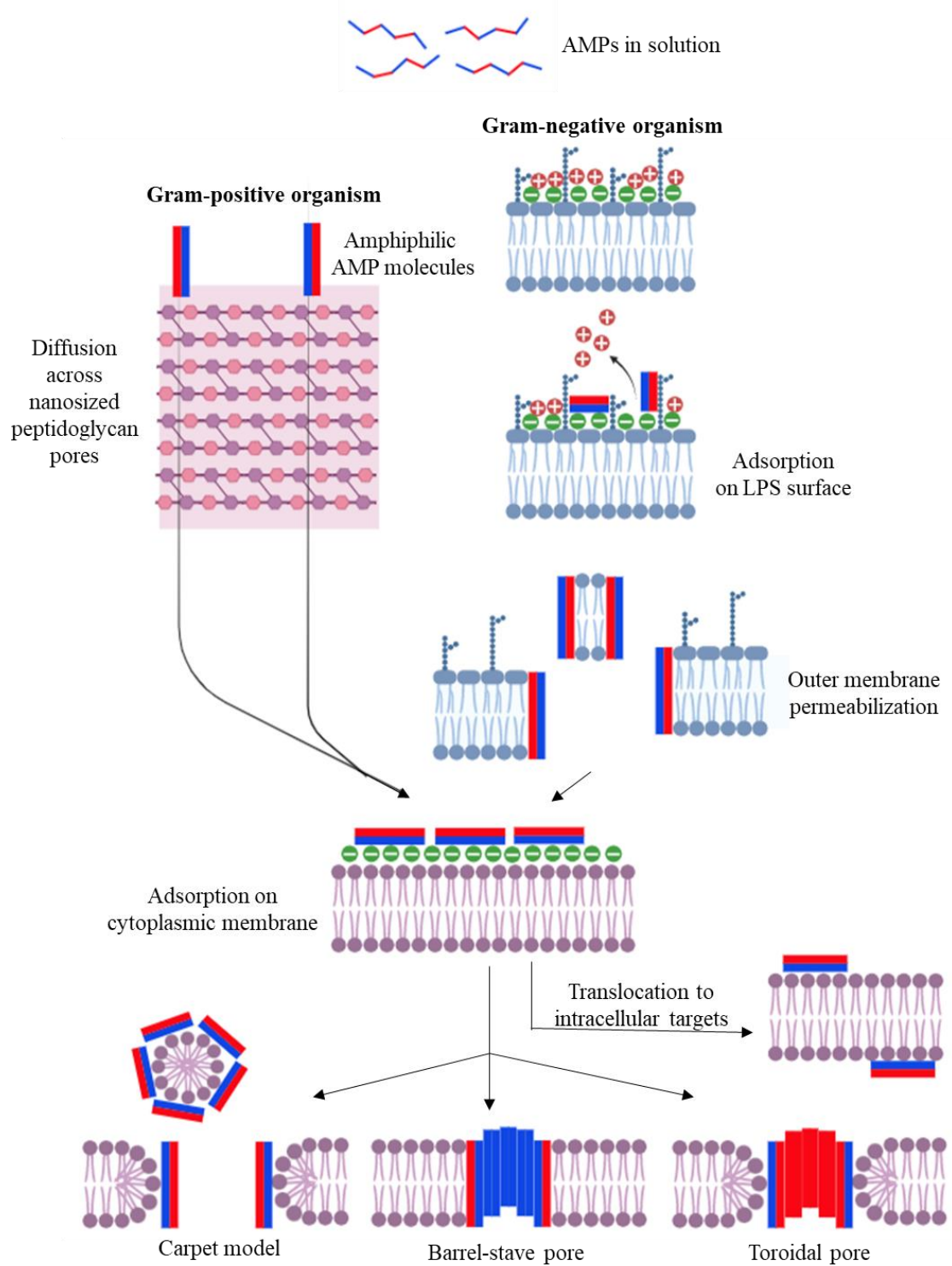
- The **carpet mechanism**<sup>56,57</sup> is a detergent-like effect exerted by some AMPs which accumulate parallel on the bilayer surface and at high concentrations, after reaching the surface coverage, disrupt the membrane via the formation of micelles and pores. This model is used to explain the mode of action of peptides such as ovispirin,<sup>58</sup> dermaseptin<sup>57</sup> or some cecropins.<sup>59</sup>
- The **barrel-stave model** is the classical picture to explain the transmembrane pore formation. According to this model, at given threshold concentration peptides insert perpendicularly in the bilayer such that their hydrophobic regions interact with the non-polar lipid region, while the hydrophilic surface of the peptide is oriented inwards, producing a hydrophilic channel across the membrane.<sup>56</sup> Barrel-stave model was first postulated in 1970s<sup>60</sup> and due to the lack of alternatives, during several years, peptide pores were often attributed incorrectly to this model,<sup>61,62</sup> but in fact, only the  $\alpha$ -helical alamethicin is consistent with the barrel-stave model, which created aqueous pores approximately greater than 18 Å in diameter.<sup>63,64</sup> Derivations of the barrel-stave model have also been reported for dermcidin<sup>65</sup> or pardaxin.<sup>66</sup>
- The **toroidal pore model**, also known as wormhole model, was proposed to describe magainin-induced pores in 1996 for first time,<sup>67,68</sup> this model represents

an extension of the barrel-stave model and it is the most cited mechanism for membrane permeabilization. As the barrel-stave model, it consists in a pore forming mechanism where AMPs insert perpendicularly in the bilayer, but in this case, the peptides impose a local membrane curvature around the pore in such a way that the hydrophilic site of the peptide is always interacting with the polar lipid headgroups, whereas the hydrophobic part forms the internal aspect. This model describes the mechanism of action of magainin and LL-37<sup>69</sup> among others.

- A large number of variants of the toroidal pore model have been proposed, such as the **aggregate model** or **disordered toroidal pore model**.<sup>54,70</sup> In these models, the formation of unstable pores, with heterogeneous shapes and sizes, facilitates the peptide uptake to the cell interior, followed by their rapid disintegration with the minimal disruption of the bacterial membrane. This is the case of melitin<sup>70</sup> and buforin II.<sup>71</sup>

After membrane penetration, some AMPs may exert their activity through **intracellular mechanisms**. It has been reported that AMPs can bind the negatively charged nucleic acids (DNA/RNA), enzymes or other intracellular targets. This model is used by AMPs such as indolicin, which inhibits DNA synthesis in *E. coli* cells at concentrations at which RNA and protein synthesis are either partially affected,<sup>72</sup> whereas pyrrolicin inhibits their correct protein folding.<sup>73</sup> In the case of Gram-positive bacteria, for example, nisin generates pores in cell membrane and inhibit cell wall biosynthesis by interrupting the peptidoglycan production.<sup>74</sup>

Thus, the study of all the events that occur when an AMP encounters a cell is a notoriously difficult task since AMPs can exert their antimicrobial activity through more than one mechanism of action simultaneously and there does not appear to be one model that fits all peptides.



**Figure 4:** Schematic illustration of direct antibacterial mode of action of AMPs. The hydrophilic and hydrophobic regions of the peptide are depicted in blue and red respectively.

## **d. Resistance**

Antimicrobial peptides are unlikely to spur the development of resistant organisms due to their rapid bactericidal effects and the multiple bacterial targets of these compounds. However, there is evidence of bacterial resistance to AMPs through diverse mechanisms, briefly described below.

### **d.1. Extracellular proteins**

The proteases or peptidases are the first bacterial defense mechanisms that AMPs encounter when interacting with bacteria. Produced by either Gram-negative or Gram-positive bacterial species, these proteolytic enzymes contribute to the degradation of active AMPs into inactive fragments. Examples include the cleavage of AMPs such as LL-37 by the metalloprotease aureolysin of Gram-positive *Staphylococcus aureus*<sup>75</sup> or the ompTn proteases in Gram-negative bacteria, such as protein OmpT in *Escherichia coli*.<sup>76</sup>

Along with proteolysis, some secreted molecules can bind and neutralize the microbicidal activity of AMPs, this resistance method is known as trapping or sequestration. As an example, SIC proteins, produced by *Streptococcus pyogenes*, bind and inactivate LL-37 and human  $\alpha$ -defensin, blocking their antimicrobial activity.<sup>77</sup>

### **d.2. Biofilms**

Biofilms are microbial communities of bacterial cells attached to a surface, which are encased in a self-produced matrix of extracellular proteins, DNA and exopolysaccharides.<sup>78</sup> These grouped bacteria show 100-1000-fold higher resistance than planktonic microbes<sup>79-81</sup> and they can be formed in every surface such as natural, medical or industrial settings, being one of the main causes of persistent infections. This increased resistance could be caused by the decreased penetration of the drugs through the matrix and the higher mutation rate of bacteria in biofilm communities.<sup>82,83</sup>

Different evidences of biofilm mediated resistance to AMPs have been reported such as the trapping of magainin II and cecropin P1 by the anionic alginate overproduced in *Pseudomonas aeruginosa* biofilms,<sup>84</sup> or the electrostatic repulsion of cationic AMPs such as LL-37 or human  $\beta$ -defensin caused by the positively charged exopolymer PIA present in *Staphylococcus epidermis* and *Staphylococcus aureus*.<sup>85</sup> Even so, AMPs represent a

promising approach for the eradication of biofilms, for instance, LL-37 and indolicidin can prevent the formation of *Pseudomonas aeruginosa* biofilms<sup>86</sup> and nisin A, lactacin Q, and nukacin ISK-1 can destroy biofilms of methicillin resistant *Staphylococcus aureus*.<sup>87</sup>

### **d.3. Surface modification**

As explained above, the antimicrobial action of AMPs is mainly exerted at the cytoplasmic membrane of bacteria. But to reach this target, the peptides should first penetrate the outer membrane or the peptidoglycan layer of bacteria, and on this stage, bacteria can modify their cell wall components and consequently, develop resistance. One of the best well-known surface-remodeling bacterial strategies is the loss of negative surface charges by, for example, the incorporation of D-alanine into free hydroxyls of teichoic acid in Gram-positive bacteria<sup>88</sup> or amine-containing compounds such as phosphoethanolamine (pEtN) or 4-amino-4-deoxy-L-arabinose (Ara4N) into the lipid A head groups of LPS in Gram-negative bacteria.<sup>89</sup> On the other hand, there are capsule-forming bacteria which are protected by an external polysaccharides layer that limits the interaction of AMPs with their targets, this is the case of *Klebsiella pneumoniae* capsule resistant to cationic defensins, lactoferrins and polymyxins.<sup>90</sup>

### **d.4. Cytoplasmic membrane alteration**

After passing through the outer membranes, AMPs must interact with the cytoplasmic membrane to exert their antimicrobial action. To decrease the peptide attraction and insertion, bacteria can modify the electronegativity of the cytoplasmic membrane, by altering the phospholipid composition. The most abundant phospholipids in bacterial inner membranes are the anionic phosphatidylglycerol (PG) and diphosphatidylglycerol (DPG, also known as cardiolipin), which can be modified to produce aminoacyl esters of PG that localize positive or zwitterionic charges onto the membrane.<sup>91-93</sup> For example, *Staphylococcus* and *Bacillus* species, modify their membranes by the production of Lys-PG<sup>94</sup> while other such as *Pseudomonas aeruginosa* produce Ala-PG,<sup>95</sup> these charge alteration result in AMP resistance by electrostatic repulsion.

### **d.5. Efflux pumps**

Once AMPs are inserted into the cytoplasmic membrane, bacteria can still remove them using efflux pumps, which are one of the major causes of multidrug resistance. Efflux

pumps are energy-dependent transport proteins involved in the extrusion of toxic molecules from within cells to the external environment. These proteins are found in both Gram-positive and Gram-negative bacteria as well as in eukaryotic organisms. As examples, the MtrCDE RND transporter of the Gram-negative *Neisseria gonorrhoeae* and *Neisseria meningitides* is responsible for resistance to LL-37 and protegrin-1<sup>96,97</sup> and the VraFG ABC transporter of the Gram-positive *Staphylococcus aureus* confers resistance to nisin, bacitracin, vancomycin, indolicidin, LL-37 and HBD-3.<sup>98</sup>

#### **d.6. Modulation of AMP gens expression**

The interference or suspension of host pathways for AMP expression appears to be another mechanism through which several pathogens achieve maximal resistance to AMPs. For example, downregulation of host AMP expression is a typical survival strategy of Gram-negative pathogens, such as *Shigella spp.*, which was shown to overturn the immune system by downregulating the expression of LL-37 and hBD-1.<sup>99</sup>

#### **e. Antimicrobial peptides as therapeutic agents**

In the last decades, peptides have also become outstanding candidates in the therapeutic anti-infectives field due to their broad-spectrum activity, including MDR bacteria, alongside to their low propensity to develop resistance. Nevertheless, AMPs present several drawbacks for their successful clinical development, such as their low metabolic stability and bioavailability owing to the proteolytic degradation in presence of proteases. To overcome this issue, unusual amino acids (mainly D-form or non-natural amino acids) have been introduced in peptide sequences,<sup>100,101</sup> as well cyclic structures and modified terminal regions by acetylation<sup>102</sup> or amidation.<sup>103</sup> The use of efficient drug delivery systems, such as liposome encapsulation, can also improve the peptide stability and reduce toxicity.<sup>104</sup> Another important disadvantage of peptides is their costly associated production. In this regard, many efforts have been made, including the development of active shorter peptides or alternative production methods, such as biotechnological engineering or fermentation.<sup>105</sup>

The factors above mentioned and the low financial support in research are limiting the growth of the AMPs market across the globe. Even so, to date, there are several AMP-based drugs in the market and many others currently in clinical trials (Tables 2 and 3).



**Table 2:** Representative AMPs as anti-infective therapeutics approved by FDA. Data collected from Drugs@FDA (<http://www.fda.gov/drugsatfda>) and DrugBank.<sup>106</sup>

AMP	Description	FDA approval	Medical use	Mechanism
<b>Bacitracin</b>	Cyclic peptide	1948	Skin lesions, surface wounds and eye infections caused by Gram-positive bacteria.	Cell wall synthesis inhibition
<b>Colistin<sup>a</sup></b>	Cyclic lipopeptide	1970	Bacterial infections caused by MDR Gram-negative bacteria including pneumonia.	Membrane disruption
<b>Gramicidin D</b>	Linear peptide	1955	Skin lesions, surface wounds and eye infections caused by Gram-positive bacteria.	Membrane pores formation
<b>Dalbavancin</b>	Lipoglycopeptide	2014	ABSSSI <sup>b</sup> caused by Gram-positive bacteria.	Cell wall and RNA synthesis inhibition and membrane permeabilization
<b>Daptomycin</b>	Cyclic lipopeptide	2003	ABSSSI <sup>b</sup> , endocarditis and bacteremia caused by Gram-positive bacteria.	Membrane depolarization and permeabilization
<b>Oritavancin</b>	Lipoglycopeptide	2014	ABSSSI <sup>b</sup> caused by Gram-positive bacteria.	Cell wall synthesis inhibition
<b>Polymyxin B</b>	Cyclic lipopeptide	2011	Bacterial infections caused by MDR Gram-negative bacteria including pneumonia.	Membrane disruption
<b>Teicoplanin</b>	Lipoglycopeptide	No FDA <sup>c</sup>	Septicemia, endocarditis, bone, and joint infections caused by Gram-positive.	Cell wall synthesis inhibition
<b>Telavancin</b>	Lipoglycopeptide	2009	HAP <sup>d</sup> , VAP <sup>e</sup> and ABSSSI <sup>b</sup> caused by Gram-positive bacteria.	Cell wall synthesis inhibition and membrane depolarization
<b>Vancomycin</b>	Tricyclic glycopeptide	1955	Serious or severe infections caused by MRSA and <i>Clostridium difficile</i> .	Cell wall and RNA synthesis inhibition and membrane permeabilization

<sup>a</sup>Approved as colistimethate sodium (CMS). <sup>b</sup>Treatment of acute bacterial skin and skin structure infections.

<sup>c</sup>Authorized in the EU *via* national procedures, first marketed in 1987. <sup>d</sup>Hospital-acquired bacterial pneumonia.

<sup>e</sup>Ventilator-associated bacterial pneumonia.

**Table 3:** Non-exhaustive list of AMPs as anti-infective therapeutics in clinical trials. Adapted from refs.<sup>107,108</sup>

AMP	Description	Stage of development	Medical use	Mechanism
<b>SPR206</b>	Polymyxin analogue	I	Severe Gram-negative bacterial infections	Membrane disruption
<b>QPX9003</b>	Polymyxin analogue	I	Severe Gram-negative bacterial infections	Membrane disruption
<b>MRX-8</b>	Polymyxin analogue	I	Severe Gram-negative bacterial infections	Membrane disruption
<b>Murepavidin (POL7080)</b>	Protegrin analogue	I	Lower respiratory infections caused by <i>Pseudomonas aeruginosa</i> and VAP <sup>a</sup>	Targets the outer membrane LPS
<b>Friulimicin</b>	Cyclic lipopeptide	I	MRSA, pneumonia.	Membrane disruption
<b>hLF1-11</b>	Fragment of human lactoferrin	I (completed)	MRSA, <i>K. pneumoniae</i> , <i>L. monocytogenes</i> infections.	DNA binding
<b>P-113 (PAC-113)</b>	Fragment of Histatin-5	I (completed)	Chronic infections caused by <i>Pseudomonas aeruginosa</i> , gingivitis, and periodontal diseases.	Membrane disruption/immunomodulation
<b>LTX-109</b>	Tripeptide	II	Uncomplicated skin infections caused by Gram-positive bacteria.	Membrane permeabilization
<b>PMX-30063 (Brilacidin)</b>	Defensin mimetic	II	ABSSSI <sup>b</sup>	Membrane permeabilization
<b>XF-73</b>	Porphyrin derivative	II (recruiting)	<i>Staphylococcal</i> infections.	Membrane permeabilization
<b>DPK060</b>	Kininogen derivative	II (completed)	Infections caused by eczematous lesions.	Membrane disruption/immunomodulation
<b>OP-145</b>	LL-37 derivative	II (completed)	Chronic middle ear infections.	Immunomodulation
<b>P2TA (AB103)</b>	CD28 mimetic peptide	III	Necrotic tissue infection	Immunomodulation
<b>Omiganan (MBI-226, MX-594AN)</b>	Indolicin derivative	III (completed)	Infections associated with catheters.	Membrane permeabilization

<b>Dusquetide (IMX942, SGX942)</b>	Analogue of IDR-1	III (recruiting)	Oral mucositis.	Immunomodulation
<b>XOMA-629</b>	BPI derivative	III (failed)	Impetigo, acne, rosacea.	Membrane permeabilization
<b>Surotomycin</b>	Cyclic lipopeptide	III (failed)	Diarrhea caused by <i>Clostridium difficile</i> .	Membrane depolarization
<b>Iseganan (IB-367)</b>	Protegrin analogue	III (failed)	VAP <sup>a</sup> and oral mucositis.	Membrane permeabilization
<b>Pexiganan (MSI-78, locilex)</b>	Magainin analogue	III (failed)	Infections caused by diabetic foot ulcer.	Membrane disruption/ immunomodulation

---

<sup>a</sup>Ventilator-associated bacterial pneumonia. <sup>b</sup> Treatment of acute bacterial skin and skin structure infections.

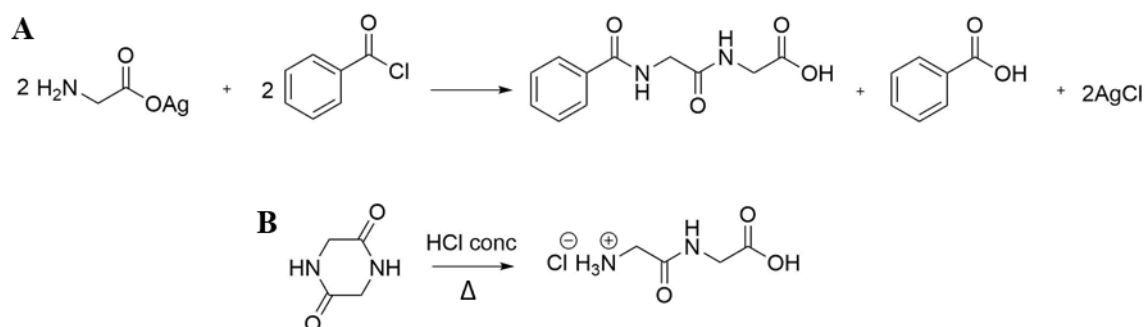
## f. Antimicrobial peptide synthesis

As mentioned above, antimicrobial peptides are active biomolecules that contain less than 100 amino acid residues joined by amide bonds. Many AMPs can be directly obtained by isolation from their natural sources; however, they are produced in limited quantities in nature. As a result, the current state of the art of peptide synthesis involves different methodologies, such as chemical synthesis,<sup>109</sup> DNA recombinant techniques,<sup>110,111</sup> enzymatic synthesis<sup>112</sup> or combinations of these technologies.<sup>113</sup> The peptide length and the production scale determine the most suitable methodology for its production. Thus, the total enzymatic synthesis is restricted to the production of short peptides which contain less than 10 residues, whereas recombinant DNA technology represents the most cost-effective option for large-scale production of peptides with large sequences, such as insulin or other hormones.<sup>114</sup> On the other hand, chemical synthesis is applied for the production of short or medium length peptides and it is currently the most widely used approach on a laboratory scale, hence the present thesis focuses on chemical peptide synthesis.

### f.1. Brief history of chemical peptide synthesis

The first peptide was synthesized and characterized by Curtius in 1882,<sup>115</sup> it was the *N*-protected dipeptide benzoylglycylglycine, prepared by treatment of the silver salt of glycine with benzoylchloride (Figure 5A). Twenty years later, Fisher first introduced the terminology ‘peptides’, and furthermore, he reported the synthesis of the first free

dipeptide, the glycineglycine,<sup>116</sup> which was synthesized using the hydrolysis of the diketopiperazine of glycine (Figure 5B).



**Figure 5:** First synthesized dipeptides by A) Curtius B) Fisher.

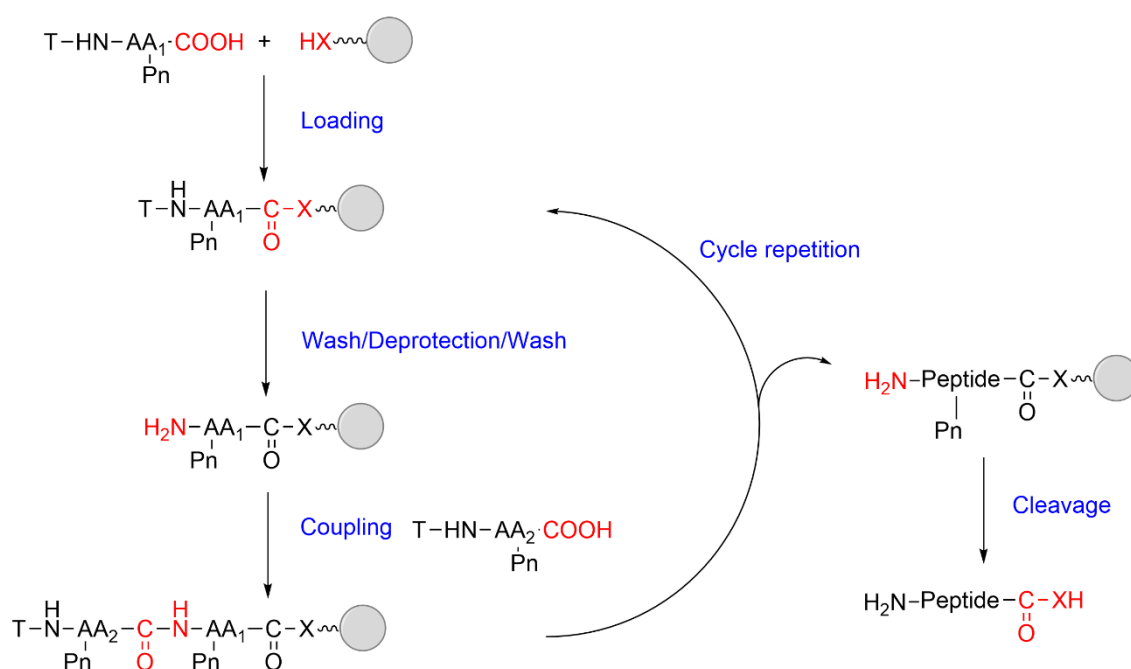
Afterwards, these researchers continued their investigation on peptide synthesis and developed two different synthetic methodologies: the azide-coupling method developed by Curtius<sup>117,118</sup> and the use of acylchloride coupling reactions employed by Fisher.<sup>119</sup> But both methods present important limitations such as the absence of an easily removable protecting group or high racemization propensity. To overcome these difficulties, Bergmann and Zervas in 1932<sup>120</sup> reported the use of benzyloxycarbonyl group (first abbreviated as Cbz, now Z) as a temporary amino protecting group, which permitted the synthesis of peptides containing amino acid residues with reactive side chains (e.g. Asp, Glu, Lys or Arg). The concept of temporarily protecting groups revolutionized the peptide chemistry and led to intensive research toward discovering new protecting groups and coupling reagents. Remarkable innovations in this regard were the introduction of the *tert*-butoxycarbonyl (Boc) protecting group,<sup>121,122</sup> carbodiimides<sup>123</sup> or 1-hydroxybenzotriazole (HOBt).<sup>124</sup>

Along with these advances, du Vigneaud described the chemical synthesis of the first natural peptide, oxytocin, in 1953.<sup>125</sup> The described synthesis was laborious and the yield was low because it was carried out in solution, which means that all intermediates were isolated and characterized after each coupling. Few years later, Merrifield reported a revolutionary new methodology, the Solid Phase Peptide Synthesis (SPPS),<sup>126</sup> which briefly consists of successive addition of protected amino acid derivatives to a growing peptide chain immobilized on a solid support, including deprotection and washing steps to remove unreacted and also side products, thereby simplifying the demanding steps of purification associated with solution phase synthesis. Later, in 1970, the base-labile 9-

fluorenylmethoxycarbonyl (Fmoc) amino-protecting group<sup>127</sup> was introduced and therewith orthogonal protection strategies were widely applied. Nowadays, a century ago since the first simple peptides were synthesized, the methodology of peptide synthesis has undergone dramatic development, allowing the preparation of highly complex peptides.

## f.2. Fundamentals on solid phase peptide synthesis

Solid phase peptide synthesis is currently one of the most frequent and simple methodology to obtain peptides in a laboratory scale and it was the methodology employed during this thesis for the peptide synthesis. The principles of SPPS are summarized in Figure 6.



**Figure 6:** General scheme of SPPS. X: O or NH; Pn: permanent protecting group; T: temporary protecting group.

Briefly, a *N*-protected *C*-terminal amino acid is anchored to an insoluble polymeric support and then, the peptide is assembled by the successive addition of protected amino acids from the *C*-terminus to the *N*-terminus by repetitive cycles of *N*- $\alpha$  deprotection and amino acid coupling reactions. To prevent the peptide polymerization and epimerization, the synthetic process is performed following an orthogonal protection strategy, which means that the side-chain functional groups of amino acids are masked with permanent protecting groups (Pn) stable in the reaction conditions, whereas the  $\alpha$ -amino groups are

protected by temporary protecting groups (T), which are easily removed during the synthetic process under mild conditions. After each reaction step, excess reagents and by-products can be easily removed from the growing and insoluble peptide by filtration and washings. In a final step, the peptide is released from the solid support and the permanent protecting groups (Pn) concomitantly removed.

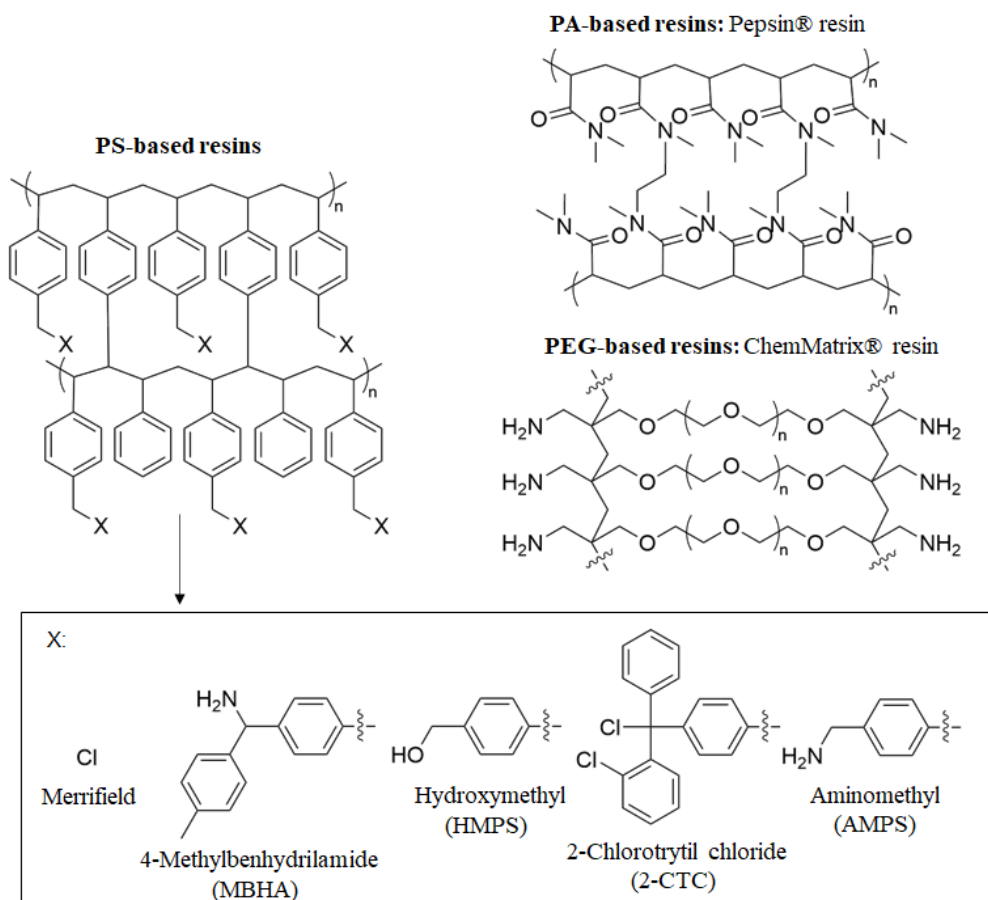
Below, the most important aspects of SPPS are briefly introduced:

- **Polymeric solid support:** A useful support must contain reactive sites where the polypeptide chain could be attached and subsequently removed, and it must be completely insoluble and stable to the physical and chemical conditions of the synthesis.

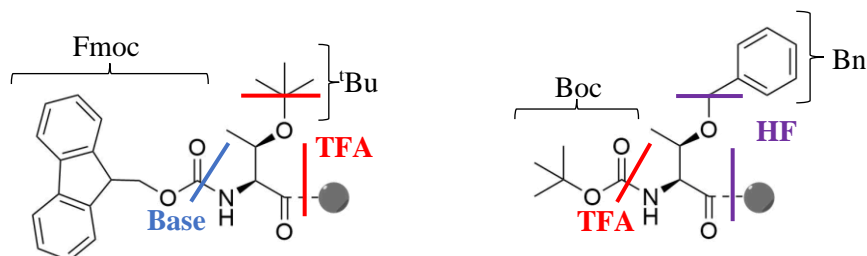
The solid support, also named resin, is composed of a polymer matrix functionalized or derivatized with an appropriate linker. Crosslinked polystyrene (PS)-based resins are the most commonly used for routine SPPS. There are also other supports much more hydrophilic such as the crosslinked polyamide (PA)-based resins and composite PS-polyethylene glycol (PEG)-based resins, which may represent an alternative to standard crosslinked PS resins for the synthesis of difficult sequences and large peptides.<sup>128</sup>

Many different resins are commercially available nowadays, containing different linkers anchored on the matrixes above mentioned. The most suitable option should be properly chosen for each synthesis, depending on the C-terminal functional group of target peptide (such as acid, amide, thioacid or aldehyde). The most frequently used resins are represented in Figure 7.

- **Protection strategies:** Protection of the  $\alpha$ -amino group of each amino acid is a common way to prevent unwanted side reactions avoiding its polymerization during the coupling reaction. The  $\alpha$ -amino-protecting groups should also prevent or minimize epimerization. Furthermore, as they are removed several times during the synthesis, they should be easily removed under mild conditions without affect the remaining side-chain protectors (permanent or semi-permanent protecting groups) or even the peptidic chain. In addition, this removal should be free of side reactions and should render easily eliminated by-products. For that purpose, the most common  $\alpha$ -amino-protecting groups for SPPS are the *tert*-butoxycarbonyl (Boc) and the 9-fluorenylmethoxycarbonyl (Fmoc) groups, used in Boc/benzyl (Bn) and Fmoc/*tert*-butyl (<sup>t</sup>Bu) strategies respectively (Figure 8).

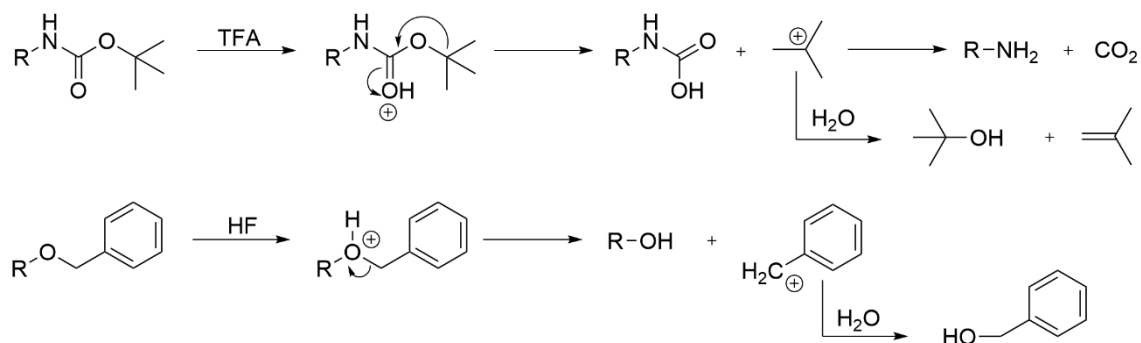


**Figure 7:** Polymeric solid supports commonly used in SPPS.



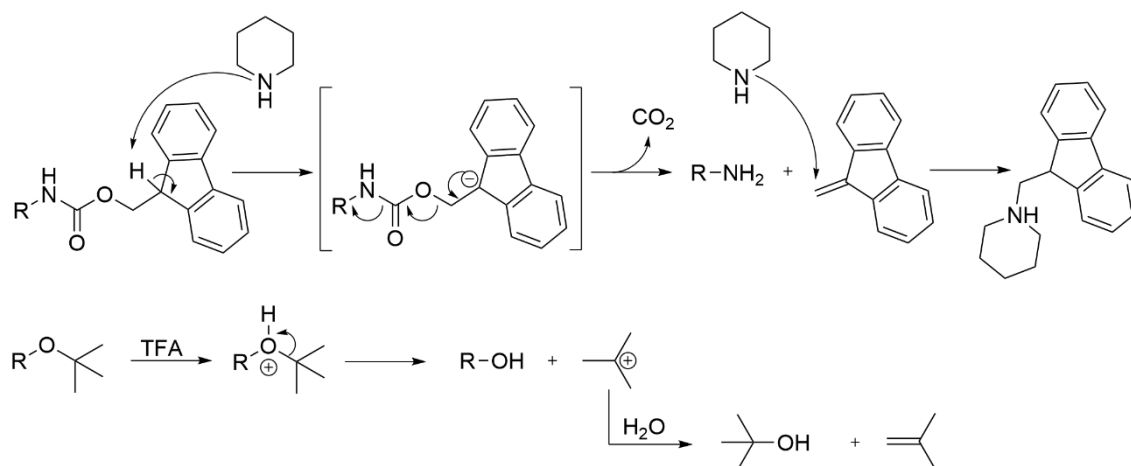
**Figure 8:** Comparison of the Fmoc/<sup>t</sup>Bu (left) and Boc/Bn (right) protection strategies.

The Boc/Bn approach is based upon the different acid lability of the protecting groups. In this strategy, Boc groups protect temporarily the  $\alpha$ -amino functions, and they are successively removed by trifluoroacetic acid (TFA). Whereas side chain protecting groups and peptide–resin linkages are removed at the end of the synthesis under a strong acidic treatment with anhydrous hydrogen fluoride (HF). Removal mechanisms are shown in Figure 9. This methodology allows the synthesis of large peptides, but it presents several drawbacks such as the high toxicity of HF and the need for special laboratory equipment.



**Figure 9:** Removal mechanisms of Boc and Bn protecting groups.

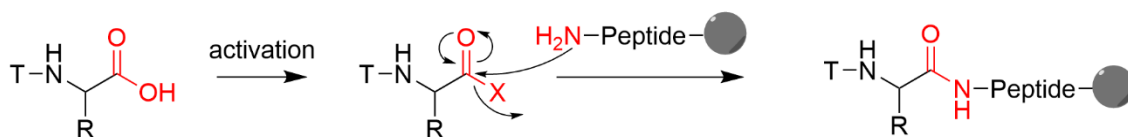
The Fmoc/<sup>t</sup>Bu strategy is nowadays the most common methodology for the routine peptide synthesis. It is based on an orthogonal protection, which means that temporary and permanent protections are removed by different mechanisms allowing the use of milder acidic conditions for final deprotection and cleavage of the peptide from the resin. In this case, the base-labile Fmoc group is used to protect the  $\alpha$ -amino functions, while acid-labile groups protect the side-chain reactive groups. Removal mechanisms are shown in Figure 10.



**Figure 10:** Removal mechanisms of Fmoc and <sup>t</sup>Bu protecting groups.

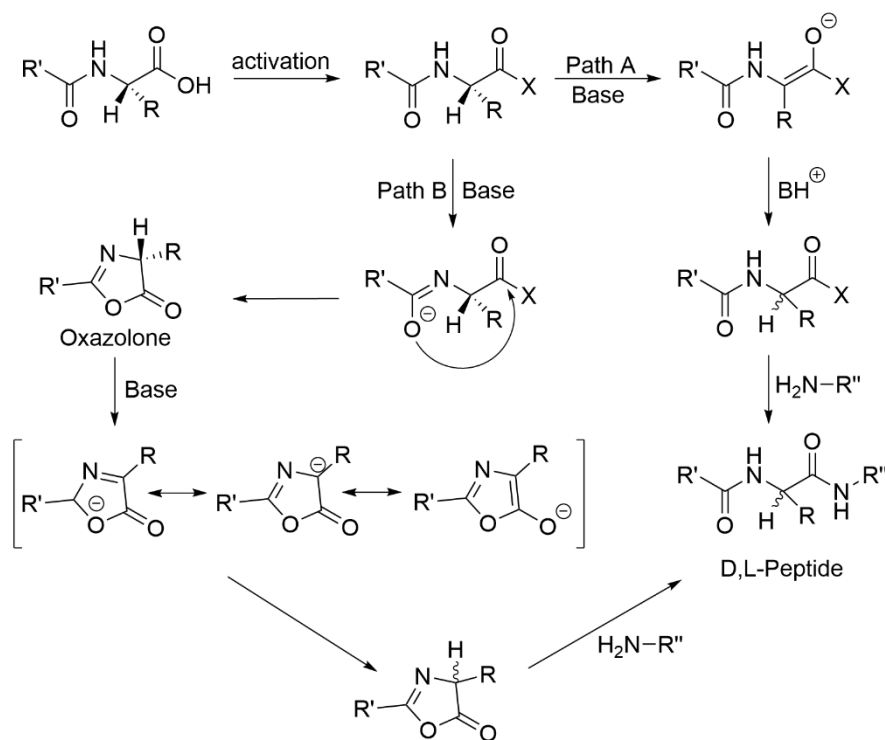
**- Chain elongation and coupling agents:** Peptides are assembled by an amide bond between two adjacent amino acids through the so-called coupling reaction. The obtention of this amide bond is not directly accessible, because the direct treatment of a carboxylic acid with an amine undergoes an acid–base reaction. To tackle this problem, an additional reagent known as a coupling reagent is added to activate the carboxy group by the introduction of an electro-withdrawing group, thus the carboxy group is activated toward nucleophilic attack of the  $\alpha$ -amino function of another residue (Figure 11).





**Figure 11:** Peptide bond formation. T: temporary protecting group; X: halide, N<sub>3</sub>, OR (activated ester), OCOR (mixed or symmetric anhydride).

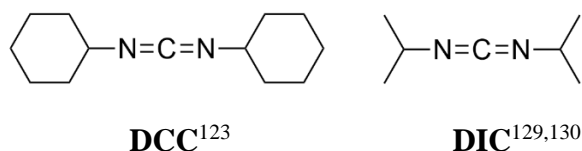
Coupling conditions are a key factor of the peptide synthesis since they determine the acylation rate, as well as the extent of side reactions. For instance, racemization is a side-reaction produced during the peptide bond formation under basic conditions, which causes a loss of configuration at the activated carboxyl residue. Two major pathways for racemization have been reported: the direct enolization due to the acidic behaviour of the  $\alpha$ -hydrogen when the carboxyl function is activated, and 5(4H)-oxazolone formation, both shown in Figure 12.



**Figure 12:** Racemization mechanisms. Path A: direct enolization; Path B: oxazolone formation. X: activating moiety.

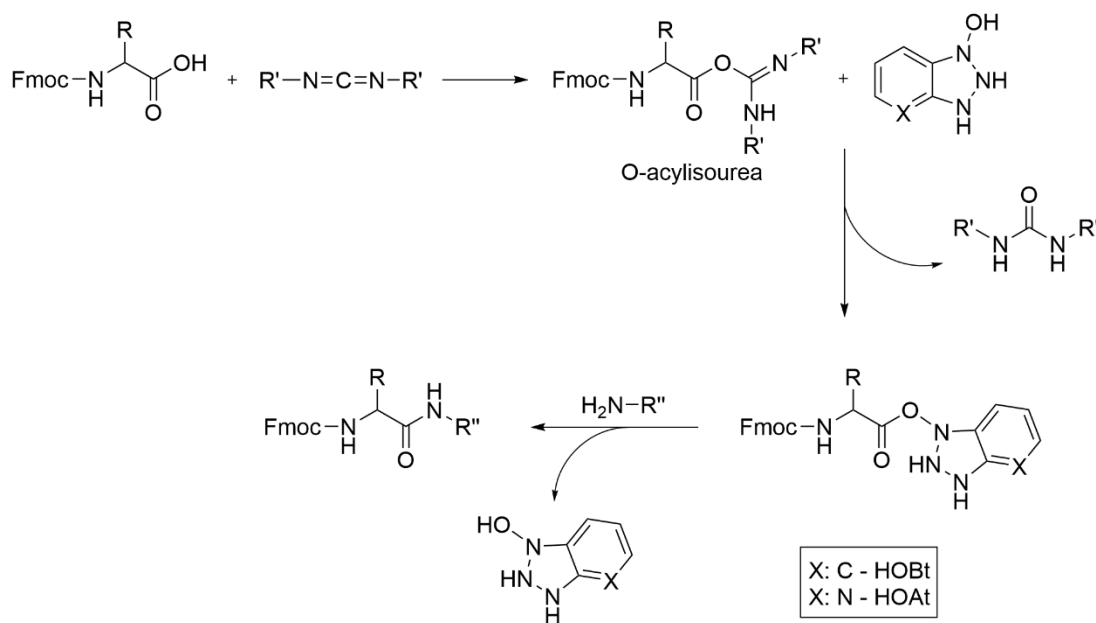
A diverse range of coupling reagents is used in stepwise peptide chain elongation, such as carbodiimides (Figure 13), among which *N,N'*-dicyclohexylcarbodiimide (DCC) has been widely used in the peptide synthesis since its introduction in 1955.<sup>123</sup> DCC produces

a dicyclohexylurea by-product, which is nearly insoluble in most organic solvents. Hence DCC is appropriated in solution phase reactions, but it has been substituted by *N,N'*-diisopropylcarbodiimide (DIC) in SPPS, which generates an urea by-product soluble in organic solvents that may be eliminated by washing the resin after coupling completion.



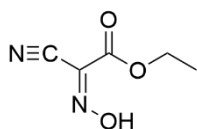
**Figure 13:** Common carbodiimides used in peptide synthesis.

The reaction between the carbodiimide and an acid generate the O-acylisourea of an *N*-alkoxycarbonylamino acid or peptide (Figure 14), which is one of the most reactive species and rapidly undergoes aminolysis in the presence of the amine component to yield the peptide. However, the strong activation of carboxy groups by carbodiimides sometimes leads to a partial racemization as it was discussed above. For that reason, *N*-hydroxylamine-based additives are typically added to minimize racemization rate. The positive effect of these additives is explained by the formation of a transient active ester that is slightly less reactive than previously formed intermediates, but reactive enough to successfully lead to the desired peptide bond. The most commonly used additives are 1-hydroxybenzotriazole (HOBt) or 1-hydroxy-7-azabenzotriazole (HOAt).



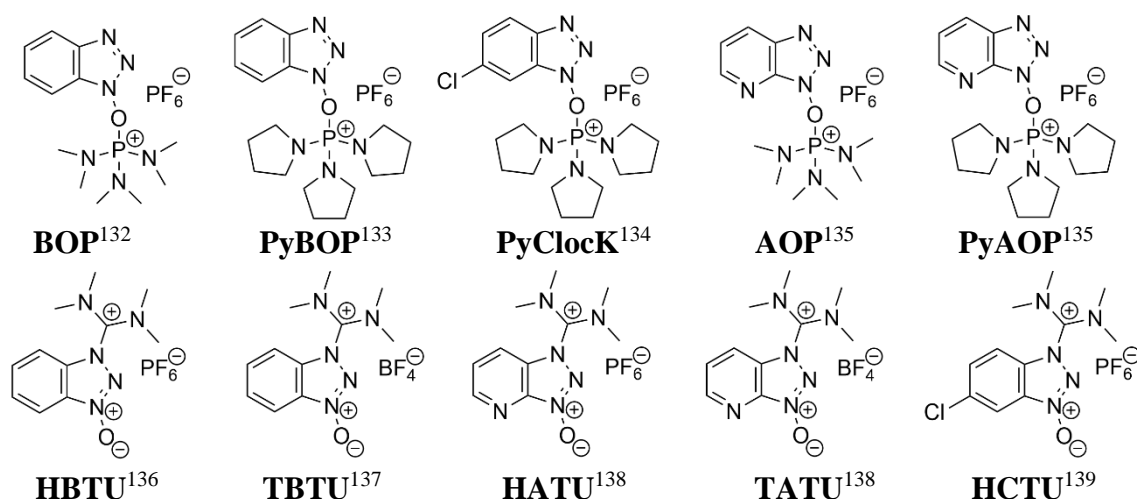
**Figure 14:** Mechanism of peptide bond formation from a carbodiimide-mediated reaction.

Moreover, ethyl 2-cyano-2-(hydroxyimino)acetate (Oxyrna) (Figure 15) is a safe and highly efficient additive to be used in the carbodiimide approach for peptide bond formation. Oxyrna possesses a remarkable capacity to suppress racemization, high coupling efficiency and it is a valuable alternative to the use of HOBt and HOAt, which exhibit explosive properties.



**Figure 15:** Oxyrna.<sup>131</sup>

As alternative to carbodiimides, other activating agents have become vastly used in SPPS, such as the phosphonium and aminium-based reagents, which are HOBt or HOAt derivatives, the most widely used are shown in Figure 16. Coupling reactions with these agents are rapid, being nearly complete within a few minutes and devoid of racemization.

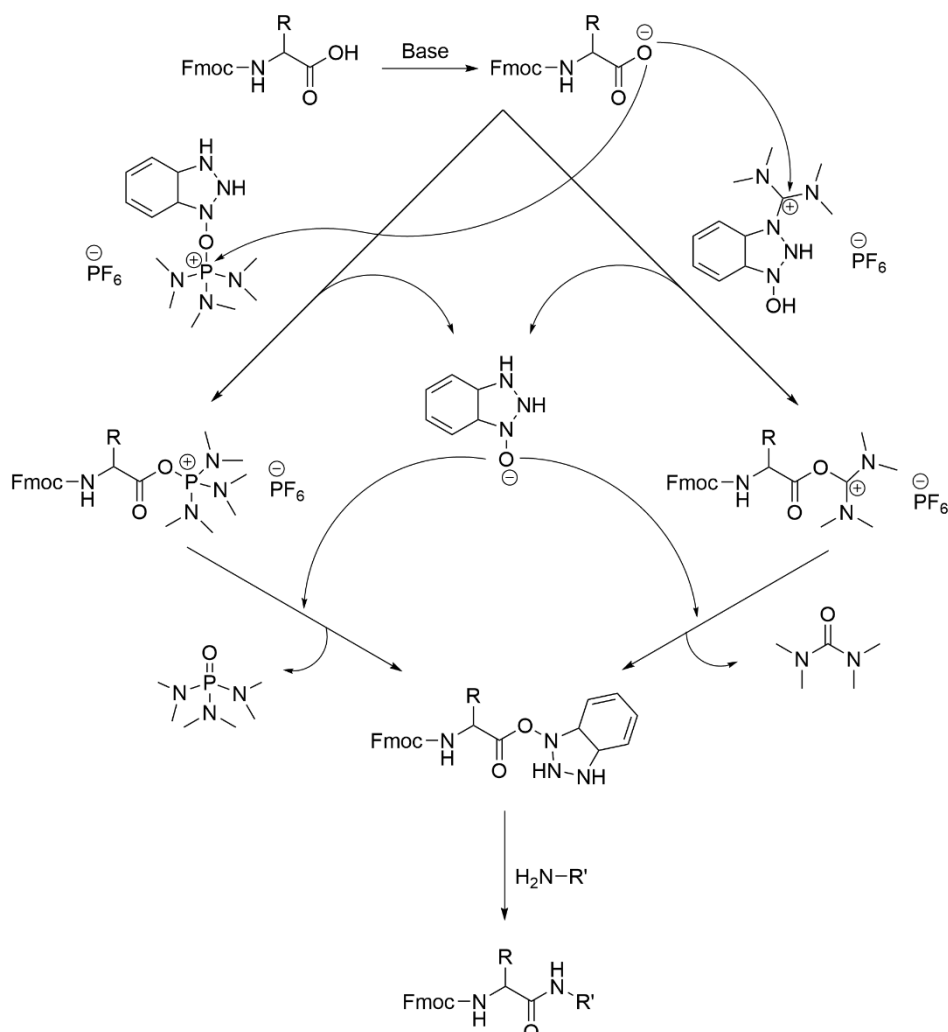


**Figure 16:** Common phosphonium and aminium salts used in SPPS.

These salts, unlike the carbodiimides, generate active esters in situ by their reaction with the carboxylate function, being so necessary the addition of base, typically a hindered tertiary amine such as *N,N*-Diisopropylethylamine (DIPEA), *N*-methylmorpholine (NMM) or collidine (TMP). The reaction mechanism is shown in Figure 17.

In addition to the above mentioned, there are various other activating reagents such as symmetric and mixed anhydrides, acylazoles, acyl azides, acyl halides,

organophosphorus reagents, organosulfur reagents or pyridinium reagents. All these activating methodologies have been extensively studied and reviewed in literature.<sup>140-143</sup>



**Figure 17:** Mechanism of peptide bond formation with phosphonium and aminium salts. BOP (left); HBTU (right).

- **Cleavage:** On completion of chemical peptide synthesis, the final step requires the removal of the peptide from the solid support while removing the protecting groups from the sidechains. Many different approaches have been established depending on the protection strategy, resin or the amino acids used for each synthesis. Briefly, for all Boc/Bn-based peptides highly strong acidic cleavage conditions are required, such as treatments with anhydrous HF, trifluoromethanesulfonic acid (TFMSA), trimethylsilyl trifluoromethanesulfonate (TMSOTf) or HBr. Whereas milder acidic conditions are necessary for peptides synthesized following the Fmoc/<sup>t</sup>Bu methodology, generally cleaved by TFA treatments.

In both methodologies, during the cleavage, sidechain protecting groups produce stabilized carbocations, which can readily react with the electron rich sidechain of amino acids (such as Cys, Met, Tyr, Thr, Ser or Trp), leading to undesired by-products. To minimize this side reaction, scavengers are added to the cleavage reagent, which trap carbocations. Some of the most widely used are water, thiols, anisole, dimethyl sulfide, p-cresol or silane-based compounds (triethylsilane or triisopropylsilane).

- **Purification:** Peptide purification methodologies involve different techniques such as reversed-phase high-performance liquid chromatography (RP-HPLC), flash chromatography, ion-exchange chromatography, hydrophobic interaction chromatography, gel filtration chromatography, size exclusion chromatography, and hydrophilic interaction chromatography.<sup>144</sup> The final purity of the product depends on the method used and the nature of the prepared sample.

## **GENERAL OBJECTIVES**



The main goal of this thesis is to provide an approach to the fight against antimicrobial resistance with the design, synthesis, and characterization of novel antimicrobials with improved properties, and to get insight into the interaction of antimicrobial peptides with the lipid component of the membrane.

The specific objectives were the following:

- Development of a new synthetic approach to the total synthesis and characterization of polymyxin B<sub>3</sub> and other antimicrobial peptides.
- Design and synthesis of new polymyxin B analogues in order to obtain novel antimicrobial compounds with improved activity and reduced toxicity compared to the natural compound.
- Study the antimicrobial activity and mechanism of action of the synthesized polymyxin analogues using different techniques, such as *in vitro* assays with bacteria, transmission electron microscopy, or biophysical techniques with model membranes.
- Selection of the most promising hit compounds to advance them according to the hit-to-lead stage of development. Scale-up their synthesis and evaluate their potency and toxicity using *in vitro* and *in vivo* models.
- Study the mechanism of action of BP100 by using a series of peptides of different lengths based on the same BP100 repeating units.





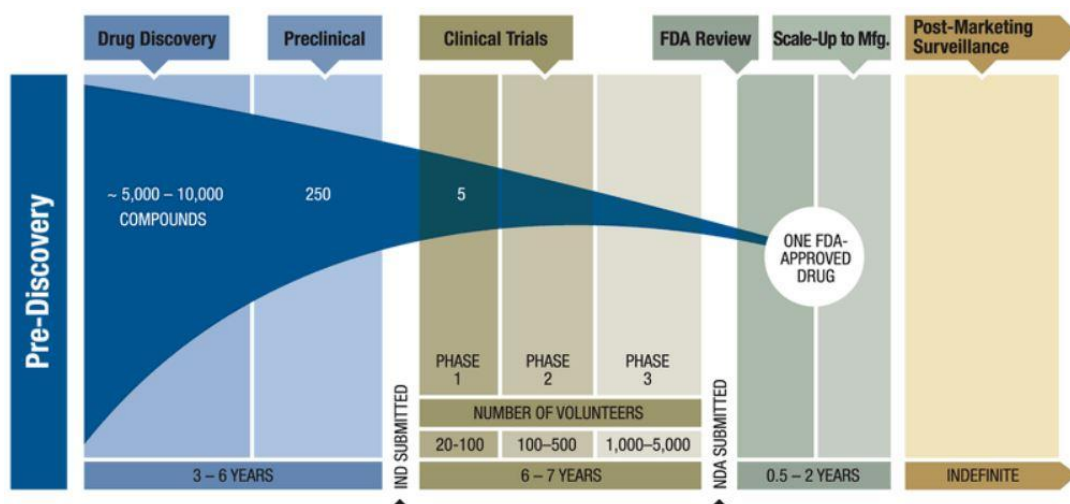
**CHAPTER 1:**  
**Development of new polymyxin B-based drugs**



## 1.1. Introduction

### 1.1.1. Drug development process

The introduction of a new drug product into the market requires of an extensive discovery and development process, involving design and chemistry work in research laboratories, followed by *in vitro* and animal studies, clinical trials, the approval of all regulatory requirements controlled by the Food and Drug Administration (FDA) in the USA and European Medicines Agency (EMA) in Europe, as well as the scale-up of the drug production. This is a complicated and lengthy process that can take between 10 and 15 years, and its average cost is estimated to \$1.3 billion.<sup>145</sup> Figure 18 shows the abbreviated chronology of the introduction of a new drug in the market, each stage will be further discussed below.



**Figure 18:** Drug discovery and development timeline. IND: Investigational new drug application; NDA: New drug application. Image credit: American Association for Cancer Research, Philadelphia, 2011.<sup>146</sup>

#### 1.1.1.1. Drug discovery

Historically, drugs have mainly been discovered by serendipity or by isolation of the active molecules from plant extracts used as medicines. Afterward, the rise of synthetic organic chemistry became one of the main drivers of drug discovery, which permitted the preparation of non-natural drug candidates. In more recent times, with the current technological development such as molecular modelling, combinatorial chemistry, automated high-throughput screening, or the emergence of recombinant DNA technology, rapid advances occurred in drug discovery.

This stage is divided in the following sub-processes:

- Target identification and validation: Study of the disease pathways and identification of a drug target involved in the progression of the disease.
- Hit discovery process: Development of screening assays in order to find compounds (hits) with the desired activity against the previously identified drug target. At this stage thousands of compounds are evaluated, such as new synthetic compounds, analogues of already existing drugs or naturally occurring compounds that can be re-purposed as drugs.
- Hit to lead (H2L): Hits are further evaluated and undergo limited optimization to narrow the field of compounds to a small number of promising lead compounds.
- Lead optimization (LO): Lead compounds are finally optimized to improve their efficacy and safety. Pharmacodynamic, pharmacokinetic and toxicological properties are carefully evaluated *in-vitro* and even in some animal models such as mice and rat. The resulting compound or compounds of this stage are the final candidate drugs that will undergo years of testing on this way to the market.

#### 1.1.1.2. Preclinical research

Once one or more lead compounds have been identified, preclinical research is performed to evaluate the drug's toxicity in animal species before their administration to humans. Different pharmacology tests are also carried out to study the absorption, distribution, metabolization, and excretion of the drug. These studies provide valuable information to select the proper formulation, dosage, and administration form (topical, oral, or parenteral) of the new drug.

On completion of the preclinical studies, the corresponding regulatory authorities must approve the Investigational New Drug application (IND), where the following information must be included: the pharmacologic profile of the drug and determination of its toxicity, drug manufacturing information, clinical protocols for the next stage of development, and relevant information about the principal investigator.

At this point in time, it is highly important to study the scale-up of the drug production, since the small quantities usually obtained in research laboratories are often not enough to carry out experiments in animals and humans and the techniques used in small scale may not translate easily to longer production.

#### 1.1.1.3. Clinical trials

After preclinical research, clinical trials are conducted in human volunteers to fine-tune the drug for its final medical use. This process follows the following stages: <sup>147</sup>

- Phase 1: The new drug is tested in 20 - 100 healthy volunteers to determine how the drug interacts with the human body and to establish dose adjustment. It takes several months, and according to the FDA, approximately 70 % of drugs move to the next phase.
- Phase 2: Between 100 and 500 people with disease are treated with the drug to evaluate its effectiveness and adverse effects. This phase is prolonged from several months to 2 years. Approximately 33 % of drugs move to the next phase.
- Phase 3: Phase 3 studies are developed to study less common side effects that might have gone previously undetected, for that purpose larger tests (1000 to 5000 patients) of longer in duration (1 to 4 years) are performed. Only 25 - 30 % of drugs make it through this stage.

#### 1.1.1.4. Drug approval

Once clinical trials have succeeded, a New Drug Application (NDA) is submitted to the appropriate regulatory authorities. The aim of this document is to demonstrate that the new drug is safe and effective for its medical use. It must include all the information collected during the preclinical and clinical trials, as well as a proposed labelling, and information about safety, directions of use, drug abuse, and patenting state.

The NDA is carefully analysed by a review team composed of medical doctors, chemists, statisticians, microbiologists, pharmacologists, and other experts during about 6 to 10 months. If it is finally approved, the labelling processes begins, which consists of the development of the prescribing information that accompanies all prescription medications.

#### 1.1.1.5. Scale-up of the manufacturing process

The scale-up process should be considered during each above-mentioned development stages, since any processes involved in the drug's obtention must be scalable in terms of safety, efficacy, and economic viability.

In moving from R&D to market, the drug is first obtained at laboratory scale, which is those that produce from milligrams to grams of product, and it is used when the drug is still being tested in preclinical trials. The following level is the pilot scale which is often used for the production during clinical trials and represents about 10 % of the production scale. Finally, when a drug is approved and in demand stage, it is produced at commercial scale, which consists of kilograms or even tones of product.

The scale-up represents a challenge for the pharmaceutical industry because any change introduced into the process could modify the characteristics of the final compound or change its final purity, which can ruin all the safety studies done previously. Scale-up problems sometimes require post-approval changes that affect formulation, composition, and manufacturing process or equipment.

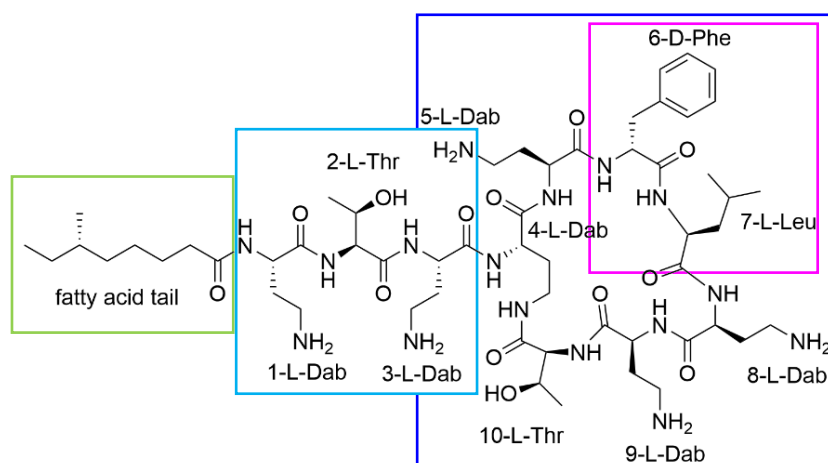
#### 1.1.1.6. FDA Post-Market Safety Monitoring

Once the drug has been approved, the regulatory authorities require drug companies to monitor the safety of the new drug, this post-market monitoring is also known as Phase 4. It involves continuous observational strategies to evaluate the drug efficacy, long term side effects, and cost-effectiveness relationship.

### **1.1.2. Polymyxins**

Polymyxins are antimicrobial cyclic lipopeptides produced by the Gram-positive bacterium *Paenibacillus polymyxa* that present a potent and selective activity against Gram-negative bacteria, including the majority of Enterobacteriaceae family (*Escherichia coli*, *Enterobacter* spp., *Klebsiella* spp., *Citrobacter* spp., *Salmonella* spp., and *Shigella* spp.) as well as *Pseudomonas aeruginosa*, *Acinetobacter baumannii*, *Haemophilus* spp., and *Pasteurella* spp. However, *Proteus* spp., *Burkholderia* spp., *Serratia* spp. and genera *Brucella*, *Neisseria*, *Chromobacterium* and *Providencia*, have intrinsic resistance to polymyxins.<sup>148,149</sup>

In terms of their chemical structure, polymyxins are polycationic lipopeptides formed by a cyclic heptapeptide core linked to a linear tripeptide with an *N*-terminal fatty acid tail (Figure 19). Polymyxins present an amphipathic structure as a result of the combination of five L-2,4-diaminobutiric acid (Dab) residues that are positively charged at physiological pH, and hydrophobic domains, that includes the *N*-terminal acyl chain and several non-polar amino acids.



**Figure 19:** Polymyxin B<sub>1</sub> structure. The functional segments are color coded as follows: hydrophobic *N*-terminal fatty acid chain (green), linear tripeptide segment (light blue), polar residues of the heptapeptide ring (dark blue) and hydrophobic motif within the cycle (pink).

Polymyxins were first reported in 1947, when Benedict and Langlykke,<sup>150</sup> Stansly et al.,<sup>151</sup> and Ainsworth et al.,<sup>152</sup> reported simultaneously the obtention of polymyxins A and D. Later Brownlee and Bushby<sup>153</sup> isolated a third polymyxin, named polymyxin B. Currently, there are reported up to 30 naturally occurring polymyxins, some of whose structures are shown in Table 4.

The most well-known members of this family are polymyxin B (PxB) and polymyxin E (PxE, also named colistin), because they were introduced into the clinical practice in mid 1950s and where used until the late 1970s, when their systemic use were gradually abandoned due to the widely reported cases of neuro- and nephrotoxic adverse effects.<sup>148,154</sup> In the last two decades, as a consequence of the alarming situation of bacterial resistance, polymyxins have reemerged as last line therapy in hospitals to treat ventilator associated pneumonia, sepsis and catheter-related infections caused by Gram-negative MDR bacteria.

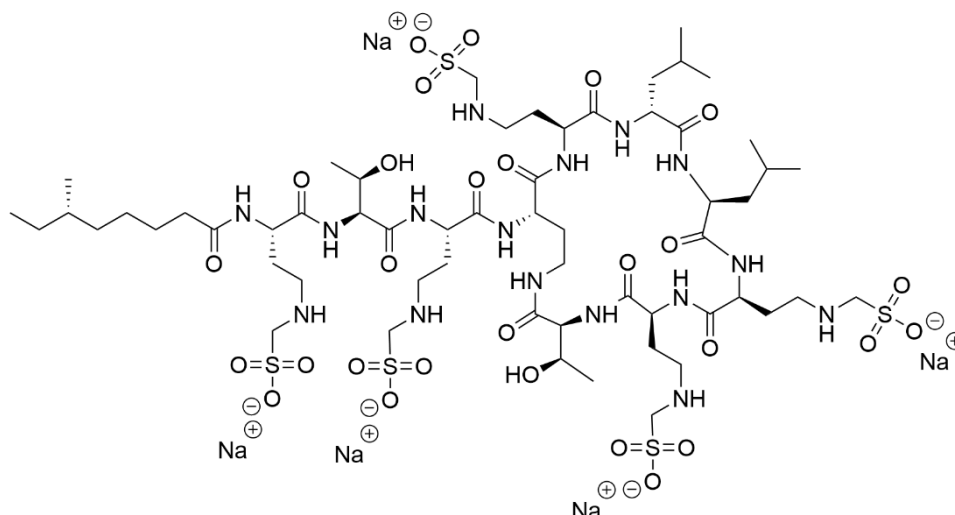


**Table 4:** Structure of some relevant naturally occurring polymyxins. All amino acids refer to the L-configuration unless otherwise specified.

Polymyxin	Fatty acid tail	AA-3	AA-6	AA-7	AA-10
<b>B<sub>1</sub></b>	6-MOA	Dab	D-Phe	Leu	Thr
<b>B<sub>1</sub>-Ile</b>	6-MOA	Dab	D-Phe	Ile	Thr
<b>B<sub>2</sub></b>	6-MHA	Dab	D-Phe	Leu	Thr
<b>B<sub>3</sub></b>	Octanoic acid	Dab	D-Phe	Leu	Thr
<b>B<sub>4</sub></b>	Heptanoic acid	Dab	D-Phe	Leu	Thr
<b>B<sub>5</sub></b>	Nonanoic acid	Dab	D-Phe	Leu	Thr
<b>E<sub>1</sub></b>	6-MOA	Dab	D-Leu	Leu	Thr
<b>E<sub>1</sub>-Ile</b>	6-MOA	Dab	D-Leu	Ile	Thr
<b>E<sub>1</sub>-Val</b>	6-MOA	Dab	D-Leu	Val	Thr
<b>E<sub>1</sub>-Nva</b>	6-MOA	Dab	D-Leu	Nva	Thr
<b>E<sub>2</sub></b>	6_MHA	Dab	D-Leu	Leu	Thr
<b>E<sub>3</sub></b>	Octanoic acid	Dab	D-Leu	Leu	Thr
<b>E<sub>4</sub></b>	Heptanoic acid	Dab	D-Leu	Leu	Thr
<b>E<sub>7</sub></b>	7-MOA	Dab	D-Leu	Leu	Thr
<b>A<sub>1</sub></b>	6-MOA	D-Dab	D-Leu	Thr	Thr
<b>C<sub>1</sub></b>	6-MOA	Dab	Phe	Thr	Thr
<b>D<sub>1</sub></b>	6-MOA	D-Ser	D-Leu	Thr	Thr
<b>M<sub>1</sub></b>	6-MOA	Dab	D-Leu	Thr	Thr
<b>S<sub>1</sub></b>	6-MOA	D-Ser	D-Phe	Thr	Thr
<b>T<sub>1</sub></b>	6-MOA	Dab	D-Phe	Leu	Leu
<b>P<sub>1</sub></b>	6-MOA	D-Dab	D-Phe	Thr	Thr

6-MOA, (S)-6-methyl octanoic acid; 7-MOA, 7-methyl octanoic acid; Nva: L-norvaline.

Colistin is the most frequently used polymyxin, it is commercially available as colistin sulfate, and is currently used orally for bowel decontamination or topically, as powder, for skin infections. It can also be administered parenterally, intrathecally, intraventricularly or by inhalation through its inactive prodrug, named colistimethate sodium (CMS) (Figure 20), which is produced by the reaction of colistin with formaldehyde and sodium hydrogensulfite. CMS is less toxic than the parent drug but also less potent because it lacks antibacterial activity and should be converted *in vivo* into colistin after its administration.<sup>155</sup> Polymyxin B is available for clinical use as polymyxin B sulfate, and it is used parenterally, topically (ophthalmic and otic instillation) or intrathecally.



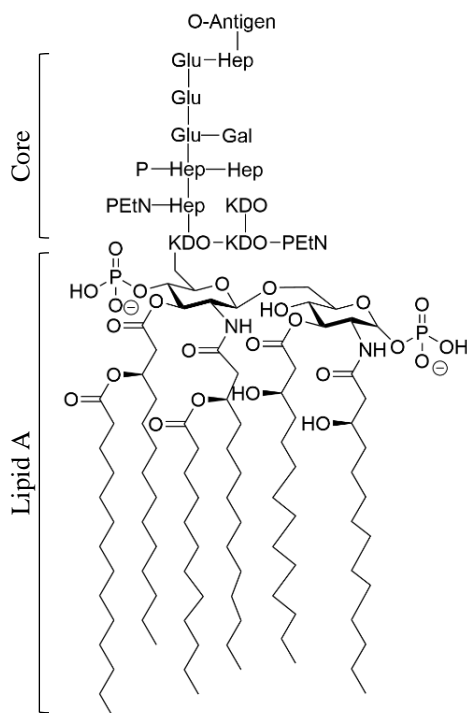
**Figure 20:** Structure of colistimethate sodium (CMS), the prodrug of colistin.

In contrast to human medicine, polymyxins have been used extensively in veterinary. For example, colistin is usually administered orally with complete feed, milk, or water to poultry and pigs to treat infections related to Enterobacteriaceae and to promote the animals' growth. This indiscriminate use has led to the appearance of polymyxin resistance in Asia<sup>156</sup> and other parts of the world and, as a result, the use of polymyxin in veterinary medicine is being re-evaluated and largely banned.<sup>157–159</sup>

#### 1.1.2.1. Mode of action

Polymyxins present a narrow antibacterial spectrum, due to their selective interaction with the LPS and phospholipids unique to the outer membrane of Gram-negative bacteria. LPS (Figure 21) is in turn composed of three structural domains: the hydrophobic lipid A, the hydrophilic core of polysaccharides, and the hydrophilic O-antigen polysaccharide side chain. Lipid A, which is the principal target of polymyxins, lies on the outer membrane of bacteria and is the responsible of its tightly packed structure due to the divalent calcium and magnesium cations that bridge adjacent LPS molecules. Meanwhile, the core and O-antigen polysaccharides extend outside the cell and are responsible of cell growth and bacterial resistance.<sup>160,161</sup>

Despite that it has been extensively reported that Gram-negative outer membrane is the primary target for polymyxins, the exact mode of action of this drug is still under discussion and there are several models proposed and reviewed in literature.<sup>148,160,162</sup>



**Figure 21:** Structure of *Escherichia coli* LPS. EtN, ethanolamine; Gal, D-galactose; Glu, D-glucose; Hep, L-glycero-D-manno-Heptose; KDO, 3-deoxy-D-manno-oct-2-ulonic acid; P, phosphate.

A widely accepted model is the ‘self-promoted uptake’<sup>54</sup> which postulates that the antimicrobial activity of polymyxins begins by the competitive displacement of divalent cations  $\text{Ca}^{2+}$  and  $\text{Mg}^{2+}$  and the subsequent electrostatic interaction between the positively charged polymyxin and the Lipid A phosphate groups, allowing the uptake of polymyxin and the upcoming insertion of its fatty acid tail and hydrophobic motif into the outer membrane. Such insertion weakens the packing of LPS and causes outer membrane expansion, which leads to the entrance of polymyxin to the periplasmic space. Subsequent interaction with the cytoplasmic membrane results in loss of the physical integrity of the phospholipid bilayer, leakage of intracellular contents, and bacterial cell death.<sup>163,164</sup>

The vesicle-vesicle contact pathway proposes that once in the periplasmic space, polymyxin creates contacts between the inner leaflet of the outer membrane and the outer leaflet of the cytoplasmic membrane, inducing a fast and selective phospholipid exchange between the two leaflets that modifies the overall phospholipid composition and potentially causes an osmotic imbalance that culminates in cell death.<sup>165,166</sup>

A third model suggest that polymyxin kills bacteria through oxidative stress and reactive oxygen species (ROS) generation. According to this model, polymyxin potentiate the

electron extraction from molecular oxygen, causing a dramatic rise of superoxide levels and stimulating the hydroxyl radical production.<sup>167,168</sup> These oxidated species adversely affect the activity of enzymes and the integrity of DNA, lipids, and proteins of the bacteria, thereby resulting in bacterial death.<sup>169</sup>

Additional models have been proposed, for example, there is evidence that polymyxins inhibit key respiratory enzymes present in inner bacterial membranes,<sup>170</sup> or alter the mechanical properties and morphology of the bacterial outer membrane, perturbing the normal cell division.<sup>171</sup>

In conclusion, in addition to the classical proposed mechanisms affecting bacterial membranes that cause the membrane lysis and subsequent cell death, there is substantial evidence of secondary pathways through which polymyxins could exert their antimicrobial action after cell permeabilization.

#### 1.1.2.2. Toxicity

The use of polymyxin, colistin and colistimethate has always been associated with reports of adverse renal and neurological effects in considerable number of patients,<sup>172,173</sup> for that reason, their clinical use declined in the 1970s. Nowadays, close monitoring of patients is mandatory to identify the optimal dose from both efficacy and toxicity perspectives, due to their narrow therapeutic window.

The major dose-limiting toxicological drawback of polymyxins is nephrotoxicity. Systemic use of polymyxin therapy is often associated with acute kidney injury (AKI), in fact, recent meta-analysis of 95 observational studies demonstrated that the overall nephrotoxicity rate in patients treated with polymyxins is 28.1 %.<sup>174</sup> Polymyxins nephrotoxicity is dose dependent, mostly reversible, and it is highly increased by the co-administration with other nephrotoxic drugs (vancomycin, aminoglycosides or anti-inflammatory drugs) and patient related factors (advanced age, pre-existing kidney diseases, hyper and hypoalbuminemia). Nephrotoxicity is associated with acute tubular necrosis in the kidneys provoked by the polymyxin reabsorption and accumulation in the tubular cells. This hypothesis was recently supported by a detailed study using Mass Spectroscopy Imaging (MSI), which revealed the preferential accumulation of polymyxin B and colistin in their non-metabolized form in the renal cortical region.<sup>175</sup>

On the other hand, the reported cases of neurotoxicity do not exceed 7 % and generally present mild symptoms<sup>174</sup> such as paraesthesia (commonly known as ‘pin and needles sensation’), ataxia, vertigo, confusion, seizures, visual and speech disturbances, partial deafness or neuromuscular blockade.<sup>176</sup>

The mechanism of polymyxin-induced toxicity has not been completely described, but structure-activity data suggest that toxicity is closely related with the presence of D-amino acids, the *N*-terminal fatty acid tail and charged Dab residues.<sup>162</sup>

#### 1.1.2.3. Resistance

Even though polymyxins are less prone to develop resistance than other antibacterial agents, due to the increase in their use in medicine and especially in agriculture and in livestock, bacterial resistance to polymyxins has recently emerged worldwide.<sup>156</sup> Furthermore, there are some Gram-negative bacterial species intrinsically resistant to polymyxins, including for example, *Neisseria meningitidis*, *Proteus mirabilis* or *Burkholderia* spp.<sup>96,177</sup>

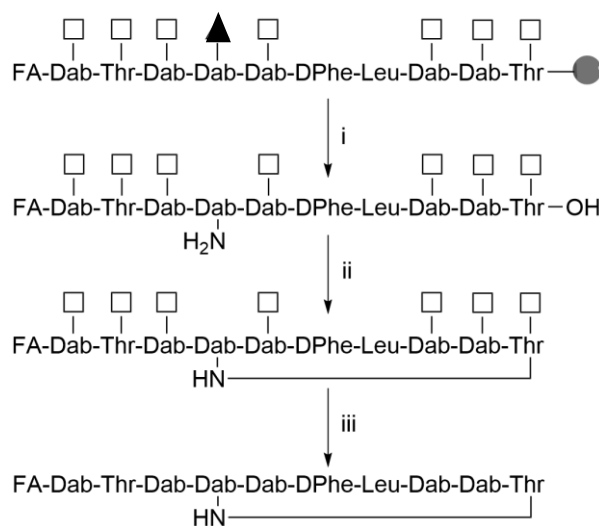
Briefly, polymyxin resistance in Gram-negative bacteria is primarily due to post-translational modifications of the phosphates of Lipid A with cationic groups such as 4-amino-4-deoxy-L-arabinose (L-Ara4N), phosphoethanolamine (pEtN) or galactosamine. With these modifications the net negative charge of the bacterial membrane is decreased and therefore, there is a reduction of polymyxin-LPS binding, thus avoiding the polymyxin uptake into the cell interior.<sup>178–180</sup> These chromosomal mutations are adaptive and regulated by environmental stimuli such as the drug presence. However, the first transmissible plasmid-mediated colistin resistance mechanism, caused by the novel pEtN transferase gen *mcr-1*, in Enterobacteriaceae was reported by Liu et al.<sup>181</sup> in 2016 and then, different isolates of Gram-negative bacteria with this acquired resistance have been found in livestock in the southeast of Asia, and some countries of Europe and America.<sup>160</sup> Worryingly, this resistance can be passed between different bacterial strains increasing the dissemination of polymyxin resistance.

#### 1.1.2.4. Synthetic preparation of polymyxins

The preparation of novel polymyxin analogues can be performed following two different techniques: semi-synthesis and total chemical synthesis. Semi-synthesis is used to create

polymyxin analogues with truncations or substitutions in the linear lipotriptide by the chemical or enzymatic manipulation of natural polymyxin product, usually obtained by fermentation procedures. Whereas total chemical synthesis involves the complete peptide assembly by the construction of peptide bonds, this methodology can be performed in solution or using solid phase peptide synthesis (SPPS).

The total chemical synthesis of polymyxin has always been challenging due to the presence of the macrolactam ring. The first total synthesis was achieved by Vogler et al.<sup>182</sup> in 1964 using a solution-phase condensation approach. Then, Sharma et al.<sup>183</sup> employed Fmoc/<sup>t</sup>Bu based SPPS where the 4-Dab was protected with Dde on Sasrin resin. The partially protected linear precursor was obtained after treatment with 2 % hydrazine and cleavage with 1 % TFA. The cyclization was performed in solution with diphenylphosphorylazide (DPPA), and then, the peptide was fully deprotected with 95 % TFA (Figure 22). Similarly, Tsubery et al.<sup>184</sup> used Mtt protecting group in the 4-Dab position, and afterwards, Sakura et al.<sup>185</sup> and Vaara et al.<sup>186</sup> reported polymyxin synthesis on Wang resin with Boc protection for 4-Dab and Bn-type protecting groups in the other residues. The partially protected peptide was obtained after TFA treatment, whereas the complete deprotection was obtained employing stronger acidic conditions.



**Figure 22:** Generalized scheme for polymyxin synthesis. From Sharma et al.<sup>183</sup> ● = Sasrin resin; ▲ = Dde protecting group; □ = Boc/<sup>t</sup>Bu protection; FA= fatty acid; i= 2 % hydrazine and 1 % TFA; ii= DPPA; iii= TFA/H<sub>2</sub>O (95:5). From Tsubery et al.<sup>184</sup> ● = 2-CTC resin; ▲ = Mtt protecting group; □ = Boc/<sup>t</sup>Bu protection; FA= fatty acid; i= 1 % TFA; ii= PyBOP; iii= TFA/H<sub>2</sub>O (95:5). From Sakura et al.<sup>185</sup> and Vaara et al.<sup>186</sup> ● = Wang resin; ▲ = Boc protecting group; □ = Z/Bn protection; FA= fatty acid; i= 95 % TFA; ii= PyBOP or DPPA; iii= HF or hydrogenation.

#### 1.1.2.5. Design of new polymyxins

Most of the above-mentioned antibiotics discovered during the ‘golden age’ have been replaced by their optimized versions. This is the case of drug derivatives such as penicillin G, chlortetracycline, streptomycin, or erythromycin. Nevertheless, there are still some antibiotics, such as polymyxins, that were discovered decades ago and remain in current use.

Considering the excellent activity displayed by polymyxins against Gram-negative bacteria, there have been several research initiatives to study their structure-activity relationship and develop new polymyxin analogues with improved microbiological, pharmacological, and toxicological profiles, an effort that has been going on for several decades.<sup>162</sup>

Strategies for polymyxin improvement have included modifications in the length and size of the *N*-terminal fatty acid chain, the net charge of the molecule, hydrophobicity, the size of peptide ring and the length of the *N*-terminal linear tripeptide.

##### *1.1.2.5.1. N-terminal fatty acid modifications*

*N*-terminal fatty acid is an indispensable component of polymyxins for antimicrobial activity because, as previously mentioned, it interacts with the hydrophobic fatty acid layer of the Lipid A, causing the permeation of the outer membrane of Gram-negative bacteria.

The importance of the *N*-terminal fatty acid first became evident when the polymyxin B nonapeptide (PBNP) was reported.<sup>187</sup> PBNP is the truncated version of polymyxin B which lacks the *N*-terminal fatty acid and the 1-L-Dab residue, and it displays a significantly reduced toxicity, but is also devoid of antimicrobial activity, suggesting that the activity and toxicity of polymyxins can partly be attributed to *N*-terminal fatty acid. Accordingly, many research efforts have focused in the generation of *N*-terminal analogues of the polymyxin molecule.<sup>188–190</sup> Collectively, these studies revealed that the antibacterial activity appears to be correlated to the length and bulkiness of the *N*-terminal substituent. As per the naturally occurring polymyxins, the ideal fatty acyl chain length appears to be C7 - C9. The introduction of shorter chains decreases the LPS-binding affinity, and longer chains reduce the antimicrobial activity potentially by steric

hinderance. However, the activity of *N*-terminal fatty acid analogues containing C9-C14 chains show more activity against resistant strains and Gram-positive bacteria, which is usually accompanied by a toxicity increase.

#### 1.1.2.5.2. *Hydrophobic motif*

The segment formed by the amino acids D-Phe<sup>6</sup>/D-Leu<sup>6</sup> and Leu<sup>7</sup> constitutes the second hydrophobic region of the polymyxin B and colistin molecules. Similarly to the *N*-terminal fatty acid, the lateral chains of these amino acids contribute to the polymyxin-LPS binding through their interactions with the fatty acid tails of the Lipid A.

In order to study the influence of the hydrophobic motif, the activity of different polymyxin analogues, which contained more polar amino acids, such as tyrosine, alanine or glycine, or inverse optical configuration at position 6 have been reported.<sup>185,191</sup> Both modifications resulted in almost complete loss of outer membrane permeabilization.

#### 1.1.2.5.3. *Dab residues*

Polymyxins are cationic peptides containing five positive charges at physiological pH, located in the amino groups of Dab residues. These charges enable the first contact of polymyxin and LPS through electrostatic interactions between the peptide and the phosphate groups of Lipid A, and they are also important for subsequent inner membrane interaction. They have been proven to be crucial for the antimicrobial activity, in fact, if the five lateral chains of Dab are blocked, for example with methanesulfonate groups, an inactive compound is obtained.<sup>192</sup>

Numerous synthetic modifications targeted at the Dab residues have been introduced in polymyxin analogues,<sup>185,186,193,194</sup> based on this studies, there is evidence that the key features of the Dab residues that affect polymyxin activity are: the positive net charge of the molecule, the length of the lateral chain and their specific order in the sequence, which confers the appropriate spatial distribution for the electrostatic interaction with the phosphate groups of Lipid A. In general, only the 1-Dab residue can be modified without a dramatic decrease in the antimicrobial activity.



#### 1.1.2.5.4. *Cyclic peptide ring size*

There are many biologically active peptides, natural or synthetic, that contain cyclic ring structures. This is the case of vancomycin, bacitracin, daptomycin or polymyxins among others. In this case, the structure of polymyxin comprises a lactam ring of 23 atoms formed between the  $\gamma$ -amino group of 4-Dab residue and the  $\alpha$ -carboxylic acid of 10-Thr. The polymyxin's cycle has been proven to present several advantages compared to its linear analogue, such as an increase in the rigidity, resistance to endopeptidases or better permeability across cell membranes.<sup>195,196</sup>

Some studies demonstrated that the 23-atom ring is precisely the size that provides the molecule with the best electrostatic and hydrophobic points of contact with the LPS. As an example, Tsubery et al.<sup>184,197</sup> synthesized a library of 6 analogues of the non-active polymyxin B nonapeptide wherein the size ring varied from 20 to 26 atoms and all of them shown less potency to sensitize bacteria to novobiocin (aminocoumarin antibiotic) than the native 23 atom ring.

#### 1.1.2.5.5. *Linear tripeptide*

The linear tripeptide segment (1-Dab–2-Thr–3-Dab) serves to bridge the heptapeptide ring to the *N*-terminal fatty acid, and it contributes with two positive charges towards the binding polymyxin-LPS. Several analogues which include amino acid deletions and substitutions into the tripeptide have been studied,<sup>185,186,189</sup> and finally, it was concluded that the linear tripeptide segment can only be truncated at position 1 with a negligible loss of antimicrobial activity. Regarding the substituted analogues, only conservative amino acid substitutions appear to be tolerated.

#### 1.1.2.6. State of the art in new polymyxins development

Over the last years, various academic groups and pharmaceutical and biotech companies have focused great efforts on the discovery of novel polymyxins devoid of nephrotoxicity, some of the most important reported analogues are shown in Table 5.

CB-182,184 was the first polymyxin analogue that reached Phase I clinical trials. It was originally developed by BioSource Pharm and then licensed to Cubist Pharmaceuticals (now Merck Pharmaceuticals). CB-182,184 is a polymyxin decapeptide derivative with an aryl urea substituent at the *N*-terminus. The analogue showed comparable activity to

natural polymyxins and reduced nephrotoxicity in monkey models during the preclinical studies,<sup>198</sup> but unfortunately, its development was discontinued in 2010, apparently due to non-published toxicity issues.

Later on, Pfizer reported their lead compound Pfizer 5x, which contains an *N*-phenyl pyridone at the *N*-terminal position, and the Dab residue at position 3 substituted by L-2,3-Diaminopropanoic acid (Dap).<sup>199</sup> Despite the fact that comparable or even two-fold lower MIC values than the natural polymyxins were obtained, the toxicological studies performed in rat and dog models showed that there was no significant safety improvement, and the compound was also discontinued.

Northern Antibiotics followed the positive net charge reduction strategy to obtain less nephrotoxic derivatives. NAB739, is a polymyxin B derivative which lacks the Dab residue at position 1 and has the third Dab replaced with D-Ser. It displayed good *in vitro* and *in vivo* activities against *Escherichia coli* but not against *Acinetobacter baumannii* and *Pseudomonas aeruginosa*.<sup>186,200</sup> On the other hand, the non-active but membrane sensitizing compound NAB741 was tested in Clinical Phase I by Spero Therapeutics named as SPR741,<sup>201</sup> but it was finally discontinued because Spero Therapeutics acquired other polymyxin analogue, SPR206, which presents a potency and safety profile superior to SPR741.

SPR206 (formerly CA1206) has recently reached Phase I trials.<sup>202,203</sup> It was originally developed by Cantab anti-infectives. This company also developed CA824, which lacked the Dab at position 1 and contained piperazine instead of the *N*-terminal fatty acid. The *in vitro* activity of this analogue was similar or slightly improved compared with polymyxin. CA824 progressed to *in vivo* efficacy experiments, and it proved to be superior to polymyxin B against *Acinetobacter baumannii* and *Pseudomonas aeruginosa*.<sup>204</sup>

The team at Monash Biomedicine Discovery Institute described a series of polymyxin analogues where positions 6 and 7 were replaced by more hydrophobic residues. The design of more hydrophobic analogues resulted in a substantial improvement of *in vitro* potency against resistant strains, this is the case of FADDI-002 (L-2-amino decanoic acid at position 7 and n-octanoyl *N*-terminus) and FADDI-003 (L-2-amino decanoic acid at position 7 and biphenyl acyl *N*-terminus)<sup>205</sup>. FADDI compounds are currently under

development by Qpex Biopharma. In fact, a promising new generation polymyxin agent designed by the team of Monash University, Qpx9003 has recently reach Phase I.<sup>206-208</sup>

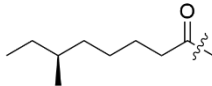
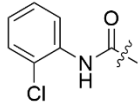
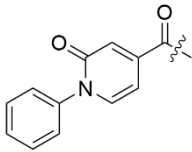
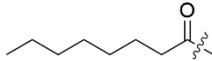
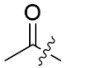
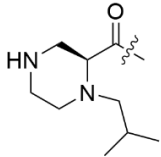
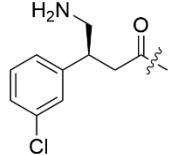
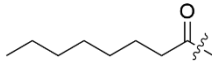
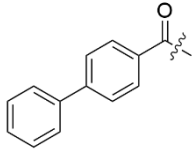
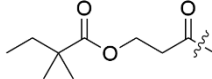
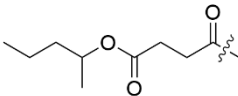
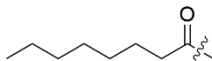
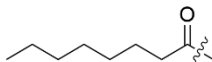
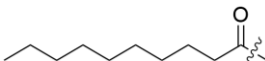
MicuRx reported analogues that incorporate ester, carbamate and phosphate/phosphonate/ phosphoramidate bonds within the *N*-terminal part of polymyxin, aiming to reduce the toxicity by introducing fewer stable bonds in the peptidic structure. MicuRx 12 and 18 analogues showed comparable *in vitro* activity and *in vivo* efficacy than polymyxin and lower nephrotoxicity in rat models.<sup>209</sup> Nowadays, MicuRx is conducting Phase I clinical trials on compound MRX-8.<sup>210,211</sup>

The group at the Institute for Molecular Bioscience at the University of Queensland detailed the synthesis and *in vitro* screening of several compounds focused on the reduction of nephrotoxicity and structure-activity relationship studies.<sup>212</sup>

Finally, our group designed and synthesized polymyxin analogues where the amide bond between the  $\gamma$ -amino group of 4-Dab residue and the  $\alpha$ -carboxylic acid of 10-Thr was replaced by a disulphide bond between two Cys residues.<sup>213</sup> This modification was inspired in the natural occurring ranalexin, an antimicrobial peptide from bullfrog skin which is closely related to polymyxin and contains a disulphide linkage in its sequence.<sup>214</sup> Rustici et al.<sup>215</sup> introduced this modification into polymyxin backbone and the effective binding between the polymyxin derivatives and LPS was demonstrated, but the analogues were devoid of antibiotic activity.

In order to perform an isosteric replacement and maintain the appropriate configuration of the  $\alpha$ -carbon; L-Cys was placed at position 4 and D-Cys at 10. The disulphide bond potentially confers enough stability to the molecule to readily display its antimicrobial action but after an eventual accumulation in the kidneys, it could be broken as a consequence of the reductant intracellular environment (reduced glutathione and oxidoreductases), thus opening the cycle, facilitating the proteolytic degradation of the molecule, and reducing the polymyxin associated toxicity. The disulphide analogues previously synthesized in our group displayed comparable activity to polymyxin, and an *in vivo* acute toxicity test showed that LD<sub>50</sub> of analogue 39 was clearly superior (283 mg·kg<sup>-1</sup>) to that reported for polymyxin B (59.5 mg·kg<sup>-1</sup>). New results about these analogues are presented in the present thesis.

**Table 5:** Relevant polymyxin analogues under development. Cyclic ring indicated with brackets.

Compound	<i>N</i> -terminal fatty acid	Amino acid sequence
PxB <sub>1</sub>		-Dab-Thr-Dab-[Dab-Dab-DPhe-Leu-Dab-Dab-Thr]
CB-182,804		-Dab-Thr-Dab-[Dab-Dab-DPhe-Leu-Dab-Dab-Thr]
Pfizer 5x		-Dab-Thr-Dap-[Dab-Dab-DPhe-Leu-Dab-Dab-Thr]
NAB739		-Thr-DSer-[Dab-Dab-DPhe-Leu-Dab-Dab-Thr]
SPR741 (NAB741)		-Thr-DSer-[Dab-Dab-DPhe-Leu-Dab-Dab-Thr]
CA824		-Thr-Dab-[Dab-Dab-DPhe-Leu-Dab-Dab-Thr]
SPR206 (CA1206)		-Thr-Dap-[Dab-Dab-DPhe-Leu-Dab-Dab-Thr]
FADDI-002		-Dab-Thr-Dab-[Dab-Dab-DPhe-Adec-Dab-Dab-Thr]
FADDI-003		-Dab-Thr-Dab-[Dab-Dab-DPhe-Adec-Dab-Dab-Thr]
MicuRx-12		-Dab-Thr-Dab-[Dab-Dab-DPhe-Leu-Dab-Dab-Thr]
MicuRx-18		-Dab-Thr-Dab-[Dab-Dab-DPhe-Leu-Dab-Dab-Thr]
Queensland-38		-Dab-Thr-Gly-[Dab-Dab-DPhe-Leu-Dab-Dab-Thr]
Barcelona-38		-Dab-Thr-Dab-[Cys-Dab-DPhe-NLe-Dab-Dab-DCys]
Barcelona-39		-Dab-Thr-Dab-[Cys-Dab-DPhe-NLe-Dab-Dab-DCys]

### 1.1.3. General considerations about the techniques employed in this chapter

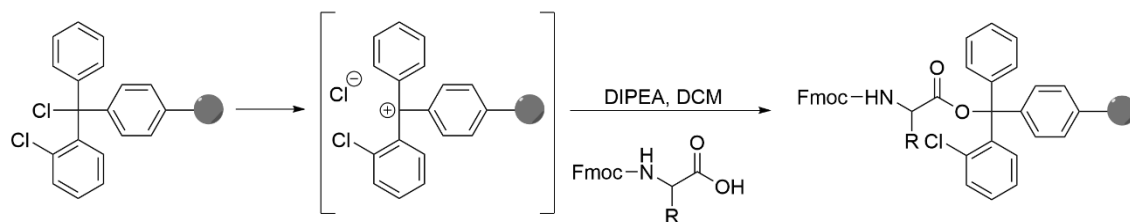
Throughout this chapter, various techniques will be sequentially mentioned. For clarity, the basics of each are briefly presented below and further detailed information can be found in the experimental section 3.1.2.

#### 1.1.3.1. Solid phase peptide synthesis

The synthesis of all analogues was conducted manually by conventional solid-phase chemistry applying the most suitable conditions depending on the peptide characteristics.

##### 1.1.3.1.1. Solid supports

The elongation of the target molecules was performed in three different resins, being 2-chlorotrityl chloride (2-CTC) the most suitable resin for the synthesis of peptides that contain the C-terminus as free carboxylic acid functionality. The starting point of the synthesis with this polymeric support consist of the addition of the desired Fmoc-protected amino acid by standard means though a nucleophilic attack ( $S_N1$  reaction) of the carboxylate form of the amino acid to form an ester (Figure 23).

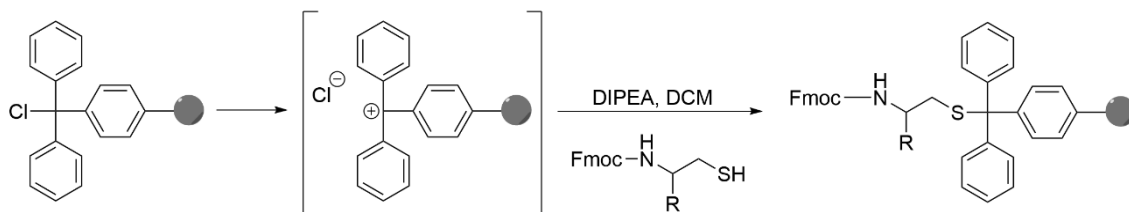


**Figure 23:** Coupling of the first amino acid onto 2-CTC resin.

The optimal loading of this resin for common peptides range from  $0.5 - 1 \text{ mmol} \cdot \text{g}^{-1}$ , for that purpose the reaction was performed overnight using 1 or 1.2 equivalents of amino acid and 4-fold molar excess of the non-nucleophile base *N,N'*-diisopropylethylamine (DIPEA). The real substitution level was determined by Fmoc UV quantification at  $\lambda = 301 \text{ nm}$  and then, the resin was treated for additional 30 minutes with an excess of MeOH, to link a small nucleophile to the unreacted positions of the resin.

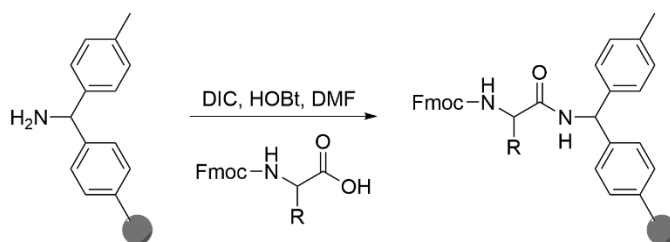
The 2-chlorotrityl chloride resin and trityl chloride resin (Trt-Cl) were also used in section B to attach the thiol functionality of an amino acid derivative forming a thioether bond (Figure 24). In this case, a molar excess of 2 equivalents of amino acid and 4 equivalents of DIPEA were used in dichloromethane, and the nucleophilic substitution was also led

to react overnight. The loading of the first amino acid was determined by Fmoc absorbance after deprotection with 20 % piperidine in DMF. Finally, resin was capped with MeOH.



**Figure 24:** Coupling of the first amino acid onto Trt-Cl resin.

Finally, peptides containing C-terminal carboxamide form were synthesized onto a 4-methylbenzhydrylamine resin (MBHA) (Figure 25), which was generally functionalized with Fmoc-Rink linker in order to enhance the acid lability of the resin. Amino acids were coupled onto MBHA resin using standard amide forming conditions such as DIC/HOBt, with 3-fold molar excess of each reagent in DMF for 1 hour. Full residue incorporation was ensured by Kaiser test.



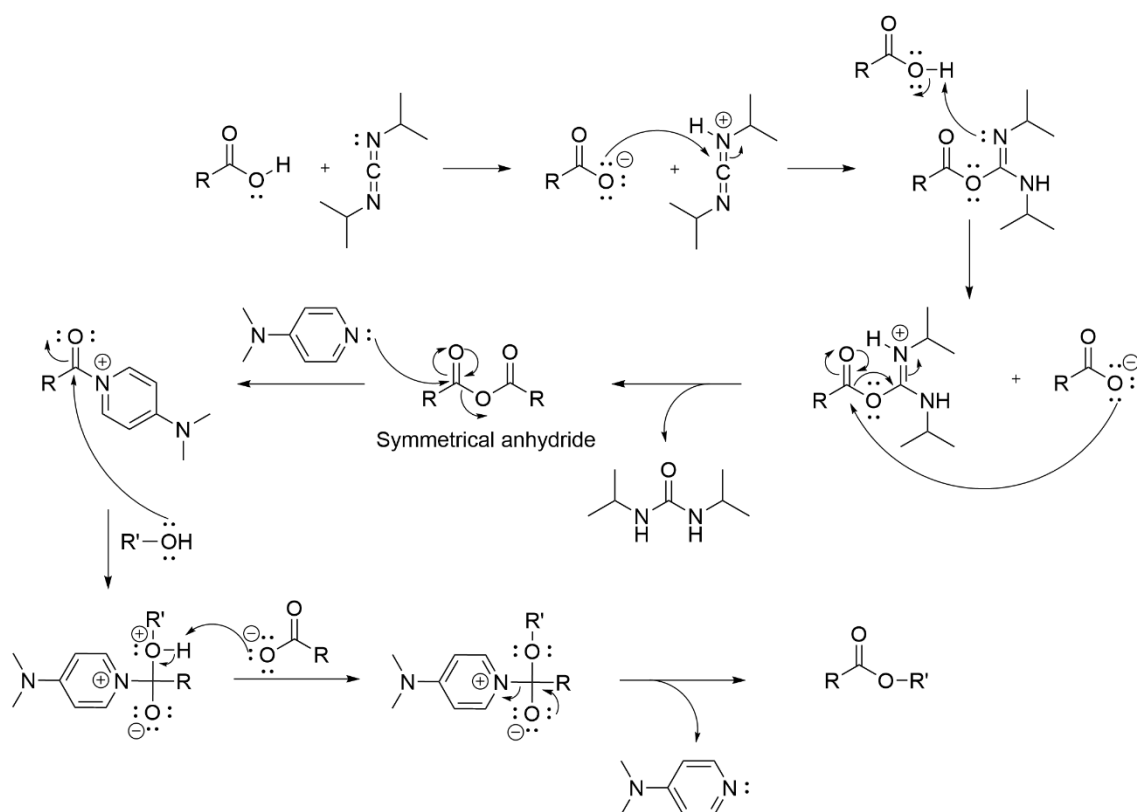
**Figure 25:** Coupling of the first amino acid onto MBHA resin.

#### 1.1.3.1.2. Chain elongation

The peptide chain elongation consisted of coupling and deprotection repetitive cycles using Fmoc/<sup>t</sup>Bu or Fmoc/Bn protection strategies. Couplings were generally carried out using the AA-DIC-HOBt (3:3:3 eq.) system in DMF for 1 hour. If the coupling was not complete, 1.5 eq. of the reagents were added for 30 additional minutes. Additional coupling systems such as AA-HATU-HOAt-DIEA (3:3:3:6 eq.) or AA-DIC-K-Oxyma (3:3:3 eq.) were used upon mild and neutral conditions, hence preventing the premature release of peptide chains in highly acid labile resins.

The Steglich esterification or carbodiimide/4-Dimethylaminopyridine (DMAP) coupling method<sup>216</sup> was used for depsipeptide synthesis. The amino acid was activated with

diisopropylcarbodiimide, via the symmetrical anhydride formation mechanism (AA/DIC ratio 2:1) (Figure 26). Then, the activated specie reacts with the free alcohol in presence of catalytic DMAP. It should be noted that the free alcohol had been previously introduced in the growing peptide chain using AA-DIC-HOBt (2:2:4 eq.) system, containing a large excess of HOBt order to prevent the polymerization of the alcohol containing moiety.



**Figure 26:** Steglich esterification mechanism.

#### 1.1.3.1.3. Solid-phase reaction monitoring

The Kaiser test was performed to monitor coupling completion, it consists of a colorimetric test that enables the qualitative detection of primary amines. Briefly, when ninhydrin reacts with the  $\alpha$ -amino group of primary amino acids produces 'Ruhemann's purple' which indicates that the coupling reaction is not completed.

Additionally, difficult steps during the synthesis of the target compounds were monitored by acidolytic cleavage of a small aliquot of the peptidyl resin using. The sample was then subjected to HPLC and ESI-MS analysis.

#### 1.1.3.1.4. *Cleavage*

Cleavage and full or partial deprotection of the lateral chains were carried out using different acidic mixtures depending on the synthesis strategy. Basically, chlorotriptyl-based resins are easily removed under very mild conditions such as 25 % of HFIP or 1 - 2 % of TFA, whereas Rink amide MBHA resin requires longer treatments of 95 % of TFA and even more acidic conditions such as HF or hydrogenolysis treatments are necessary to cleave peptides directly attached to MBHA resins.

Once the acidic treatment was performed, the peptides were precipitated with cold diethyl ether or water.

#### 1.1.3.1.5. *Purification*

All peptides were purified using a RP-HPLC equipment and conventional gradients of acetonitrile–water–trifluoroacetic acid. The crude purity was assessed by analytical RP-HPLC and collected samples with purity >95 % were lyophilized.

#### 1.1.3.1.6. *Counter ion Exchange*

After cleavage and purification with TFA-containing mixtures, residual acid remains in the peptide preparation in anionic form, and therefore, the cationic peptides are generally obtained as TFA salts. These counter ions can affect both biological and physico-chemical properties of the peptides,<sup>217-219</sup> For instance, according to Johansson et al.,<sup>220</sup> the secondary structure of a peptide is closely related with the different counter ion composition, and Pini and et al.,<sup>221</sup> reported substantial differences in toxicity signs presented by mice after the administration of peptide M33 as TFA or acetate salt.

All of our analogues were obtained as chloride salt by repetitive cycles of lyophilization of the peptide in the presence of an excess of the desired acid.

#### 1.1.3.2. Antimicrobial activity assays

To evaluate the *in vitro* antimicrobial activity of all polymyxin analogues synthesized during the present thesis, their minimum inhibitory concentration (MIC) was determined using three different Gram-negative and one Gram-positive bacterial ATCC strains recommended for antibiotic susceptibility testing. These bacteria were chosen considering the guidelines for the research and development of new therapeutic agents



published by the WHO.<sup>27</sup> All of them also belong to the most alarming species highlighted by IDSA (the ESKAPE pathogens).<sup>27</sup>

The microorganisms used were the following:

- *Pseudomonas aeruginosa* is a Gram-negative aerobic rod-shaped bacterium belonging to the bacterial family Pseudomonadaceae. This bacterium is commonly found in soil and water, and it can cause pneumonia, bacteremia, dermatitis, urinary tract infections, bone and joint infections, gastrointestinal infections, and a variety of systemic infections. *Pseudomonas aeruginosa* is commonly referred as an opportunistic pathogen since it particularly affects patients with severe burns, organ transplants, or cancer and AIDS patients who are immunosuppressed.
- *Escherichia coli* is a Gram-negative rod-shaped bacterium belonging to the Enterobacteriaceae family, which is mainly found in the digestive tracts of humans and animals and benefit their hosts by producing vitamin K and preventing colonization of the intestine with pathogenic bacteria. Otherwise, some *Escherichia coli* strains can cause bloody diarrhea, severe anemia, or kidney failure as well as urinary tract infections. The transmission of these hazardous strains to humans is related with the consumption of contaminated foods, such as raw or undercooked products.
- *Acinetobacter baumannii* is an aerobic, rod-shaped, Gram-negative bacterium of the Moraxellaceae family. It is commonly found in soil and water, and moreover, it has the ability to survive for long periods on surfaces and equipment, for that reason it is considered an opportunistic pathogen which is one of the major causes of nosocomial infections in healthcare system. *Acinetobacter baumannii* can cause infections in the blood, urinary tract, wounds, and lungs, and is associated with high mortality.
- *Staphylococcus aureus* is a facultative anaerobe, round-shaped Gram-positive bacteria. It is commonly found on the skin and hair as well as in the noses and throats of people and animals. This bacterium can produce a wide range of diseases, ranging from skin infections, such as dermatitis or folliculitis, until

disease life-threatening illnesses, such as osteomyelitis, meningitis, sepsis, endocarditis, or pneumonia. Along with *Acinetobacter baumannii* it is currently one of the main causes of nosocomial infections.

The MIC assay, which is further detailed in experimental section 3.1.2.3., was based on the method reported by Wiegand et al.<sup>222</sup> Briefly, it consisted of serial two-fold dilutions of peptide which were inoculated with a standardized number of microorganisms and incubated at 37°C for the prescribed time. The MIC of our analogues against the different bacterial strains was considered to be the lowest concentration inhibiting bacterial growth.

#### 1.1.3.3. Hemolysis assay

Cationic lipopeptides are often highly toxic because they display a non-selective detergent membrane-lytic effect. Drug candidates must be selective for prokaryotic membranes, and therefore, in drug development it is crucial to verify the ability of the compounds to damage eukaryotic cell membranes. In that context, an *in vitro* hemolysis assay was performed to evaluate the hemoglobin released in the plasma after drug exposure, thus indicating the red blood cell lysis. Hemolysis of our peptides was examined using blood from a healthy rabbit as it is explained in experimental section 3.1.2.4. Briefly, the protocol consists in a dilution series of peptide with a standard number of erythrocytes, which was incubated for 1 hour at 37 °C. The degree of hemolysis is then measured by separating the plasma from the red blood cells and analyzing the amount of cell-free hemoglobin using a spectrophotometer.

#### 1.1.3.4. Transmission electron microscopy

Transmission electron microscopy (TEM) imaging is a microscopy technique in which the interaction between a high-energy electron beam and a solid sample forms an image that is magnified and focused onto an image device. This allows the investigation of sample morphology down to nanometric scale.

Applied to the antibacterial development field, TEM is used to visualize ultrastructural damage produced by a drug on a cell membrane, and therefore it helps to identify potential drug targets and clarify the mechanism of cell death. For that purpose, antimicrobials are incubated with a standardized number of bacteria during the prescribed time. Prepared

samples are fixed and embedded on epoxy resin and finally examined in an electron microscope.

#### 1.1.3.5. Biophysical studies

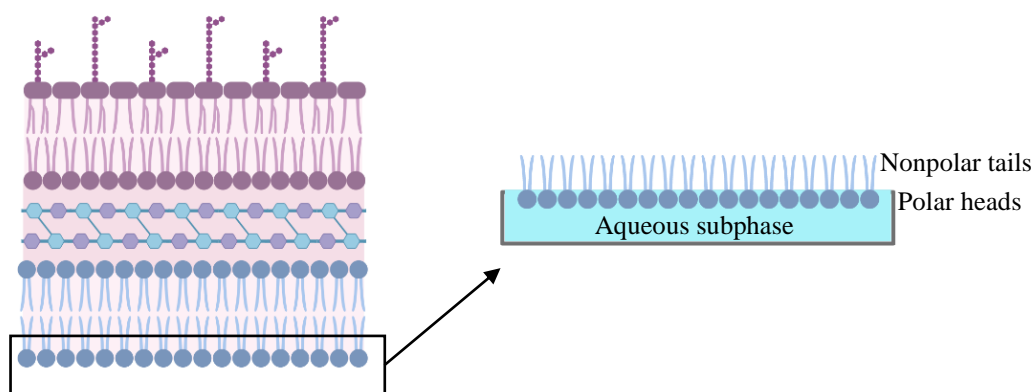
The mechanism of action of polymyxin and its analogues was studied in the present thesis using well-established model membranes such as monolayers and liposomes. The composition of such models was chosen based on the reported membrane composition of the different biological membranes.<sup>223</sup> In general, cytoplasmic membranes of Gram-positive bacteria are mostly composed by anionic lipids, such as phosphatidylglycerol (PG), whereas Gram-negative bacteria generally have a high content of the zwitterionic lipid phosphatidylethanolamine (PE) in addition to variable proportions of anionic lipids. In order to mimic both membrane types, pure POPG was used as a model of cytoplasmic membranes of Gram-positive bacteria, and POPE/POPG (6:4) mixture, to mimic Gram-negative membranes. Finally, given that the main component of the cytoplasmic membranes of eukaryotic cells is the zwitterionic phosphatidylcholine, POPC was used to model the eukaryotic membrane. All the phospholipids used in our membrane models are synthetic and contain well defined fatty acids. In many reports, a second model of Gram-positive inner membrane is used, to take into account the presence of positively charged molecules that can be important for the interaction with the polycationic antimicrobial peptides. For that purpose, POPG/DOTAP (8:2) vesicles were used as a new model of Gram-positive cytoplasmic membranes, due to the presence of positively charged lysyl-PG lipids on some Gram-positive bacteria such as *Staphylococcus aureus*.<sup>224</sup> Lysyl-PG is PG derivative which contains a lysine residue bonded to the PG headgroup, thus conferring an overall positive charge to the lipid. It usually presents low stability, and for that reason, it is often replaced by the more stable and affordable lipid, DOTAP, which is also positively charged.<sup>225,226</sup>

Phospholipids are vital to living cells, since they are the main components of the cell membrane, a structure that must be at the same time flexible and selectively permeable. For that purpose, the majority of phospholipids found in cell membranes are asymmetrical concerning their fatty acyl chains and contain one saturated and one unsaturated chain. In our case, there chains are a palmitoyl (saturated 16:0) and an oleoyl (unsaturated 18:1).

Finally, as mimic of the outer layer of the outer membrane of Gram-negatives, we used commercial LPS of *Salmonella enterica* serotype Minnesota Re 595 (Re mutant), therefore modelling the outer membrane of Gram-negative bacteria. The structure of the lipids is shown in detail in Appendix VIII.

#### 1.1.3.5.1. Monolayers as model membranes

Langmuir monolayers are considered one of the simplest models of biomembranes to study the specific interactions produced between lipids and peptides, as they represent half of a cellular membrane. They consist of single molecular layer formed by amphipathic phospholipids extended through the air/liquid interface of a polar solvent, generally water (Figure 27).<sup>227</sup> The main advantage of this model compared to other more complex systems such as lipid bilayers, lays on the possibility of controlling the order of the molecules, the molecular area or the surface pressure of the monolayer.

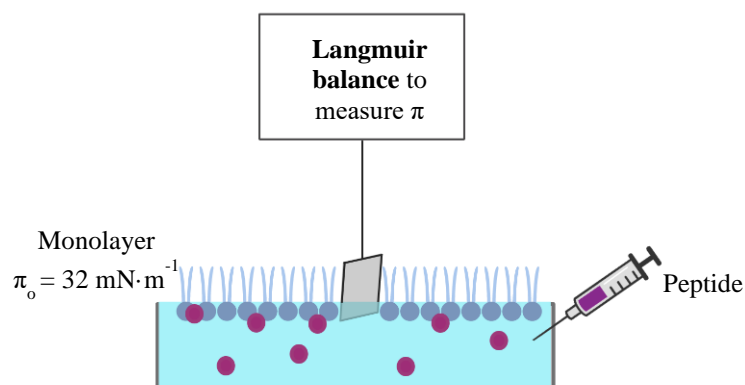


**Figure 27:** Graphic representation of a monolayer as a model of cytoplasmic membrane of Gram-negative bacteria.

To characterize the interaction between our analogues and monolayers, kinetics of penetration at constant area were carried out. The technique is based in the measure of the surface pressure by the Wilhemy method, first described in 1863,<sup>228</sup> which consists of the partial introduction of a platinum plate (Wilhemy plate) in the aqueous subphase, linked to an electrobalance that measures the force that the liquid exerts on the plate (Figure 28).

This assay consist of the preparation of monolayers of different composition stabilized at  $32 \text{ mN}\cdot\text{m}^{-1}$ , a surface pressure that is considered equivalent to the natural bacterial membranes.<sup>229</sup> Peptides are then injected into the subphase, and the peptide-membrane

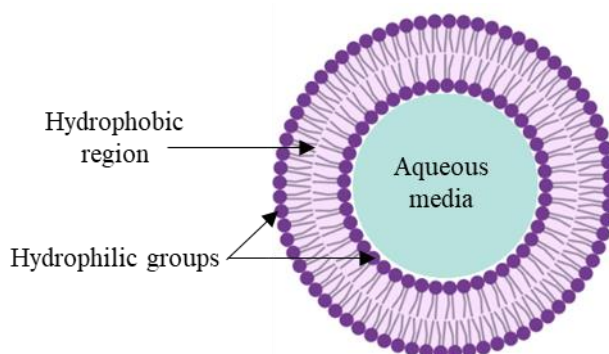
binding is followed by the increase in surface pressure ( $\Delta\Pi$ ) as a function of time. Detailed information about this technique can be found in experimental section 3.1.2.6.1.



**Figure 28:** General scheme of the procedure for the measurement of the interaction between peptides and lipid monolayers at constant area.

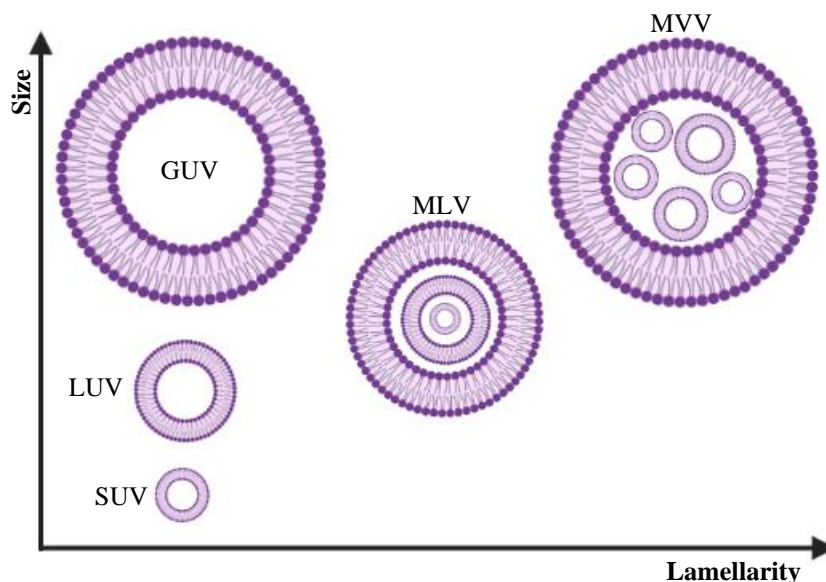
#### 1.1.3.5.2. Liposomes as model membranes

Liposomes are composed of amphipathic phospholipids that self-organize spontaneously in contact with water, forming spherical bilayers where the polar part remains exposed to the aqueous media, whereas the hydrophobic region is located in the interior, avoiding the contact with the aqueous media (Figure 29). Liposomes had been firstly described by Bangham et al. in 1964,<sup>230</sup> and nowadays they have become an important tool in biophysical, pharmaceutical and medical research. Their main biophysical application is as model membranes, due to their similarity with cellular membranes.<sup>231</sup> Additionally, because of their ability to compartmentalize their aqueous environment from the external environment, they are currently being used as drug delivery systems to introduce different agents into the cells and to potentially reduce the toxicity of the encapsulated drugs.<sup>232</sup>



**Figure 29:** Transversal section of a liposome.

The liposome size can vary from 0.025  $\mu\text{m}$  to 2.5  $\mu\text{m}$ . Moreover, liposomes may have one or multiple bilayer membranes. On the basis of their size and number of bilayers, liposomes can be classified as shown in Figure 30.<sup>233,234</sup>



**Figure 30:** Liposome classification according to their size and lamellarity. Unilamellar vesicles: Giant unilamellar vesicles (GUVs):  $>1 \mu\text{m}$ ; Large unilamellar vesicles (LUVs): 100 nm - 1  $\mu\text{m}$ ; Small unilamellar vesicles (SUVs): 20 - 100 nm. Multilamellar vesicles (MLVs):  $>500 \text{ nm}$ . Multivesicular vesicles (MVVs):  $>1 \mu\text{m}$ .

Liposomes can be prepared using different methodologies such as sonication, extrusion, freeze-thaw cycling or reverse phase evaporation among others.<sup>234</sup> All these methods are based on the spontaneous self-organization of the lipids in bilayers upon contact with aqueous media. The correct choice of liposome preparation method depends on diverse parameters, such as the desired liposome size, the nature of the medium in which the lipid vesicles are dispersed or the batch-to-batch reproducibility. In our case, the liposomes used in this chapter were SUVs or LUVs obtained by extrusion.

There are several spectroscopical techniques where liposomes can be used to discriminate between the different mechanistic possibilities that an antimicrobial peptide can exert on biological membranes (Table 6). In the present thesis, light scattering, fluorescent resonance energy transfer (FRET), ANTS-DPX leakage, pyrene fluorescence and depolarization experiments were performed on the polymyxin analogues to further investigate their mechanism of action.

**Table 6:** Summary of the most used biophysical techniques based on UV-visible and fluorescence spectrometry to investigate the mechanism of action of drugs on the lipid membrane.

Process	Scheme	Biophysical technique
<b>Aggregation:</b> - No lipid mixing - No permeabilization		- Light scattering - FRET (NBD - Rh)
<b>Liposome mixing</b> - Selective exchange of certain phospholipids - No permeabilization - No flip-flop		- FRET (NBD - Rh) - Pyrene fluorescence
<b>Hemifusion</b> - Exchange of external monolayers - No permeabilization		- FRET (NBD - Rh) - ANTS/DPX leakage
<b>Fusion</b> - Full mixing of layers - With or without permeabilization		- FRET (NBD - Rh) - ANTS/DPX leakage
<b>Lysis</b> - Detergent effect - Permeabilization		- Light scattering - ANTS/DPX leakage - NBD/Dithionite - Confocal microscopy
<b>Channel formation</b> - Permeabilization - No aggregation - No lipid mixing		- ANTS/DPX leakage - Confocal microscopy - Membrane depolarization
<b>Flip-Flop</b> - Transmembrane movement of lipids - No permeabilization - No fusion		- NBD/Dithionite
<b>Translocation</b> - No permeabilization - No lysis - No flip-flop		- Fluorescence confocal microscopy

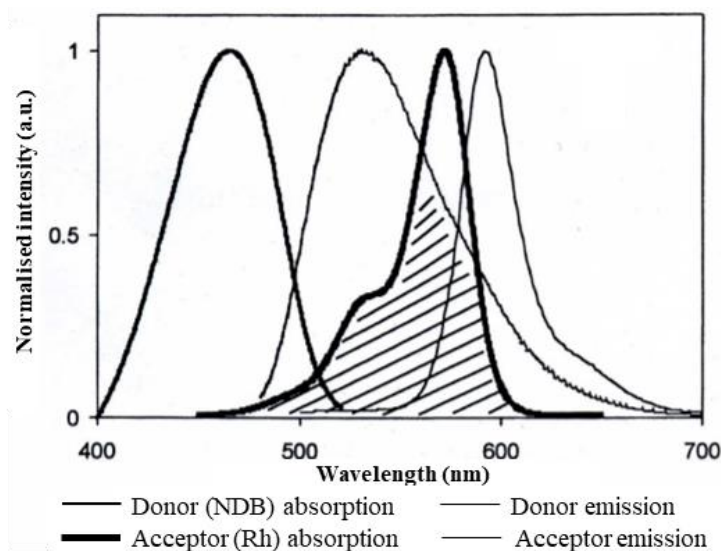
● Peptide

## 1.1.3.5.2.1. Light scattering

Peptide-induced aggregation of liposomes can be studied by monitoring changes in turbidity as a function of time. Recording the changes in 90° angle light scattering, an increase in light dispersion would be a clear indicator that there was an increase in particle size and consequently that the vesicle aggregation has taken place. On the other hand, if there was a lytic effect, a decrease in turbidity would be produced due to the destruction of the vesicles and formation of smaller sized particles, generally micelles.

## 1.1.3.5.2.2. Fluorescence resonance energy transfer

This method is based on the non-radiative transfer of the excited state energy from 7-nitrobenz-2-oxa-1,3-diazol-4-yl (NBD) as a donor fluorophore to the rhodamine (Rh) acceptor molecule, which in turn emits a fluorescent photon. The necessary condition for energy transfer to take place is that the emission spectrum of the donor molecules overlaps the absorption spectrum of the acceptor, as it is shown in Figure 31. The extent of energy transfer depends mainly on the distance between the two molecules,<sup>235</sup> the Förster distance, which represents the molecular separation at which energy transfer is 50 % efficient, and is usually limited to only a few nanometers; in the case of NBD-Rh pair, the Förster distance is of 5 nm.<sup>236</sup>

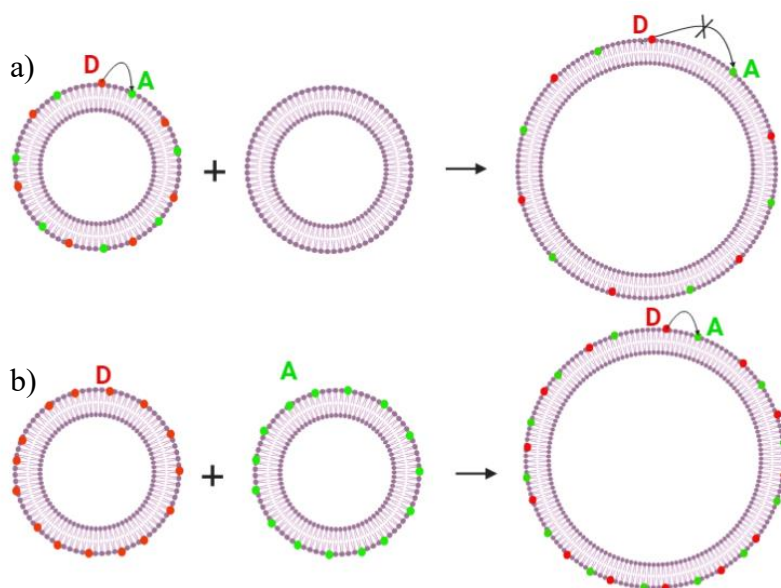


**Figure 31:** Excitation and emission spectra of NBD-PE and Rh-PE. Adapted from Baptista et al.<sup>237</sup>

FRET phenomenon finds significant application in membrane fusion assays when liposomes are labeled with lipid probes. In this chapter, two different experiments based on NBD-rhodamine energy transfer were performed (Figure 32):



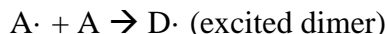
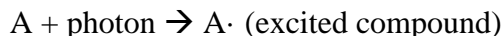
- A) Using vesicles containing both classes of chromophores at 0.3 mol% each, as both dyes are closely located on the liposome bilayer, FRET takes place, and exciting the NBD donor molecule, emission of fluorescence from Rh acceptor molecule can be observed. Thus, if an excess of dye-free vesicles is added and fusion between the two LUVs classes occur, donor and acceptor molecules will be surface diluted in such a way that no significant FRET will occur, because the distance will be clearly higher than the Förster distance of this pair. This event will be measured as a decrease in the fluorescence emission from Rhodamine as a function of time.
- B) Monitoring the changes in FRET between two populations of vesicles, one containing 0.6 mol% of the donor fluorophore NBD, and another with 0.6 mol% of the acceptor molecule, Rh. In the event of aggregation, hemi-fusion or fusion, the two probes will come at a close distance and FRET will take place, resulting in an increase in the fluorescence emission from Rh.



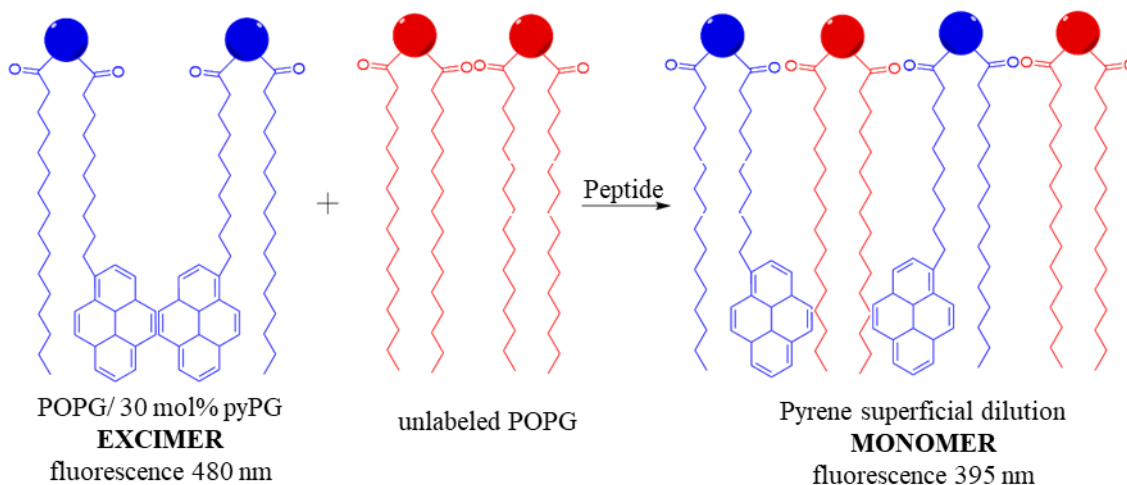
**Figure 32:** Schematic representation of FRET experiments: a) fusion between vesicles containing the two fluorophores: donor (D) and acceptor (A) 0.3 mol% each and blank vesicles; b) fusion between vesicles containing the 0.6 mol% donor (D) with a second type of vesicles containing 0.6 mol% of acceptor (A).

#### 1.1.3.5.2.3. Pyrene fluorescence emission to determine lipid mixing

Pyrene is a fluorescent dye that can form excited state dimers (excimers) upon close encounter of an excited state molecule with another ground state molecule. Monomer and excimer forms of pyrene have separated fluorescence emission spectra.



In addition to FRET experiments described previously, pyrene fluorescence can be used to monitor lipid mixing providing complementary information. In brief, locally concentrated pyrene-labeled (py) vesicles have a broad emission band centered at 480 to 500 nm, due to formation of excimers. In a mixture of pyrene-labelled vesicles with excess unlabeled ones with the same lipid composition, peptide-induced lipid mixing will result in a surface dilution of the pyrene fluorophore, with an increase in monomer emission and a concomitant decrease in excimer fluorescence (Figure 33). Monomeric pyrene spectrum is composed of vibronic bands around 370 - 400 nm. Therefore, lipid mixing can be easily monitored following the intensity increase of the monomer band at 395 nm.



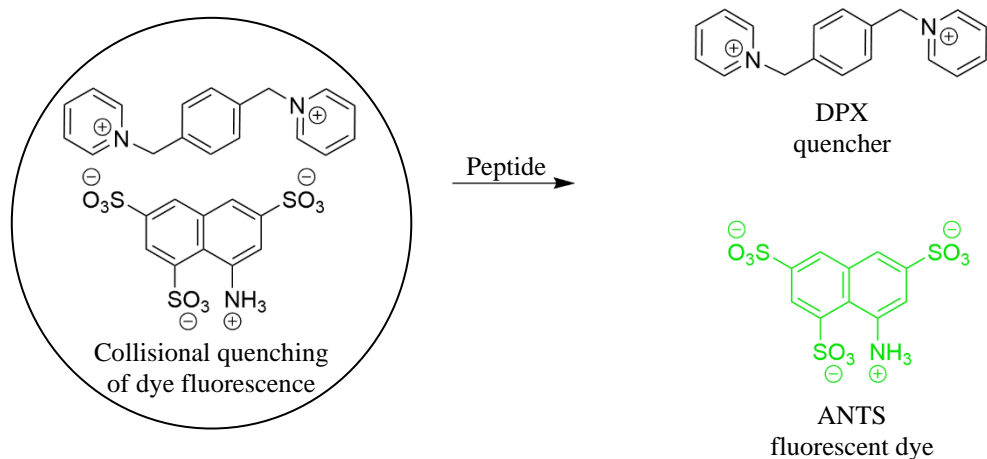
**Figure 33:** Schematic representation of lipid-mixing assay based on pyrene fluorescence.

#### 1.1.3.5.2.4. Leakage of aqueous contents

Many antimicrobial peptides induce the bacterial death due to pore formation, leaky fusion induction, or even due to a detergent effect. In order to study these mechanisms of action, the leakage of aqueous contents from liposomes can be studied.

Leakage assay is based on the collisional quenching of ANTS fluorescence by the fluorescence quencher DPX, both initially co-encapsulated in liposomes. If the peptides

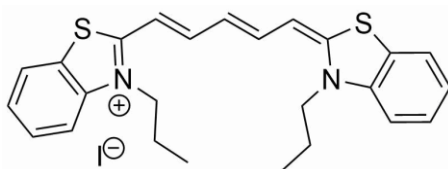
permeabilized the membrane, liposome contents would be released into the media and the induced leakage could be monitored by the ANTS-fluorescence increase, because the low DPX concentration leaked into the medium would not be effective in quenching ANTS any longer (see Figure 34).



**Figure 34:** Schematic representation of the ANTS/DPX leakage assay.

#### 1.1.3.5.2.5. Bacterial cytoplasmic membrane depolarization assay

The ability of our analogues to permeabilize the cytoplasmic membrane of viable bacteria as a function of time was assessed with the membrane potential-sensitive fluorescent probe, 3,3-dipropylthiadicarbocyanine iodide (diSC<sub>3</sub>(5)) (Figure 35).



**Figure 35:** Chemical structure of diSC<sub>3</sub>(5).

This cyanine dye has been shown to exhibit large fluorescent alterations in response to changes in membrane potential when it is added at relatively low concentrations to cell suspensions.<sup>238</sup> DiSC<sub>3</sub>(5) is a cationic fluorescent dye, which can penetrate lipid bilayers and accumulate in polarized cells. The strong accumulation in energized cells results in quenching of the overall fluorescence.<sup>239,240</sup> Upon depolarization, the dye is rapidly released to the media, which is reflected as an increase in fluorescence. Hence, control cells produce a low fluorescent signal, while peptide-mediated depolarization of cells result in high fluorescence.

## 1.2. Objectives of chapter 1

The main objectives of this chapter were the following:

- Development of an efficient novel cleavage reagent for the removal of Bn-type protecting groups that enables the total synthesis of the natural polymyxin B<sub>3</sub> following a Fmoc/Bn protection strategy and using a more accessible condition than those previously reported in literature (hydrogenolysis and anhydrous HF treatments). Application of this methodology to synthesize other relevant C-terminal amidated peptides directly attached to MBHA resins, avoiding the use of bifunctional linkers.
- Design, synthesize and characterize novel polymyxin analogues with reduced nephrotoxicity and wider therapeutic window amenable for future development as antibiotic drugs.
- Investigate the antimicrobial activity and mechanism of action of the synthesized analogues using different techniques, such as *in vitro* assays with bacteria, transmission electron microscopy, or biophysical experiments using liposomes and monolayers as model membranes.
- Based on the previously mentioned microbiological and biophysical evaluation, select the most promising compound to progress into the drug development process as hits. Scale-up their synthesis and evaluate their potency and toxicity using different *in vivo* and *in vitro* assays, such as efficacy, pharmacokinetic and nephrotoxicity assays in mice models or evaluation of their *in vitro* activity using resistant bacterial strains.

## 1.3. Design of novel polymyxin analogues

With the principal aim to obtain novel drug candidates with comparable or improved activity than natural polymyxin B, while reducing its nephrotoxic adverse effects, 31 polymyxin analogues were designed (Table 7).

The designed analogues included different modifications, such as the introduction of potentially metabolizable bonds in the backbone scaffold of the molecule in order to prevent their accumulation in kidneys, changes in hydrophobicity, or C-terminal and N-terminal modifications.

**Table 7:** Sequence and numeration of the designed polymyxin analogues displayed in three-letter code.

The cyclic structure is denoted in brackets.

Peptide	Sequence
PxB <sub>3</sub>	C8-Dab-Thr-Dab-[Dab-Dab-DPhe-Leu-Dab-Dab-Thr]
<b>1</b>	C8-Dab-Thr-Dab-[Dab-Dab-DPhe-ALeu-Dab-Dab-Thr]
<b>2</b>	C9-Dab-Thr-Dab-[Dab-Dab-DPhe-ALeu-Dab-Dab-Thr]
<b>3</b>	DAdec-Thr-Dab-[Dab-Dab-DPhe-ALeu-Dab-Dab-Thr]
<b>4</b>	C6-Dab-Thr-Dab-[Cys-Dab-DPhe-Leu-Dab-Dab-DCys]
<b>5</b>	C8-Dab-Thr-Dab-[Cys-Dab-DPhe-Leu-Dab-Dab-DCys]
<b>6</b>	C10-Dab-Thr-Dab-[Cys-Dab-DPhe-Leu-Dab-Dab-DCys]
<b>7</b>	C12-Dab-Thr-Dab-[Cys-Dab-DPhe-Leu-Dab-Dab-DCys]
<b>8</b>	C8-Dab-Thr-Dab-[Cys-Dab-DPhe-Nle-Dab-Dab-DCys]
<b>9</b>	C9-Dab-Thr-Dab-[Cys-Dab-DPhe-Nle-Dab-Dab-DCys]
<b>10</b>	C10-Dab-Thr-Dab-[Cys-Dab-DPhe-Nle-Dab-Dab-DCys]
<b>11</b>	C12-Dab-Thr-Dab-[Cys-Dab-DPhe-Nle-Dab-Dab-DCys]
<b>12</b>	C6-Dab-Thr-Dab-[Cys-Dab-DTrp-Nle-Dab-Dab-DCys]
<b>13</b>	C7-Dab-Thr-Dab-[Cys-Dab-DTrp-Nle-Dab-Dab-DCys]
<b>14</b>	C8-Dab-Thr-Dab-[Cys-Dab-DTrp-Nle-Dab-Dab-DCys]
<b>15</b>	C6-Dab-Thr-Dab-[Cys-Dab-DAoc-ALeu-Dab-Dab-DCys]
<b>16</b>	C7-Dab-Thr-Dab-[Cys-Dab-DAoc-ALeu-Dab-Dab-DCys]
<b>17</b>	C8-Dab-Thr-Dab-[Cys-Dab-DAoc-ALeu-Dab-Dab-DCys]
<b>18</b>	DAoc-Thr-Dab-[Cys-Dab-DAoc-ALeu-Dab-Dab-DCys]
<b>19</b>	DAoc-Thr-Dab-[Cys-Dab-DAoc-Leu-Dab-Dab-DCys]
<b>20</b>	C9-Dab-Thr-Dab-[Cys-Dab-DPhe-Leu-Dab-Dab-DCys-NHOH]
<b>21</b>	C9-Dab-Thr-Dab-[Cys-Dab-DPhe-Leu-Dab-Dab-Cys-NHOH]
<b>22</b>	C9-Dab-Thr-Dab-[Cys-Dab-DPhe-ALeu-Dab-Dab-DCys-NHOH]
<b>23</b>	C9-Dab-Thr-Dab-[Cys-Dab-DPhe-ALeu-Dab-Dab-Cys-NHOH]
<b>24</b>	C8-Dab-Thr-Dab-[Cys-Dab-DPhe-Leu-Dab-Dab-Trt]
<b>25</b>	DAdec-Thr-Dab-[Cys-Dab-DPhe-Leu-Dab-Dab-Trt]
<b>26</b>	C8-Dab-Thr-Dab-[Cys-Dab-DPhe-ALeu-Dab-Dab-Trt]
<b>27</b>	DAdec-Thr-Dab-[Cys-Dab-DPhe-ALeu-Dab-Dab-Trt]
<b>28</b>	C8-Dab-Thr-Dap-[Cys-Dab-DPhe-Abu-Dab-Dab-Trt]
<b>29</b>	DAdec-Thr-Dap-[Cys-Dab-DPhe-Abu-Dab-Dab-Trt]
<b>30</b>	C8-Dab-Thr-Dab-[Cys-Dab-DPhe-Nva-Dab-Dab-Trt]
<b>31</b>	DAdec-Thr-Dab-[Cys-Dab-DPhe-Nva-Dab-Dab-Trt]

For clarity, the peptides are divided into five different series depending on the modifications introduced in each case:

- The first series was composed by three depsipeptide analogues of polymyxin.
- The second and the third series enclosed 16 different analogues that form their cyclic structure by a disulfide bond between two cysteine analogues.
- The fourth series was formed by four *C*-terminal modified peptides with hydroxamic acid.
- The fifth series contained nine analogues cycled through a disulfide bond between a cysteine residue and a threonine derivative (Ttr).

### 1.3.1. Depsipeptide polymyxin analogues

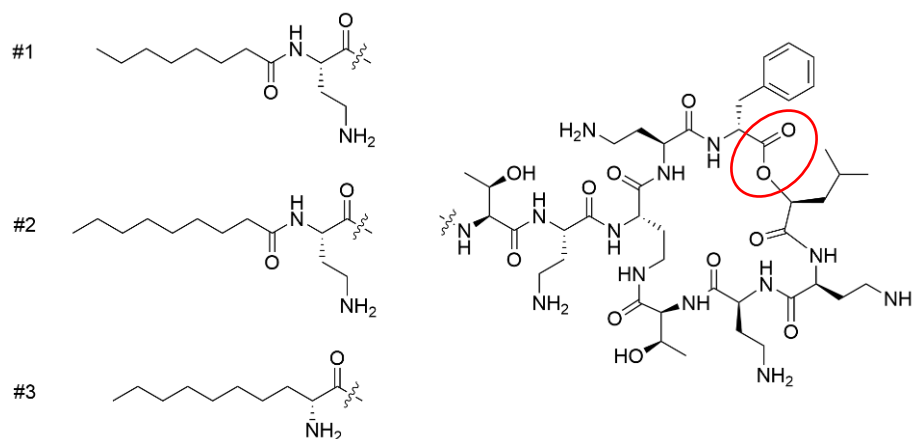
Depsipeptides are biomolecules commonly found in nature that are characterized by the presence of at least one ester bond within the peptide backbone. Excellent examples of depsipeptide AMPs are the naturally occurring cyclic lipodepsipeptides daptomycin and ramoplanin.

Inspired by the idea that the lower stability to degradation inherent to ester bonds will reduce the nephrotoxicity, we firstly designed 3 depsipeptide polymyxin analogues which should be stable enough in biological medium but would be metabolized by detoxifying enzymes (kidneys esterases), and therefore potentially reduce the nephrotoxicity associated with the polymyxin accumulation.

Our cyclic depsipeptide analogues were created by the replacement of the amide bond between the positions 6 and 7 by an ester bond. So that, the metabolization of the ester bond would facilitate the ring opening, and the subsequent proteolysis and elimination of the linear peptide. To do so, the commercially available (S)-2-hydroxy-4-methylpentanoic acid (L-leucic acid), was placed at position 6 allowing the selective introduction of the ester bond.

The general structure of the designed depsipeptides is shown in Figure 36. Analogue #1 maintained the structure of polymyxin B<sub>3</sub> with an octanoic acid in the *N*-terminal position. Whereas analogue #2, which contains *N*-terminal nonanoic acid, was the canonical depsipeptide analogue of polymyxin B<sub>5</sub>. Finally, analogue #3 included the D-Adec moiety at position 1, which mimics the *N*-terminal portion of polymyxins, by substituting

the 1-Dab residue and *N*-terminal fatty acid. The replacement of these two residues, which contribute actively to the overall toxicity of the molecule, may influence in the improvement of the therapeutic window of polymyxins.



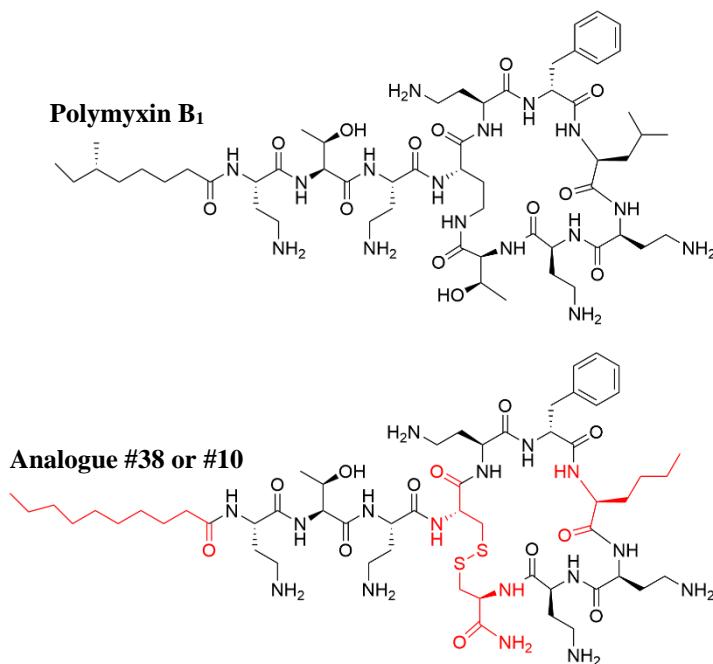
**Figure 36:** Structure of the analogues #1, #2 and #3. The ester bond is highlighted in red.

### 1.3.2. Cysteine analogues

As previously introduced, our group reported in 2015 the design and synthesis of new polymyxins with a chemically accessible scaffold and reduced toxicity.<sup>213</sup> Those polymyxin analogues were based on the isosteric modification of the lactam bond that forms the cycle between 4-Dab and 10-Thr by a disulfide bond between two cysteine residues. The *C*-terminal cysteine was derivatized as a carboxamide to mimic the neutral hydroxyethyl threonine moiety being substituted. To maintain the natural configuration of polymyxins 4-Cys–10-D-Cys link was used. The most active compound previously reported by our group was analogue #38 (also used in the present thesis named as #10 and shown in Figure 37), this analogue displayed excellent activity against both Gram-negative and Gram-positive clinically relevant bacteria and showed low toxicity *in vitro*. Thus, suggesting that after eventual accumulation in renal cells, the disulfide bond of the molecule would presumably be reduced and the cycle would be open up due to the reducing intracellular environment (reduced glutathione and oxidoreductases) and therefore, the proteolysis and degradation of the linear sequence would be facilitated.

Based on the previous investigation performed in the group, we designed a series of cysteine analogues to further explore the influence of hydrophobicity in the antimicrobial activity and the mechanism of action of polymyxin analogues (analogues #4 - #11 of

Table 7). Briefly, in analogues #4 to #7, the branched octanoic acid chain of the natural polymyxin B<sub>1</sub> was substituted by linear C6 to C12 chains. Whereas, on the analogues #8 to #11, a norleucine (Nle) residue was introduced at position 7. Nle is the unbranched isomer of leucine, it is longer and flexible and consequently, it may favor the hydrophobic interactions with bacterial membranes. It should be noted that compounds #6, #10 and #11 correspond to analogues #37, #38 and #39 previously reported by our group.<sup>213</sup>



**Figure 37:** Comparison of the chemical structure of PxB<sub>1</sub> with peptide #38<sup>213</sup> (also renumbered #10 in the present thesis). Modifications are highlighted in red.

Afterward, a new series of cysteine compounds was designed aiming to redistribute the hydrophobicity by increasing the one within the macrocycle, while reducing the corresponding to the fatty acid tail. For that purpose, the Nle<sup>7</sup> residue was maintained, and a D-Trp residue was placed at position 6 instead of D-Phe of the natural polymyxin B. Conversely, the fatty acid of those compounds was shortened to a C6, C7 or C8 acyl chain (analogues #12, #13 and #14 of Table 7).

In addition, to further explore the influence of changes at position 6, analogues #15 to #19 included a 2-D-aminooctanoyl (D-Aoc) unit at position 6 instead of the D-Phe residue. In this case, the hydrophobic aromatic ring of phenylalanine was replaced by a long and flexible hydrocarbon chain composed of 6 methylene units. Analogues #15, #16 and #17 had C6, C7 or C8 N-terminal chains. Whereas analogues #18 and #19, contained

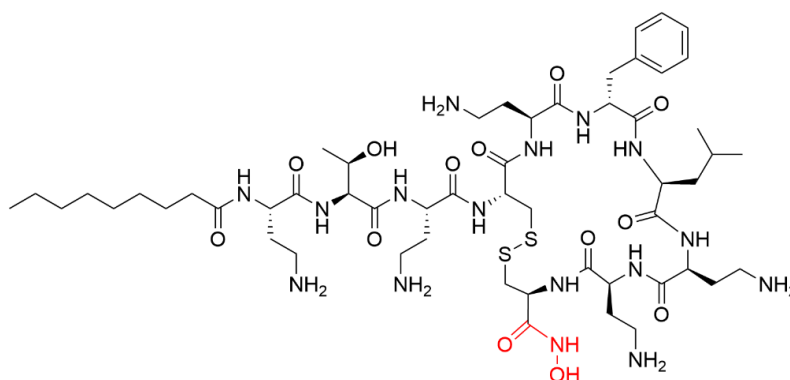


the D-Aoc residue instead of 1-Dab and *N*-terminal fatty acid. Moreover, some compounds included an extra scissile ester bond placed between the positions 6 and 7.

### 1.3.3. Hydroxamic acid analogues

In recent years, there has been a growing interest in developing bacterial peptide deformylase (PDF) inhibitors as novel antibiotics. PDF is metalloenzyme which utilize  $\text{Fe}^{2+}$  as catalytic metal for *N*-formyl hydrolysis, and it has been recognized as an essential component for both Gram-positive and Gram-negative bacteria to complete protein biosynthesis and maturation.<sup>241,242</sup> Therefore, due to the wide distribution of PDF in bacteria and its absence in mammalian cells, it represents an attractive target for the discovery of broad spectrum antibacterial drugs. In that field, hydroxamic acids are currently under study due to their strong metal ion chelating properties. As an example, actinonin is a natural hydroxamic acid derivative that inhibits bacterial growth of Gram-negative and Gram-positive bacteria through the inhibition of PDF activity.<sup>243</sup>

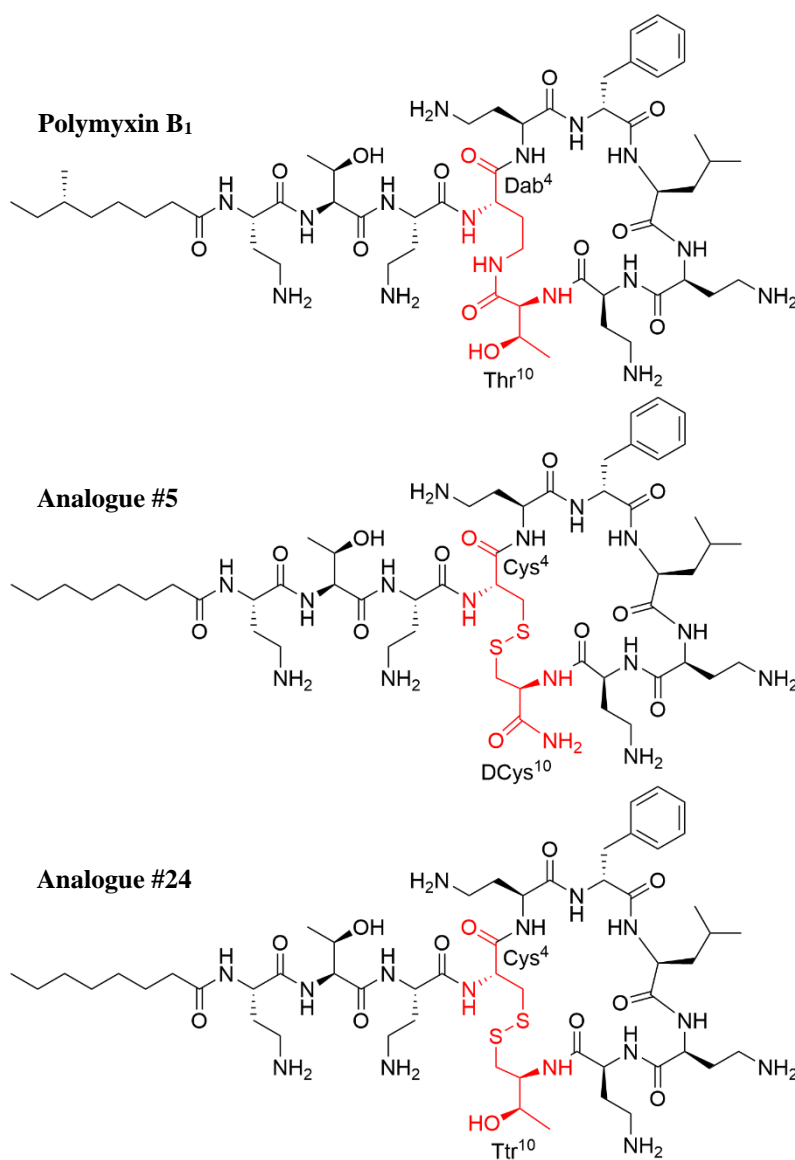
In that context, a new series of polymyxin analogues with *C*-terminal hydroxamic acid was designed (analogues #20 - #24 of Table 7). In this new series, the macrocycle formation by the disulfide bond between two cysteine residues was maintained, and the hydroxamic acid was created by the addition of a hydroxylamine onto the  $\alpha$ -carboxylic group of the cysteine residue at position 10 (Figure 38). The analogues #20 and #22 included D configuration on the cysteine placed at position 10, as the previously discussed cysteine analogues. Contrastingly, analogues #21 and #23 contained L-Cys at position 10 to study if the configuration of this new *C*-terminal modification influence the peptide activity. Finally, an ester bond between position 6 and 7 were also included in analogues #22 and #23. All analogues had a nonanoyl *N*-terminal fatty acid chain.



**Figure 38:** Chemical structure of analogue #20. Hydroxamic acid is highlighted in red.

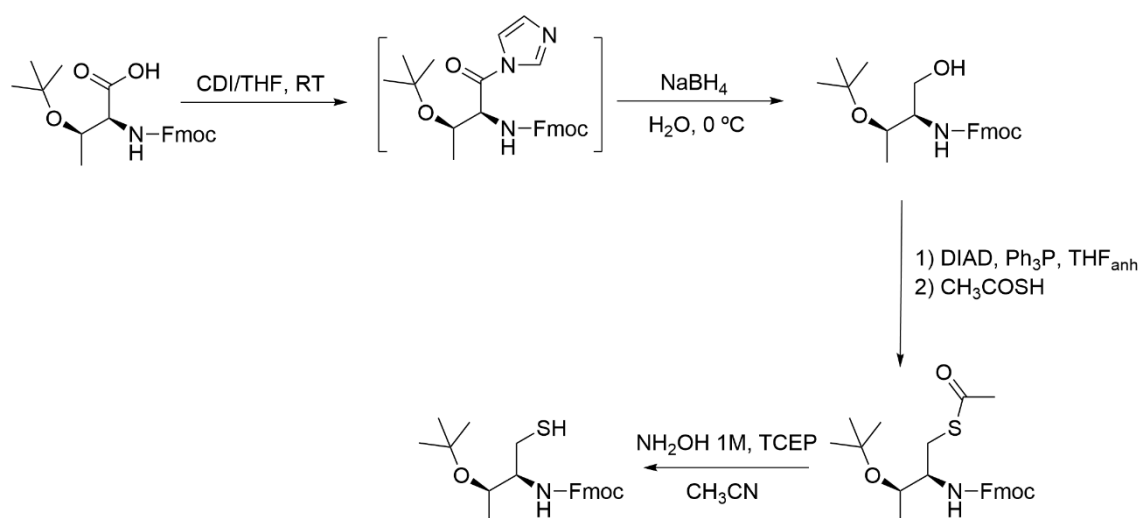
### 1.3.4. Thiiothreonine analogues

As previously discussed, the introduction of a disulfide bond into the polymyxin structure facilitates the synthetic process and could prevent the peptide accumulation in the kidneys, reducing its nephrotoxic effects. Unfortunately, as it will be discussed in section 1.6, this modification produces a 2 or 4-fold reduction of activity in comparison with polymyxin. For that reason, a new synthetic moiety was designed in order to mimic the Thr<sup>10</sup> residue of the natural polymyxin and reduce the impact caused by the introduction of a D-Cys residue (Figure 39). This new moiety was the (2R,3S)-3-amino-4-mercaptobutan-2-ol, also referred in the present thesis as thiiothreonine or Ttr.



**Figure 39:** Structural comparison of Polymyxin B<sub>1</sub>, cysteine analogues (compound #5) and thiiothreonine analogues (compound #24). Amino acids involved in the cyclization are highlighted in red.

The thiothreonine building block and the synthetic route to obtain it (Figure 40) were designed in our group, but the synthesis was optimized and produced at the “Plataforma de Química i Anàlisi” at the Parc Científic de Barcelona in order to speed up the obtention of the analogues and be developed within the ENABLE European consortium of antibiotics (<https://www.imi.europa.eu/projects-results/project-factsheets/enable>).



**Figure 40:** General scheme of the synthesis of the thiothreonine residue.

Analogues #24 to #27 contained an octanoyl chain in the *N*-terminal position or a D-Adec amino acid. Analogues #26 and #27 also contained the scissile labile ester bond placed between positions 6 and 7.

Finally, to explore further the possibilities of substitutions, we also introduced L-2-aminobutanoic acid (Abu) and L-norvaline (Nva) at position 6, shorter residues compared with the parent Leu<sup>6</sup>. Compounds #28 and #29 also included L-2,3-diaminopropanoic acid (Dap) at position 3.

## 1.4. Synthesis of polymyxin analogues

### 1.4.1. Novel acydolitic methodology for the total synthesis of polymyxin B<sub>3</sub> and other relevant peptides

To date, the previously discussed Fmoc/Bn protection strategy applied by Vaara<sup>186</sup> and Sakura<sup>185</sup> constitutes the most successfully and widely used method for polymyxin synthesis; however, the use of Bn-type protecting groups represent a serious concern due to the strong and hazardous conditions required for their removal.

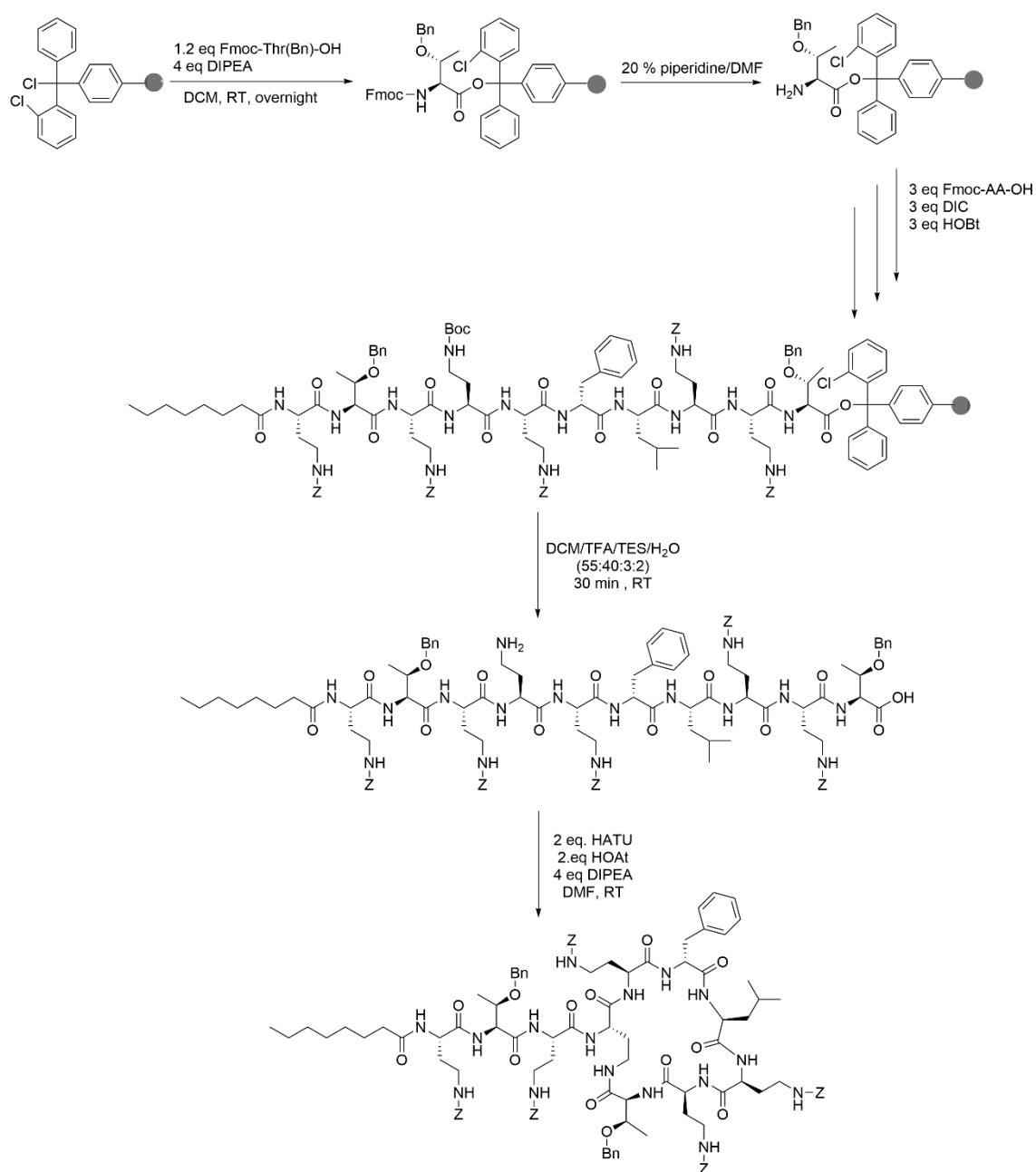
Ben-Ishai and Berger<sup>244</sup> were the first who demonstrated that carbobenzoxy- $\alpha$ -amino acids are cleaved at room temperature by HBr in AcOH to the corresponding amine hydrobromides, benzyl bromide, and carbon dioxide. This deprotecting procedure was then applied to the solid phase peptide synthesis by Merrifield<sup>126</sup> in 1963. However, this method did not gain wide acceptance in peptide synthesis since the anhydrous HF methodology reported by Sakakibara et al.<sup>245</sup> in 1967 was found to be more useful in small scale synthesis. Nowadays, the procedure described by Tam et al.<sup>246</sup> in 1983, consisting on a two-stage procedure named the “low-high HF deprotection procedure”, is the most widely applied in peptide research. It incorporates an initial cleavage of most of the side chain protecting groups under treatment with HF, Me<sub>2</sub>S and p-cresol (25:65:10, v/v/v), followed by a second standard HF cleavage step to remove the more resistant protecting groups. Nevertheless, this methodology still presents several drawbacks such as the handling of the acid (extremely toxic, corrosive, and volatile) and its caustic action on glass, which requires special and costly Teflon® labware. Trifluoromethanesulfonic acid (TFMSA) represents an alternative to HF which do not require special resistant material, but TFMSA-cleaved peptides are susceptible to salt and scavenger association and should be neutralized and desalted before further purification.<sup>247</sup>

Catalytic hydrogenation and catalytic transfer hydrogenation on palladium have also gained broad acceptance as an easy method to cleave benzyl protecting groups and it is widely employed in peptide synthesis, since it is potentially less damaging to the peptide by preventing strong acidic conditions for which peptides are very sensitive.<sup>248</sup>

#### 1.4.1.1. Synthesis and cyclization of polymyxin B<sub>3</sub>

The synthesis of polymyxin B<sub>3</sub> was conducted manually following conventional Fmoc protection strategy onto a 2-CTC resin, as it is summarized in Figure 41. The  $\gamma$ -amino group of the 4-Dab residue involved in cyclization of the peptide was protected by the acid-labile Boc group, whereas all the other amino acids with functional side chain groups were protected by benzyloxycarbonyl (Z) or benzyl (Bn) groups, which are only removed under strong acidic conditions. All couplings were carried out using 3-fold molar excess of DIC/HOBt coupling reagents, for 1 hour in DMF, and the successive Fmoc removal treatments were performed with 20 % piperidine in DMF.

On completion of the synthesis, the peptide was removed from the resin by reaction with a solution of 40 % TFA for 30 minutes at room temperature, to yield the partially protected linear peptide after precipitation in cold diethyl ether. The resulting peptide was cyclized using HATU-HOAt-DIPEA system, and the progress of the cyclization reaction was monitored by TLC revealed by spraying with ninhydrin reagent. Finally, the cyclized protected peptide was precipitated and washed by the addition of cold water, and the product was dried by lyophilization.



**Figure 41:** Complete scheme of the synthesis of cyclic protected polymyxin B<sub>3</sub>.

#### 1.4.1.2. Bn-type protecting groups removal

In order to develop a new efficient reagent for the deprotection of Bn-type protecting groups, different acidic mixtures based on HBr were used onto the cyclic protected peptide to finally obtain the fully deprotected polymyxin B<sub>3</sub>, as it is shown in Table 8.

All experiments involved in the deprotection optimization process were performed at small scale. Briefly, 5 mg of cyclic protected peptide were dissolved in 2 mL of tested solution and left to react over the desired time. The reaction crude was obtained after precipitation in cold diethyl ether, and the scope of each reaction was evaluated by analytical HPLC and ESI-MS spectrometry.

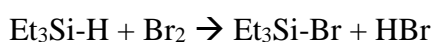
**Table 8:** The optimization of the PxB<sub>3</sub> deprotection conditions.

	Acidic mixture	HBr w/v%	Volume ratio	Temperature	Time	Crude purity
1	TFA/TES	-	95:5	RT	5 h	0 %
2	TFA/TES	-	95:5	50 °C	2 h	0 %
3	TFA/TES	-	95:5	50 °C	5 h	0 %
4	TFA/TES	-	95:5	50 °C	8 h	3 %
5	TFA/TMSCl/TES/HBr 33 % in AcOH	2.2	64.2:25.8:5:5	RT	1 h	1 %
6	TFA/TMSCl/TES/HBr 33 % in AcOH	2.2	64.2:25.8:5:5	RT	2 h	6 %
7	TFA/TES/ Br <sub>2</sub>	12	47.5:45:7.5	RT	1 h	0 %
8	TFA/TES/ Br <sub>2</sub>	4	82.5:15:2.5	RT	30 min	60 %
9	TFA/TES/ Br <sub>2</sub>	4	82.5:15:2.5	RT	45 min	75 %
10	TFA/TES/ Br <sub>2</sub>	4	82.5:15:2.5	RT	90 min	71 %

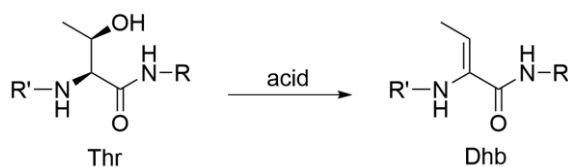
The optimization process was initiated by the study of a simple TFA/TES solution (95:5, v/v) at room temperature (entry #1 Table 8), but the peptide remained totally protected after 5 hours of treatment (chromatogram not shown). Afterwards, the same acid mixture was employed, but heating up the reaction to 50 °C, and as a result, a complex chromatogram was obtained due to the partial deprotection of some Z groups. In fact, only a 3 % of the desired product was obtained after 8 hours of treatment (entry #4 Table 8, Figure 43A).

An acidic mixture composed of HBr solution 33 wt. % in AcOH, TMSCl and TES (entries #5 and #6 Table 8) was then tested. This acidic mixture has been previously studied and patented by our group<sup>249,250</sup> with excellent results in the obtention of model peptides protected with Boc and <sup>t</sup>Bu groups. Unfortunately, after 2 hours of treatment at room temperature only 6 % of the final compound was obtained. These conditions appear to be not acidic enough to obtain the fully deprotected Polymyxin B<sub>3</sub>, although the reaction contained 2.2 w/v % of HBr along with 25.8 v/v % of TMSCl and 64.2 v/v % of TFA. The obtained crude corresponded to a highly complex mixture of partially protected peptides and other minor byproducts (Figure 43B).

In order to obtain stronger acidic mixtures and avoid the use of acetic acid, which could also generate acetylation side reactions, we then explored the *in-situ* generation of HBr in TFA. The *in-situ* generation of hydrogen halides by the reaction of halogens (X: Br, Cl and I) with trialkyl silanes (R<sub>3</sub>Si-H) was firstly described by Deans et al. in 1954.<sup>251</sup> Therefore, the reaction of TES and Br<sub>2</sub> in TFA provides the reactive mixture with two strong protic acids (HBr and TFA), one Lewis acid (TES-Br) and a carbocation scavenger (TES in excess) under very simple experimental conditions. Briefly, Br<sub>2</sub> (1 eq) was dissolved in TFA in a glass conical vial with gentle agitation and the reaction mixture was cooled to 0 °C with an ice bath. TES (1.9 eq) was then added dropwise until the total disappearance of the reddish-brown color characteristic of the molecular bromine, according to the following reaction:

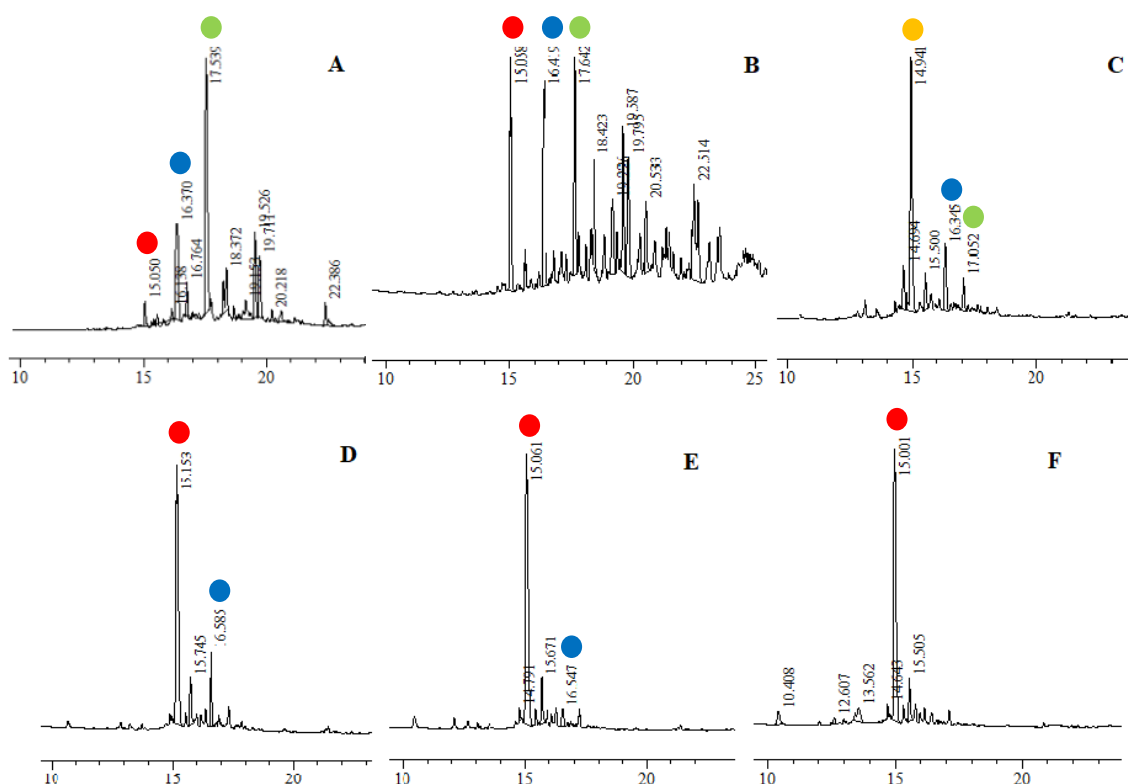


Thus, the protected peptide was treated during 1 hour with a solution of 12 w/v % of generated HBr (entry #7 Table 8), and a 40 % of a main product was obtained (Figure 43C), but ESI-MS revealed that the major peak was a M-36 byproduct, probably due to dehydration of the two Thr lateral chains, resulting in the formation of dehydrobutyrine (Dhb) (Figure 42).



**Figure 42:** Thr residue dehydration.

To avoid the dehydration byproducts originated by an excess of acid, these conditions were optimized reducing the total percentage of generated HBr and the exposure time. Remarkably, the acidic deprotection with 4 w/v % of HBr for 45 minutes (entry #9 Table 8) appear to be the most effective treatment, resulting in a peptide yield of 75 % (Figure 43E). Applying the same treatment for 90 minutes (entry #10 Table 8), very similar results were obtained (Figure 43F), whereas a 30-minute treatment yield to 15 % of semi-protected polymyxin B<sub>3</sub> (Figure 43D).



**Figure 43:** PxB<sub>3</sub> crude HPLC chromatograms run at G0595t30 and processed at 220 nm. Crudes obtained after treatment of: A) TFA/TES (95:5) for 8 hours at 50 °C; B) TFA/TMSCl/TES/HBr 33 % in AcOH (64.2:25.8:5:5) for 2 h at RT; C) TFA/TES/Br<sub>2</sub> (47.5:45:7.5) for 1 h at RT; D) TFA/TES/Br<sub>2</sub> (82.5:15:2.5) for 30 min at RT; E) TFA/TES/Br<sub>2</sub> (82.5:15:2.5) for 45 min at RT; F) TFA/TES/Br<sub>2</sub> (82.5:15:2.5) for 90 min at RT. ● = PxB<sub>3</sub>, C<sub>55</sub>H<sub>96</sub>N<sub>16</sub>O<sub>13</sub>, exact mass: 1188.7, found 1189.7 [M + H]<sup>+</sup>; ● = PxB<sub>3</sub> + Bzl, C<sub>62</sub>H<sub>102</sub>N<sub>16</sub>O<sub>13</sub>, exact mass: 1278.8, found 1279.7 [M + H]<sup>+</sup>; ● = PxB<sub>3</sub> + 2Bzl, C<sub>69</sub>H<sub>108</sub>N<sub>16</sub>O<sub>13</sub>, exact mass: 1368.8, found 1370.1 [M + H]<sup>+</sup>; ● = PxB<sub>3</sub> - 2H<sub>2</sub>O, C<sub>55</sub>H<sub>92</sub>N<sub>16</sub>O<sub>11</sub>, exact mass: 1152.7, found 1153.8 [M + H]<sup>+</sup>.

Finally, the optimized deprotection conditions were applied in a higher scale. Starting from 254 mg of 2-CTC resin, a total amount of 257 mg of cyclic protected peptide were obtained, which were treated with 100 mL of TFA/TES/Br<sub>2</sub> (82.5:15:2.5, v/v/v) for 45 min, the product was then precipitated in cold diethyl ether, obtaining a 72 % pure solid



with a pale orange/off-white coloration, which disappeared after purification by semi-preparative HPLC. The product was finally dried by lyophilization, and 69 mg (47 mg of free base compound) of >95 % pure product were obtained. Characterization was carried out by analytical HPLC and ESI-MS, and the global yield for the total synthesis of polymyxin B<sub>3</sub> was 21 %.

#### 1.4.1.3. Other applications for the novel acidolytic methodology

The 4-methylbenzhydrylamine resin (MBHA) is a solid support which allows the preparation of C-terminal amidated peptides. This solid support is generally associated with the Boc/Bn protecting strategy since the cleavage of the carboxylic amides from the resin requires strong acids such as trimethylsilyl trifluoromethanesulfonate, trifluoromethanesulfonic acid or HF. MBHA resin is also compatible with the standard Fmoc/<sup>t</sup>Bu strategy if the support is attached to a bifunctional linker such as Rink-amide linker,<sup>252</sup> which consists of a benzhydryl amine functionalized with two methoxy groups at positions *ortho* and *para*, and increases the acid lability of the resin allowing the peptides removal by milder acidic conditions.

In order to expand the scope of the new cleavage reagent we tested its capability to cleave peptides synthesized using Fmoc/<sup>t</sup>Bu protection and directly attached to MBHA resin, avoiding the time and resource-consuming addition of a linker. Following this approach, we synthesized the C-terminal amidated peptides, dusquetide and RR4 (sequences shown in Table 9). Dusquetide is a synthetic 5-amino acid peptide derived from indolicin which is currently in Phase III clinical trials for the treatment of oral mucositis.<sup>253,254</sup> On the other hand, RR4 is a rationally-designed peptide composed of 14 amino acid residues, which present significant activity against MDR *Pseudomonas aeruginosa* and *Acinetobacter baumannii*.<sup>255</sup>

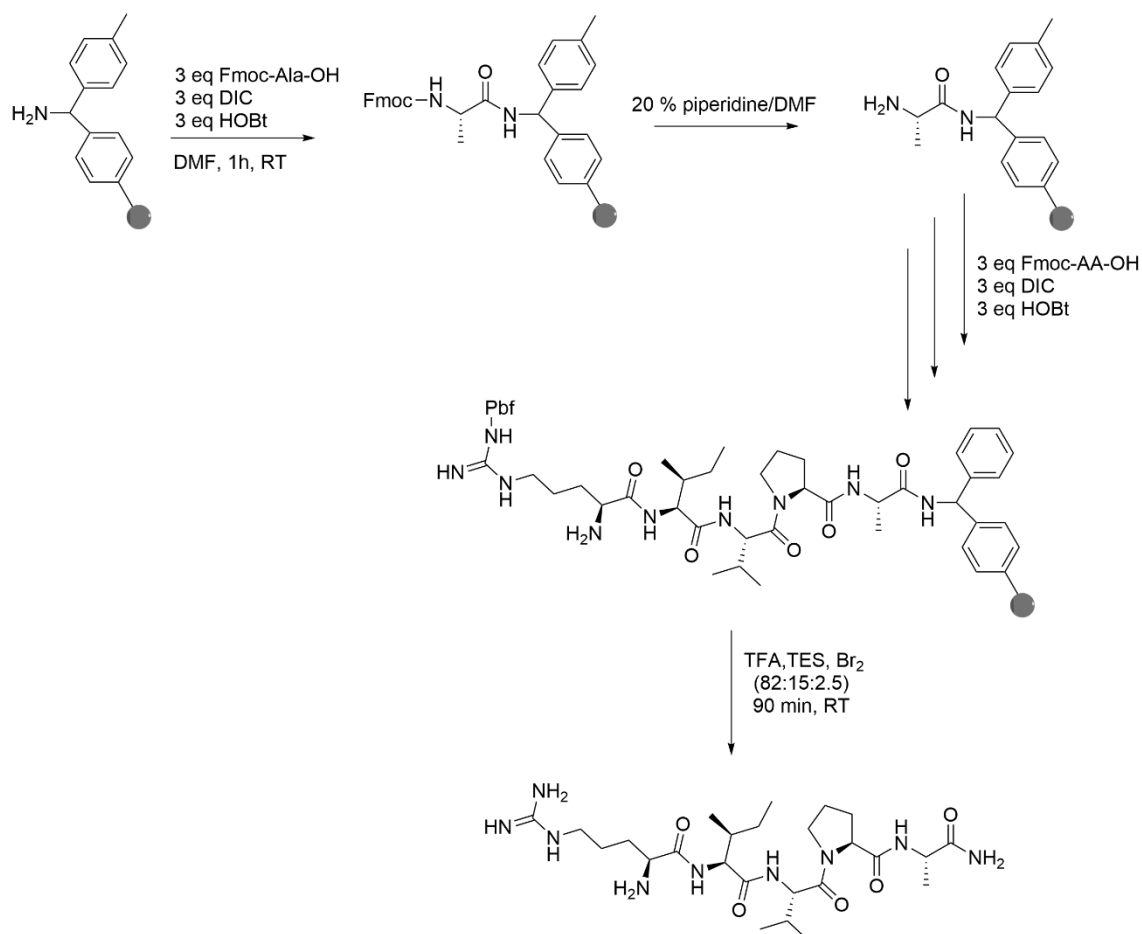
**Table 9:** Three letter code sequence of dusquetide and RR4.

Peptide	Sequence
Dusquetide	Arg-Ile-Val-Pro-Ala-NH <sub>2</sub>
RR4	Trp-Leu-Arg-Arg-Ile-Lys-Ala-Trp-Leu-Arg-Arg-Ile-Lys-Ala-NH <sub>2</sub>

## 1.4.1.3.1. Synthesis of dusquetide

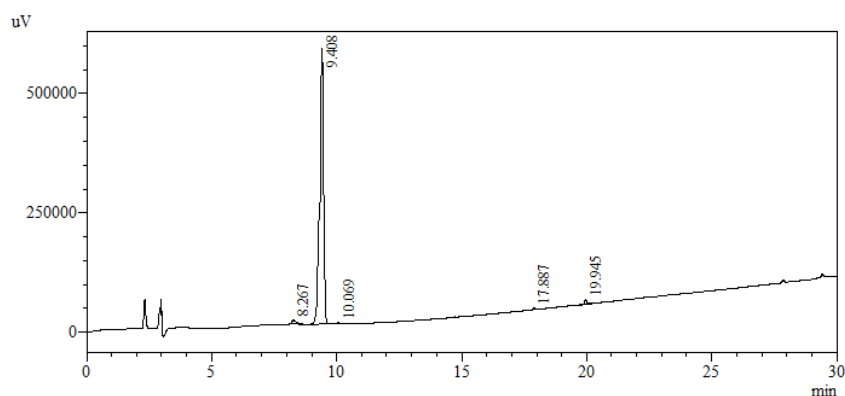
Dusquetide was synthesized manually by solid-phase chemistry following standard Fmoc/<sup>t</sup>Bu procedures on MBHA resin, the synthetic route is shown in Figure 44. The five amino acids of the sequence, Fmoc-Ala-OH, Fmoc-Pro-OH, Fmoc-Val-OH, Fmoc-Ile-OH and Fmoc-Arg(Pbf)-OH were stepwise incorporated using DIC-HOBt coupling system using 3-fold molar excess of reagent for 1 hour in DMF. Full residue incorporation was ensured by Kaiser test, and Fmoc groups were removed by successive treatments with 20 % piperidine in DMF.

On completion of the synthesis, the peptide was removed from the resin by reaction with the *in-situ* generated HBr mixture (HBr 4 w/v %), following the optimized conditions previously described. However, according to other studies on peptides cleaved directly from MBHA resin using HBr or TMSBr,<sup>256,257</sup> the reaction time was increased to 90 minutes to ensure the complete peptide release from the resin.



**Figure 44:** Complete scheme of the synthetic route of dusquetide.

Finally, the obtained results were excellent since the weight of the crude peptide yielded 42 mg (33 mg of free base peptide,  $\eta = 87\%$ ) and the reaction crude was 95 % pure (Figure 45), thus indicating that the new acidic methodology is a highly promising approach to obtain pure peptides in very good yields.



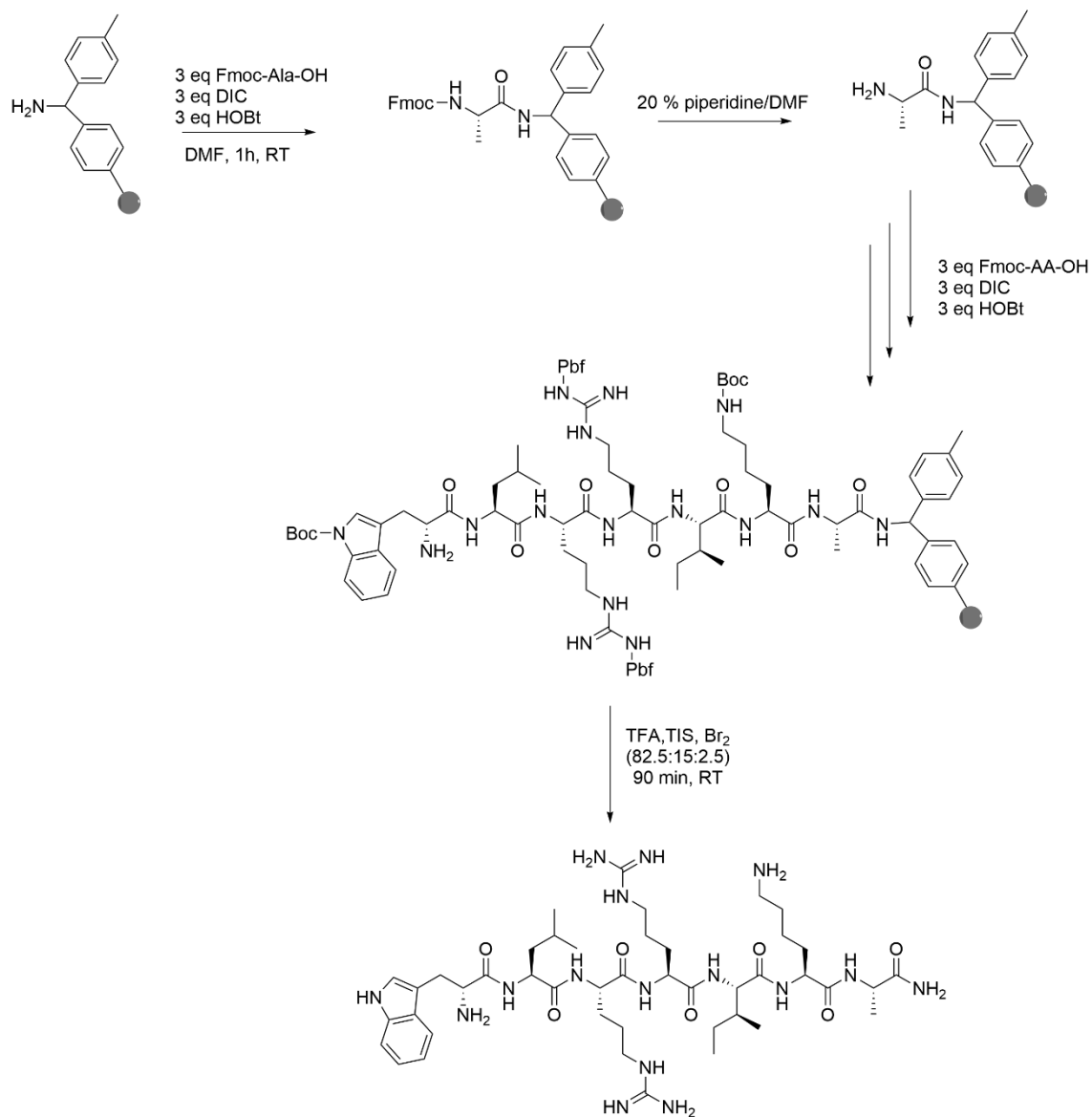
**Figure 45:** Crude dusquetide HPLC chromatogram run at G0595t30 and processed at 220 nm.

It should be noted that, as the peptide was not further purified, the obtained product with pale orange/off-white color was lyophilized three times with H<sub>2</sub>O/ACN until color disappearance.

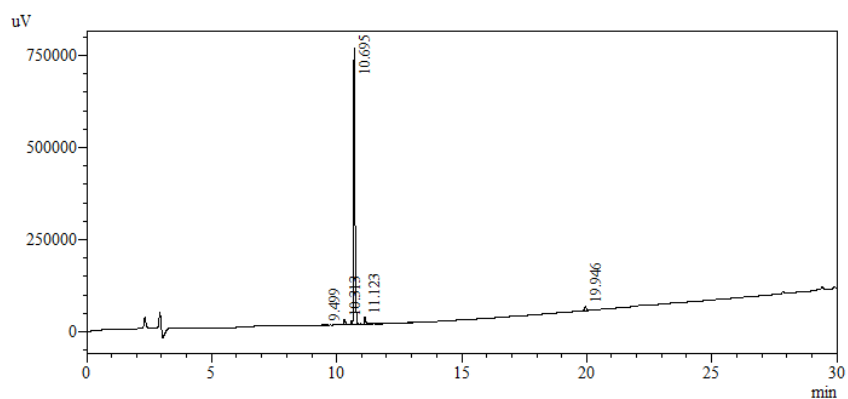
#### 1.4.1.3.2. Synthesis of RR4

We next synthesized the 8-14 segment of RR4 using the same procedure described for dusquetide. The amino acids used in this case were: Fmoc-Ala-OH, Fmoc-Lys(Boc)-OH, Fmoc-Ile-OH, Fmoc-Arg(Pbf)-OH, Fmoc-Leu-OH and Fmoc-Trp(Boc)-OH. The complete scheme of the synthesis is shown in Figure 46.

In this case, the cleavage reagent cocktail was prepared with TIS instead of TES, to prevent the indole ring reduction of Trp residue. The excellent results obtained for dusquetide were confirmed with an obtention of 92 % pure RR4 (Figure 47) and a cleavage yield of 82 % (72 mg of bromide salt, 53 mg of free base peptide). The off-white obtained peptide was also lyophilized three times in H<sub>2</sub>O/ACN solution until color disappearance and the obtained peptide was not further purified.



**Figure 46:** Complete scheme of the synthetic route of the segment 8-14 of RR4.



**Figure 47:** Crude segment 8-14 of RR4 HPLC chromatogram run at G0595t30 and processed at 220 nm.

### 1.4.2. Synthesis of depsipeptide analogues

Depsipeptides were synthesized using manual SPPS on a 2-CTC resin following a standard Fmoc protection strategy. Functional side chain groups of all amino acids, except the Dab involved in the cyclization process, were protected by Boc and <sup>t</sup>Bu protecting groups which were stable to the cleavage conditions. Whereas the amino group of the 4-Dab residue was protected by 4-methyltrityl (Mtt) group, a protecting group highly acid labile and easily removable under mild acidic conditions. The complete synthetic scheme is shown in Figure 48.

On peptide completion, it was removed from the resin by reaction with a solution of 25 % HFIP for 1 h at room temperature, to obtain the partially protected product. The resulting peptide was precipitated with cold water. The cyclization reagent, which consisted of HATU, HOAt and DIPEA, was added to the peptide dissolved in DMF using, and it was monitored by TLC exposed to ninhydrin reagent. The cyclized protected peptide was precipitated and washed by the addition of cold water, and the product was dried by lyophilization.

The remaining side chain protecting groups were removed by acidic treatment with TFA. Peptides were finally purified by semi-preparative HPLC to >95 % of purity and were characterized by analytical HPLC and ESI MS. Global yields of these analogues were around 10 %.

### 1.4.3. Synthesis of cysteine analogues

The 16 cysteine analogues were prepared on a Rink amide linker attached via alanine to MBHA resin by established manual solid phase synthesis using Fmoc-amino acids activated by 3-fold molar excess of DIC, HOBt coupling system. All coupling reactions were performed in DMF for 1 hour and their completion was assessed by Kaiser test. 20 % of piperidine in DMF was used to remove the  $\alpha$ -amino Fmoc protecting groups. The amino acids used were: Fmoc-Cys(Trt)-OH, Fmoc-DCys(Trt)-OH, Fmoc-Dab(Boc)-OH, Fmoc-DPhe-OH, Fmoc-Leu-OH, Fmoc-Nle-OH, Fmoc-Thr(<sup>t</sup>Bu)-OH, Fmoc-Trp-OH and Fmoc-DAoc-OH. The *N*-terminal fatty acid position was occupied by hexanoic, octanoic, nonanoic, decanoic or dodecanoic acid.

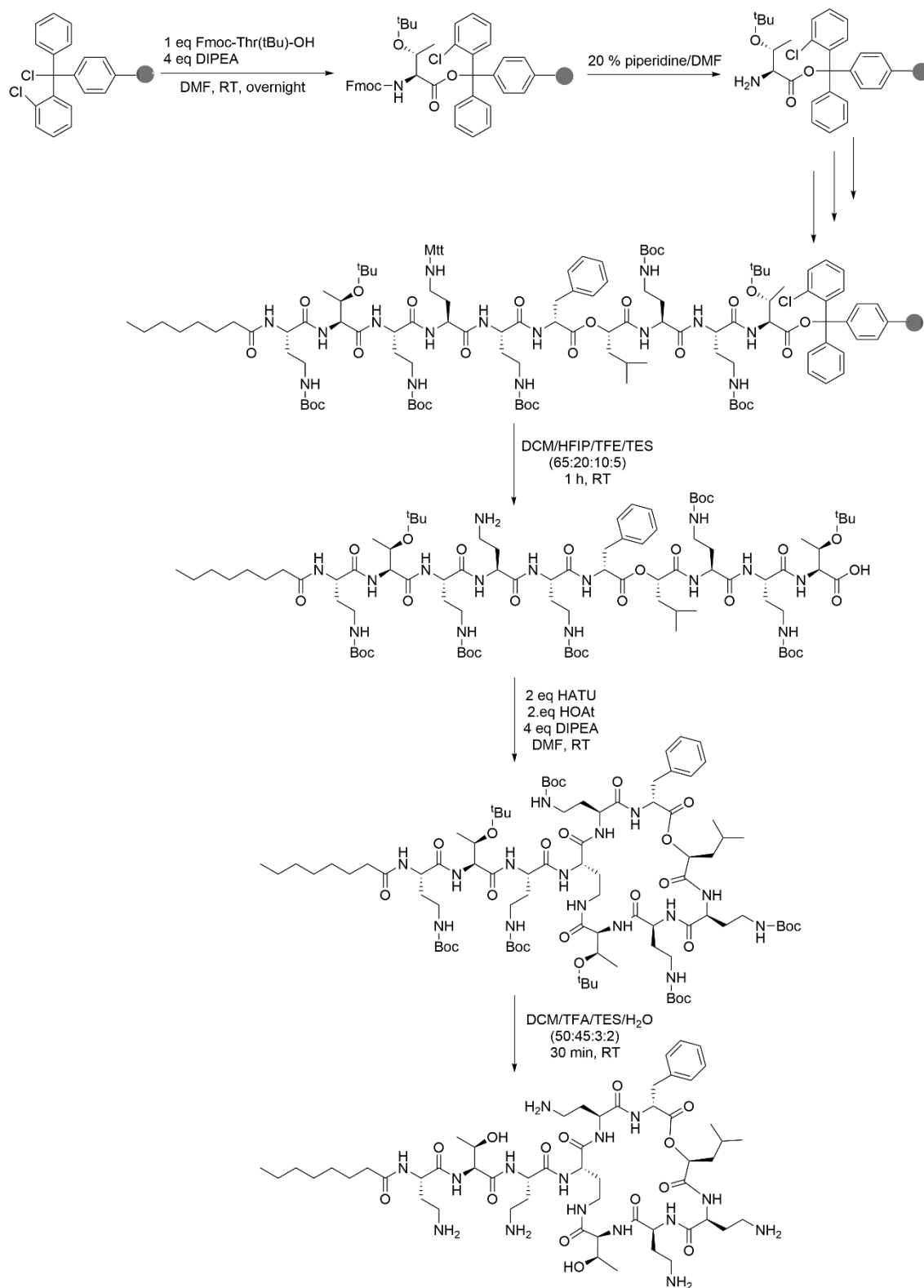
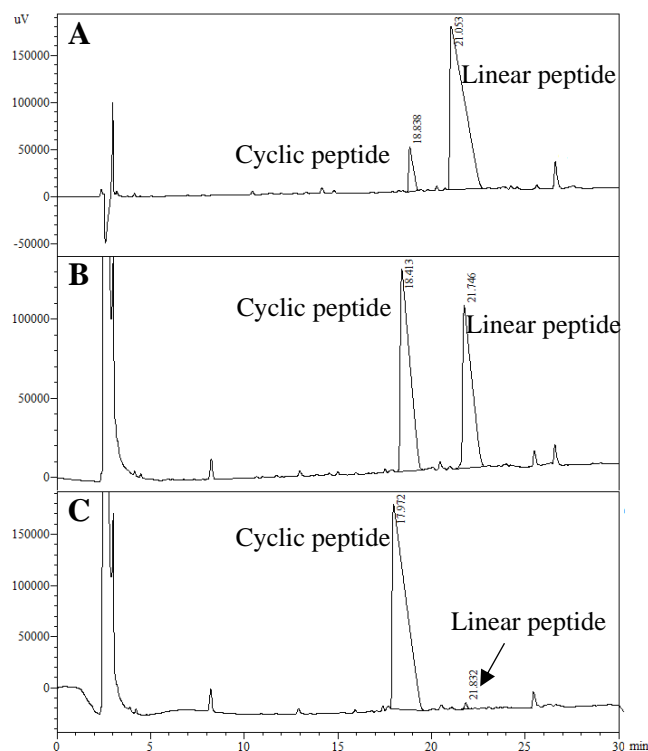


Figure 48: Synthesis scheme of analogue #1.

On completion of the synthesis, the assembled protected peptides were cleaved from the Rink-amide resin under acidic conditions using a TFA/TES/H<sub>2</sub>O solution (95:3:2, v/v/v) for 90 minutes. The acidic treatment of the resin was repeated twice in order to increase the reaction yields. Both batches were collected, and the cyclization was carried out by oxidation of cysteines in a solution of 5 % DMSO in water. The progress of the cyclization reaction was monitored by analytical HPLC (example of cyclization shown in Figure 49).



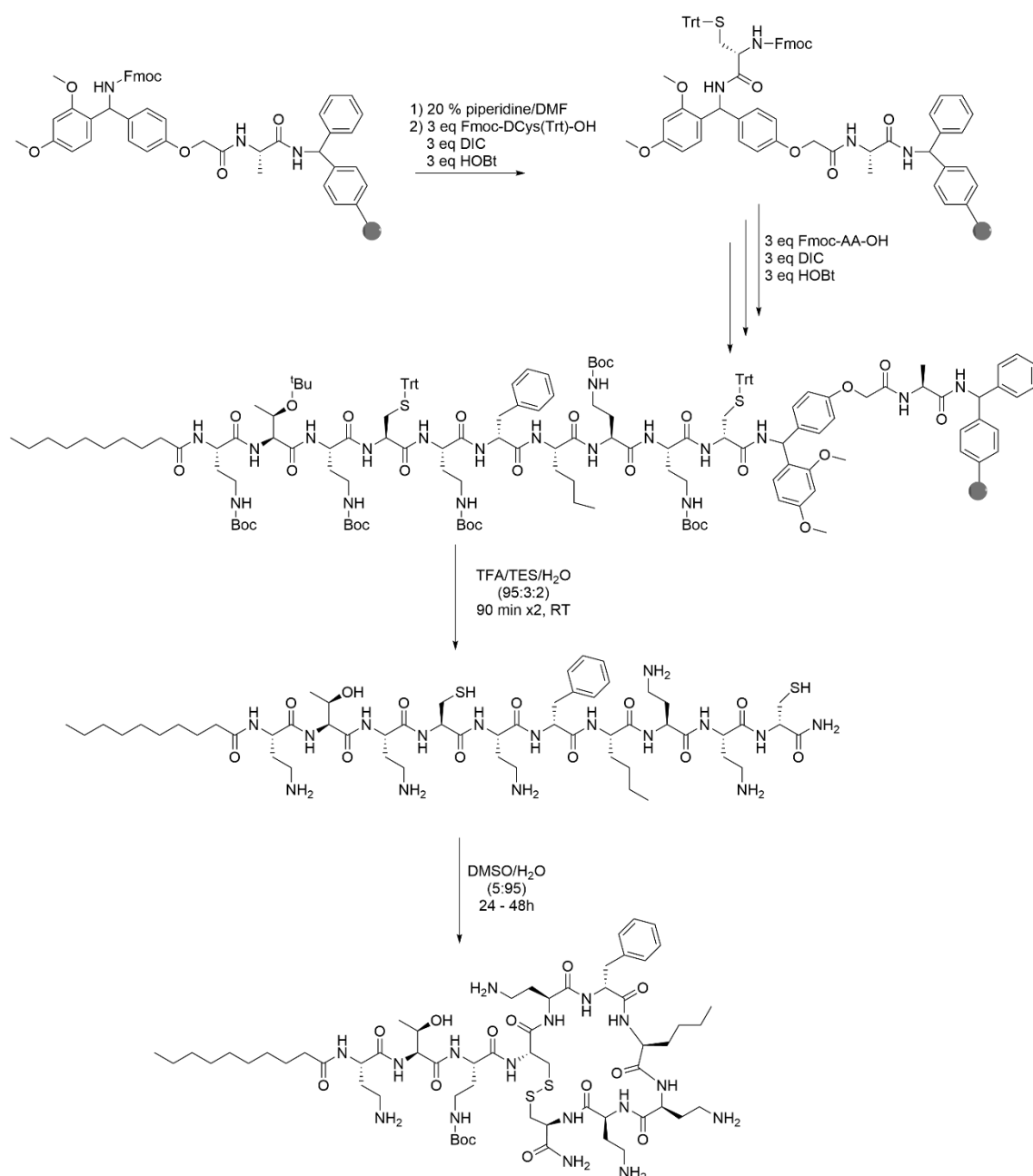
**Figure 49:** Monitoring by analytical HPLC of cyclization in DMSO 5 % solution of analogue #10: A) 0 h; B) 8 h; and C) 24 h of treatment. Chromatograms run at G2540t30 and processed at 220 nm.

Finally, peptides were purified by semi-preparative HPLC to >95 % of purity and were characterized by analytical HPLC and ESI mass spectrometry. A general scheme of the synthesis of analogue #10 is shown in Figure 50. Global yields obtained for the synthesis of cysteine analogues ranged from 15 to 28 %.

#### 1.4.4. Hydroxamic acid analogues synthesis

Hydroxamic acid analogues were synthesized by solid-phase peptide synthesis following the method described by Mellor et al.,<sup>258</sup> it consisted in the production of a *N*-Fmoc-aminoxy-2-chlorotrityl polystyrene, anchoring a previously protected *N*-Fmoc-hydroxylamine to a 2-CTC resin in presence of DIPEA for 48 hours. The real substitution

level was then determined by Fmoc UV quantification at  $\lambda = 301\text{nm}$  and unreacted chloride sites were "capped" by stirring with methanol. Peptides were then synthesized by standard means, following the Fmoc/<sup>t</sup>Bu and using 3 eq of AA-DIC-HOBt coupling system. Once the sequence was completed, peptides were cleaved from the resin under 60-minute treatment of TFA. The obtained peptides were cyclized by oxidation of cysteines, as previously explained. Cyclic crude peptides were finally lyophilized, purified, and characterized. Purities higher than 95 % and global yields of 10 % were obtained.

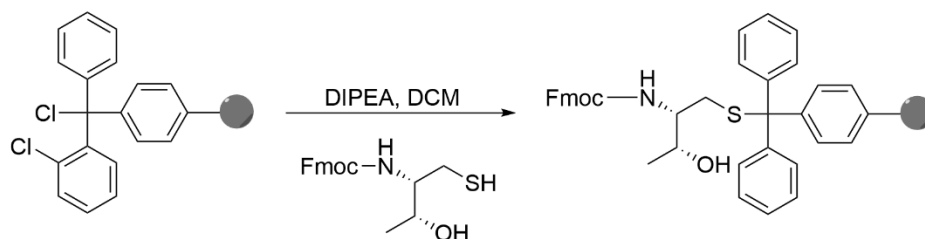


**Figure 50:** General scheme of the synthesis of analogue #10.



### 1.4.5. Synthesis of thiothreonine analogues

For the thiothreonine analogues synthesis, the Fmoc-protected thiothreonine moiety was anchored to a 2-CTC resin via a  $S_N$  reaction yielding a thioether bond (Figure 51).



**Figure 51:** First coupling of thiothreonine analogues.

Peptides were then assembled, cleaved, cyclized, purified, and characterized as explained in the previous section. Global yields obtained for thiothreonine analogues ranged from 5 to 12 %, whereby the synthesis was further studied and optimized.

### 1.4.6. Scale-up and optimization of the synthesis of thiothreonine analogues

During the discovery process only few milligrams of each peptide were necessary to perform the *in vitro* experimentation. For that reason, all analogues were first synthesized at small scale, generally obtaining around 20 mg of pure peptide per synthesis. Nevertheless, as drug development progressed, larger quantities of peptide were required in order to perform the experimentation in animals (100 mg - 1 g), and therefore the optimization and scale up of the synthesis became crucial. As it will be shown in section 1.8., thiothreonine analogues #25 and #27 were selected as the most promising compounds for further development, for that reason herein is presented their scale-up and optimization process.

#### 1.4.6.1. Compound 27

We started optimizing peptide #27 since it was the most difficult one due to the presence of the ester bond in its structure. Table 10 shows all the modifications explored in order to optimize the synthetic process and scale the production of thiothreonine analogues. Basically, we studied different coupling agents, cleavage methods, the presence of water in the synthesis and the polymeric support.

**Table 10:** Optimization and scale-up process of the synthesis of compound #27.

#	Resin type	Initial resin amount/loading	Coupling agents	Cleavage method	Cleavage yield	Crude purity	Pure peptide (free base)/ Global yield
1	2-CTC	165 mg 0.9 mmol·g <sup>-1</sup>	3 eq DIC 3 eq HOBt	TFA/TES/H <sub>2</sub> O (95:3:2) 30 min	40 %	60 %	30 mg (21 mg) 12 %
2	2-CTC	507 mg 0.8 mmol·g <sup>-1</sup>	3 eq DIC 3 eq HOBt	TFA/TES/H <sub>2</sub> O (95:3:2) 30 min	40 %	60 %	82 mg (55 mg) 12 %
3	2-CTC	550 mg 0.8 mmol·g <sup>-1</sup>	3 eq DIC 3 eq HOBt	TFA/TES/H <sub>2</sub> O (95:3:2) 60 min x 2	45 %	43 %	54 mg (36 mg) 7 %
4	2-CTC	510 mg 0.9 mmol·g <sup>-1</sup>	3 eq HATU 3 eq HOBt 6 eq DIEA	TFA/TES/H <sub>2</sub> O (95:3:2) 30 min	35 %	53 %	58 mg (39 mg) 7 %
5	2-CTC	2.003 g 0.7 mmol·g <sup>-1</sup>	3 eq HATU 3 eq HOBt 6 eq DIEA	TFA/TES/H <sub>2</sub> O (95:3:2) 30 min	29 %	33 %	76 mg (51 mg) 3 %
6	2-CTC	1.125 g 0.8 mmol·g <sup>-1</sup>	3 eq DIC 3 eq K-Oxyrna	TFA/TES/H <sub>2</sub> O (95:3:2) 30 min	30 %	33 %	51 mg (34 mg) 3 %
7	Trt-Cl	254 mg 0.9 mmol·g <sup>-1</sup>	3 eq DIC 3 eq HOBt	TFA/TES/H <sub>2</sub> O (95:3:2) 30 min	68 %	45 %	57 mg (38 mg) 14 %
8	Trt-Cl	250 mg 0.9 mmol·g <sup>-1</sup>	3 eq DIC 3 eq HOBt	TFA/TES (95:5) 30 min	68 %	58 %	79 mg (53 mg) 20 %
9	Trt-Cl	1.059 g 0.8 mmol·g <sup>-1</sup>	3 eq DIC 3 eq HOBt	TFA/TES (82:18) 30 min	72 %	56 %	234 mg (157 mg) 16 %
10	Trt-Cl	2.486 g 0.7 mmol·g <sup>-1</sup>	3 eq DIC 3 eq HOBt	TFA/TES (82:18) 30 min	70 %	60 %	543 mg (364 mg) 18 %

Initially, peptide #27 was synthesized at laboratory scale (entry #1, Table 10). Briefly, the thiol group of the Fmoc-protected thiothreonine residue was anchored to 2-CTC resin (165.0 mg, loading: 0.9 mmol·g<sup>-1</sup> resin) and then, the peptide was built up by standard solid phase procedures, following a Fmoc/<sup>t</sup>Bu protection strategy. The acidolytic cleavage was carried out with TFA/TES/H<sub>2</sub>O (95:3:2, v/v/v) for 30 minutes, obtaining a crude purity of 60 % (peak at 14.3 min, Figure 53 #1). Finally, the peptide was cyclized and purified by HPLC, and a total amount of 30 mg was obtained, which supposes a moderated global yield of 12 %. The process was then scaled to 500 mg of initial resin (entry #2, Table 10) obtaining basically the same yield.

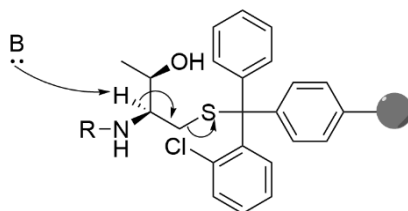
In order to optimize the process, we first addressed the low cleavage yields obtained so far, which were around 40 % and entailed a peptide loss of more than half of theoretical

amount. Firstly, we hypothesized that our peptide remained anchored to the resin after 30 minutes of acidic treatment. Hence, the acidic treatment was extended to 60 minutes and repeated 2 times (entry #3, Table 10), but the reaction yielded only 45 %, thus indicating that cleavage conditions were probably correct, and the peptide loss occurred during the peptide elongation. Moreover, the longer acidic treatment led to a less pure reaction crude (Figure 53 #3)

There is reported that premature release of peptides anchored to extremely acid labile resins could be related with the slightly acidic character of *N*-hydroxyl-amine-type additive.<sup>259</sup> In our case, HOBt ( $pK_a= 5.65$ ) had been used as coupling agent combined with DIC. To avoid this potential side reaction, HATU/HOAt/DIEA coupling system was used due to the presence of basic medium (entry #4, Table 10). Unfortunately, the obtained cleavage yield was even lower than before. Furthermore, the scale-up of these conditions (entry #5, Table 10) produced a highly complex reaction crude (Figure 53 #5).

In the view of these results, we decided to follow the methodology reported by Cherkupally et al.,<sup>260</sup> who described a new approach for the synthesis of peptides assembled on highly acid-labile solid-supports. It consisted in the use of K-Oxyma in conjunction with DIC (entry #6, Table 10), but it also resulted in a 30 % of yield and a highly impure final product (Figure 53 #6).

Under those circumstances, considering that coupling agents were not the cause of the premature peptide release, we decided to change our solid support. Similarly to our thiothreonine anchoring reaction, Diaz-Rodriguez et al.<sup>261</sup> reported the synthesis of peptides containing *C*-terminal cysteine methyl esters by anchoring the thiol group of the cysteine side chain to a trityl-based resin forming a thioether bond. They performed the synthesis on a 2-CTC resin obtaining a 45 % overall yield, and then repeated the synthesis using a chlorotriyl chloride (Trt-Cl) resin, in order to determine if the absence of the electron-withdrawing chloride would have an effect on the final yield. Surprisingly, the yield of their peptide increased from 45 % to 82 % by simply changing to the Trt-Cl resin. They hypothesized that the presence of the electron-withdrawing chloro substituent in the 2-CTC resin increases the risk of  $\beta$ -elimination by increasing the leaving group ability of the protected thiol resulting in peptide loss from the resin during each piperidine deprotection cycle, as shown in Figure 52.



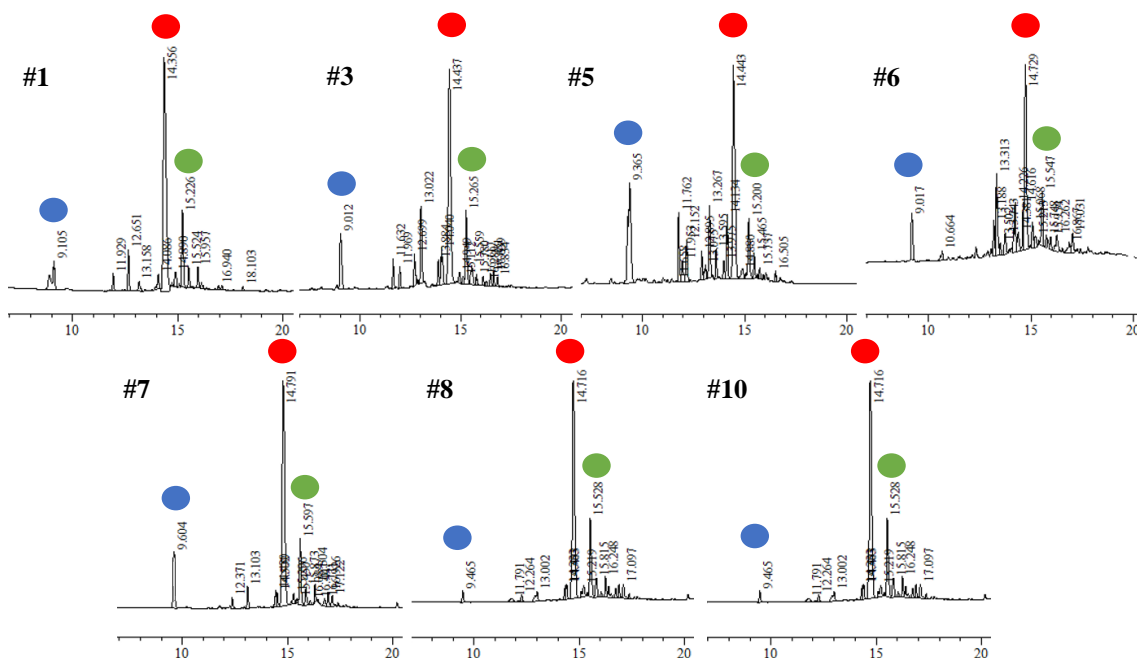
**Figure 52:**  $\beta$ -elimination side reaction produced each piperidine deprotection cycle. B: piperidine; R: growing peptide chain.

Hence, we employed Trt-Cl resin in our synthesis, firstly in small scale (entry #7, Table 10), and the cleavage yield was successfully increased from 40 % to 68 %. Regarding the purity of the obtained crude (Figure 53 #7), our compound yields only 45 % whereas 10 % corresponded to the fragment ALeu-Dab-Dab-Ttr (peak at 9.4 min), coming from the ester hydrolyzation, and 14 % of the crude corresponded to a *tert*-butylated peptide (M+56 peak at 15.59 min). In order to tackle the hydrolyzation side reaction, we removed the water from the cleavage reagent and used anhydrous Et<sub>2</sub>O to precipitate the peptide after cleavage. Moreover, we increased the cleavage treatment to 60 minutes to facilitate the deprotection of threonine *tert*-butyl group (entry #8, Table 10). As a result, water removal readily decreased the hydrolyzation of the ester bond, and only 3 % of the crude correspond to the fragment 7-10 of the peptide (Figure 53 #8). Contrarily, the 60 minutes cleavage did not produce any improvement, since 14 % of the crude remained *tert*-butylated. Additional acidic treatments up to 60 minutes were performed onto the obtained peptide, but no significant changes were observed. Thus, we hypothesized that one thiol group had reacted irreversibly with a *tert*-butyl protecting group, probably the thiol group of the thiothreonine, due to their spatial proximity.

To overcome the *tert*-butylation problem we finally increased the total amount of scavengers on the cleavage cocktail to a 18 % of triethylsilane (entries #9 and #10, Table 10), and we performed the cleavage for 30 minutes obtaining a yield of 72 %. Unfortunately, 14 % of *tert*-butylated peak was still present (Figure 53 #10), although the global yield of the synthesis increased to nearly 20 %.

Further investigation can still be performed in order to maximize the reaction yields, such as shorten the time of piperidine treatments to completely avoid the premature peptide release or change the cleavage composition and conditions to eliminate the *tert*-butylation

side reaction, but at this point in time, the optimization was stopped because we were able to produce enough peptide to perform all *in vivo* experimentation planned.



**Figure 53:** Compound 27 crude HPLC chromatograms run at G0595t30 and processed at 220 nm.

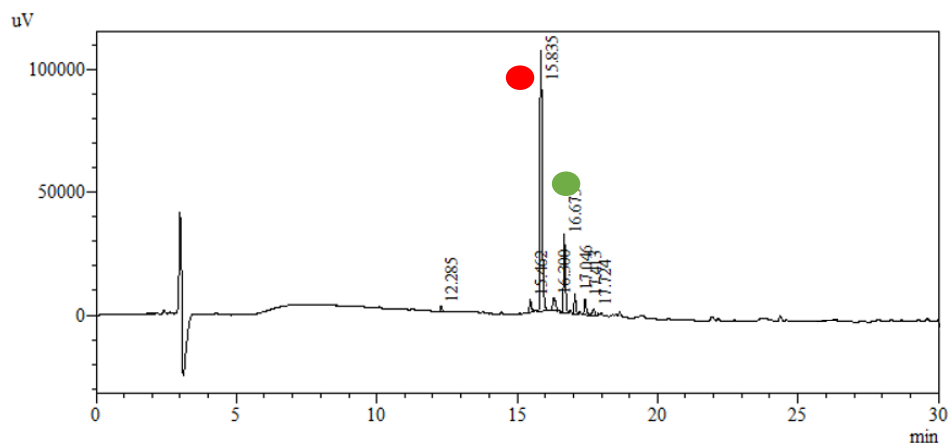
● = linear 27,  $C_{52}H_{93}N_{13}O_{12}S_2$ , exact mass: 1155.6, found 1156.7 [M + H]<sup>+</sup>; ● = hydrolyzed fragment 10-7  $C_{18}H_{37}N_5O_5S_2$ , exact mass: 435.2, found 436.2 [M + H]<sup>+</sup>; ● = *tert*-butylated peptide,  $C_{56}H_{101}N_{13}O_{12}S_2$ , exact mass: 1211.7, found 1212.5 [M + H]<sup>+</sup>.

#### 1.4.6.2. Compound 25

The previously optimized conditions used for the synthesis of peptide 27 were also employed to synthesize compound #25. Since #25 did not contain the ester bond, the synthesis was more straightforward, and the global yield increased to almost 40 % (entry #2, Table 11). Figure 54 shows the reaction crude achieved after the optimized cleavage, as observed for compound #27, a 16 % of *tert*-butylated peptide appeared at 16.67 min.

**Table 11:** Optimization and scale-up process of the synthesis of compound 25.

#	Resin type	Initial resin amount/loading	Coupling agents	Cleavage method	Cleavage yield	Crude purity	Pure peptide (free base)/ Global yield
1	2-CTC	126 mg 0.8 mmol·g <sup>-1</sup>	3 eq DIC 3 eq HOBt	TFA/TES/H <sub>2</sub> O (95:3:2) 30 min	42 %	67 %	29 mg (20 mg) 17 %
2	CTC	2.455 g 0.7 mmol·g <sup>-1</sup>	3 eq DIC 3 eq HOBt	TFA/TES (82:18) 30 min	78 %	71 %	1.197 mg (802 mg) 39 %



**Figure 54:** Compound 25 crude HPLC chromatogram run at G0595t30 and processed at 220 nm.

● = linear 25,  $C_{52}H_{93}N_{13}O_{12}S_2$ , exact mass: 1155.7, found 1156.8  $[M + H]^+$ ; ● = *tert*-butylated peptide,  $C_{56}H_{102}N_{14}O_{11}S_2$ , exact mass: 1210.7, found 1211.7  $[M + H]^+$ .

## 1.5. Peptide characterization

### 1.5.1. Complete ionic characterization of peptide salts

After cleavage and purification, cationic peptides are generally obtained as trifluoroacetate salts. Currently there are different options for the determination of counterions in pharmaceutical salts, the most commonly used in the industry are Ion Chromatography (IC) and Capillary Electrophoresis (CE).<sup>262</sup> However, there is still an important need to develop an easy and reliable method to use, for instance, in peptide laboratories. For that purpose, with the principal aim to characterize the ionic composition of our synthetic polymyxin B<sub>3</sub> depending on the exposure to different acids (HBr, TFA and HCl), we explored different techniques within our reach, such as CHNS elemental analysis, titration, or mass spectrometry. Finally, we found Electrospray Ionization High Resolution Mass Spectrometry (ESI-HR MS) to be an easy, rapid, and sensitive tool that permits the complete characterization of the counterions of a peptide salt.

#### 1.5.1.1. CHNS elemental analysis

CHNS elemental analysis provides a means for the rapid determination of carbon, hydrogen, nitrogen, and sulfur in organic matrices. This technique consists of the combustion of the sample in an oxygen-rich environment with the presence of certain catalysis where carbon is converted to carbon dioxide; hydrogen to water; nitrogen to nitrogen gas or oxides of nitrogen and sulfur to sulfur dioxide. The combustion products

are then detected by gas chromatography followed by quantification using thermal conductivity detection.

This technique is an easy, rapid, and cheap method to analyze the elemental composition of a pure peptide composed of C, N, H, S and therefore it can only provide information about sulfate counter ions, for instance, while anions such as chloride, bromide or trifluoroacetate cannot be detected using this technique. Hence this method was not sufficiently convenient for ionic content characterization of our polymyxin B<sub>3</sub> samples, which could contain bromide or trifluoroacetate or a mixture of both ions. But we decided to explore the scope of this technique using the commercially available polymyxin B sulfate.

As previously mentioned, polymyxin B is manufactured as a heterogeneous mixture of closely related lipopeptides and therefore, the empirical formula of this compound is not unique, and the obtained results can only provide approximate values. According to the supplier, each polymyxin molecule is associated with two sulfate counterions, which corresponds to an empirical formula  $C_{55}H_{96}N_{16}O_{13} \cdot 2H_2SO_4$ , and a theoretical sulfur content of 4.63 %. The experimental obtained result was close to this value, 4.22 % (Table 12), hence we can confirm that the commercial sample was composed of sulfate counterions, but this technique was not capable to completely elucidate the ionic composition of the sample because it could contain other minor non-analyzed elements.

**Table 12:** Summarized results of the NCHS analysis of Px.B.

<b>Element</b>	<b>Average</b>	<b>Standard deviation</b>	<b>% Relative SD</b>	<b>Variance</b>
<b>Nitrogen</b>	13.41	0.02887	0.2153	0.0008
<b>Carbon</b>	40.98	0.09238	0.2254	0.0085
<b>Hydrogen</b>	8.22	0.01528	0.1858	0.0002
<b>Sulphur</b>	4.22	0.05000	1.1848	0.0025

#### 1.5.1.2. Chloride determination by titration

Other interesting technique to analyze the counter ion content of a sample is titration. Specifically, Volhard's Titration Method is a very useful technique to easily analyze the chloride content of a sample quantitatively. It consists of a back titration using silver nitrate and potassium thiocyanate.

Unfortunately, this methodology is not suitable for peptide synthesis in laboratory scale, because an important amount of sample is required to perform each titration (about 70 to 100 mg). For that reason, our synthetically obtained polymyxin B<sub>3</sub> was not analyzed by this method, but we tested a polymyxin B chloride sample prepared from the commercial polymyxin B sulfate. For that purpose, the commercial sample was neutralized using equimolar amounts of KOH 0.1 M to obtain the counter-ion free polymyxin B as a solid compound completely insoluble in neutral aqueous conditions. The obtained free-base polymyxin was then redissolved in aqueous HCl until its complete dissolution, thus obtaining the commercial polymyxin B as the chloride salt.

Finally, using the titration method, a 12.70 %, (SD = 0.00087) content of chloride was obtained, which correlates perfectly with the theoretical calculated content (12.79 %). Therefore, we can conclude that titration method is an easy and rapid tool to accurately determine the chloride content of peptide samples, but it cannot detect other counter ions such as trifluoroacetates or bromides and it is not compatible to small scale synthesis.

#### 1.5.1.3. Electrospray ionization mass spectrometry

ESI-MS is typically adjusted to desolvate and remove all counter ion complexes and clusters, because clusters usually reduce analyte signals and complicate mass spectra. However, there is the possibility to modulate different parameters such as the capillary temperature and/or extraction voltages to observe clusters of the protonated peptide with its associated counter ions.<sup>263</sup>

To explore the scope of this technique three samples collected in different stages of the polymyxin B<sub>3</sub> synthesis were analyzed: (1) a crude sample collected after the treatment with HBr mixture; (2) pure polymyxin B<sub>3</sub> collected after purification using 0.1 % TFA eluents; and (3) pure polymyxin B<sub>3</sub> collected after lyophilization with an HCl excess.

The study was performed by the Mass Spectrometry and Proteomics Core Facility at the Institute for Research in Biomedicine (IRB Barcelona). Samples were analyzed in an Orbitrap Fusion Lumos™ Tribrid (Thermo Scientific) mass spectrometer with an Advion Triversa Nanomate (Advion BioSciences, Ithaca, NY, USA) electrospray source was used. The electrospray needle voltage was set to -1.7 kV, and the heated capillary was kept at



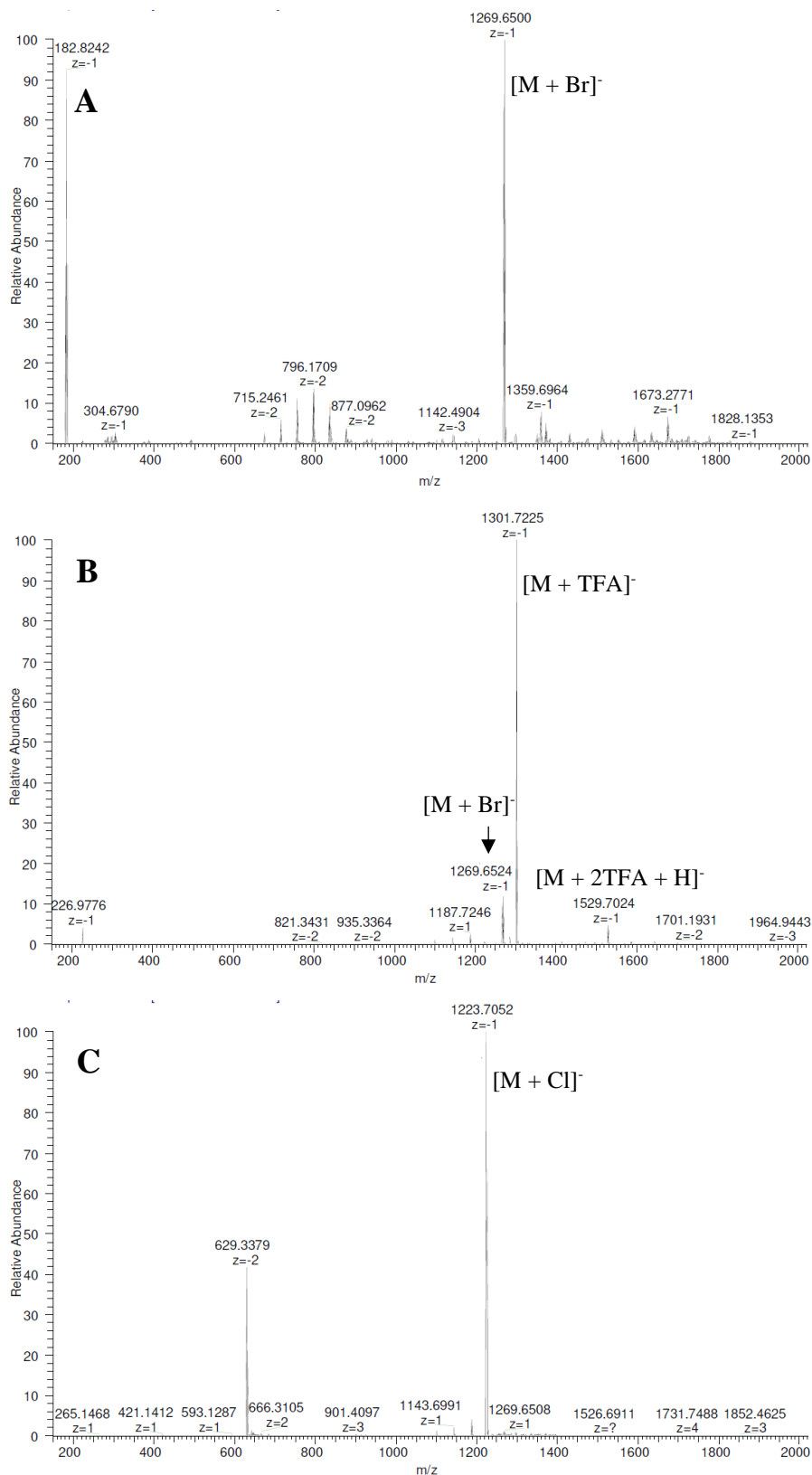
275 °C. The obtained spectra are shown in Figure 55 and the detailed analysis of each specie compared with its theoretical spectrum is shown in Appendix IX.

In the first analyzed sample, corresponding to the reaction crude after acidic treatment with HBr, the species  $[M + Br]^-$ ,  $[M + 2Br + H]^-$ ,  $[M + 3Br + 2H]^-$ ,  $[M + 4Br + 3H]^-$  and  $[M + 5Br + 4H]^-$  were detected, being  $[M + Br]^-$  the main specie. Clusters of  $PxB_3$  with TFA were not observed.

The second studied polymyxin  $B_3$  sample had been purified using conventional gradients of acetonitrile-water-trifluoroacetic acid. After purification in TFA excess, the bromide counter ions appeared to be exchanged by trifluoroacetates and our peptide was obtained as a TFA salt. The species  $[M + TFA]^-$ ,  $[M + 2TFA + H]^-$ ,  $[M + 3TFA + 2H]^-$ ,  $[M + 4TFA + 3H]^-$  and  $[M + 5TFA + 4H]^-$  were observed, whereas a unique peptide cluster with bromide was detected  $[M + Br]^-$ , being  $[M + TFA]^-$ ,  $[M + Br]^-$  and  $[M + 3TFA + H]^-$  the most abundant species. Apparently, there were no mixed species such as  $[M + Br + TFA + H]^-$ .

Finally, the hydrochloride salt of polymyxin  $B_3$  was analyzed. It was obtained after repetitive cycles of peptide dissolution and lyophilization in the presence of an excess of HCl. In this case, the detected species were  $[M + Cl]^-$ ,  $[M + 2Cl + H]^-$ ,  $[M + 3Cl + 2H]^-$ ,  $[M + 4Cl + 3H]^-$  and  $[M + 5Cl + 4H]^-$ , being  $[M + Cl]^-$  the most abundant specie. No traces of TFA salt were detected, thus indicating that the counter ion exchange had been completed.

Unlike the two techniques discussed above (CHNS elemental analysis and chloride titration), ESI-HR MS demonstrated to be a highly effective technique to study all clusters formed between a peptide and its counter ions, being possible to identify multiple counter ion species, such as bromide, trifluoroacetate and chloride anions. Furthermore, the amount of sample required for each analysis (around 0.1 mg) is perfectly compatible with peptide synthesis at the laboratory scale.



**Figure 55:** Spectra obtained by ESI-HR MS in negative mode for samples: A) PxB<sub>3</sub> after HBr deprotection treatment; B) purified PxB<sub>3</sub>; C) PxB<sub>3</sub> as hydrochloride salt.

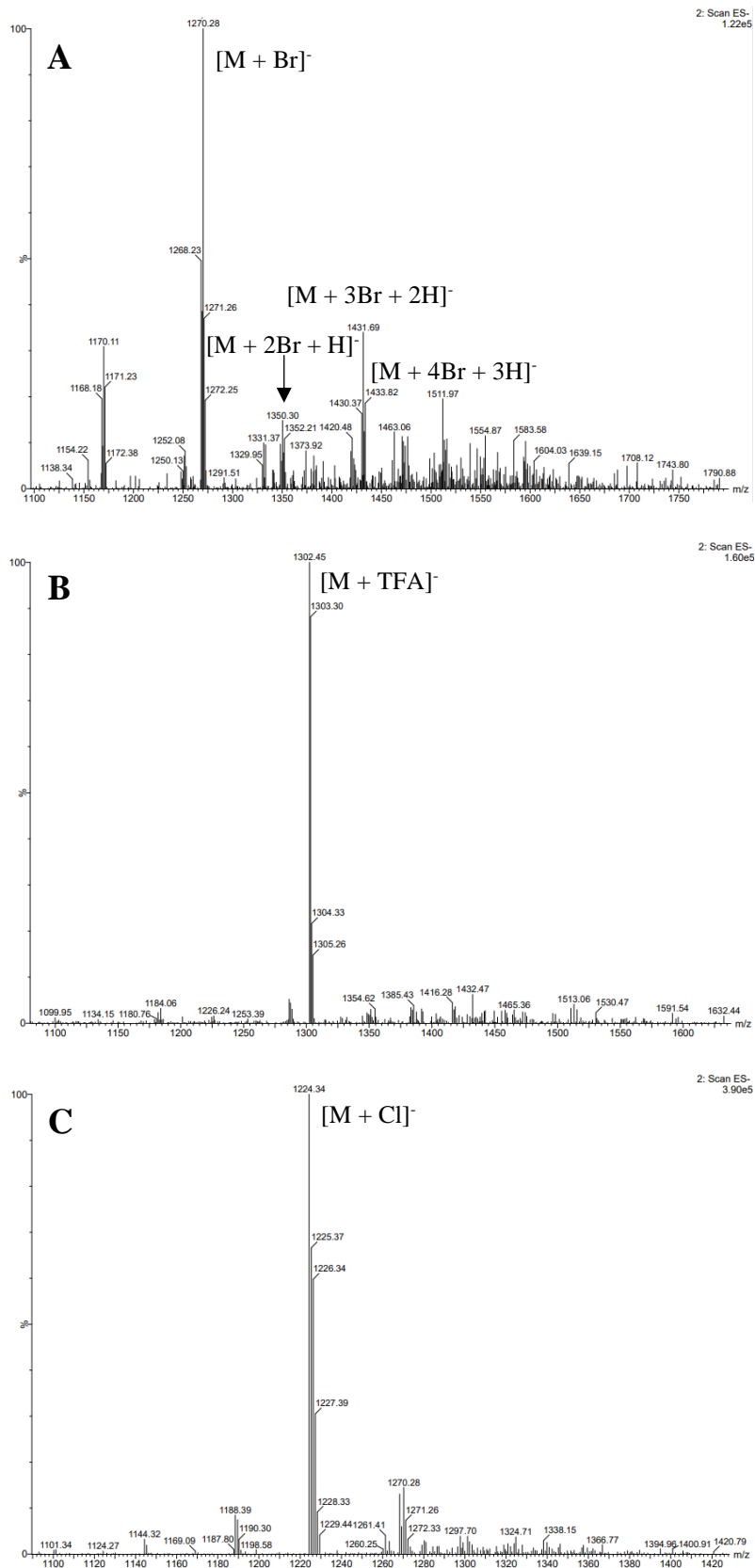
Considering these excellent results, we finally explored the technique using basic ESI MS spectrometry instead of the high-resolution instrumentation. For that purpose, a Waters instrument was employed comprising Waters 2695 separation module, a Waters 2996 photodiode array detector, a Waters ESI-MS Micromass ZQ 4000 spectrometer, and a Masslynx v4.1 system controller. The electrospray needle voltage was set to -2 kV, and the heated capillary was kept at 300 °C.

Remarkably, bromide clusters appeared to be the more easily identified with this ESI MS optimized conditions, being possible to identify the species  $[M + Br]^-$ ,  $[M + 2Br + H]^-$ ,  $[M + 3Br + 2H]^-$  and  $[M + 4Br + 3H]^-$ , whereas only  $[M + TFA]^-$  and  $[M + Cl]^-$  clusters were identified in the other samples (Figure 56). Further optimization of the ionization parameter could lead to better results for those ions.

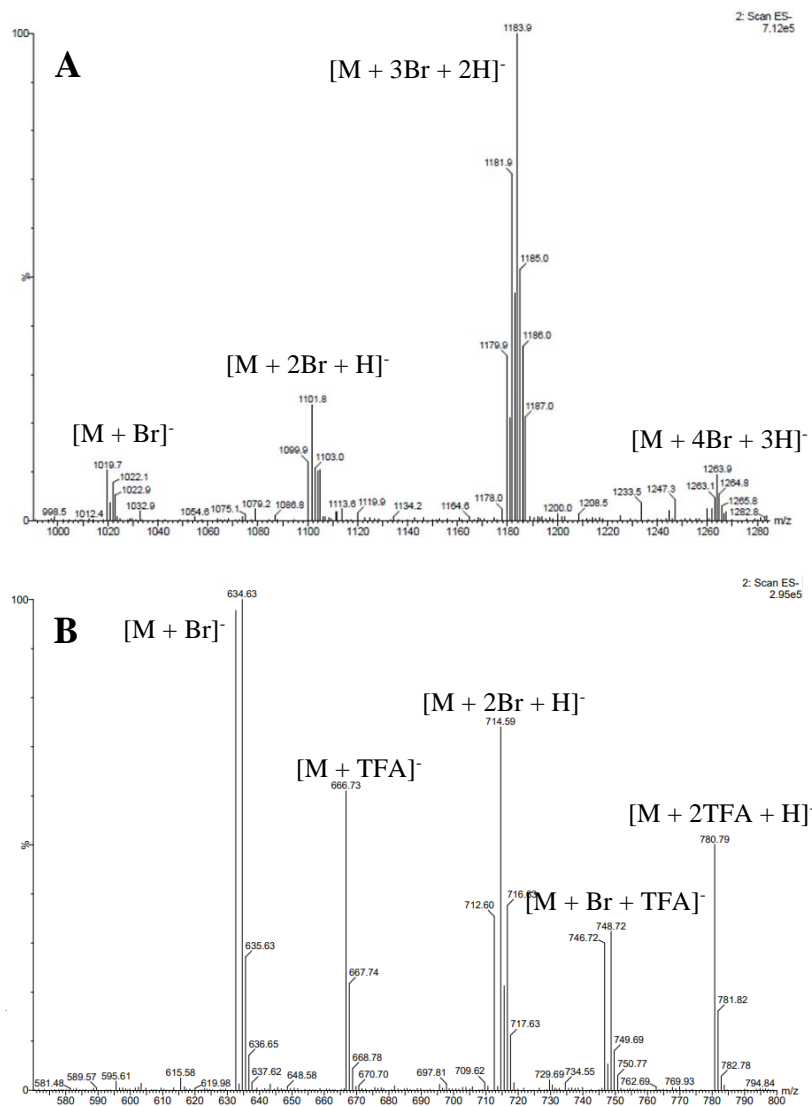
The crude of reaction of dusquetide and RR4 were also subjected to ion analysis through ESI MS. The detected species for RR4 were  $[M + Br]^-$ ,  $[M + 2Br + H]^-$ ,  $[M + 3Br + 2H]^-$ , and  $[M + 4Br + 3H]^-$ , where  $[M + 3Br + 2H]^-$  was the main ones. Regarding dusquetide, the clusters  $[M + Br]^-$ ,  $[M + TFA]^-$ ,  $[M + 2Br + H]^-$ ,  $[M + 2TFA + H]^-$ , and  $[M + Br + TFA + H]^-$  were detected. Contrary to polymyxin and RR4, mixed clusters of bromide and trifluoroacetate were detected for dusquetide. Mass spectra of both peptides are shown in Figure 57.

In conclusion, we found ESI-HR MS to be a complete and very useful technique to fully characterize the counterion composition of cationic peptides, being possible to elucidate the whole salt composition of the synthesized polymyxin B<sub>3</sub> after its exposure to different acids during the synthesis. ESI MS instrumentation proved to be less sensitive than high resolution spectrometry, as expected, but it was possible to determine the main species of each sample  $[M + Br]^-$ ,  $[M + TFA]^-$  and  $[M + Cl]^-$ .

Electrospray ionization mass spectrometry was also employed for the characterization of the 31 polymyxin analogues synthesized in the present thesis, a complete summary of the obtained results is shown in experimental section 3.1.3.



**Figure 56:** Spectra obtained by ESI MS in negative mode for samples: A) reaction crude of PxB<sub>3</sub> after HBr deprotection treatment; B) purified PxB<sub>3</sub>; C) PxB<sub>3</sub> as hydrochloride salt.



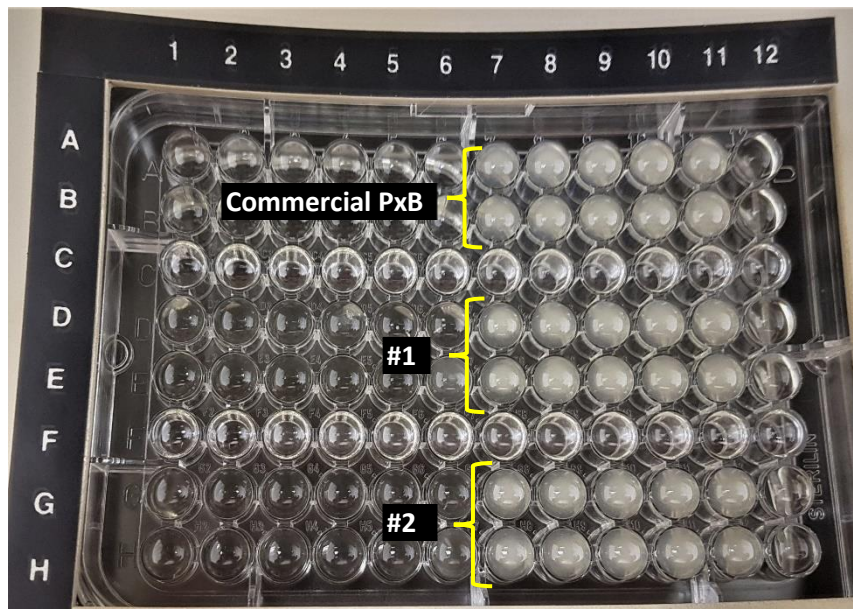
**Figure 57:** Spectra obtained by ESI MS in negative mode for samples: a) crude RR4; b) crude dusquetteide.

## 1.6. Antimicrobial activity

The antimicrobial activities of the synthesized compounds were obtained as their minimum inhibitory concentrations (MICs). The assay consisted in serial to-fold dilutions from 0.06 to 32  $\mu\text{g}\cdot\text{mL}^{-1}$  of peptide which were inoculated with a standardized number of microorganisms ( $10^6$  CFU $\cdot\text{mL}^{-1}$ ) and incubated at 37 °C for 18 h. The MIC was determined visually on the basis of turbidity as the lowest concentration inhibiting bacterial growth. Further information of the experiment is enclosed in experimental section 3.1.2.3. An example of microtiter plate used is shown in Figure 58.

Considering that the MIC of a given compound is the lowest concentration of antibacterial agent that inhibits the visible bacterial growth after 18 hours of treatment, the lower the

obtained value, the higher the antimicrobial potency of this compound. In fact, it is commonly accepted that a compound is considered to have a low activity when its MIC is higher than  $4 \mu\text{g}\cdot\text{mL}^{-1}$ .



**Figure 58:** Example of 96-well microtiter plate used in the MIC test of three different peptides (A and B: natural PxB; D and E: analogue #1; and G and H: analogue #2, C and F rows are empty) against *Pseudomonas aeruginosa*. The columns 1 - 10 contain different concentrations of the peptide tested in MHB ( $32 - 0.06 \mu\text{g}\cdot\text{mL}^{-1}$ ). Column 11 corresponds to the growth control and column 12 is the sterility control. Observing the plate used as example, MIC value of the three tested peptides is  $1 \mu\text{g}\cdot\text{mL}^{-1}$  (column 6 is the first column without bacterial growth).

### 1.6.1. Polymyxin B<sub>3</sub>

PxB<sub>3</sub> was tested with different counter ions in order to evaluate the influence of the ionic composition in the *in vitro* experimentation. Commercially available PxB sulfate, the PxB<sub>3</sub> obtained after purification, which is mainly composed by trifluoroacetate ions, and PxB<sub>3</sub> hydrochloride salt were tested. All compounds showed the same antimicrobial activities, with MICs of  $1 \mu\text{g}\cdot\text{mL}^{-1}$  against *Pseudomonas aeruginosa*. Therefore, it can be concluded that the presence of different counter ions in polymyxin has no significant impact on the antimicrobial activity.

### 1.6.2. Depsipeptide analogues

According to the obtained results summarized in Table 13, it can be concluded that the introduction of an ester bond in the peptide sequence does not affect the activity of the

polymyxin analogues, because the three synthesized compounds maintain the activity of natural polymyxin B against the Gram-negative bacterial strains. Remarkably, compound #3, which lacks 1-Dab and the *N*-terminal fatty acid, shows an even improved activity against *Acinetobacter baumannii* compared to the parent compound. This fact is highly encouraging, since the introduction of a metabolizable ester bond along with the reduction of the basicity of the amino group at position 1 and the removal of the fatty acid may reduce the toxicity of the molecule.

**Table 13:** Minimum inhibitory concentrations of the depsipeptide analogues. Peptide sequences are displayed in three-letter code, the cyclic segment is given in brackets.

	Sequence	MIC ( $\mu\text{g}\cdot\text{mL}^{-1}$ )			
		EC	PA	AB	SA
<b>PxB</b>	6MOA-Dab-Thr-Dab-[Dab-Dab-DPhe-Leu-Dab-Dab-Thr]	1	1	0.25	>32
<b>1</b>	C8-Dab-Thr-Dab-[Dab-Dab-DPhe-ALeu-Dab-Dab-Thr]	1	1	0.25	>32
<b>2</b>	C9-Dab-Thr-Dab-[Dab-Dab-DPhe-ALeu-Dab-Dab-Thr]	1	1	0.125	>32
<b>3</b>	DAdec-Thr-Dab-[Dab-Dab-DPhe-ALeu-Dab-Dab-Thr]	1	1	0.125	>32

EC: *Escherichia coli* ATCC 25922; PA: *Pseudomonas aeruginosa* ATCC 27853; AB: *Acinetobacter baumannii* ATCC 19606; SA: *Staphylococcus aureus* ATCC 25923.

### 1.6.3. Cysteine analogues

The obtained results are summarized in Table 14. Analogue #4, which contained an hexanoyl chain placed at *N*-terminal position, was devoid of antimicrobial activity, with MIC values higher than  $32 \mu\text{g}\cdot\text{mL}^{-1}$  for both Gram-negative and Gram-positive bacteria. This fact denotes that a minimum length in the hydrophobic *N*-terminus is needed for activity. Analogue #5, which was the canonical cysteine analogue of PxB<sub>3</sub>, showed some activity, especially against *Pseudomonas aeruginosa*, but lower than the natural polymyxin, thus suggesting that the modification of the macrolactam cycle reduces the potency of the drug. Interestingly, analogues with long fatty acid tails such as #6 and #7, with decanoyl and dodecanoyl respectively, were slightly active against Gram-positive bacteria, in addition to their good activity against Gram-negative bacteria.

Regarding the compounds that contain norleucine at position 7, excellent activities were obtained, some of them comparable to polymyxin B. Comparing analogue #5 with #8, which only differed in the residue at position 7, the MIC values obtained by the compound with norleucine are 8-fold lower in the case of *Escherichia coli*. As the leucine analogues,

compounds #10 and #11 with long fatty acyl chains presented high antimicrobial activity against Gram-positive *Staphylococcus aureus*.

**Table 14:** Minimum inhibitory concentration of the cysteine analogues. Peptide sequences are displayed in three-letter code, the cyclic segment is given in brackets.

	Sequence	MIC ( $\mu\text{g}\cdot\text{mL}^{-1}$ )		
		EC	PA	SA
<b>PxB</b>	6MOA-Dab-Thr-Dab-[Dab-Dab-DPhe-Leu-Dab-Dab-Thr]	1	0.5	>32
<b>4</b>	C6-Dab-Thr-Dab-[Cys-Dab-DPhe-Leu-Dab-Dab-DCys]	>32	>32	>32
<b>5</b>	C8-Dab-Thr-Dab-[Cys-Dab-DPhe-Leu-Dab-Dab-DCys]	16	8	>32
<b>6</b>	C10-Dab-Thr-Dab-[Cys-Dab-DPhe-Leu-Dab-Dab-DCys]	2	4	8
<b>7</b>	C12-Dab-Thr-Dab-[Cys-Dab-DPhe-Leu-Dab-Dab-DCys]	16	8	8
<b>8</b>	C8-Dab-Thr-Dab-[Cys-Dab-DPhe-Nle-Dab-Dab-DCys]	2	4	>32
<b>9</b>	C9-Dab-Thr-Dab-[Cys-Dab-DPhe-Nle-Dab-Dab-DCys]	2	1	16
<b>10</b>	C10-Dab-Thr-Dab-[Cys-Dab-DPhe-Nle-Dab-Dab-DCys]	2	1	4
<b>11</b>	C12-Dab-Thr-Dab-[Cys-Dab-DPhe-Nle-Dab-Dab-DCys]	4	1	2

EC: *Escherichia coli* ATCC 25922; PA: *Pseudomonas aeruginosa* ATCC 27853; SA: *Staphylococcus aureus* ATCC 25923.

Thus, considering the obtained results, it can be concluded that highly hydrophobic compounds such as #10 and #11, with C10 or C12 *N*-terminal chains and 7-Nle residue, were the most potent compounds with a broad spectrum of activity against both Gram-negative and Gram-positive bacterial strains. But there were also other interesting compounds that show considerable activity and selectivity towards Gram-negative bacteria, this is the case of #6, #8 and #9, which contained a C8 or C9 *N*-terminal fatty acyl chain.

#### 1.6.4. Second series of cysteine analogues

In the second series of cysteine analogues the hydrophobicity of the *N*-terminal fatty acid chain was transferred within the macrocycle by replacing the 6-D-Phe residue by 6-D-Trp and 6-D-Aoc. Obtained results are shown in Table 15, all analogues that included the 6-D-Trp residue in the structure were poorly active compared with polymyxin. In fact, compound #14 presented 4-fold bigger MIC values compared with compound #8, its counterpart with D-Phe. However, better results were obtained from the analogues with 6-D-Aoc, especially against *Pseudomonas aeruginosa*, being #19 the most promising compound with comparable activity to polymyxin.



Surprisingly, all analogues did not show remarkable activity against the Gram-negative bacterium *Acinetobacter baumannii*. No activity was either shown on Gram-positive bacteria, so that, the transfer of the hydrophobicity from the *N*-terminus to the macrocycle resulted in quite selective analogues against *Pseudomonas aeruginosa*.

Furthermore, contrarily to the behaviour observed in compounds #1, #2 and #3, where the introduction of an ester bond did not influence the antimicrobial activity, compound #18, which was the depsipeptide analogue of #19, presented 2-fold bigger MIC values, suggesting that the ester bond introduction weaken antibacterial potency.

**Table 15:** Minimum inhibitory concentration of the cysteine analogues. Peptide sequences are displayed in three-letter code, the cyclic segment is given in brackets.

	Sequence	MIC ( $\mu\text{g}\cdot\text{mL}^{-1}$ )			
		EC	PA	AB	SA
<b>PxB</b>	6MOA-Dab-Thr-Dab-[Dab-Dab-DPhe-Leu-Dab-Dab-Thr]	1	1	0.25	>32
<b>12</b>	C6-Dab-Thr-Dab-[Cys-Dab-DTrp-Nle-Dab-Dab-DCys]	16	16	>32	>32
<b>13</b>	C7-Dab-Thr-Dab-[Cys-Dab-DTrp-Nle-Dab-Dab-DCys]	16	8	>32	32
<b>14</b>	C8-Dab-Thr-Dab-[Cys-Dab-DTrp-Nle-Dab-Dab-DCys]	8	8	>32	32
<b>15</b>	C6-Dab-Thr-Dab-[Cys-Dab-DAoc-ALeu-Dab-Dab-DCys]	8	4	16	>32
<b>16</b>	C7-Dab-Thr-Dab-[Cys-Dab-DAoc-ALeu-Dab-Dab-DCys]	4	2	16	>32
<b>17</b>	C8-Dab-Thr-Dab-[Cys-Dab-DAoc-ALeu-Dab-Dab-DCys]	4	2	8	>32
<b>18</b>	DAoc-Thr-Dab-[Cys-Dab-DAoc-ALeu-Dab-Dab-DCys]	8	4	16	16
<b>19</b>	DAoc-Thr-Dab-[Cys-Dab-DAoc-Leu-Dab-Dab-DCys]	4	1	8	32

EC: *Escherichia coli* ATCC 25922; PA: *Pseudomonas aeruginosa* ATCC 27853; SA: *Staphylococcus aureus* ATCC 25923.

### 1.6.5. Hydroxamic acid analogues

The obtained MIC values of hydroxamic acid analogues are shown in Table 16. Analogue #p1, which had been previously synthesized in our group, was also tested to evaluate the influence of the introduction of the hydroxamic acid. Results did not demonstrate any significant improvement on the antibacterial activity. The activity was neither considerably affected by the change of D and L configuration of the cysteine at position 10. Furthermore, as it was previously discussed, polymyxin analogues containing the disulfide modification showed low activity against *Acinetobacter baumannii*.

It should be noted that hydroxamic acid analogues showed selectivity against *Pseudomonas aeruginosa*, being compound #20 the most active analogue.

**Table 16:** Minimum inhibitory concentration of the hydroxamic acid analogues. Peptide sequences are displayed in three-letter code, the cyclic segment is given in brackets.

	Sequence	MIC ( $\mu\text{g}\cdot\text{mL}^{-1}$ )			
		EC	PA	AB	SA
<b>PxB</b>	6MOA-Dab-Thr-Dab-[Dab-Dab-DPhe-Leu-Dab-Dab-Thr]	1	1	0.25	>32
<b>p1</b>	C9-Dab-Thr-Dab-[Cys-Dab-DPhe-Leu-Dab-Dab-Cys]	8	2	>32	32
<b>20</b>	C9-Dab-Thr-Dab-[Cys-Dab-DPhe-Leu-Dab-Dab-DCys-NHOH]	16	2	>32	16
<b>21</b>	C9-Dab-Thr-Dab-[Cys-Dab-DPhe-Leu-Dab-Dab-Cys-NHOH]	8	4	>32	32
<b>22</b>	C9-Dab-Thr-Dab-[Cys-Dab-DPhe-ALeu-Dab-Dab-DCys-NHOH]	16	8	>32	32
<b>23</b>	C9-Dab-Thr-Dab-[Cys-Dab-DPhe-ALeu-Dab-Dab-Cys-NHOH]	8	8	32	16

EC: *Escherichia coli* ATCC 25922; PA: *Pseudomonas aeruginosa* ATCC 27853; SA: *Staphylococcus aureus* ATCC 25923.

### 1.6.6. Thiiothreonine analogues

In Table 17 are shown the antimicrobial activity results of thiothreonine polymyxin analogues. Compounds #24 and #25 presented a high selectivity against Gram-negative bacteria, showing comparable values to polymyxin against *Escherichia coli* and *Pseudomonas aeruginosa*. Remarkably, these thiothreonine compounds presented a promising activity against *Acinetobacter baumannii*, differing from the cysteine analogues which showed low activity against this bacterial strain. Therefore, these results confirmed that the side chain of the residue located at position 10 plays a crucial role in the antimicrobial activity, and the use of the novel thiothreonine moiety is an important advance in the synthesis of new polymyxin analogues with an easily accessible backbone and a disulfide bond embedded in the structure.

As previously observed, the introduction of an extra scissile bond in the structure implies a 2-fold increase in the MIC, being less potent the depsipeptide analogues #26 and #27. However, the obtained values were highly promising considering that compound #27 contained 2 metabolizable bonds and it lacks 1-Dab residue, modifications that could potentially reduce the toxicity of the drug.

Poor antimicrobial potency was obtained for analogues #28 to #31 against *Acinetobacter baumannii* and *Escherichia coli*, however they were selective against *Pseudomonas aeruginosa*. No remarkable differences between them were observed.

**Table 17:** Minimum inhibitory concentration of the cysteine-cysteine analogues. Peptide sequences are displayed in three-letter code, the cyclic segment is given in brackets.

Sequence	MIC ( $\mu\text{g}\cdot\text{mL}^{-1}$ )			
	EC	PA	AB	SA
<b>PxB</b> 6MOA-Dab-Thr-Dab-[Dab-Dab-DPhe-Leu-Dab-Dab-Thr]	1	1	0.25	>32
<b>24</b> C8-Dab-Thr-Dab-[Cys-Dab-DPhe-Leu-Dab-Dab-Ttr]	2	1	1	>32
<b>25</b> DAdec-Thr-Dab-[Cys-Dab-DPhe-Leu-Dab-Dab-Ttr]	1	1	1	>32
<b>26</b> C8-Dab-Thr-Dab-[Cys-Dab-DPhe-ALeu-Dab-Dab-Ttr]	4	2	2	>32
<b>27</b> DAdec-Thr-Dab-[Cys-Dab-DPhe-ALeu-Dab-Dab-Ttr]	2	2	4	>32
<b>28</b> C8-Dab-Thr-Dap-[Cys-Dab-DPhe-Abu-Dab-Dab-Ttr]	8	2	>32	>32
<b>29</b> DAdec-Thr-Dap-[Cys-Dab-DPhe-Abu-Dab-Dab-Ttr]	2	1	4	>32
<b>30</b> C8-Dab-Thr-Dab-[Cys-Dab-DPhe-Nva-Dab-Dab-Ttr]	8	2	16	>32
<b>31</b> DAdec-Thr-Dab-[Cys-Dab-DPhe-Nva-Dab-Dab-Ttr]	2	1	4	>32

EC: *Escherichia coli* ATCC 25922; PA: *Pseudomonas aeruginosa* ATCC 27853; AB: *Acinetobacter baumannii* ATCC 19606; SA: *Staphylococcus aureus* ATCC 25923.

### 1.6.7. Summary

As previously mentioned, our principal objective in the design of the analogues was to include metabolizable bonds on the structure that could facilitate the ring opening upon accumulation in renal cells. We observed that the introduction of a disulfide bond formed by two cysteine residues produced an important decrease on the antimicrobial activity of polymyxin B. Therefore, following the approximation of the disulfide bond, we designed the thiothreonine analogues, which contained a synthetic residue at position 10 that mimic the structure of the natural Thr but including a thiol group that allows the formation of the disulfide bond with a cysteine residue placed at position 4. This modification led to highly active and selective compounds with comparable activities than the natural polymyxin B.

Other explored way to introduce metabolizable bonds on the structure was the design of depsipeptide analogues. We found that the introduction of an ester bond situated between positions 6 and 7 generally yielded compounds 2-fold less active.

Apart from the scissile bond introduction, we explored the influence of hydrophobicity in polymyxin analogues. Firstly, we proposed a small set of 9 polymyxin B analogues with different *N*-terminal fatty acid length and a norleucine residue at position 7. We came to the conclusion that a minimum length of C8 fatty acid tail is compulsory for

antimicrobial activity, and hydrophobicity is highly related with antimicrobial activity and hemolysis, being C12 analogues the most active and hemolytic compounds. For that reason, we explored the redistribution of hydrophobicity from the *N*-terminal end of the molecule to the macrocycle, creating new analogues with shorter fatty acid tails but larger hydrophobic side chains at positions 6 and 7. With these modifications we concluded that, in our polymyxin analogues, long fatty acid chains generate highly potent compounds active against both Gram-negative and Gram positive bacteria, whereas the redistribution of the hydrophobicity generates highly active and selective compounds.

In order to potentially reduce polymyxin toxicity, some analogues also lacked 1-Dab and *N*-terminal fatty acid chain, which were replaced by D-Adec or D-Aoc residue. This modification appeared not to reduce the activity of the natural polymyxins.

Finally, the introduction of a *C*-terminal hydroxamic acid did not improve the antimicrobial activity of polymyxins.

In the view of that results, analogues #3, #10, #19, #24, #25, #26 and #27 were selected as the most promising candidates and were then subjected to new activity studies against resistant bacterial strains and *in vivo* experiments on a mice model in order to further narrow the number of candidates to one or two hit compounds (see section 1.8).

## **1.7. Evaluation of the mechanism of action**

### **1.7.1. Cysteine analogues**

With the main goal to explore the mechanism of action of polymyxin and its analogues, and further explore the influence of the *N*-terminal fatty acid length and the hydrophobicity of the molecule, different biophysical assays were performed on compounds #4 to #11, as well as toxicity studies on rabbit blood and transmission electron microscopy.

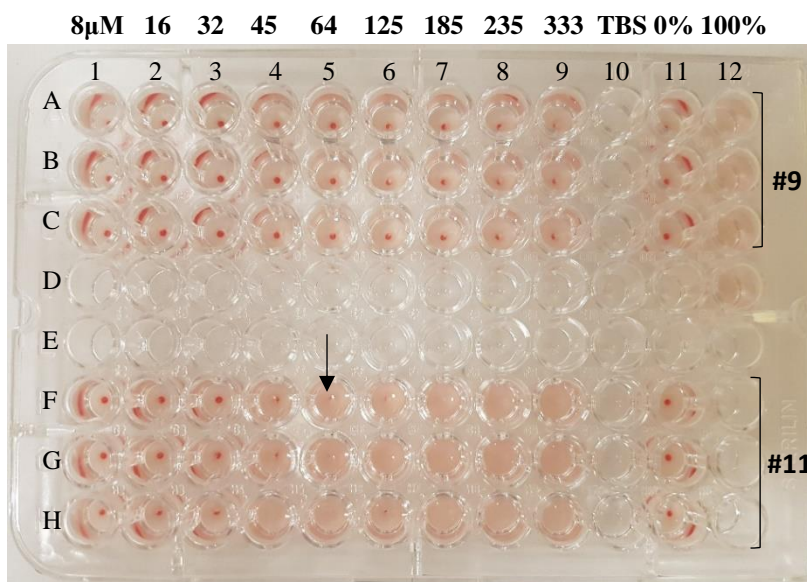
#### 1.7.1.1 Hemolysis

Antimicrobial peptides must be selective for prokaryotic membranes; a well-established method of verifying their ability to damage eukaryotic cell membranes is to measure the hemolytic activity (leakage of hemoglobin from red blood cells). Hemolysis was examined using blood from a healthy rabbit obtained from the Animal Experimentation

Unit of the Faculty of Pharmacy and Food Sciences of the University of Barcelona. Hemolytic activity was determined in a wide range of peptide concentrations, from 8  $\mu$ M to 333  $\mu$ M, which were incubated for 1 hour at 37 °C. Lipopeptide-induced hemolysis was determined by measuring the absorbance of released hemoglobin in the supernatant after sample centrifugation, and hemolysis values were calculated according to the equation:

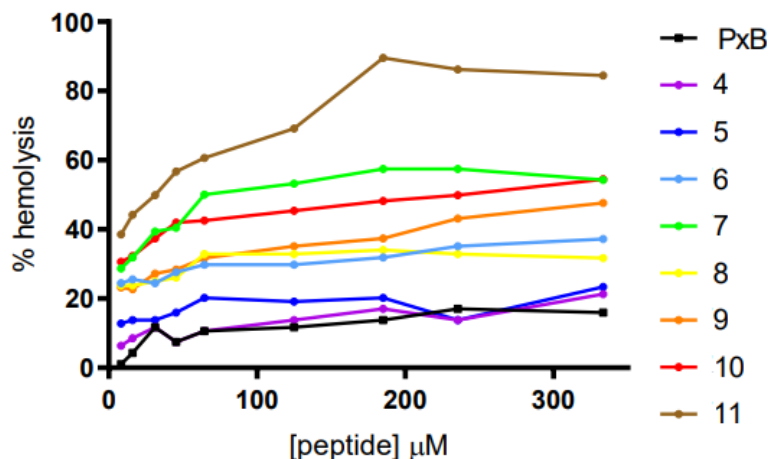
$$\% \text{ hemolysis} = [(A_{\text{obs}} - A_{0\%}) / (A_{100\%} - A_{0\%})] \cdot 100$$

Negative control (0 %) corresponds to erythrocytes exposed to TSB without peptide, whereas 100 % hemolysis corresponds to the treatment of the erythrocytes with the membrane lytic Triton X-100. An example of microtiter plate used in the assay is shown in Figure 59.

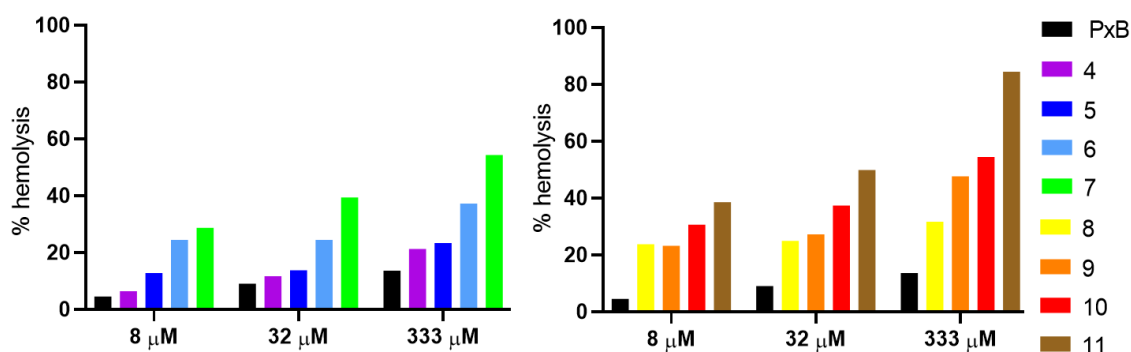


**Figure 59:** Example of 96-well microtiter plate used in the hemolysis assay of two different peptides (A to C: analogue #9; F to H: analogue #11; D and E rows are empty). The columns 1 - 9 contain the solutions of the peptide tested in the presence of rabbit erythrocytes (8 - 333  $\mu$ M of peptide) after centrifugation. Column 10 corresponds to buffer control, 11 to 0 % hemolysis and column 12 rows A to D, are the 100 % hemolysis. It could be observed that analogue #11 is highly hemolytic above 45  $\mu$ M (pointed out with an arrow), since there are not visible precipitated erythrocytes (red dots at the bottom) because red blood cells had been lysed.

Induction of hemolysis as function of peptide concentration is shown in Figure 60, and the percentages of hemolysis at some selected concentrations are presented in Figure 61.



**Figure 60:** Hemolysis induced by the synthetic analogues of PxB. Data corresponds to the average of three independent experiments (error <8 %).



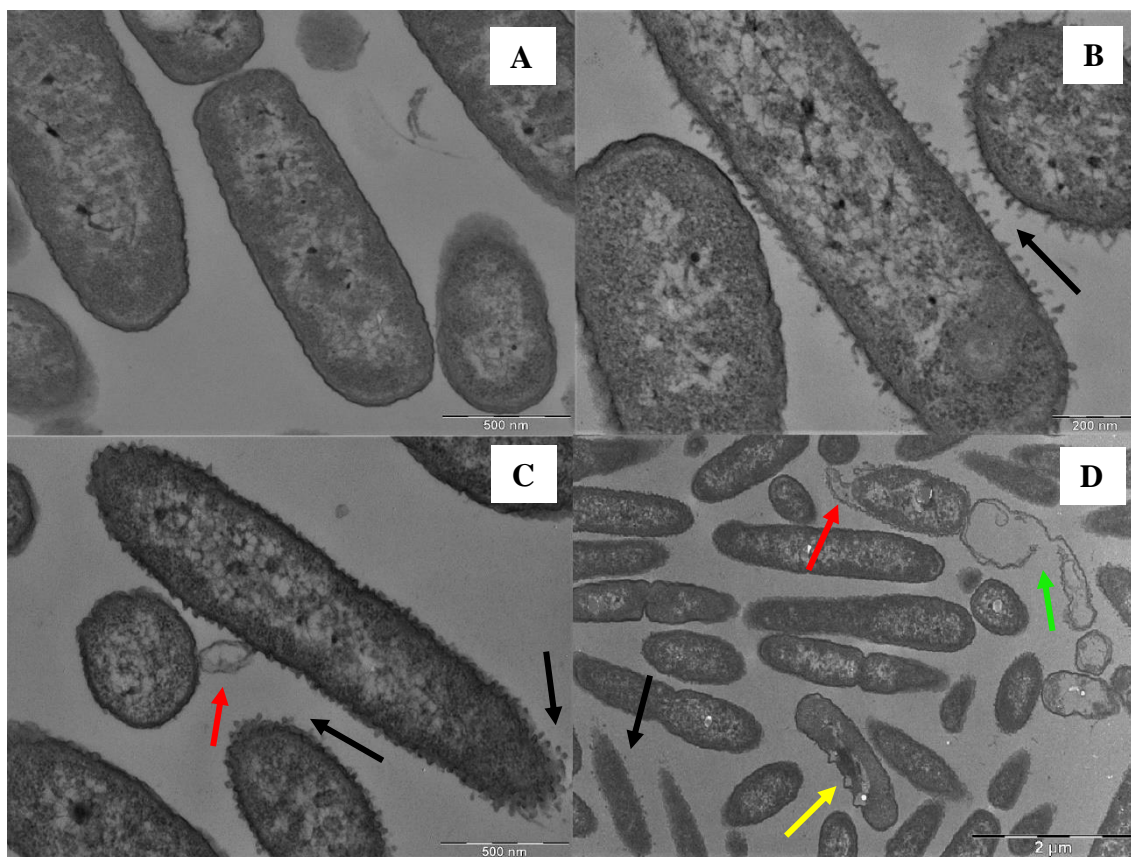
**Figure 61:** Summary of hemolysis induced by the synthetic analogues of PxB at 8, 32 and 333  $\mu\text{M}$ .

All analogues resulted mildly hemolytic at 8  $\mu\text{M}$ , concentration that is representative of the MIC of all compounds (MICs compressed between 1 and 13  $\mu\text{M}$ ). As it could be observed in Figure 61, there is a clear correlation between induction of hemolysis and the length of the fatty acid, being #4, which contains a C6 tail, the less hemolytic analogue and #7 and #11, the C12 analogues, the most lytic. Unfortunately, the introduction of a norleucine residue in the sequence increased the hemolytic effect.

Thus, it was demonstrated that the most hydrophobic compounds, which previously showed the most potent antibacterial activities, were also the most hemolytic compounds. However, #6, #8, #9 and #10 analogues, which presented good antimicrobial potency, maintained low levels of hemolysis, near 20 % at their MIC, suggesting that C8, C9 or C10 are the optimal fatty acid lengths for polymyxin analogues.

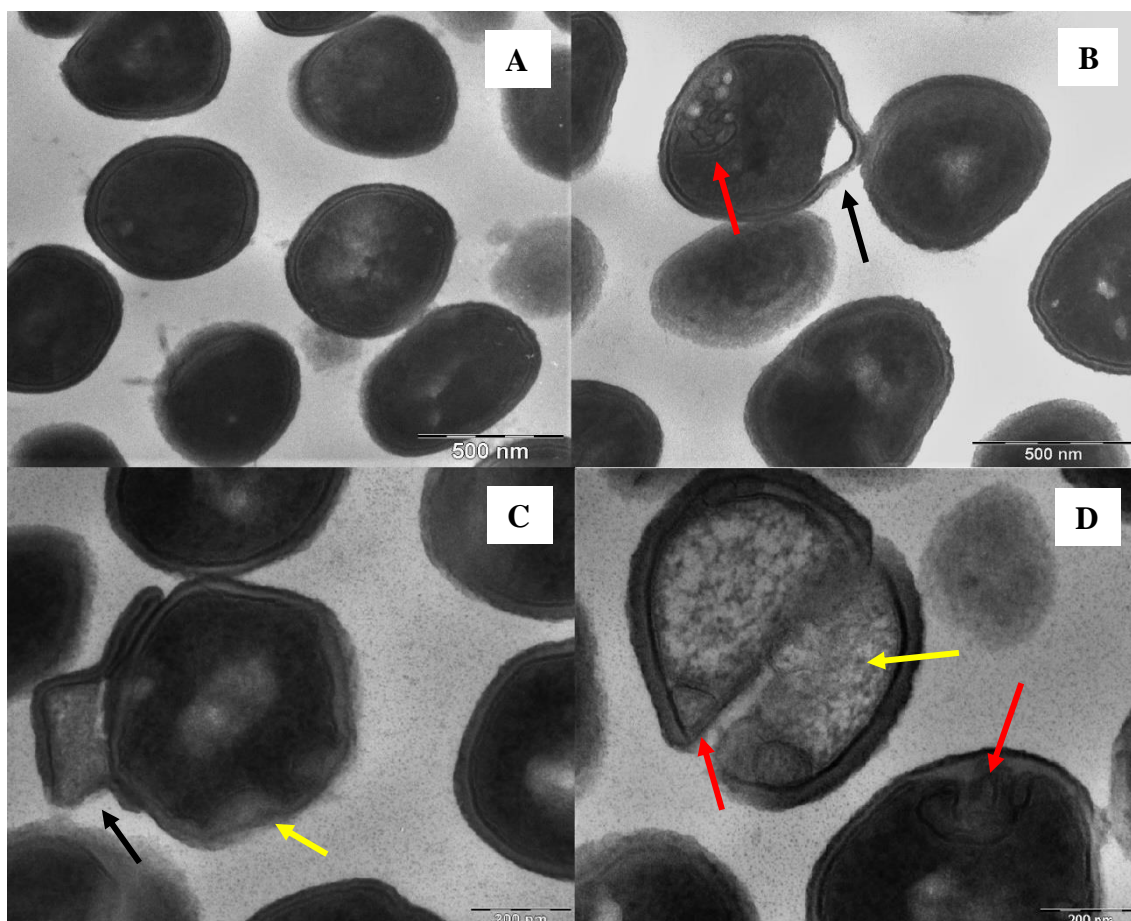
### 1.7.1.2. Transmission Electron Microscopy

Transmission electron microscopy was carried out to examine the membrane damage caused by analogue #6 in *Pseudomonas aeruginosa* and *Staphylococcus aureus* cells. Figure 62A shows untreated cells of *Pseudomonas aeruginosa* in tryptone water medium, with a normal rod shape, an undamaged inner membrane, and intact but slightly waved outer membrane. Incubation of this bacterium with compound PxB at the MIC ( $1 \mu\text{g}\cdot\text{mL}^{-1}$ ) caused the formation of outer membrane vesicles, also known as blebs, that protrude from the outer membrane (Figure 62B). Blebbing is an evidence of cell death,<sup>205,264</sup> and it is also caused by other AMPs such as gramicidin.<sup>265</sup> Compound #6 showed similar blebbing behaviour (Figure 62C), and occasioned the complete lysis of membranes and the leakage of the cytoplasmic material (Figure 62D).



**Figure 62:** Comparative TEM micrographs of *Pseudomonas aeruginosa*. A) untreated bacteria; B) after treatment with PxB at the MIC ( $1 \mu\text{g}\cdot\text{mL}^{-1}$ ); C and D) after treatment with compound #6 at the MIC ( $4 \mu\text{g}\cdot\text{mL}^{-1}$ ). Lipopeptides caused alteration of the membrane (yellow arrow), blebs (black arrows), leakage of intracellular contents (red arrows), and even ghost cells (green arrow).

The effects of compound #6 on Gram-positive bacteria were also determined. In Figure 63A, untreated *Staphylococcus aureus* shows a round shape and intact cell envelope. Upon incubation with compound #6 at the MIC ( $8 \mu\text{g}\cdot\text{mL}^{-1}$ ), we observed the formation of spherical mesosome-like structures (Figure 63B). Mesosomes are intracytoplasmic membrane inclusions which appear to be formed under conditions that affect bacterial viability. In fact, since cytoplasmic membrane is instrumental in cell wall synthesis and turnover, the perturbations produced by mesosome formation directly affect cell wall integrity.<sup>266</sup> Mesosome-like structures have also been reported in Gram-positive bacteria treated with amikacin, gentamicin or vancomycin.<sup>267</sup> Bacteria also exhibited important deformation of the cell envelope (Figure 63C) and cytoplasmic areas of low electron density, suggesting peptide-induced release of cytoplasmic material (Figure 63D).

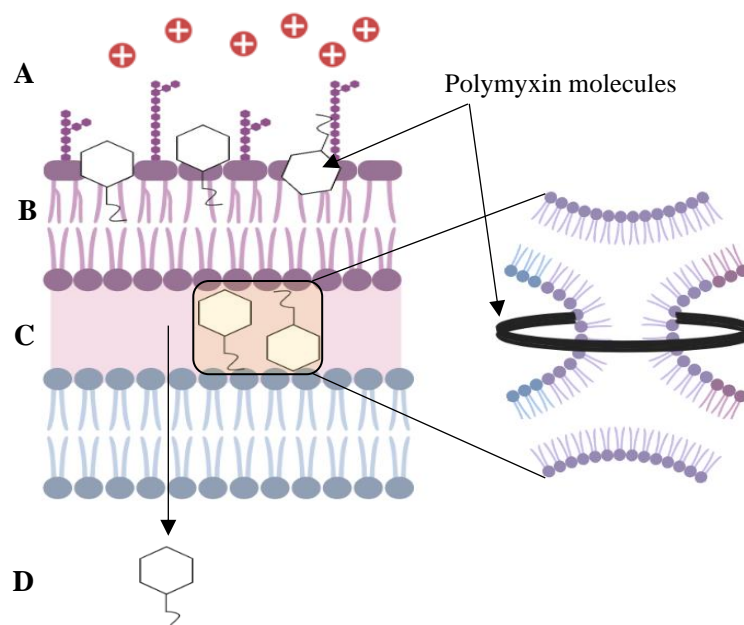


**Figure 63:** Comparative TEM micrographs of *Staphylococcus aureus*. A) untreated bacteria; B, C and D) after treatment with #6 at the MIC ( $8 \mu\text{g}\cdot\text{mL}^{-1}$ ). The polymyxin analogue caused alteration of the membrane (black arrows), mesosome-like structures (red arrows), and possible leakage of cytoplasmic material (yellow arrow).



### 1.7.1.3. Biophysical evaluation of the mechanism of action

As previously introduced, the mode of action of polymyxins is complex and not totally understood yet. However, there is wide acceptance on the model which postulates that the antimicrobial activity begins with the electrostatic and hydrophobic interactions of the peptide with the components of the bacterial outer membrane, LPS and phospholipids, facilitating peptide penetration into the periplasmic space. Then, the peptide establishes contacts between the inner leaflet of the outer membrane and the outer leaflet of cytoplasmic membrane (see Figure 64), and induces a selective mixing of anionic phospholipids through those contacts, resulting in the alteration of the specific phospholipid composition of each membrane and causing an osmotic imbalance that produces the cell death.<sup>165,166,268</sup>



**Figure 64:** Representation of the putative mechanism of action of polymyxins against Gram-negative bacteria. Stage A) displacement of  $\text{Ca}^{2+}$  and  $\text{Mg}^{2+}$  and binding to Lipid A; B) self-promoted uptake of the molecule to the periplasmic space; C) contacts between outer and inner membranes and lipid exchange; D) entry to the cytoplasm and access to intracellular targets.

The mechanism of action of our analogues was further studied using synthetic model membranes such as monolayers and liposomes composed of anionic and zwitterionic lipids that mimic the bacterial biological membranes. As previously introduced, anionic POPG was used to model cytoplasmic membranes of Gram-positive bacteria, whereas zwitterionic POPE was added to mimic the Gram-negative membranes with a POPE/POPG (6:4) mixture. The zwitterionic phospholipid POPC was employed to model

the eukaryotic membrane. Additionally, LPS of the bacteria *Salmonella enterica* serotype Minnesota Re 595 (Re mutant) was used to model the outer membrane of Gram-negative bacteria.

The novel polymyxins should have the following characteristics:

- Interact with model membranes and present high affinity to LPS .
- Form molecular contacts between membranes, that give place to phospholipid exchange, as previously reported for natural polymyxins.
- Show no lytic effect on the model membranes of eukaryotic cells.

#### 1.7.1.3.1. Monolayers as model membranes

Lipid monolayers were prepared as explained in section 1.1.3.5.1. and used to determine peptide binding to outer and inner bacterial membrane lipids. Monolayers were compacted at an initial pressure that is equivalent to the biological membrane pressure ( $32 \text{ mN}\cdot\text{m}^{-1}$ ),<sup>229</sup> and the desired peptide was injected underneath, in such a way that insertion into the monolayer will result in an increase in surface pressure.

Table 18 shows the surface pressure increases obtained 25 minutes after peptide addition.

**Table 18:** Increase in surface pressure upon penetration of the antimicrobial lipopeptides into monolayers at an initial pressure of  $32 \text{ mN}\cdot\text{m}^{-1}$ .

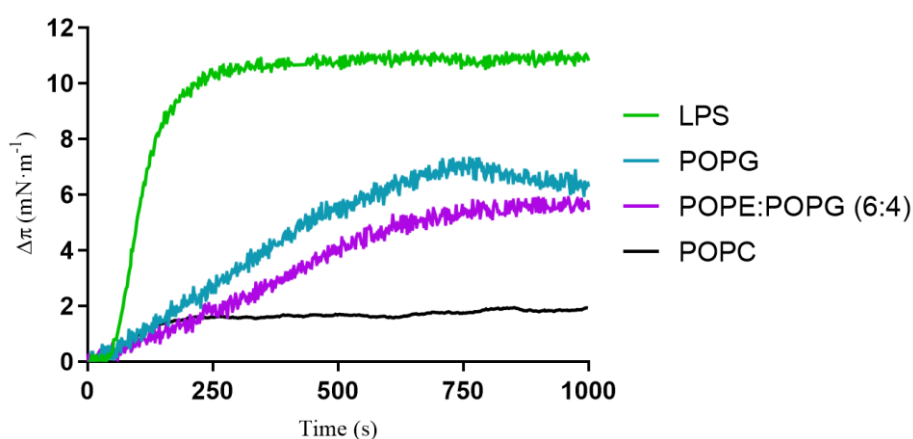
Composition	$\Delta\pi \text{ (mN}\cdot\text{m}^{-1}\text{)}$								
	PxB	4	5	6	7	8	9	10	11
POPC	2.4	0.9	1.8	2.0	2.5	0.8	0.4	2.1	1.7
LPS	11.4	12.1	12.6	11.0	12.2	10.6	10.8	9.3	11.2
POPE/POPG (6:4)	7.2	4.6	5.5	6.0	5.0	6.5	5.0	6.5	6.2
POPG	5.9	5.7	7.0	6.2	6.7	7.3	6.0	4.2	3.8

The obtained results show that polymyxin B has very low affinity to bind the zwitterionic phospholipid POPC, which model the eukaryotic plasma membrane. This behavior could be easily explained due to the lack of electrostatic interaction of the cationic antibiotic with the zwitterionic monolayer. Our synthesized analogues share the same affinity, with no noticeable or very low pressure change in POPC monolayers, fact that is paramount to reduce toxicity towards mammalian cells.

As previously introduced, LPS is the major component of the outer membrane of Gram-negative bacteria and therefore, the binding of our peptides to LPS is a necessary first step for their activity. Natural polymyxin B showed high affinity and insertion in the LPS layer, with an increase in surface pressure of  $11.4 \text{ mN}\cdot\text{m}^{-1}$ . All the synthetic derivatives inserted into LPS monolayer with similar levels of penetration, fact that is consistent with a mainly electrostatic interaction, since all analogues are equally protonated at pH 7.4. Clearly, the contribution of the hydrophobic interactions is not strictly necessary for LPS binding even though it seems crucial for antibacterial activity. This is the case of analogue #4, which contains an hexanoyl *N*-terminal tail and was not active towards Gram-negative bacteria, but it possesses similar binding affinity to the LPS than polymyxin B according to the monolayer penetration assay.

Regarding the binding to cytoplasmic bacterial membrane lipids, insertion into anionic POPG or POPE/POPG monolayers showed no relevant differences in the different analogues assayed, with increases of  $4 - 7 \text{ mN}\cdot\text{m}^{-1}$ , thus indicating that the insertion into the phospholipid layer requires both electrostatic and hydrophobic interactions.

Finally, Figure 65 shows the kinetics of insertion of analogue #6 as a representative example of the time-dependent increase in surface pressure in the four different models. It could be observed that insertion is very fast for LPS, but penetration into phospholipid monolayers is time-dependent, although the maximum increase in pressure is reached in less than 15 minutes.



**Figure 65:** Kinetics of insertion of compound #6 into monolayers of different composition at constant area and initial surface pressure of  $32 \text{ mN}\cdot\text{m}^{-1}$ . Peptide concentration  $0.48 \mu\text{M}$ .

#### 1.7.1.3.2. Liposomes as model membranes

Large unilamellar vesicles (LUVs) of different compositions were prepared by sonication and extrusion as explained in detail in experimental section 3.1.2.6.2., typically obtaining liposomes with a mean diameter between 90 and 117 nm.

##### 1.7.1.3.2.1. Aggregation of vesicles

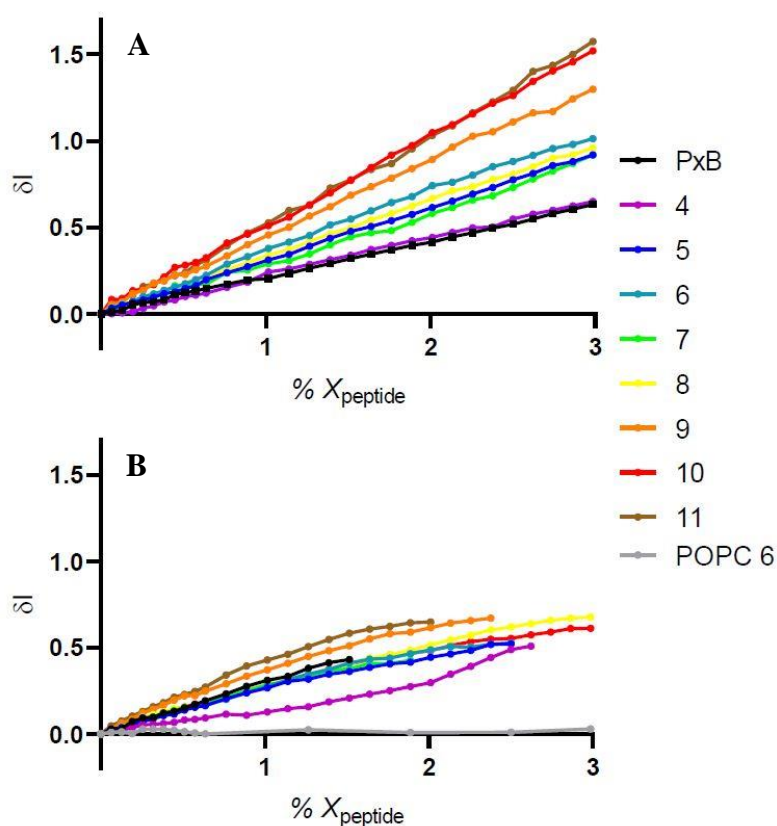
As previously demonstrated with the monolayer experiments, our cationic lipopeptide analogues readily interact with anionic phospholipid membranes. We next used liposomes formed by only one lipid bilayer to study the possible effects of lipid-peptide interaction. Once bound to the lipid vesicles, the new lipopeptides may induce the formation of bigger particles, for example inducing aggregation or even membrane fusion, or they can induce vesicle lysis, with a reduction of particle size due to formation of micelles, in what is known as an unspecific detergent effect.

A change in the size of the particles is accompanied by a change in the turbidity, that can be monitored as the change in the 90° scattered intensity at 360 nm upon peptide addition. An increase in the relative change in the intensity of the scattered light,  $\delta I$ , would be a clear indicator that there was an increase in particle size and consequently there was aggregation between vesicles. Contrarily, if there was a lytic effect, a decrease in turbidity would be produced due to the destruction of the vesicles and formation of smaller sized particles.

As shown in Figure 66, a linear increase of the 90° scattered intensity of both anionic vesicles, POPG and POPE/POPG, at low mole fractions of peptide (below 3 %) was observed, indicating vesicle aggregation, and ruling out the possibility of a detergent or lytic effect. No precipitation or increase in scatter with peptides alone was observed, hence the increase in scatter was a direct consequence of the association of peptides with lipid vesicles.

Interestingly, for a given peptide, increase was higher for pure POPG vesicles than for mixed POPE/POPG meaning that bigger aggregates are formed in the Gram-positive membrane model. It could be also observed that aggregation is related to the hydrophobicity of the molecule, since analogues with longer fatty acid chains and a Nle residue at position 7 (#9, #10, and #11) showed the highest increases in

scattered light, whereas low aggregating capacity was observed with the C6 analogue. Results are in good agreement with previously reported experiments conducted with natural PxB (also included here as a control).<sup>194,269,270</sup> At high peptide concentrations we observed the formation of optically visible particles that tended to precipitate, as is also the case with PxB above 5 - 6 mol%, however these elevated concentrations are not relevant for activity, and in this work, we focused on the low peptide concentration range (below 3 mol%). None of the analogues had any effect on the zwitterionic POPC vesicles, with no changes in light scattering even at 3 mol% of each peptide, (compound #6 is shown as a representative example).



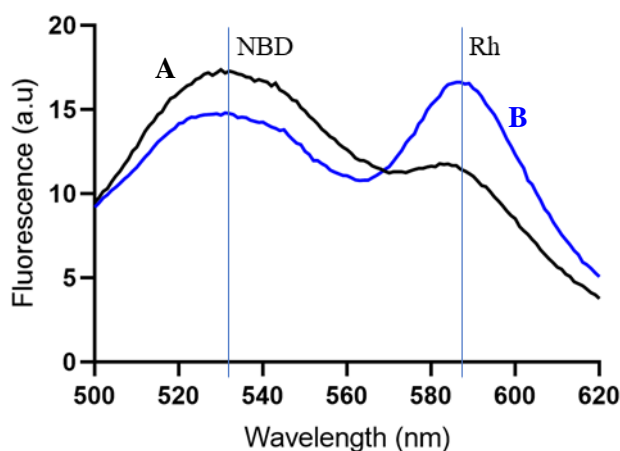
**Figure 66:** Effect of polymyxin analogues on the intensity of scattered light of: A) POPG vesicles and B) POPE/POPG (6:4) vesicles. Changes in light scattering of peptide #6 on POPC is shown in graph B as a representative example of the non-aggregating effect caused by the lipopeptides in eukaryotic model membranes.

#### 1.7.1.3.3. Fluorescence resonance energy transfer to study peptide-lipid interaction

The previously observed increase in light scattering can arise either due to simple aggregation or a combination of aggregation and vesicle fusion/lipid mixing. For that

reason, fusion experiments were carried out by measuring the fluorescence intensity change resulting from the fluorescence resonance energy transfer (FRET) between 7-nitrobenz-2-oxa-1,3-diazol-4-yl (NBD) (donor) and rhodamine (Rh) (acceptor). Both labels were covalently attached to a PE phospholipid headgroup, and mixed with the regular phospholipids during the preparation of the LUVs.<sup>271</sup>

As previously explained, fluorescence resonance energy transfer from NBD-PE to Rh-PE is significant when these probes are in close proximity, such as in the same vesicle, since the Förster distance for this pair is ~5 nm (Figure 67).



**Figure 67:** Change in the spectrum due to FRET between: A) an equimolar mixture of vesicles of 0.6 mol% NBD-PE/POPG and 0.6 mol% Rh-PE/POPG (107  $\mu$ M total lipid), without peptide and B) the same lipid mixture with 6.7  $\mu$ M analogue #7, which causes aggregation or fusion of vesicles. Excitation 460 nm, excitation and emission band passes 4 nm.

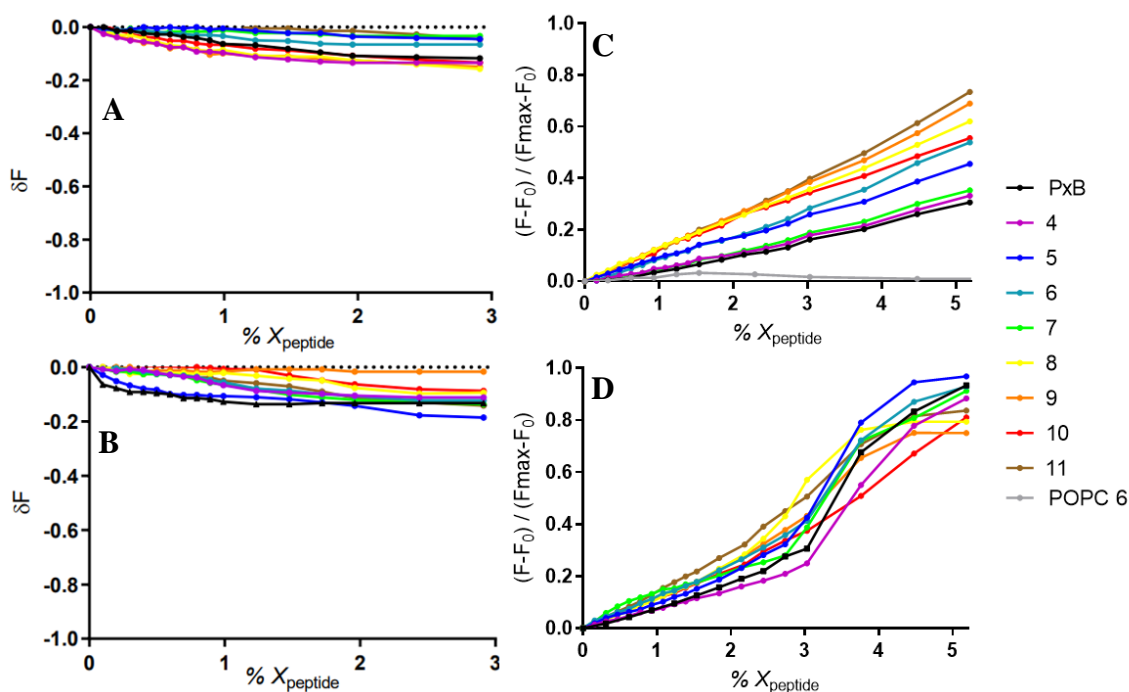
In a first experimental design to detect lipid mixing, vesicles of the desired composition containing the two probes at 0.3 mol% each, were mixed with unlabeled vesicles of the same composition in a 1:24 ratio. In this case, FRET is maximal in the beginning of the experiment, before peptide addition, and a reduction in energy transfer will be expected in the event of peptide-induced fusion (for details see experimental section 3.1.2.6.4.).

The FRET intensity did not present a significant change on the addition of <3 % mole fraction of peptide (Figure 68A and B). This result means that average distance between NBD-PE and Rh-PE was not altered upon peptide addition, as it would be in case of fusion events.

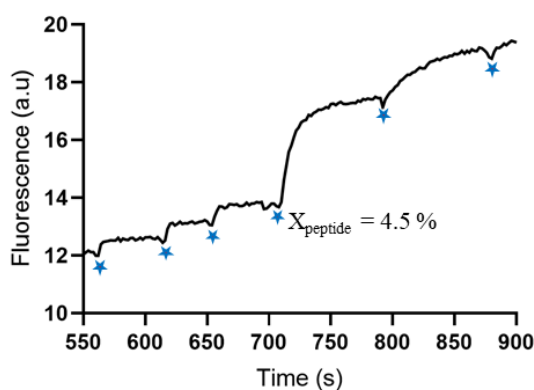
In a second experimental design, vesicles containing 0.6 mol% of only NBD-PE or Rh-PE labelled lipids were mixed in an equimolar ratio. In this case, in the beginning of the experiment, before peptide addition, there will be no significant FRET, since the distance between donor and acceptor is too big. In the event of aggregation or lipid mixing, an increase in the FRET signal will be detected. As shown in Figures 68B and C, addition of the polymyxin analogues induced a clear increase in FRET intensity in all cases, as in the case with natural polymyxin B. These results clearly show that polymyxin analogues induced the aggregation of the anionic vesicles, however the head-group labelled phospholipids are not significantly crossing those peptide-mediated contacts according to the experiment in Figure 68A/B, at least at low peptide concentrations. This is the same behaviour described for polymyxin B, and it is probably due to the bulky structure of the fluorescent probes, that are located at the lipid interface. However, as it will be shown later with pyrene-labelled phospholipids where the fluorescent probe is located at the acyl chain of the phospholipids, under these conditions peptide-mediated lipid exchange takes place.

Summarizing, the increase in FRET in Figure 68C/D, combined with the non-fusogenic effect at low peptide mole fractions demonstrated in Figure 68A/B, along with the increase in light scattering, creates a scenario where vesicles do not fuse in a unspecific way, but there is peptide-mediated aggregation and, as it will be demonstrated later, a selective lipid exchange.

In addition, it should be noted that, especially in POPE/POPG vesicles, the FRET increase versus peptide mole fraction showed a biphasic behavior, where the magnitude of the energy transfer was considerably higher as fusion and nonspecific lipid mixing took place (at mole peptide fractions  $>4\%$ ), as it was demonstrated for natural polymyxin.<sup>165</sup> As an example the time-dependent change in fluorescence for analogue #5 is shown in Figure 69, at low peptide concentration, below 3 mol%, the change in fluorescence is fast after peptide interaction and the signal is rapidly stabilized, but at high peptide concentrations, for example 4.5 mol% in the figure, there is a time-dependent increase in fluorescence that is characteristic of membrane fusion.



**Figure 68:** Changes in FRET intensity resulting from the addition of peptide to different LUV vesicles containing the fluorophores NBD-PE and Rh-PE. Left: Vesicles co-labeled with NBD and Rh mixed with excess unlabeled vesicles of A) POPG; B) POPE/POPG (6:4). Right: NBD-labeled vesicles mixed with Rh-labeled vesicles C) POPG; D) POPE/POPG (6:4). Changes in FRET of peptide #6 on POPC is shown in graph C as a representative example of the non-aggregating or fusiogenic effect caused by the lipopeptides in eukaryotic model membranes.



**Figure 69:** Time-dependent FRET produced by the addition of peptide #5 to 0.6 mol% NBD-PE/POPE/POPG and 0.6% Rh-PE/POPE/POPG vesicles. At low peptide concentrations the change in fluorescence is fast after peptide addition. However, under addition of >4 mol% of peptide, there is a time-dependent FRET increase, characteristic of membrane fusion. Stars denote peptide addition from a stock solution.

It could be also observed that on the second experiment, POPE/POPG vesicles (Figure 68D) at a given peptide-lipid ratio, presented a higher increase of FRET than for



POPG. For example, at 4.5 mol% of compound #6 relative change in fluorescence was 0.87, while for POPG vesicles it was of 0.46. This effect has been described before, and is attributed to the pronounced effect of POPE on the membrane lateral pressure, with an increase in acyl chain packing and induction of negative curvature.<sup>194,272</sup> Also, it is well possible that the cationic peptides induce phase segregation upon binding, leading to the formation of phase boundaries that allow the formation of packing defects and making the vesicles more prone to destabilization of the membrane and fusion. The higher fluorescence increases on POPE/POPG vesicles, together with the lower scattering increase, indicates that even though small sized clusters are formed in the mixed POPE/POPG vesicles, the number of clusters is higher than for POPG vesicles.

No fusion or lipid mixing was observed with liposomes of pure POPC (compound #6 is shown as a representative example in Figure 68C), which suggests that our lipopeptides and polymyxin B present selectivity towards anionic membranes.

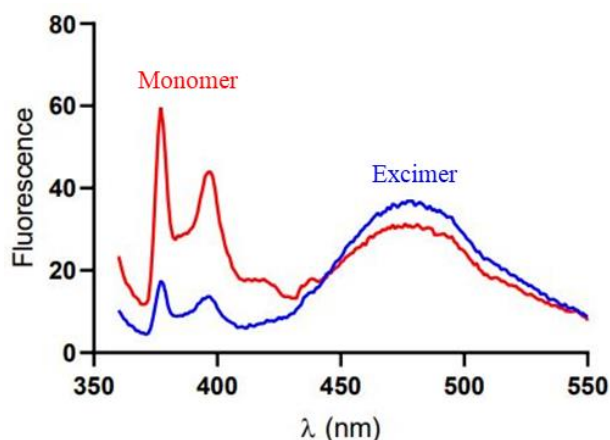
Finally, the hydrophobicity of the compounds appears not to be highly related with the lipid mixing ability of the compounds since even the short C6 analogue (compound #4) showed similar values than commercial polymyxin B.

#### *1.7.1.3.4. Changes in excimer-to-monomer ratio of pyrene fluorescence to detect lipid mixing*

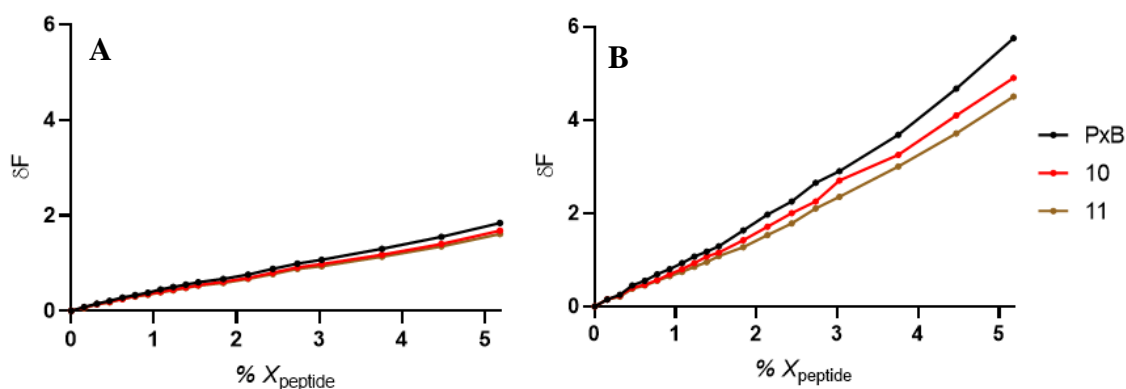
Peptide-mediated exchange of phospholipids was determined by monitoring the change in the pyrene monomer fluorescence emission of a mixture of pyPG-containing vesicles and a 100-fold excess of unlabeled vesicles. As described previously in section 1.1.3.5.2.3, the induction of lipid mixing will result in surface dilution of the fluorescent probe, which is located at the acyl chain of the phospholipids, decreasing the intensity of the excimer band and increasing the monomer band at 395 nm (Figure 70).

Due to time issues, this experiment was only performed in the most active compounds #10 and #11, results are summarized in Figure 71. Both lipopeptides and natural polymyxin B showed very similar effects, it could be observed that at very low peptide concentration (less than 1 mol%) there is a rapid increase in the fluorescence, indicating that pyPG molecules are transferred into POPG or POPE/POPG unlabeled vesicles. The extent of lipid mixing for the same peptide concentration is significantly higher in the

Gram-negative model membranes containing a mixture of anionic and zwitterionic POPE/POPG lipids.



**Figure 70:** Example of lipid-mixing assay based on pyrene excimer formation. Blank POPG LUVs were mixed with POPG/ 30 mol% py-PG. Upon addition of compound #11 8. 3 $\mu$ M, the initial excimer fluorescence (blue line) was clearly diminished, and the intensity of the fluorescence corresponding to py-monomers around 370 - 400 nm increased (red line).



**Figure 71:** Changes in the pyrene monomer fluorescence intensity as a result of the lipopeptide-mediated transfer of pyPG from donor vesicles (pyPG 0.83  $\mu$ M) to acceptor vesicles (106  $\mu$ M) of: A) POPG vesicles; B) POPE/POPG vesicles (6:4).

#### 1.7.1.3.5. Correlation between the antimicrobial activity of the analogues and their biophysical properties

We studied the cysteine polymyxin analogues combining biophysical studies with *in vitro* activity on bacteria, observation of alterations in bacterial membrane integrity by electron microscopy, and induction of hemolysis.

Some of the new molecules shown a broad spectrum of action against Gram-positive and Gram-negative bacteria, together with low levels of induction of hemolysis, similar to

those presented by natural polymyxins. We demonstrated that increasing the length of the *N*-terminal acyl chain above C8 results in relevant antibacterial activity not only on *Pseudomonas aeruginosa* and *Escherichia coli*, but also against the Gram-positive *Staphylococcus aureus*. Combining this longer acyl chain with a 7-Nle residue, to increase the length of the side chain of the hydrophobic residue 7-Leu, resulted in very potent broad-spectrum compounds, being the C12-Nle analogue (compound #11) the most active peptide, showing similar potency than polymyxin B. But the increase in the overall hydrophobicity of the molecule produced a dramatic increase of the hemolytic activity of the antimicrobial lipopeptides. Therefore, C8, C9 and C10 appear to be the optimal length of the *N*-terminal fatty acyl tail.

Peptide interaction with model membranes indicated selective binding of peptides to anionic membranes containing LPS, a model of Gram-negative outer membrane, or to specific phospholipids that mimic the inner membrane of Gram-negative and Gram-positive bacteria, with formation of clusters of vesicles, and induction of selective anionic lipid exchange starting at very low peptide concentrations (<1 mol%). Increase in light scattering suggests that the mechanism of action is not based on a detergent or lytic effect. Bacterial membrane alteration was confirmed by electron microscopy observation, with formation of blebs on Gram-negative bacteria, in a similar way as natural polymyxins, or formation of mesosomes in Gram-positive *Staphylococcus aureus*.

### **1.7.2. Thiiothreonine analogues**

The previously discussed techniques were also used to explore the mechanism of action of thiiothreonine analogues. In this case, compounds #25 and #27 were selected as the most promising candidates for the study.

#### 1.7.2.1. Hemolysis

Thiiothreonine analogue-induced hemolysis was examined within the ENABLE European consortium of antibiotics by our collaborators at Cardiff University. The assay was performed using blood from healthy human donors, and both lipopeptides as well as natural polymyxin B displayed excellent results, with less than 1 % of red blood cell lysis at 10  $\mu$ M, concentration almost 10-fold higher than the MIC of these compounds (0.85  $\mu$ M for PxB and #25, and 1.74  $\mu$ M for compound #27).

### 1.7.2.2. Transmission electron microscopy

As previously discussed for cysteine analogues, TEM imaging was performed to evaluate the damage caused by our thiothreonine analogues to Gram-negative bacterial membranes. Results are shown in Figure 72. The untreated cells of *Pseudomonas aeruginosa* in tryptone water medium showed normal cell shape, an intact inner and outer membrane. Incubation of this bacterium with natural polymyxin B, #25, and #27 at their MIC (1, 1 and 2  $\mu\text{g}\cdot\text{mL}^{-1}$  respectively) caused similar effects than the observed for cysteine analogues, with evident blebbing, important deformation of the outer membrane, as well as cytoplasmatic areas of low electron density.

### 1.7.2.3. Biophysical assays with liposomes

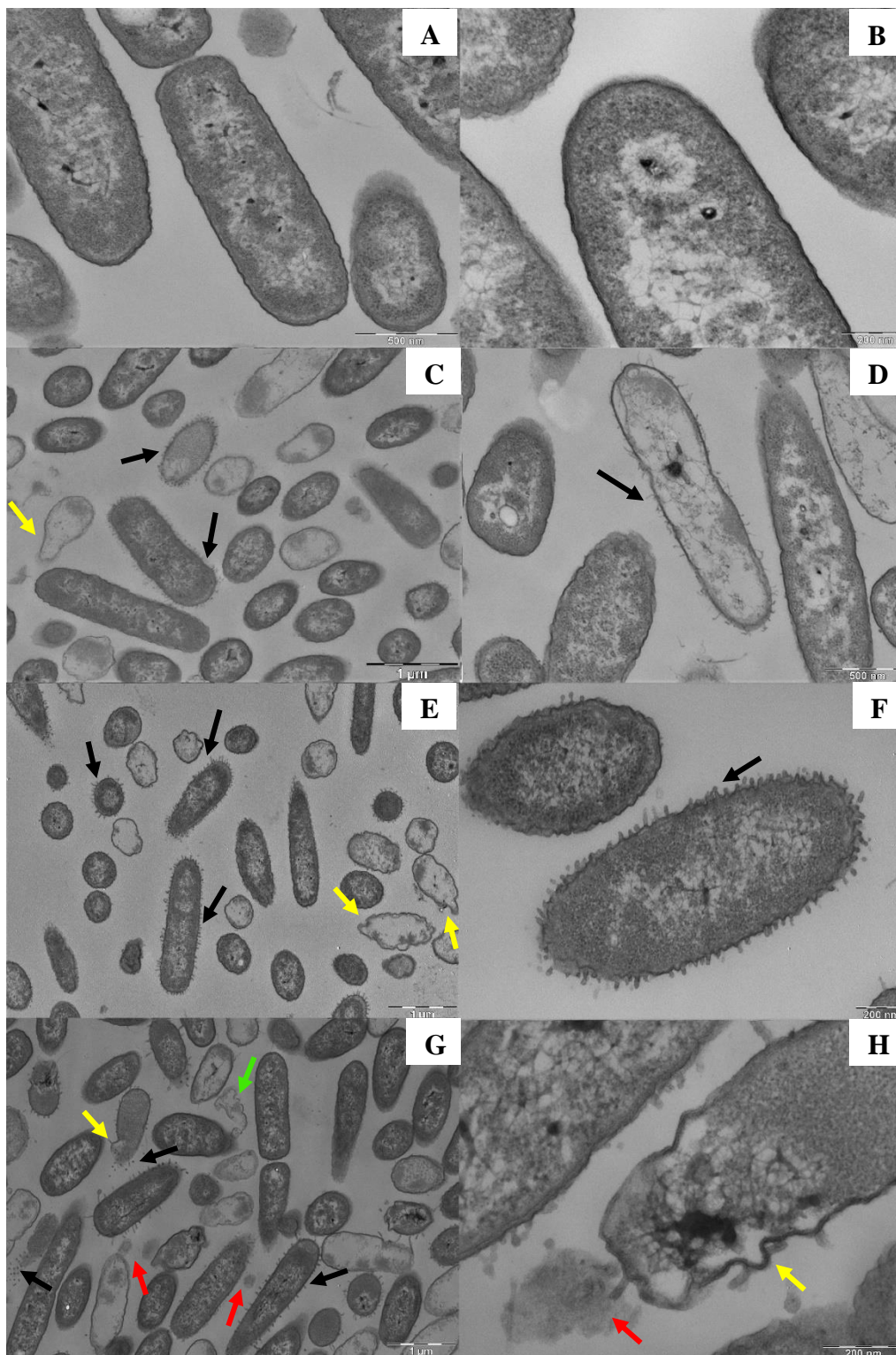
Liposomes were used as model membranes to study the mechanism of action of analogues #25 and #27. As previously explained for cysteine analogues, LPS of *Salmonella enterica*, pure POPG, POPE/POPG (6:4), and the zwitterionic POPC vesicles were used to model bacterial and eukaryotic membranes. Additionally, POPG/DOTAP (8:2) vesicles were used as a new model of Gram-positive to simulate the positively charged lysyl-PG lipids on some Gram-positive bacteria such as *Staphylococcus aureus*.<sup>224–226</sup>

#### 1.7.2.2.1. Insertion in monolayers

Thiothreonine peptides binding to different model membranes was first studied. Lipopeptides were injected at the aqueous subphase underneath monolayers of different compositions, which had been compacted at an initial pressure equivalent to the biological membrane pressure,  $32 \text{ mN}\cdot\text{m}^{-1}$ .<sup>229</sup> Table 19 shows the surface pressure increases 25 minutes after peptide addition.

**Table 19:** Increase in surface pressure upon penetration of the thiothreonine analogues into monolayers.

Composition	$\Delta\pi \text{ (mN}\cdot\text{m}^{-1}\text{)}$		
	PxB	25	27
POPC	1.4	1.2	2.5
LPS	13.8	12.6	13.7
POPE/POPG (6:4)	8.2	7.0	6.5
POPG	6.7	5.7	5.9

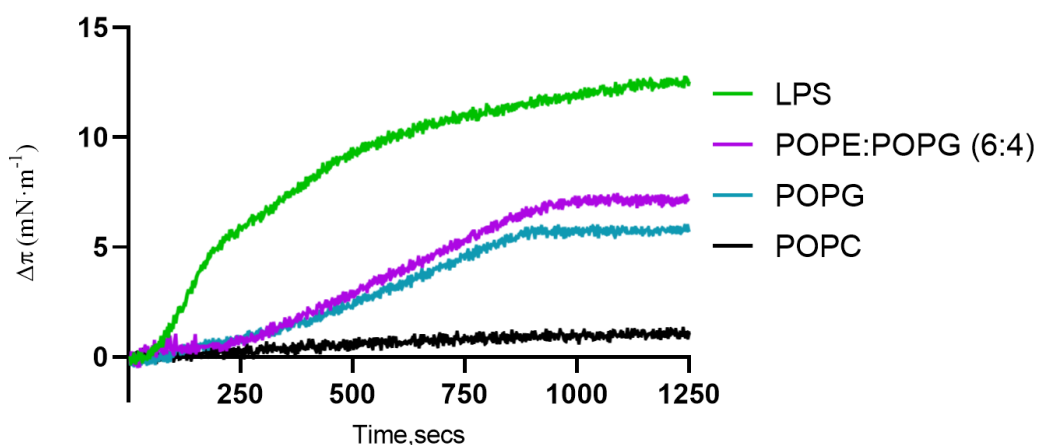


**Figure 72:** Comparative TEM micrographs of *Pseudomonas aeruginosa*. A and B) untreated bacteria; C and D) after 2 h of treatment with PxB at the MIC ( $1 \mu\text{g}\cdot\text{mL}^{-1}$ ); E and F) after 2 h of treatment with #25 at the MIC ( $2 \mu\text{g}\cdot\text{mL}^{-1}$ ); G and H) after 2 h of treatment with #27 at the MIC ( $2 \mu\text{g}\cdot\text{mL}^{-1}$ ). Lipopeptides caused alteration of the membrane (yellow arrow), blebs (black arrows), leakage of intracellular contents (red arrows), and even completely lysed membranes (green arrow).

Thiothreonine analogues insertion into the lipid monolayers was very similar to the previously described for cysteine analogues (Table 18). As previously discussed, polymyxin B has very low binding affinity towards the zwitterionic phospholipid POPC, which mimics the eukaryotic cell membranes, and our synthesized thiothreonine analogues share the same low affinity, with very low increase in surface pressure upon peptide addition.

The new lipopeptides and the natural polymyxin B, displayed high affinity to bind LPS, which is the major component of the outer membrane of Gram-negative bacteria. Increases in surface pressure around  $13.0 \text{ mN}\cdot\text{m}^{-1}$  were observed. Regarding the binding to cytoplasmic bacterial membrane lipids, insertion into anionic POPG or POPE/POPG monolayers showed no relevant differences in the different analogues assayed, with increases of  $6 - 8 \text{ mN}\cdot\text{m}^{-1}$ .

Figure 73 shows the kinetics of insertion of analogue #25 in the four different membrane models. As it was previously discussed for cysteine analogues, the insertion of thiothreonine analogues is very fast for LPS, but penetration into phospholipid monolayers is slower and time dependent.



**Figure 73:** Kinetics of insertion of compound #25 into monolayers of different composition at constant area and initial surface pressure of  $32 \text{ mN}\cdot\text{m}^{-1}$ . Peptide concentration  $0.48 \mu\text{M}$ .

#### 1.7.2.2.2. Fluorescence resonance energy transfer to study peptide-lipid interaction

As previously explained for cysteine analogues, fusion and lipid mixing events can be studied by measuring the fluorescence resonance energy transfer (FRET) between NBD

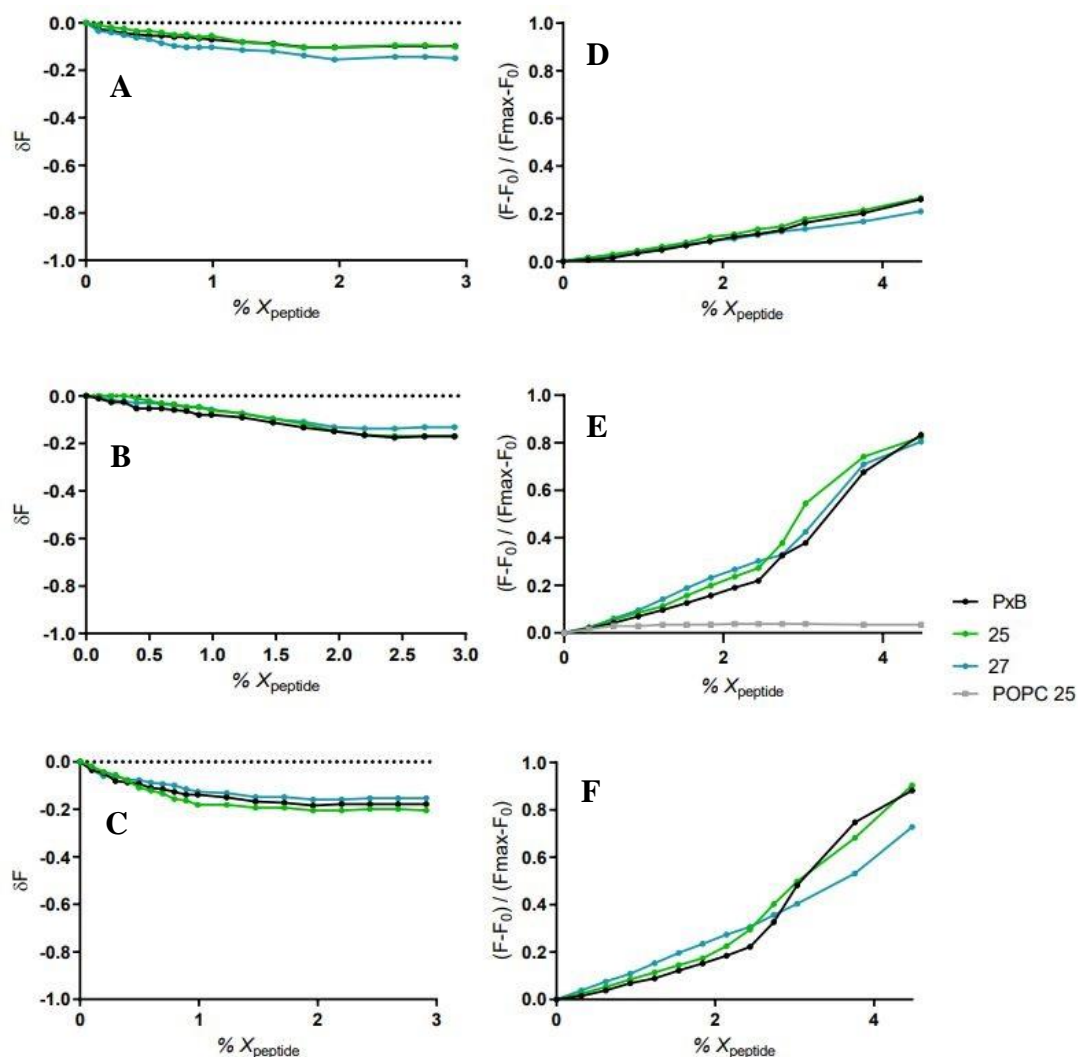
and Rh fluorophores, which are covalently attached to phospholipid headgroups and used in the preparation of liposomes.

According to the changes of FRET upon addition of peptides to co-vesicles containing 0.3 mol% of each probe, mixed with an excess population of unlabeled vesicles of the same lipid composition, both lipopeptides and natural polymyxin did not show remarkable tendency to produce fusion between anionic vesicles at low peptide-lipid ratios, independently of the lipid composition (Figures 74A, B, and C). In contrast, when anionic vesicles containing 0.6 mol% NBD-PE were mixed with vesicles of the same composition containing 0.6 mol% Rh-PE, an important increase in FRET was observed (Figures 74D, E, and F). This indicates that all compounds, at low peptide mole fraction, induced the mixing of lipids between anionic vesicles of POPG and POPE/POPG.

In consistency with the previous results of cysteine analogues, in POPE/POPG vesicles the increase in FRET intensity versus peptide mole fraction showed a biphasic behavior, where the energy transfer was considerably higher as fusion and nonspecific lipid mixing took place (at mole peptide fractions  $>4\%$ ). Mixed vesicles containing anionic POPG and cationic DOTAP vesicles appeared to behave in the same manner that mixed POPE/POPG, with a large increase in FRET above 2 mol% that is not seen in pure POPG vesicles.

The increase in FRET signal for a given analogue was also higher on the POPE/POPG and POPG/DOTAP vesicles compared to the POPG ones, indicating that the number of clusters formed on these model membranes was higher. As previously discussed for cysteine analogues, this fact could be related with the different bilayer properties of POPG and POPE or DOTAP, in which due to relative geometries of headgroups, POPG chains are less tilted (more ordered) and less densely packed than those of POPE or DOTAP.<sup>273</sup>

No fusion or lipid mixing was observed with liposomes of pure POPC (compound #25 is shown as a representative example in Figure 74E), which indicates that our thiothreonine derivatives and polymyxin B present selectivity towards anionic membranes.



**Figure 74:** Changes in FRET intensity resulting from the addition of peptide to different LUV vesicles containing NBD-PE and Rh-PE. Left: Vesicles co-labeled with NBD and Rh mixed with excess blank unlabeled vesicles of: A) POPG; B) POPG/DOTAP (8:2); C) POPE/POPG (6:4). Right: NBD-labeled vesicles mixed with Rh-labeled vesicles (1:1): D) POPG; E) POPG/DOTAP (8:2); F) POPE/POPG (6:4).

#### 1.7.2.2.3. Changes in excimer-to-monomer ratio of pyrene fluorescence to detect lipid mixing

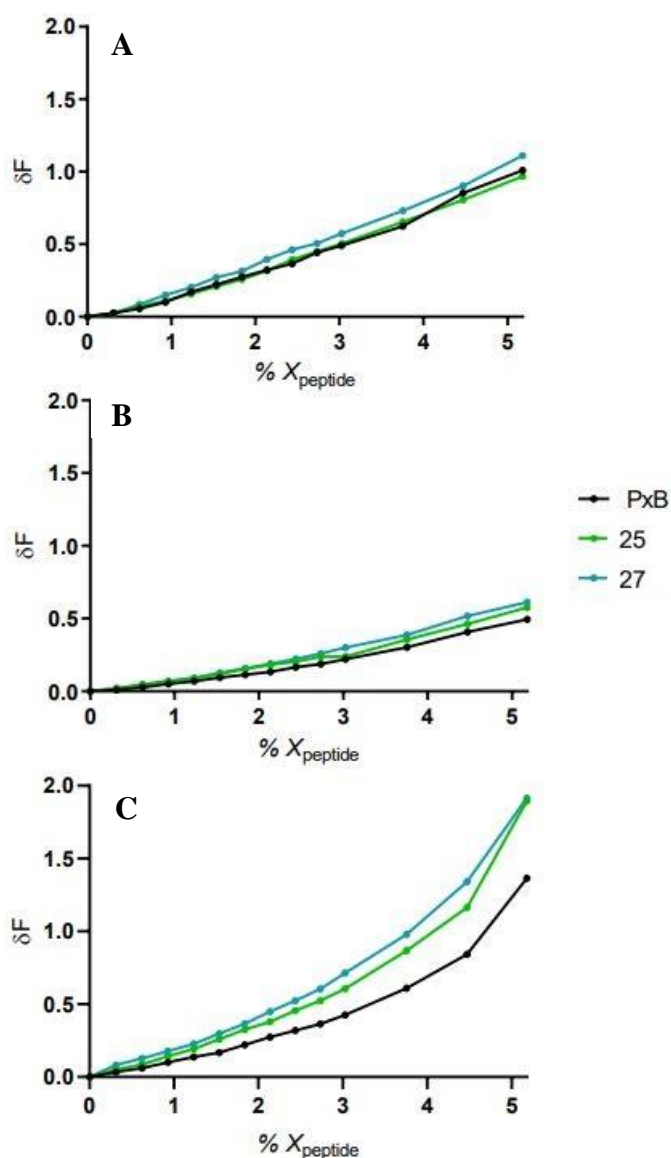
Peptide-induced lipid exchange was determined by monitoring the change in the pyrene monomer fluorescence emission of a mixture of pyPG-containing vesicles and a 100-fold excess of unlabeled vesicles, as above described for cysteine analogues.

Results are summarized in Figure 75. Briefly, both lipopeptides and natural polymyxin B induced fast exchange of pyPG in a concentration dependent manner. The extent of lipid



mixing for the same peptide concentration was significantly higher in the Gram-negative model membranes containing a mixture of anionic and zwitterionic POPE/POPG lipids.

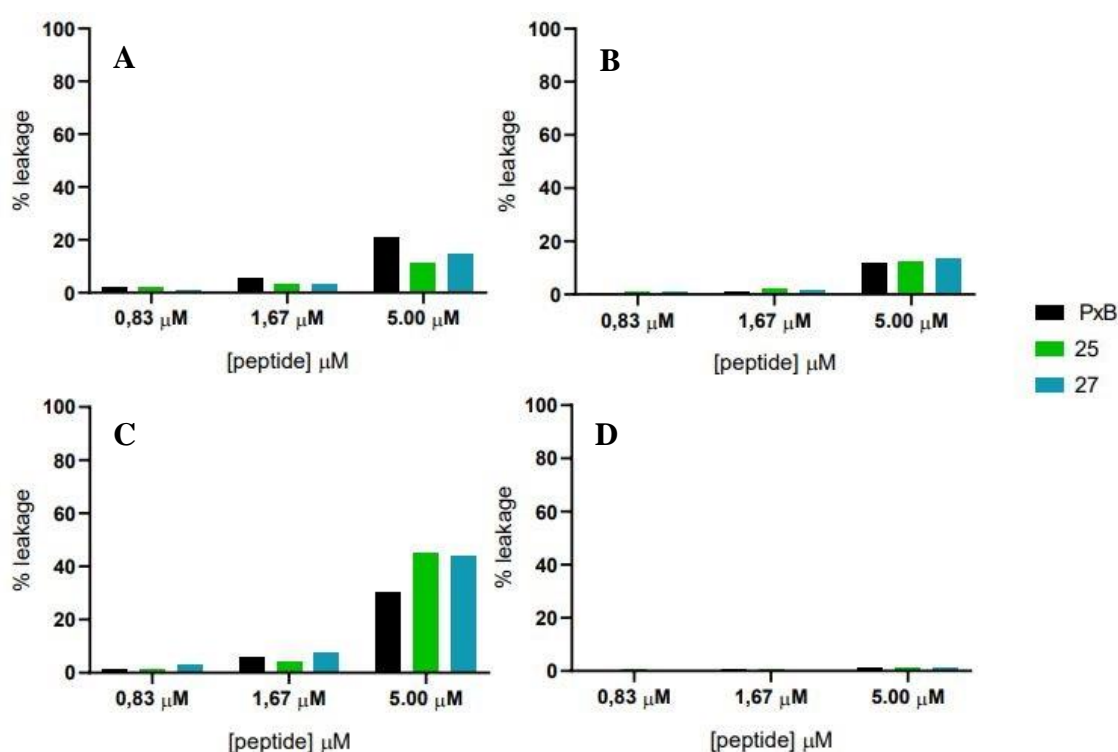
Furthermore, in POPE/POPG vesicles, the increase in the monomer fluorescence emission intensity versus mole fraction of PxB showed biphasic behavior, and the intercept of the two slopes corresponds to the onset of vesicle fusion (around 4 % peptide mole fraction). This interpretation is consistent with the fact that with the onset of fusion there is a significant decrease in the excimer fluorescence.



**Figure 75:** Graphic representation of the increase of the monomer fluorescence induced by the addition of peptide. A) POPG vesicles; B) POPG/DOTAP (8:2) vesicles; C) POPE/POPG (6:4) vesicles.

## 1.7.7.2.4. Leakage of aqueous contents

Once demonstrated that the antibiotic lipopeptides induced lipid mixing between anionic vesicles, the next question is if this is also accompanied by the leakage of aqueous contents, indicating membrane lysis or pore formation. In Figure 76, leakage at three relevant peptide concentrations is shown, being 0.83  $\mu\text{M}$  close to the MIC of PxB and analogue #25 against Gram-negative bacteria, and 1.67  $\mu\text{M}$  a concentration representative of the MIC of analogue #27. In addition, results at 5  $\mu\text{M}$  peptide are indicative of the behavior of the synthetic analogues at a high peptide concentration.



**Figure 76:** Leakage from vesicles of: A) POPG; B) POPG/DOTAP (8:2); C) POPE/POPG (6:4); and D) POPC at three peptide concentrations. Lipopeptides were added to liposomes co-encapsulating ANTS (12.5 mM) and DPX (45 mM), and leakage was determined as the increase in ANTS fluorescence intensity at 530 nm (lipid concentration 115  $\mu\text{M}$ ).

In membranes of POPE/POPG (6:4), modeling the cytoplasmic membrane of Gram-negative bacteria, leakage remained below 8 % at the MIC of each antibiotic. At high peptide concentration of 5  $\mu\text{M}$ , a dramatic increase in permeability was observed, with leakage values near 40 %. This behavior was previously demonstrated for PxB, with low induction of leaky fusion at the MIC.<sup>193</sup>

In the case of POPG and POPG/DOTAP vesicles, which mimic Gram-positive inner membranes, the permeabilization effect was also concentration-dependent and negligible at low concentrations. At the highest peptide concentration of 5.0  $\mu\text{M}$ , leakage values remained below 20 %, and were comparable to polymyxin.

Finally, leakage from POPC vesicles was negligible in all cases.

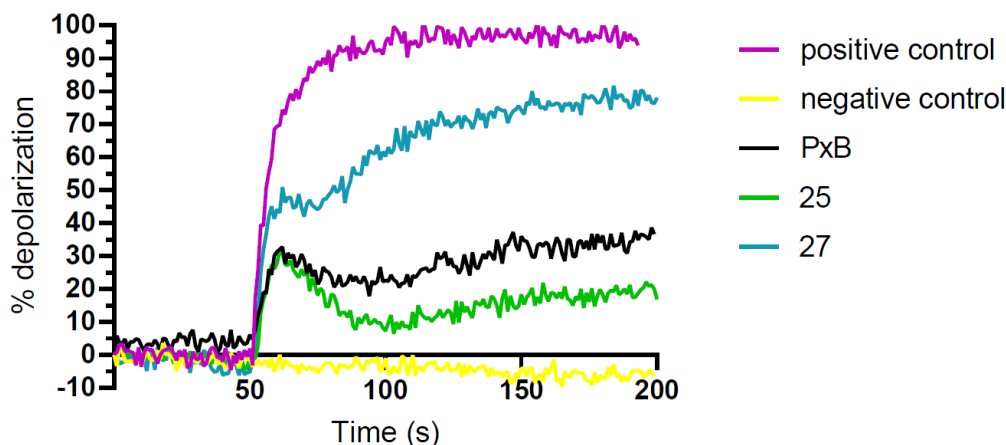
Therefore, these results are consistent with the formation of vesicle-vesicle contacts, forming clusters of vesicles (aggregation), and the mixing of lipids from the outer monolayers of the vesicles in contact, but without causing fusion and permeabilization of the inner compartments. This is the mechanism of action of natural polymyxins and other antimicrobial peptides, inducing cell death by the loss of compositional specificity in the inner and outer membranes of Gram-negative bacteria, causing osmotic shock.

#### 1.7.7.2.5. Cytoplasmic membrane depolarization assay

The ability of the new analogues to depolarize the cytoplasmic bacterial membrane was tested in *Pseudomonas aeruginosa* with the potentiometric fluorescent probe diSC<sub>3</sub>(5). Briefly, the probe is able to penetrate lipid bilayers and accumulate in viable bacteria due to the membrane potential (negative inside), resulting in a decrease in fluorescence. If any compound alters the membrane potential of the bacterial cell, the probe will be released to the media, which will result in an increase in fluorescence emission.

Results showed that three peptides induced an immediate increase in diSC<sub>3</sub>(5) fluorescence intensity, reflecting cytoplasmic membrane depolarization (Figure 77).

Compound #27, at its MIC of 2  $\mu\text{g}\cdot\text{mL}^{-1}$ , caused rapid depolarization of the cytoplasmic membrane, resulting in more than 75 % maximal release of diSC<sub>3</sub>(5) in 200 seconds. Otherwise, compound #25 and natural polymyxin B showed lower depolarization ability, with a maximal release of diSC<sub>3</sub>(5) nearly to 20 and 35 % respectively at their MIC (1  $\mu\text{g}\cdot\text{mL}^{-1}$ ). Since both polymyxin analogues shared the same structure except the ester bond between positions 6 and 7 in the analogue #27, the depsipeptide structure appears to highly enhance the depolarization of the cytoplasmic membrane.



**Figure 77:** Kinetics data for the change in diSC<sub>3</sub>(5) dye fluorescence upon exposure of the *Pseudomonas aeruginosa* ATCC 27853 cells to polymyxin analogues at their MIC. Antibacterial agents were added at 50 seconds. The detergent Triton X-100 was used as positive control. Negative control corresponds to the bacterial suspension without peptide addition.

### 1.7.2.3. Proposed mechanism of action for thiothreonine analogues

To recapitulate, the thiothreonine analogues of polymyxin present high selectivity for anionic membranes, comparable to natural polymyxin B and cysteine analogues, whereas they do not cause any effect on zwitterionic membranes.<sup>165,268</sup>

By combining the membrane potential-sensitive dye diSC<sub>3</sub>(5) with the previously discussed ANTS/DPX leakage assay, it was possible to distinguish between two different modes of peptide-membrane interaction, the peptide-induced membrane depolarization due to ion movements across the membrane, and membrane permeabilization due to the formation of pores. At concentrations relevant for the antimicrobial activity, these analogues do not cause significant leakage from liposomes that mimic Gram-negative bacteria, but they cause a fast depolarization of the membrane potential.

Peptide-mediated molecular contacts between the cytoplasmic and outer membranes are plausible mechanism for selective intermembrane transfer of phospholipids, which could result in membrane depolarization and will cause osmotic imbalance and cell death, but without causing fusion or membrane permeabilization. Lipopeptide-induced bacterial membrane alteration was confirmed by electron microscopy observation, with formation of blebs and leakage of the cytoplasmic material.

## 1.8. Hit validation

As previously discussed, analogues #3, #10, #19, #24, #25, #26 and #27 were selected as the most promising candidates to continue the development and further explore their properties *in vivo*. In this section, these studies are presented in order to designate the most promising hit compound that will initiate the ‘Hit to Lead’ phase in the drug development process.

### 1.8.1. Antimicrobial activity against resistant bacteria

In order to deep in our knowledge about the lipopeptides antimicrobial activity, a first screen of MIC values of the potential hit compounds was performed against 13 different multi-drug resistant strains isolated from hospitalized patients. The resistance profile of the selected bacterial strains is shown in Appendix X. This assay was performed in collaboration with the group of Professor Jordi Vila at the ‘Institut de Salut Global de Barcelona (ISGlobal)’, where a large collection of clinical strains is available.

The MIC values obtained are shown in Table 20. All MIC values above 8  $\mu\text{g}\cdot\text{mL}^{-1}$  are indicative of resistance and shown in red, whereas all values lower than 8  $\mu\text{g}\cdot\text{mL}^{-1}$  are indicative of bacterial susceptibility and shown in green. Our analogues maintained excellent activities, with very low MIC values against most of the multi-drug resistant strains tested. It should be noted that some compounds such as #3 or #25 even improved polymyxin’s activity, being active against strains such as *Acinetobacter baumannii* CR17 or *Klebsiella pneumoniae* MB1052, which are resistant to polymyxin, colistin and other frequently used antibiotics such as imipenem, meropenem, ceftazidime, or ciprofloxacin among others.

Interestingly, if we compare compounds with *N*-terminal D-Adec (compounds #25 and #27), with their counterparts having a C8-Dab (compounds #24 and #26), better activities were achieved with D-Adec-containing analogues. On the other hand, depsipeptide analogues (analogues #26 and #27 compared to #24 and #25 respectively) produced a 2 or 4-fold loss on antimicrobial potency, in accordance with our previous results in susceptible strains. In brief, compound #25 presented the best activity profile, while the cysteine analogue #19 was the less potent antimicrobial agent.

**Table 20:** MIC results against resistant strains. Resistant bacteria are colored in red, susceptible in green.

Bacterial strain		PxB	#3	#19	#24	#25	#26	#27
<i>Escherichia coli</i>	ATCC 25922	0.25	1	4	4	1	4	2
	MB799	2	4	4	4	2	4	4
	C22	4	8	16	8	4	8	4
	MB1410	0.5	0.5	4	0.5	1	1	1
<i>Klebsiella pneumoniae</i>	ATCC 13883	4	4	>32	16	2	32	8
	MB674	0.25	0.5	2	1	1	1	2
	MB1052	>32	8	>32	32	4	>32	8
<i>Acinetobacter baumannii</i>	ATCC 19606	0.5	1	32	8	8	4	8
	ATCC 17978	0.5	1	8	2	4	2	4
	CR17	16	4	>32	>32	2	16	32
<i>Pseudomonas aeruginosa</i>	ATCC 27853	1	1	2	1	2	2	2
	36A	1	1	1	1	2	2	2

### 1.8.2. *In vivo* nephrotoxicity assay

The major toxicological concern of polymyxins is nephrotoxicity. Both polymyxin B and colistin/colistimethate are known to produce adverse side effects in the kidneys. Polymyxin-induced nephrotoxicity has been associated with acute tubular necrosis in the kidneys and with rising creatinine levels in the blood.<sup>148</sup> In order to assess the nephrotoxicity of the synthetic analogues, *in vivo* toxicity experiments on mice were performed using CD-1 mice.

#### 1.8.2.1. First *in vivo* nephrotoxicity assay

The assay was carried out with the depsipeptide compound #3, which was selected to evaluate the influence of the *N*-terminal D-Adec residue and the introduction of an ester bond in the peptide scaffold. Cysteine analogues #10 and 19 along with the analogue p1, that had been previously synthesized in the group, were used to evaluate the effect of the cysteine-mediated disulfide bond and the modifications on hydrophobicity. Finally,

thiothreonine analogues #24 and #25 were tested to study the nephrotoxicity of thiothreonine compounds with and without *N*-terminal fatty acid.

The assay was performed in collaboration with Dr. Javier González Linares in “Centre de Recerca en Toxicologia (CERETOX)”. Briefly, after an acclimatization period of 5 days, randomly selected animals were weighed, and administered subcutaneously 6 doses of antibiotic at 2-hour intervals. Peptides were dissolved in physiological saline solution (NaCl 0.90 % w/v , 308 mOsm·L<sup>-1</sup>). After 20 hours from the last administration, the animals were anesthetized with isoflurane, blood was extracted for biochemical parameters determination (urea and creatinine), and both kidneys were extracted and weighed for histopathological analysis. later they were sacrificed by rupture of the diaphragm. The kidneys were fixed in 10 % buffered formalin and routinely embedded in paraffin. Subsequently, blocks were cut at 5 µm in a Leica RM2 145 microtome, stained with hematoxylin and eosin and evaluated in a Nikon Eclipse 300 microscope.

Histopathological evaluation was carried out and the observed nephrotoxic effects were classified as cell vacuolization, tubular necrosis, tubular casts, cell desquamation and cloudy swelling of tubular cells. Each one of these parameters had been scored with values from 0 to 4 for each animal, as a global estimate of kidney damage. Partial scores were added to obtain a final score for each animal (animal score), and the mean of animal score were then obtained to define the Group Score (GS), which is used as a nephrotoxicity indicator. An elevated value of GS will imply higher nephrotoxic effects. A summary of the obtained results is provided in Table 21. It should be noted that the experiment was performed in a very limited number of animals and therefore the results should only be considered as a first attempt to discriminate between the synthesized analogues.

Surprisingly, compound #3 presented an alarming 8-fold increase in the GS value and mean urea compared to natural polymyxin B, which indicates that the introduction of an ester bond and/or the D-Adec modification did not improve the toxicological profile of the parent peptide.

Regarding the cysteine-mediated cyclisation, analogue p1, which only differed from polymyxin B<sub>5</sub> in the disulfide bond and the lateral chain of the amino acid at position 10, did not present any toxicity improvement. Furthermore, analogues #10 and #19 presented

important toxic effects, with 2 and 3 dead animals respectively due to their increased hydrophobicity. These results suggest that the increase in the hydrophobicity of the molecule is not a good approach to design new polymyxin analogues.

Finally, thiothreonine compounds showed excellent results with lower associated nephrotoxicity parameters compared to natural polymyxin. Considering these first results, it was not possible to detect any significant difference between the D-Adec modified analogue #25 and the conservative C8-Dab analogue #24.

**Table 21:** Summary of the nephrotoxicity study.

Compound	Dose (mg·Kg <sup>-1</sup> )	Total dose (mg·Kg <sup>-1</sup> )	Animals	Dead	GS	Mean urea (mg·dL <sup>-1</sup> )	Mean creatinine (mg·dL <sup>-1</sup> )
Saline	0	0	3	0	0	36.3	0.13
PxB	12	72	3	0	2.3	32.3	0.21
#3	12	72	3	1	16	231.5	0.58
#p1	12	72	3	0	4	67.3	0.18
#10	12	72	3	2	4	31.0	0.17
#19	12	72	3	3	-	-	-
#24	12	72	3	0	1	40.7	0.18
#25	12	72	3	0	1	37.3	0.18

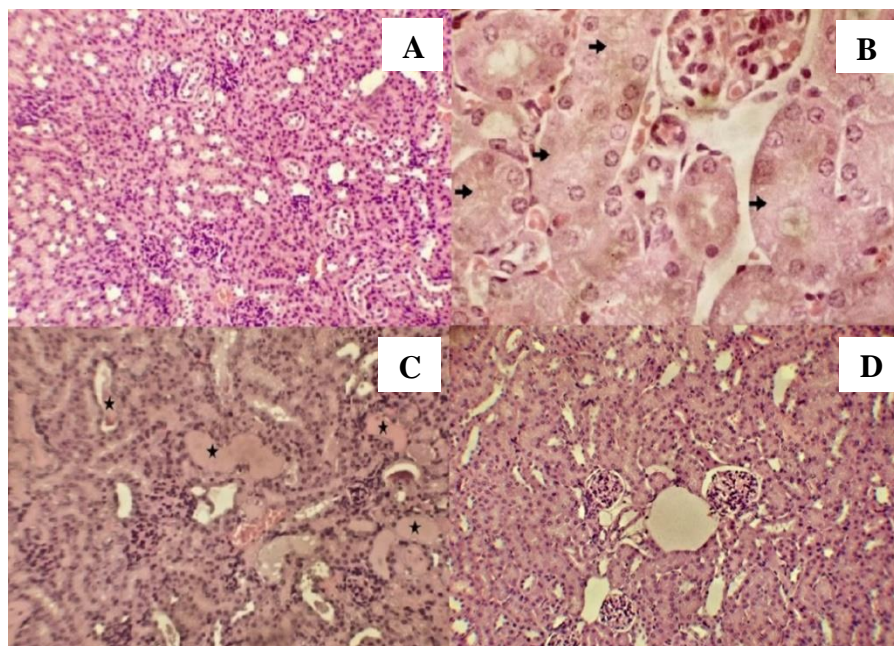
#### 1.8.2.2. Second *in vivo* study

Considering the interesting results above-mentioned, we realized a more detailed *in vivo* assay using a bigger number of animals. On this occasion, we tested again compounds #24 and #25 and included their depsipeptide analogues #26 and #27. Moreover, we studied the pharmacokinetic profile of the compounds after subcutaneous administration.

##### 1.8.2.2.1. *In vivo* nephrotoxicity assay

Nephrotoxicity was studied as explained above. Figure 78 shows an example of the histopathological images evaluated, using these images, the damage in kidney was scored with the numeric values which are summarized in Table 22.





**Figure 78:** Histopathological signs detected on kidney tissue after administration of: A) physiological saline: normal cortical structure without pathologies; B) PxB: arrows show the turbid edema of tubular cells (cloudy swelling); C) compound #24: stars indicate the presence of tubular casts; D) compound #27: normal cortical structure without pathologies.

**Table 22:** Summary of the nephrotoxicity study.

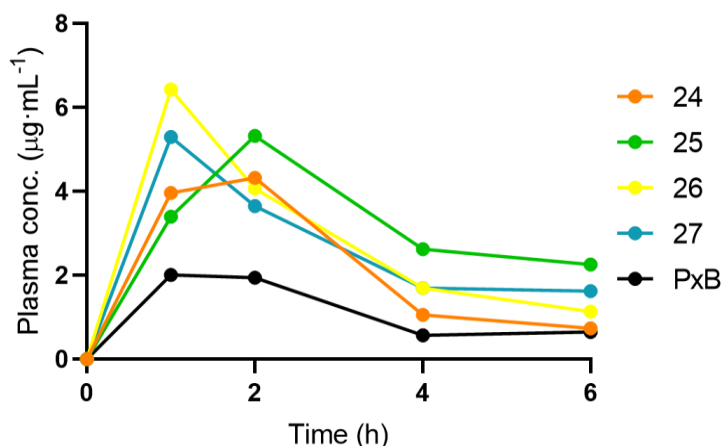
Compound	Dose (mg·Kg <sup>-1</sup> )	Total dose (mg·Kg <sup>-1</sup> )	Animals	Dead	GS	Mean urea (mg·dL <sup>-1</sup> )	Mean creatinine (mg·dL <sup>-1</sup> )
Saline	0	0	8	0	0	41.5	0.16
PxB	12	72	8	0	3.4	42.6	0.24
#24	12	72	8	0	2	54.8	0.23
#25	12	72	8	0	0.4	39.0	0.20
#26	12	72	3	1	0	32.5	0.10
#27	12	72	3	0	0	35.0	0.19

This second *in vivo* study confirmed the low nephrotoxicity of thiothreonine analogues. Furthermore, it was possible to detect an important difference between compounds #24 and #25, which confirmed the hypothesis about the reduction of toxicity by replacing the *N*-terminal fatty acid and 1-Dab residue by D-Adec moiety. The animals treated with depsipeptide analogues #26 and #27 showed normal cortical structures, with a GS of 0. However, these compounds were tested in only 3 animals each, and these promising results should be confirmed in further *in vivo* experiments that are currently underway.

#### 1.8.2.2.2. Pharmacokinetics assay

A total number of 20 animals were used for the pharmacokinetic study. Mice were distributed in 5 groups of 4 animals each. After 5 days of acclimatization, animals were randomly selected, weighed and administered subcutaneously with the appropriate dose of peptide suspended in physiological saline ( $12 \text{ mg} \cdot \text{Kg}^{-1}$ ). Afterward, four blood samples were obtained on different time points, a single animal was used per extraction.

Plasma was separated from blood samples by centrifugation, and it was precipitated by using a crash solution of TCA 30 %. Samples were mixed and centrifuged, and the supernatant was injected in a LC-MS/MS system. Finally, a noncompartmental pharmacokinetic analysis of the different plasma levels of polymyxin analogues was performed using the PKPlus® software, 1.0 (Simulations Plus). Figure 79 shows the comparative graphs of plasma concentration profiles *versus* time.



**Figure 79:** Individual plasma concentration *versus* time profiles.

The pharmacokinetic study demonstrated that thiothreonine compounds were detected non-metabolized in the blood of the mice 6 hours after their administration with higher concentrations than natural polymyxin, so that the previously discussed low toxicity presented by compounds such as #25, was not caused by a premature peptide degradation *in vivo*.

The area under the concentration-time curve from 0 to the last measurable concentration ( $\text{AUC}_{0-t}$ ) and the maximum observed concentration ( $C_{\text{max}}$ ) are summarized in Table 23. It could be observed that  $\text{AUC}_{0-t}$  and  $C_{\text{max}}$  are much higher for our compounds than for polymyxin B which indicates higher exposure in mouse plasma.

**Table 23:** Summarized information obtained from the pharmacokinetic assay.  $C_{\max}$  and  $AUC_{0-t}$  ratio of each compound was calculated with regard PxB.

Compound	$C_{\max}$ ratio	$AUC_{0-t}$ ratio
<b>PxB</b>	1.0	1.0
<b>24</b>	1.9	2.1
<b>25</b>	2.1	3.2
<b>26</b>	2.5	2.9
<b>27</b>	2.1	2.7

### 1.8.3. Study of polymyxin analogues metabolization

To further investigate the nephrotoxicity associated with polymyxins, mass spectrometry was used to detect the presence of polymyxin analogues and their metabolites upon accumulation in kidneys, and urine collected at 24 and 48 hours after peptide administration.

The HPLC-Mass spectrometry study was performed by Dr. Olga Jauregui in “Unitat de Tècniques Separatives” in the Centres Científics i Tecnològics of Universitat de Barcelona (CCiTUB). Briefly, samples from animals treated with polymyxin B, analogue #25, or #27 from the last nephrotoxicity assay previously discussed were stored at -80 °C until their use. Solid kidney tissues were then homogenized into a liquid form using mechanical power to disrupt the tissues and disperse them into plasma control and ultra-pure water. Then, liquid samples were precipitated by using a crash solution (TCA 30 %), these samples were then mixed and centrifuged, and the supernatant was collected and stored. Urine samples were mixed with ACN, formic acid and ultra-pure water, vortexed, centrifuged, and the supernatant was separated and analyzed.

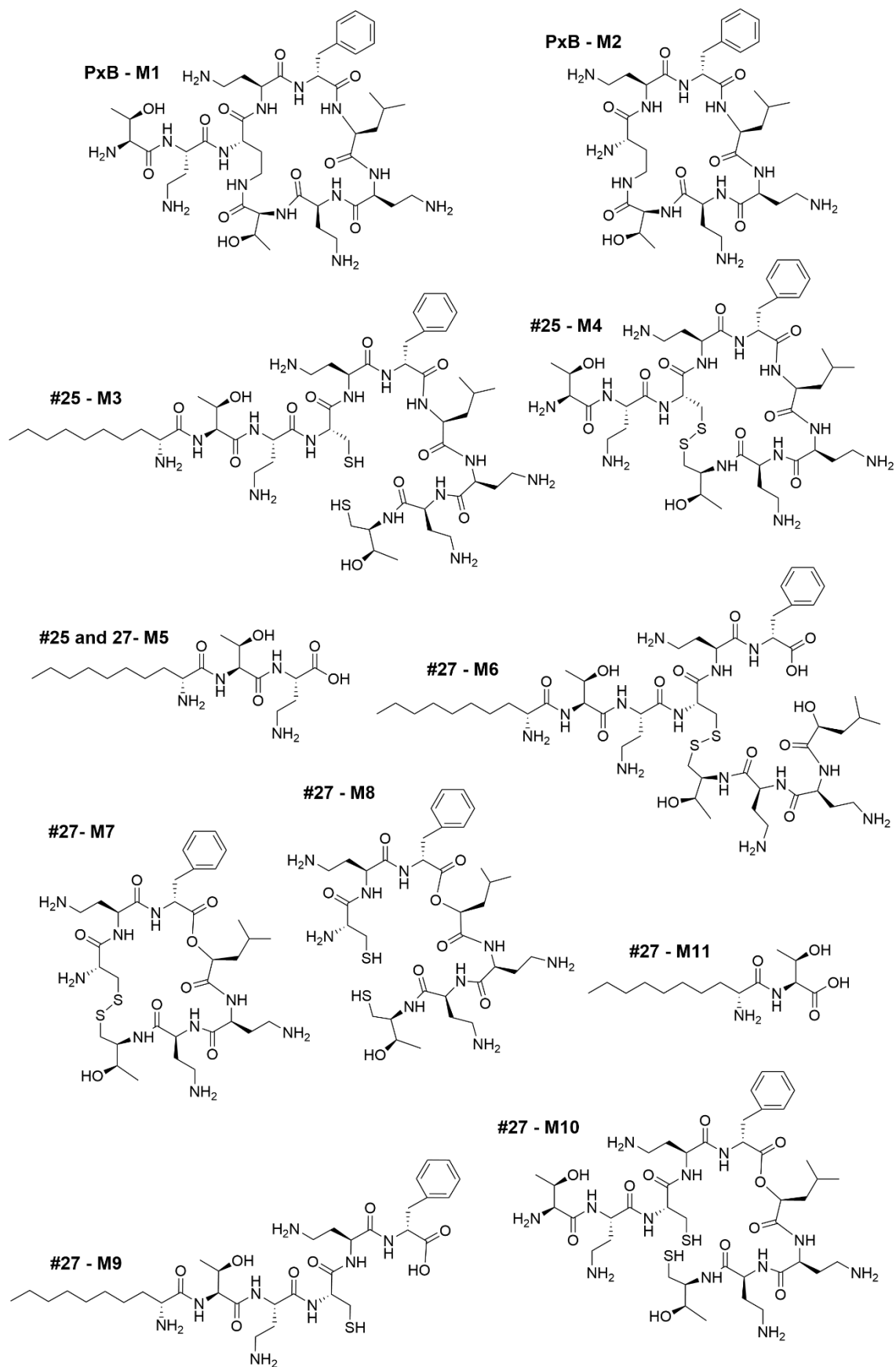
Calibration curves were constructed for each matrix by spiking the corresponding blank matrix with the compound under study at 5 levels accordingly to the concentration in samples. After the spiking, samples were treated as described above.

Finally, both tissue homogenates and urine samples were analyzed using an UHPLC system (Agilent, Model 1260 binary pump, Santa Clara, CA, USA). A linear ion trap quadrupole LC-MS/MS 4000 QTRAP mass spectrometer (ABSciex, Framingham, MA, USA) was used to obtain the MS and MS/MS data. Table 24 and Figure 80 summarize the metabolite identification for polymyxin B<sub>1</sub> and compounds #25 and #27.

Eleven different metabolites were identified, and only two of them corresponded to the amide hydrolysis of PxB, however, there is reported in literature that it is also metabolized by other mechanisms such as oxidation or demethylation.<sup>175</sup> Animals treated with lipopeptide #27 presented up to 7 different metabolites corresponding to amide, ester and disulfide bonds hydrolysis or reduction.

**Table 24:** Metabolite identification summary.

Metabolite	Transformation	Detected ion	Exact mass	$t_r$	Sample			
					Urine 24 h	Urine 48 h	Kidney	
PxB	PxB	-	[M + 2H] <sup>2+</sup> [M + 3H] <sup>3+</sup>	602.3822 401.9239	5.72	Y	Y	Y
	M1	Amide hydrolysis	[M + 2H] <sup>2+</sup>	482.2903	5.72	Y	N	N
	M2	Amide hydrolysis	[M + 2H] <sup>2+</sup> [M + 3H] <sup>3+</sup>	381.7346 254.8255	1.67	Y	Y	Y
25	25	-	[M + 3H] <sup>3+</sup>	385.2243	6.42	Y	Y	Y
	M3	Disulfide reduction	[M + 3H] <sup>3+</sup>	385.8962	6.46	Y	Y	N
	M4	Amide hydrolysis	[M + 3H] <sup>3+</sup>	328.8421	6.46	Y	Y	N
	M5	Amide hydrolysis	[M + H] <sup>+</sup>	389.2758	4.55	Y	Y	Y
27	27	-	[M + 3H] <sup>3+</sup>	385.5523	7.24	Y	Y	Y
	M6	Ester hydrolysis	[M + 2H] <sup>2+</sup> [M + 3H] <sup>3+</sup>	586.8301 391.5559	5.67	Y	Y	N
	M7	Amide hydrolysis	[M + 2H] <sup>2+</sup> [M + 3H] <sup>3+</sup>	262.1330 392.6959	3.04	Y	N	N
	M8	Disulfide reduction + amide hydrolysis	[M + 2H] <sup>2+</sup> [M + 3H] <sup>3+</sup>	262.8049 393.7037	7.47	Y	N	N
	M9	Disulfide reduction + ester hydrolysis	[M + 2H] <sup>2+</sup>	370.2122	7.26	Y	Y	N
	M10	Disulfide reduction + amide hydrolysis	[M + 2H] <sup>2+</sup>	494.2594	7.57	N	N	Y
	M5	Amide hydrolysis	[M + H] <sup>+</sup>	389.2758	4.55	Y	Y	Y
	M11	Amide hydrolysis	[M + H] <sup>+</sup>	289.2122	6.50	Y	Y	Y



**Figure 80:** Proposed molecular structures for the identified metabolites.

These results along with the low nephrotoxicity values previously obtained for compounds #25 and #27, point to that our primary hypothesis of design was consistent: polymyxin nephrotoxicity could be modulated by the introduction of scissile bonds in its scaffold, which facilitates the metabolization of the macrocycle and contributes to molecule detoxification.

#### 1.8.4. *In vivo* efficacy study

Considering the excellent antimicrobial activity showed by compound #25 and the remarkable decrease of nephrotoxicity displayed by this lipopeptide in the previously discussed *in vivo* assays, this compound was selected as the most promising therapeutic agent.

In order to study the efficacy of the potential hit candidate, an efficacy assay was performed in an experimental pneumonia model of infection caused by the clinical strain of *Pseudomonas aeruginosa*, Pa01, specifically in a previously characterized murine pneumonia model.<sup>274</sup> This experiment was performed by our collaborators in the group of Dr. María Eugenia Pachón of the Institute of Biomedicine of Seville (IBiS).

Briefly, anesthetized C57BL/6 female mice were infected intratracheally, using the minimal lethal dose (MDL) calculated for each strain, and the therapies were initiated 2 hours post-infection. Mice were randomly included into four different therapeutic groups: i) controls (CON, untreated), ii) CMS, 20 mg·Kg<sup>-1</sup>/8h, iii) PxB, 12 mg·Kg<sup>-1</sup>/8 h, and iv) #25, 12 mg·Kg<sup>-1</sup>/8 h. Mice were administered intraperitoneally with the desired dose of each peptide and monitored over 72 hours. Then, survivor mice were sacrificed, and samples were extracted and processed immediately after their death. Lungs were aseptically extracted, weighed, and homogenized in sterile and quantitative cultures (CFU·g<sup>-1</sup>) were performed.

The results obtained are shown in Table 25. Analogue #25 significantly reduced the bacterial count in lungs compared to controls. Remarkably, the obtained counts were comparable to the obtained by natural polymyxin B. and it reduced the bacterial count compared to the colistimethate sodium. New efficacy studies on peptide #27 are currently underway.

**Table 25:** In vivo efficacy in pneumonia model caused by *Pseudomonas aeruginosa* Pa01.

Strain	Group	Peptide	Animals	Dose (mg·Kg <sup>-1</sup> /8 h/ip)	Lung (CFU·g <sup>-1</sup> )
Pa01	I	CON	5	-	10.81 ± 0.64
	II	CMS	5	20	9.21 ± 1.42
	III	PxB	6	12	6.85 ± 0.38
	IV	#25	5	12	6.92 ± 0.41

## 1.9. Conclusions

- A novel cleavage reagent for the deprotection of Bn-type protecting groups has been described and optimized. This methodology consists of a 45-minute treatment with HBr *in-situ* generated from a solution of TFA/TES/Br<sub>2</sub> (82.5:15:2.5, v/v/v). It allowed the total synthesis of the model peptide polymyxin B<sub>3</sub> with a satisfactory global yield of 21 % comparable to common SPPS techniques.<sup>183,275</sup> The new methodology was also effective for the cleavage and deprotection of peptides directly attached to MBHA resins (synthesis of dusquetide and RR4), which were synthesized following Fmoc/<sup>t</sup>Bu procedures. Both model peptides were obtained with excellent cleavage yields and purities around 80 and 95 % respectively.

- We explored different methodologies for the whole characterization of the peptide salts. CHNS elemental analysis and titration gave us quantitative information about the ionic content of the polymyxin samples which contain certain counter ions such as sulphate or chloride, but they presented drawbacks such as the required sample amount and the limited number of ions detected. Finally, we found ESI-HR MS to be a complete and very useful technique to fully characterize the counterion composition of cationic peptides, being possible to elucidate the whole salt composition. ESI MS instrumentation proved to be less sensitive than high resolution spectrometry, as expected, but there was possible to determine the main species of each sample [M + Br]<sup>-</sup>, [M + TFA]<sup>-</sup> and [M + Cl]<sup>-</sup>.

- A set of 31 polymyxin-based compounds were designed and synthesized, introducing modifications that could reduce the polymyxin associated toxicity such as the introduction of scissile bonds in the structure (esters and disulfide linkages) and modifications on the *N*-terminal fatty acid or hydrophobicity.

- The antimicrobial activity of all synthesized compounds was examined. The introduction of an ester bond in the backbone of polymyxin generally produce a 2-fold increase in the MIC value. Cysteine analogues also displayed a reduced activity in comparison with natural PxB, but their activity can be modulated by modifying the hydrophobicity of the molecule. Compounds with long *N*-terminal fatty acid chains showed broad-spectrum activity, while the redistribution of the hydrophobicity into the macrocycle produced highly selective compounds against the Gram-negative *Pseudomonas aeruginosa* strain. Hydroxamic acid analogues did not improve the activity of natural polymyxin. Finally, peptides containing the thiothreonine building block showed comparable activity to polymyxin B.

- The mechanism of action of cysteine and thiothreonine compounds was studied, both analogue types showed selective binding to specific phospholipids that mimic the outer and the inner membrane of Gram-negative and Gram-positive bacteria, with formation of clusters of vesicles, and induction of lipid exchange starting at very low peptide concentrations (<3 %), in absence of any lytic effect. Lipopeptide-induced bacterial membrane alteration was confirmed by electron microscopy observation and disC<sub>3</sub>(5) depolarization assay.

- *In vivo* experimentation was performed in seven polymyxin analogues. According to the first obtained results, compounds #25 and #27 were selected as promising hit candidates for further development; then, their efficacy, and nephrotoxicity were studied, showing excellent results with good antimicrobial activity and lower nephrotoxicity than natural polymyxins. The metabolization of these peptides upon accumulation in mouse kidney was studied and the hypothesis of ester hydrolysis and disulfide reduction was confirmed.

- The synthesis of #25 and #27 was optimized and scaled by using Trt-Cl resin instead of 2-CTC resin, which prevents the premature peptide release produced in each piperidine deprotection treatments, water was also removed from the cleavage to prevent the ester bond hydrolyzation of peptide #27. Global yields about 20 % of >95 % of pure peptides were achieved and the production was scaled from 20 mg to nearly 900 mg and 400 mg respectively.





## **CHAPTER 2:**

### **Length dependent activity of $\alpha$ -helical antimicrobial peptides based on BP100**



## 2.1. Introduction

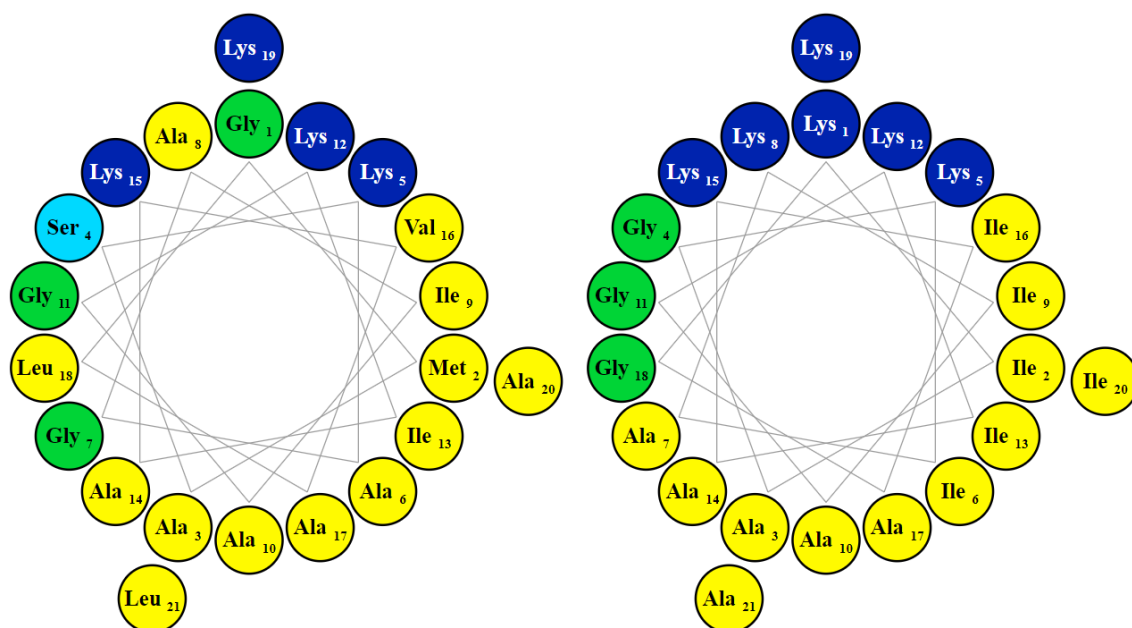
As previously introduced, AMPs are commonly classified based on their secondary structure into four major classes,  $\alpha$ -helix,  $\beta$ -sheet, extended helices and loop structures.<sup>46</sup> Among them,  $\alpha$ -helical antimicrobial peptides have been thoroughly investigated as one of the most abundant and widespread in nature. These peptides are often unstructured in aqueous solution but adopt an amphipathic helical structure in contact with biological membranes.<sup>276,277</sup> They tend to be short (<50 amino acid residues), with relatively simple structures; and they are active against a wide range of pathogens, including Gram-positive and Gram-negative bacteria, fungi, and protozoa. Numerous studies have been performed to further investigate the mechanism of action  $\alpha$ -helical AMPs. In this chapter, we will focus on the study of the  $\alpha$ -helical MSI-103 and BP100.

### 2.1.1. Peptidyl-glycine-leucine-carboxamide and its derivative MSI-103

Peptidyl-glycine-leucine-carboxamide (PGLa) is a member of the magainin family of antibiotic peptides found in frog skin and its secretions.<sup>278-280</sup> PGLa is a linear peptide with 21 amino acid residues (GMASKAGAIAGKIAKVALKAK-NH<sub>2</sub>). It is positively charged and has hydrophobic residues, due to these properties, PGLa can bind preferentially the negatively charged outer leaflet of cytoplasmic bacterial membranes.<sup>281</sup> It was shown to exhibit antifungal and antimicrobial activity towards Gram-positive and Gram-negative bacteria, and in contrast to other amphiphilic peptides, PGLa does not cause hemolysis of human red blood cells.<sup>282</sup>

MSI-103, with sequence (KIAGKIA)<sub>3</sub>-NH<sub>2</sub>, was designed starting from the sequence of PGLa (Figure 81). It was optimized and simplified through SAR studies by increasing the basicity and the amphipathicity of the molecule and it is formed by only four different amino acids in a repeated heptamer.<sup>283</sup> This designed peptide has a high antimicrobial activity, low hemolytic side effects and it adopts an  $\alpha$ -helical structure in a lipid environment.<sup>284</sup>

PGLa was proposed to kill bacteria through formation of transmembrane channels.<sup>285</sup> With the main goal to further investigate the action mechanism of MSI-103 and BP100, Anne S. Ulrich's group in the Karlsruhe Institute of Technology (KIT) have extensively studied them using different techniques, especially solid-state NMR.



**Figure 81:** Helical wheels of PGLa (left) and MSI-103 (right). Amino acids are color-coded as follows: hydrophobic residues in yellow; cationic in dark blue; polar in light blue; and Gly in green. Image created using the Protein Origami software.<sup>286</sup>

As previously introduced, many naturally produced peptides, such as antimicrobial peptides and toxins, are known to spontaneously induce transmembrane pores in lipid bilayers under certain conditions. Such pores are proposed to be formed either with peptides alone forming the walls of the pores, in a so called “barrel-stave pore” found for alamethicin,<sup>287</sup> or with lipid headgroups intermixed with peptides in the pore walls, so called “toroidal pores”, as it is the case of melittin.<sup>288</sup>

It is known that PGLa, the parent peptide of MSI-103, permeabilizes membranes by forming pores.<sup>68,289</sup> With the aim to investigate the action mechanism of MSI-103, peptides of 14-28 amino acids in length based on MSI-103 were designed with the same repetitive sequence KIAGKIA, therefore called KIA peptides (Table 26).<sup>290,291</sup> If these peptides also were to form pores built from transmembrane helices, a minimum peptide length would be required to span the membrane.

It was found that membrane activity of the KIA peptides strongly depends on their length. In particular, the peptides must be long enough to span the hydrophobic thickness of a membrane to induce vesicle leakage, and there was also a clear threshold length for antimicrobial activity and hemolytic activity.<sup>290</sup> For example, to kill *E. coli* bacteria and to induce leakage of POPC/POPG (1:1) vesicles, KIA peptides must have at least 17

amino acids; shorter peptide were inactive, while all longer peptides were also active. The length of an ideal  $\alpha$ -helix with 17 amino acids is 25.5 Å, and the hydrophobic thickness of POPC or POPG bilayer is around 27 Å, in thicker membranes longer peptides were needed. It was proposed therefore, that KIA peptides form pores in the membrane and must be long enough to span the membrane for such pores to be formed.

**Table 26:** Sequences of KIA peptides.

Peptide name	Sequence	Charge
<b>KIA14</b>	KIAGKIA KIAGKIA-NH <sub>2</sub>	5
<b>KIA15</b>	KIAGKIA KIAGKIA K-NH <sub>2</sub>	6
<b>KIA17</b>	KIAGKIA KIAGKIA KIA-NH <sub>2</sub>	6
<b>KIA19</b>	KIAGKIA KIAGKIA KIAGK-NH <sub>2</sub>	7
<b>KIA21 = MSI-103</b>	KIAGKIA KIAGKIA KIAGKIA-NH <sub>2</sub>	7
<b>KIA22</b>	KIAGKIA KIAGKIA KIAGKIA K-NH <sub>2</sub>	8
<b>KIA24</b>	KIAGKIA KIAGKIA KIAGKIA KIA-NH <sub>2</sub>	8
<b>KIA26</b>	KIAGKIA KIAGKIA KIAGKIA KIAGK-NH <sub>2</sub>	9
<b>KIA28</b>	KIAGKIA KIAGKIA KIAGKIA KIAGKIA-NH <sub>2</sub>	9

In a second study, modified KIA peptides were studied, also of length from 14 to 28 amino acids, but with a constant charge of +7 for all peptides in the series.<sup>292</sup> In this case the same length dependence was found, suggesting that the different charge of the KIA peptides was not responsible for the activity, but it is the length of the sequence that really matters. In particular, shorter peptides with less than 17 amino acids, but with a charge of +7, were also inactive against *E. coli* bacteria, and did not induce leakage of POPC/POPG (1:1) vesicles.

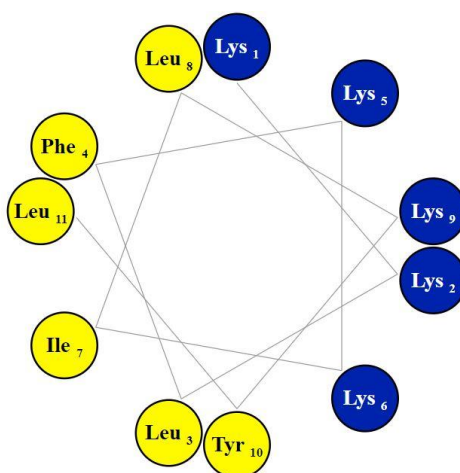
It was found from a more detailed analysis of the activity, that KIA peptides with a charged Lys residue at the *C*-terminus were less active than peptides with a hydrophobic Ile-Ala *C*-terminal sequence.<sup>290,292</sup> From further studies, it was also found that peptides with a charged Lys on the *N*-terminus were more active than peptides of the same length with a hydrophobic Ile-Ala sequence at the *N*-terminus.<sup>293</sup>

### 2.1.2. Melittin, cecropin A and its derivative BP100

Melittin (GIGAILKVLSTGLPALISWIKRKRQE-NH<sub>2</sub>) is a 26-residue peptide, which is the main component (about 50 %) of the venom of the honeybee *Apis mellifera*. It is a basic, amphipathic  $\alpha$ -helical and membrane-lytic peptide, and it causes significant

hemolysis in human blood cells.<sup>294</sup> On the other hand, cecropin A (KWKLFFKKIEKVGQNIRDGIIKAGPAVAVVGQATQIAK-NH<sub>2</sub>) is a 37-amino acid linear and highly basic  $\alpha$ -helical peptide, which was first found in the giant silk moth *Hyalophora cecropia*.<sup>295</sup> It displays powerful lytic activity against Gram-positive and Gram-negative bacteria but has no cytotoxic effects on eukaryotic cells.<sup>296</sup>

Searches for shorter, more potent, nontoxic, and more stable peptides have led to the identification of synthetic peptides with broader and higher activity than the natural melittin and cecropin.<sup>297-299</sup> BP100 (KKLFFKKILKYL-NH<sub>2</sub>) is a successful example of an 11-residue peptide derived from the well-known cecropin A(1-7)-melittin(2-9) hybrid peptide (Figure 82).<sup>300</sup> It is potent against Gram-negative bacteria and it possesses low hemolytic side effects.<sup>301</sup> An atomic force microscopy study found that BP100 destroys the cell envelope of Gram-negative bacteria,<sup>302</sup> this fact suggests that the lipid bilayer is the target of the peptide, and therefore, membrane damage is the primary cause of the antibacterial effect. Its mechanism of action, however, has not been completely understood yet. It is known to have a high antimicrobial and cell penetrating activity but with only 11 amino acids,<sup>303</sup> BP100 seems not long enough to span a lipid bilayer and form a transmembrane pores, so it is unlikely to operate by the mechanism that has been proposed for longer amphipathic peptides, such as KIA peptides.<sup>290</sup>



**Figure 82:** Helical wheels of BP100. Amino acids are color-coded as follows: hydrophobic residues in yellow; cationic in dark blue. Image created using the Protein Origami software.<sup>286</sup>

The short multifunctional peptide BP100 was studied in the Ulrich group, and solid-state NMR and oriented circular dichroism (OCD) data showed that the surface-bound peptide

does not undergo a re-alignment in the membrane over a wide range of peptide-lipid ratios from 1:3000 up to 1:10, in contrast with the pore forming peptides which have been found to bind parallel to the membrane surface only at low concentration.<sup>304</sup>

BP100 was also studied by alanine scan over all 11 amino acids. This technique consists of the replacement of a specific amino acid of the sequence by an alanine in order to determine the contribution of this specific residue. It was found that not all of the 6 positive charges are required for BP100 antimicrobial activity, but a certain level of hydrophobicity is necessary. Furthermore, the replacement of 2-Lys or 9-Lys by alanine reduced the hemolytic activity while the antimicrobial activity was conserved, giving rise to BP100 analogues with improved therapeutic index.<sup>305</sup>

These results are compatible with the view that BP100 can damage bacterial membranes *via* the so-called “carpet” mechanism, from where it is able to insert dynamically into the bilayer without pore formation. However, further studies were needed to understand how the peptide is capable to act as an antimicrobial membrane-permeabilizing agent, and on the other hand, as an efficient cell penetrating peptide without causing leakage in eukaryotic cells or significant hemolytic side effects. In that regard, we studied the length dependence of peptides of different length based on the sequence of BP100, to determine if there is also a length dependence, and how it differs from that of KIA peptides.

### **2.1.3. General considerations about the techniques used in this chapter**

#### 2.1.3.1. Antimicrobial activity

The antimicrobial activities of BP100 analogues, expressed as the minimum inhibitory concentration (MIC), were determined on standard reference DSM collection strains. Two Gram-negative bacteria, *Escherichia coli* and *Acinetobacter sp.*, were used as well as two Gram-positive strains, *Bacillus subtilis*, and *Staphylococcus xylosus*.

The MIC assay was performed as explained in chapter 1, and it is further detailed in experimental section 3.2.2.1.

#### 2.1.3.2. Hemolysis

As previously explained in chapter 1, The *in-vitro* hemolysis assay evaluates hemoglobin release in the plasma (as an indicator of red blood cell lysis) following test agent exposure.



The hemolytic activity of BP100 analogues was examined with a serial 2-fold dilution assay.<sup>284</sup> Briefly, the protocol consists of a series of dilutions of peptide which were mixed with a standard amount of erythrocytes and incubated for 30 minutes at 37 °C. The samples were then centrifuged and the absorbance of the supernatant, which includes hemoglobin, was measured.

### 2.1.3.3. Biophysical evaluation of the mechanism of action

Large and small unilamellar vesicles of different compositions were used as model membranes to further investigate the mechanism of action of BP100.

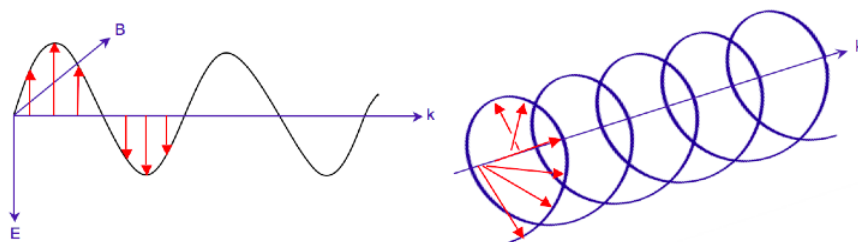
Liposomes of different compositions were used, all of them designed to model biological membranes of different compositions and thickness. In brief, DMPC/DMPG (3:1) were used for CD measurements, POPC/POPG (1:1) and DErPG/DErPC (1:1) in binding and leakage experiments, and POPC/POPG (1:1) and DMPC/lysoMPC (2:1) vesicles for solid state NMR.

#### *2.1.3.3.1. Circular dichroism spectroscopy*

Circular dichroism (CD) is an excellent tool for rapid determination of the secondary structure and folding properties of proteins and peptides. To fully understand this technique, hereunder some key concepts are briefly introduced.

##### *2.1.3.3.1.1. Light polarization*

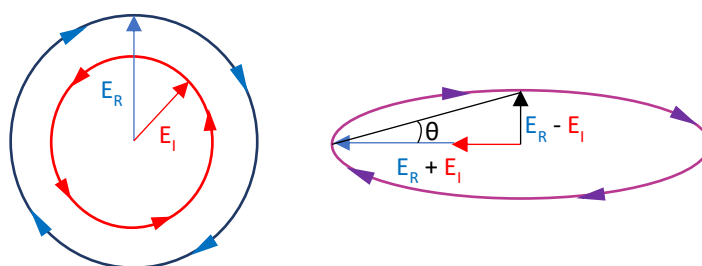
Light is an electromagnetic radiation that consists of oscillating electric (E) and magnetic (B) fields perpendicular to each other and the direction of propagation. If the light is unpolarized, the electrical field vector oscillates in many planes, which are perpendicularly oriented to the direction of the beam, whereas if light is linearly polarized by passing through suitable prisms or filters, its electric field oscillates in a single plane. Otherwise, in circularly polarized light, the electric field vector rotates around the propagation axis maintaining a constant magnitude. As the radiation propagates, the electric field vector traces out a helix, see Figure 83. Light can be circularly polarized in two directions: clockwise ( $E_R$ ) and counterclockwise ( $E_L$ ), the waves are 90 degrees out of phase with each other and can be separated using a variety of prisms or electronic devices.<sup>306</sup>



**Figure 83:** Linearly (left) and circularly (right) polarized lights.

#### 2.1.3.3.1.2. Origin of the CD effect

CD is a phenomenon that results when chromophores in an asymmetrical environment interact with circularly polarized light. When this occurs, the molecule absorbs right and left-handed circularly polarized light to different extents and also have different indices of refraction for the two waves. This differential absorption results in the  $E_R$  and  $E_L$  vectors having different amplitudes, and leads to an elliptically polarized wave, see Figure 84.



**Figure 84:** Elliptically polarized light (purple) is the superposition of  $E_L$  (red) and  $E_R$  (blue) light.  $\theta$  is the angle between the magnitude of the electric field vector at its maximum and its minimum.

CD is reported either in units of  $\Delta E$ , the difference in absorbance of  $E_R$  and  $E_L$ , or in degrees ellipticity ( $\theta$ ). Thus, CD bands can be either positive or negative, depending on which type of light is absorbed more strongly. For peptides and proteins, the mean residue ellipticity,  $[\theta]_{MRE}$ , is used. It reports the molar circular dichroism for individual residues instead of whole molecules, and therefore, it allows an easy comparison of peptides with vastly different molecular weights. Mean residue ellipticity is calculated according to the following equations:

$$[\theta]_{MRE} = \theta / 10 \cdot C_r \cdot d \quad \text{in } [\text{deg} \cdot \text{cm}^2 \cdot \text{dmol}^{-1}]$$

$$C_r = n \cdot c_g / M_w \quad [\text{mol} \cdot \text{L}^{-1}]$$

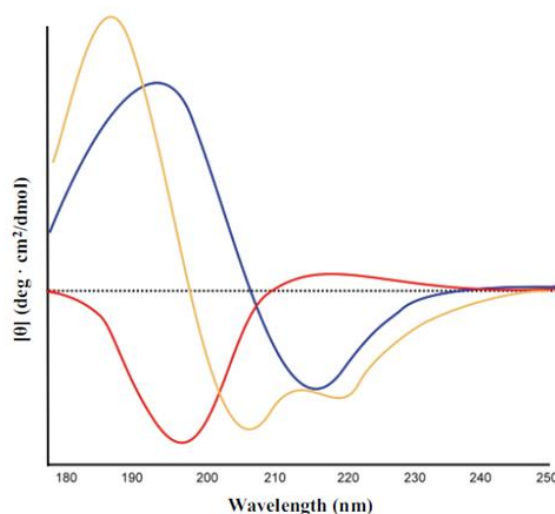
where  $\theta$  is the observed ellipticity;  $d$  is the path length of the optical cell;  $C_r$  is the molar concentration per peptide bond;  $n$  is the number of peptide bonds in the molecule;  $c_g$  is the peptide concentration; and  $M_w$  is the molecular weight of the peptide.

## 2.1.3.3.1.3. CD spectroscopy as a tool to determine peptide secondary structure

Circular dichroism (CD) spectroscopy is the most widespread technique used for estimating the secondary structures of proteins and polypeptides in solution.

The main optically active groups of the peptide backbone are the amide bonds; therefore, secondary structures of proteins and peptides can be analyzed using the far-UV (190 - 250 nm) region of light. Depending on the orientation of these bonds in the arrays, their characteristic optical transitions ( $n \rightarrow \pi^*$  at 222 nm and  $\pi \rightarrow \pi^*$  at 200 nm) can be shifted and/or split into multiple transitions.

Different common secondary structural motifs have characteristic CD spectra,<sup>307,308</sup> as it is shown in Figure 85. For example, the CD spectrum of unordered peptides is usually characterized by a single negative band below 200 nm, whereas  $\alpha$ -helical structures usually present two negative bands at 208 and 222 nm along with one positive band at 192 nm and  $\beta$ -sheet structures typically show a negative band at 217 nm and a positive band at 195 nm.



**Figure 85:** CD spectra associated with various types of secondary structures: (yellow)  $\alpha$ -helix; (blue)  $\beta$ -sheet and (red) random coil.

## 2.1.3.3.2. Tryptophan fluorescence to detect peptide binding to lipid membranes

The peptide binding to membrane interfaces was studied based on the solvatochromic effect of intrinsic tryptophan fluorescence. When the fluorescence emission spectra of Trp-containing peptides in buffer is recorded upon excitation at 280 nm, an emission

maximum around 350 - 355 nm is observed, indicating that the Trp residue is highly exposed to the solvent. If after addition of liposomes, an alteration of the emission spectra is observed, with the emission maximum shifted to 330 nm, it indicates that the Trp residue is now located in a more hydrophobic environment upon binding to the lipid membrane.

#### 2.1.3.3.3. *Vesicle leakage induced by the peptides*

Membrane permeability due to peptide binding was studied by leakage experiments using unilamellar lipid vesicles. The fundamentals of this technique have previously been explained in chapter 1. Briefly, the assay consists of co-encapsulating in liposomes the fluorescent probe ANTS and the cationic quencher DPX. If the peptides were capable of permeabilize the membrane, the liposome contents would be released into the medium and there would be an increase in ANTS fluorescence as the DPX diluted in the media would not be capable to efficiently quench the ANTS fluorescence.

#### 2.1.3.3.4. *Solid-state NMR of peptides bound to lipid membranes*

Solid state nuclear magnetic resonance (ss-NMR) spectroscopy is a valuable analytical tool used to determine the chemical composition, local structure, and dynamic properties of solids. In the present thesis it was used to obtain information about the structure and dynamics of peptides associated with extended lipid bilayers.

##### 2.1.3.3.4.1. NMR fundamentals

The basic principle of NMR is based on the Zeeman interaction between the nuclear spins and an external magnetic field. Briefly, when atoms containing non-zero nuclear spins (Table 27) are placed in an external magnetic field, nuclei exhibit Zeeman splitting (Figure 86), adopting different discrete energy states and leading to an energy difference,  $\Delta E$ , given by the following equations:

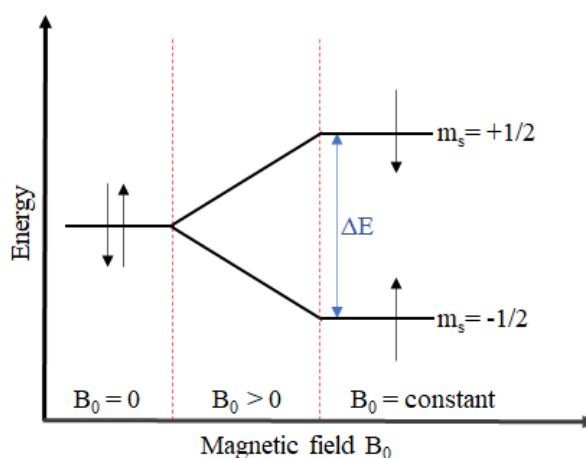
$$\Delta E = \hbar\omega_0$$

$$\omega_0 = \gamma B_0$$

where  $\hbar$  is the Planck constant;  $\omega_0$  is the Larmor frequency;  $\gamma$  is the gyromagnetic ratio, a constant associated with each isotope, and  $B_0$  is the strength of the magnetic field.

**Table 27:** Commonly studied nuclei in NMR spectroscopy.

Isotope	Spin quantum number (I)	Gyromagnetic ratio ( $\gamma$ )	Natural abundance	Sensitivity (relative to $^1\text{H}$ )
$^1\text{H}$	1/2	$2.675 \cdot 10^8$	99.98 %	1.0
$^{19}\text{F}$	1/2	$2.517 \cdot 10^8$	100 %	0.833
$^{31}\text{P}$	1/2	$1.083 \cdot 10^8$	100 %	0.0663
$^{13}\text{C}$	1/2	$6.73 \cdot 10^7$	1.1 %	0.0159
$^2\text{H}$	1	$4.11 \cdot 10^7$	0.015 %	0.0096
$^{15}\text{N}$	1/2	$-2.71 \cdot 10^7$	0.37 %	0.00104

**Figure 86:** Schematic representation of the Zeeman splitting for a  $I = 1/2$  system.

An NMR spectrum is obtained by measuring the difference in energy between the spin states. This is achieved by exciting the nuclear spins out of their thermal equilibrium using resonant radiofrequency (RF) pulses. In absence of any further perturbing radiofrequency pulse, relaxation processes eventually return the spin system to thermal equilibrium. During the process a free induction decay (FID) can be recorded in a coil wrapped around the sample. The FID contains an oscillation at the nuclear Larmor frequency, which is proportional to the Zeeman interaction and is unique to each nuclear isotope. The fluctuating FID signal is finally transformed by applying a Fourier transformation to the frequency domain signal, the NMR spectrum.

#### 2.1.3.3.4.2. NMR interactions

In addition to the Zeeman interaction, the nuclear spins are susceptible to a wide range of interactions with their surrounding environment, each interaction has contributions to the overall Larmor frequency in varying magnitudes: the Zeeman interaction is on the scale

of hundreds of MHz, dipolar coupling and chemical shift anisotropy are both on the scale of tens of kHz and J-couplings are typically 1 - 100 Hz.

$$\omega_0 \approx \text{Zeeman} + \text{Dipolar} + \text{Chemical Shift Anisotropy} + \text{Chemical Shielding} + \text{J-Coupling}$$

Depending on the states of the matter studied, the interactions affecting the Larmor frequency present significant differences. In solution NMR, compounds are dissolved in low-viscosity solvents where the molecules are rapidly tumbling through all orientations, and therefore the orientation of the nucleus with respect to the  $B_0$  field is averaged out and just the isotropic value remains. Thus, the obtained signals of solution NMR are mainly influenced by the electronic environments of the nuclei (chemical shielding,  $\delta$ ), including interactions with neighboring atoms (J-couplings).

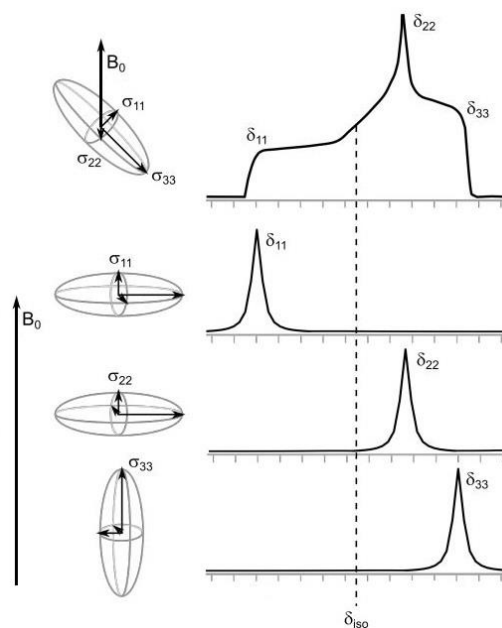
In contrast, in ssNMR the motion of the molecules is restricted, and the chemical shifts depend basically on the orientation of the molecule within the external magnetic field. This effect is commonly known as chemical shift anisotropy (CSA). In consequence, every orientation of a molecule with regard to the magnetic field contributes by a single line of a particular frequency to the overall spectrum.

The anisotropic chemical shift interactions are mathematically described by a tensor of three principal components ( $\sigma_{11}$ ,  $\sigma_{22}$  and  $\sigma_{33}$ ) that can be visualized as an asymmetric ellipsoid. The order of shielding magnitude of the tensor elements is defined as  $\sigma_{11} \leq \sigma_{22} \leq \sigma_{33}$  (the  $\sigma_{11}$  component corresponds to the direction of the least shielding, resulting in the highest field resonance).<sup>309</sup> The isotropic shift is the mean of these three components.

$$\sigma_{\text{iso}} = (\sigma_{11} + \sigma_{22} + \sigma_{33}) / 3$$

Figure 87 illustrates the effect of CSA on the chemical shift of a peak in ss-NMR spectroscopy. In an un-oriented powder, all orientations of a molecule are present with equal probability, the spectrum therefore results in a characteristic powder pattern consisting of a superposition of resonance frequencies. In solutions of low viscosity, the electronic environment is averaged out giving an isotropic value for the CSA tensor.

In the present chapter we used the CSA interactions of  $^{31}\text{P}$  ss-NMR and  $^{15}\text{N}$  ss-NMR to study phospholipid model membranes and the orientation of peptides in oriented bilayer samples. These techniques are briefly introduced below.



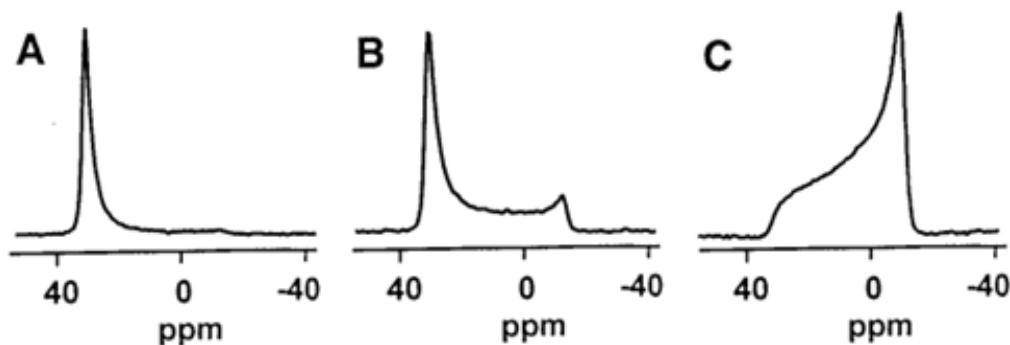
**Figure 87:** The effect of CSA on a static powder sample. The tensor ellipsoid (left) is depicted aligned with one of its principal axis along the magnetic field, resulting in the characteristic chemical shifts  $\delta_{11}$ ,  $\delta_{22}$  and  $\delta_{33}$  (right, three lower).  $\delta_{iso}$  is the isotropic chemical shift.

#### 2.1.3.3.4.3. $^{31}\text{P}$ ss-NMR as a tool to study phospholipid membranes

Phosphorus ss-NMR spectroscopy is a widely used technique to study the structure and dynamics of both model and biological membranes,<sup>310,311</sup> since they are mostly composed of phospholipids, which in turn contain only one phosphorus atom in each molecule, thus facilitating the interpretation of the spectra. Moreover, as it is not present in proteins and peptides, it provides selectivity for the lipid signal.

In our case,  $^{31}\text{P}$  ss-NMR of phospholipid bilayers were routinely used to test the quality of the alignment of phospholipid bilayers. Phospholipids in a membrane environment under physiological conditions perform rapid axial rotation around the long axis of the molecule, which results in the appearance of averaged axial symmetry of the lipid molecule and simplification of the chemical shift tensor. Therefore, when lipid bilayers are macroscopically aligned, the molecular orientation is fixed with regard to the magnetic field, and a narrow single line should be observed in the resulting spectrum, which indicates that the head group region around the phosphate atoms adopt the same conformation and are aligned in the same direction in all lipids. The exact position under a particular alignment is characteristic for a particular lipid. Bilayers of pure POPC, for example, oriented with the bilayer normal parallel to the magnetic field direction, exhibit

$^{31}\text{P}$  resonances at 30 ppm (Figure 88A). On the other hand, badly oriented lipid bilayers give rise to additional signals along the whole CSA range, in the case of POPC bilayers from approximately +30 up to -15 ppm (Figure 88B).



**Figure 88:** Proton-decoupled  $^{31}\text{P}$  ss-NMR spectra of POPC membranes. A) Well-oriented sample with the normal parallel to the magnetic field direction; B) A significant proportion of the phospholipid shows misalignment and/or conformational alterations in the headgroup; C) Powder pattern of completely un-oriented sample. Figure adapted from ref. <sup>312</sup>

#### 2.1.3.3.4.4. $^{15}\text{N}$ ss-NMR as a tool to study peptide orientation in lipid membranes

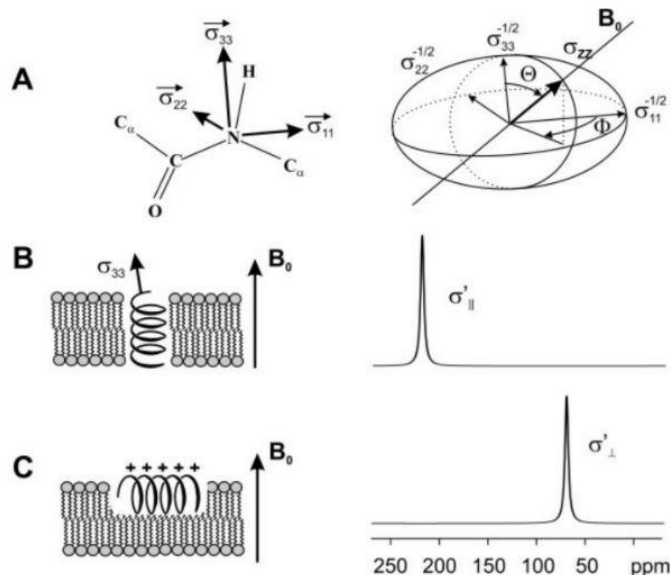
As previously shown in Table 27, the natural abundance of many interesting isotopes is low, which makes the NMR application challenging. For the purpose to study the orientation of the peptides in membranes, a single  $^{15}\text{N}$  label was introduced in the design of our peptides (see section 2.3).

In an  $\alpha$ -helix, the NH bond vector lie almost parallel to the helix axis. The  $\sigma_{33}$  component of the  $^{15}\text{N}$  CSA tensor remains aligned roughly along the NH bond vector, and also more or less parallel to the helix axis (Figure 89A). When helical peptides are reconstituted into macroscopically oriented phospholipid bilayers, the  $^{15}\text{N}$  chemical shift is a direct indicator of the approximate alignment of the helix with respect to the membrane surface. When oriented parallel to the magnetic field direction, the molecules exhibit  $^{15}\text{N}$  resonances at values above 200 ppm (Figure 89B). However, a chemical shift measurement lower than 90 ppm implies that the NH vector is oriented approximately at a right angle with respect to the magnetic field direction (Figure 89C).

It is furthermore possible to find out whether a peptide is undergoing fast long-axial rotation about the membrane normal, considering that a narrow line in the spectrum is an indicative of peptide motion. Contrarily, the broadening of the signal indicates the static



alignment in the membrane. Since  $^{15}\text{N}$  has a very low sensitivity in NMR, usually a cross-polarization sequence is used to transfer the magnetization from  $^1\text{H}$  to the neighbor  $^{15}\text{N}$  nucleus.



**Figure 89:** A) The  $^{15}\text{N}$  chemical shift tensor is represented as an ellipsoid and placed next to the molecular frame of the peptide bond.  $\sigma_{11}$ ,  $\sigma_{33}$  and the peptide bond are aligned within the plane of the paper,  $\sigma_{22}$  is oriented towards the viewer. B) Simulated proton-decoupled  $^{15}\text{N}$  solid-state NMR spectrum of a transmembrane peptide, C) same as B) for a peptide orientated parallel to the membrane surface. Figure taken from ref.<sup>313</sup>

## 2.2. Objectives of chapter 2

The main objective of this chapter was to study the mechanism of action of BP100 on lipid membranes by using peptides of different lengths based on its structure, and determine if there is a length dependence, and how it differs from that of KIA peptides.

There are several possible outcomes:

- BP100 may lay flat on the membrane surface and permeabilize it, in what is known as carpet mechanism. If this is the case, then the length of the peptide should not be important, as it does not need to span the membrane, and longer or shorter versions should be as active as BP100. However, the coverage of the surface should be important, so that we can expect that a lower molar concentration is needed for longer peptides.

- BP100 may form pores even though it is too short to span the membrane. In this case, shorter versions may not be active, and longer versions should be more active, since they should more easily span the membrane. In particular, peptides of 17 or more amino acids should be significantly more active than the shorter versions, with strong activity against *E. coli* bacteria, and with high induced leakage of POPC/POPG (1:1) vesicles.
- BP100 may work with another mechanism, and there might be an optimal length which is most active, whereas longer and shorter peptides are less active. Such a behavior has been reported for some model amphipathic  $\alpha$ -helical AMPs.<sup>314,315</sup>

### 2.3. Peptide design

The new series of peptides was analogous to the KIA series described in Table 26, but based on the sequence of BP100, and we therefore we named them BPKIA. For that purpose, an heptameric repeat from BP100 was used to generate the BPKIA peptides of different length.

We used the following design rules:

- BP100 has 6 positive charges, with 5 lysine residues in the sequence. In the first 7 residues there are 4 lysine and in the next 4 residues only one. Analogues were designed keeping the total charge and moving one charge from the first 7 residues to the last 4.
- From the KIA study, we found that *N*-terminal charges and *C*-terminal hydrophobic residues improved the activity. BP100 has two lysine residues at the *N*-terminus and two hydrophobic/ aromatic residues at the *C*-terminus, which fits with the KIA rules. Therefore, we maintained the *N*-terminal Lys-Lys and *C*-terminal hydrophobic residues.
- It was previously found in the Ala scan of BP100,<sup>305</sup> that it is possible to replace one lysine with an alanine and still keep the antimicrobial activity of the peptide, while reducing hemolytic side effects. We therefore replaced 6-Lys residue with alanine in the basic heptamer.

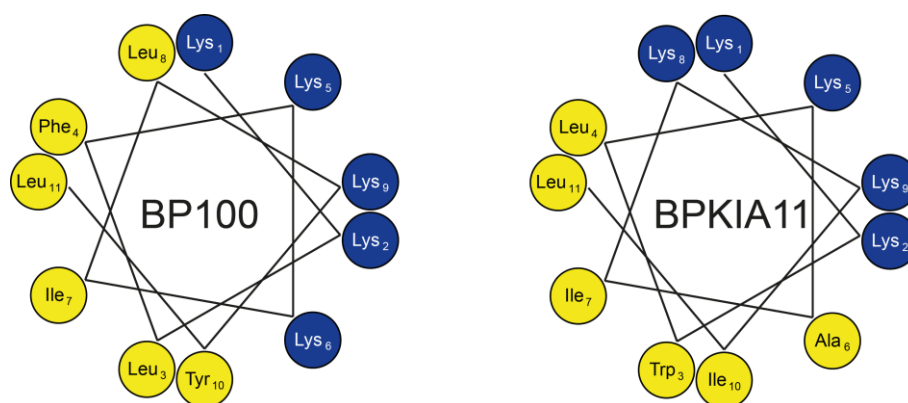
From these considerations we designed the repetitive heptameric sequence KKILAKI and planned to make a series of BPKIA peptides from 4 - 24 amino acids long.

We added in all peptides a Trp at position 3 to confer the peptides with intrinsic fluorescence, in order to study membrane binding, and to make it possible to determine the concentration of peptides accurately. Likewise, we place a  $^{15}\text{N}$  label ( $^{15}\text{N}$ -Ala) at position 6 in order to perform  $^{15}\text{N}$ -NMR experiments to determine the orientation of the peptides in the membrane and determine if pores are formed.<sup>291</sup>

The final list of BPKIA peptides is shown in Table 28. A comparison of the helical wheel projections of BP100 and BPKIA11 (with the same length) shows that both peptides form similar amphipathic helices (Figure 90).

**Table 28:** Sequences of BPKIA peptides based on BP100. All peptides contained a Trp at position 3, highlighted in bold, and a  $^{15}\text{N}$  label at Ala-6, highlighted in bold and red. Length was calculated assuming 1.5 Å per residue for an ideal  $\alpha$ -helix.

Peptide name	Sequence	C	Length (Å)
<b>KIA11</b>	KIAGKIA KIAG-NH <sub>2</sub>	5	16.5
<b>BP100</b>	KKLFFKKI LKYL-NH <sub>2</sub>	6	16.5
<b>BPKIA4</b>	KKWL-NH <sub>2</sub>	3	6
<b>BPKIA7</b>	KKWLK <b>AI</b> -NH <sub>2</sub>	4	10.5
<b>BPKIA10</b>	KKWLK <b>AI</b> KKI-NH <sub>2</sub>	6	15
<b>BPKIA11</b>	KKWLK <b>AI</b> KKIL-NH <sub>2</sub>	6	16.5
<b>BPKIA14</b>	KKWLK <b>AI</b> KKILKAI-NH <sub>2</sub>	7	21
<b>BPKIA17</b>	KKWLK <b>AI</b> KKILKAI KKI-NH <sub>2</sub>	9	25.5
<b>BPKIA18</b>	KKWLK <b>AI</b> KKILKAI KKIL-NH <sub>2</sub>	9	27
<b>BPKIA21</b>	KKWLK <b>AI</b> KKILKAI KKILKAI -NH <sub>2</sub>	10	31.5
<b>BPKIA24</b>	KKWLK <b>AI</b> KKILKAI KKILKAI KKI-NH <sub>2</sub>	12	36



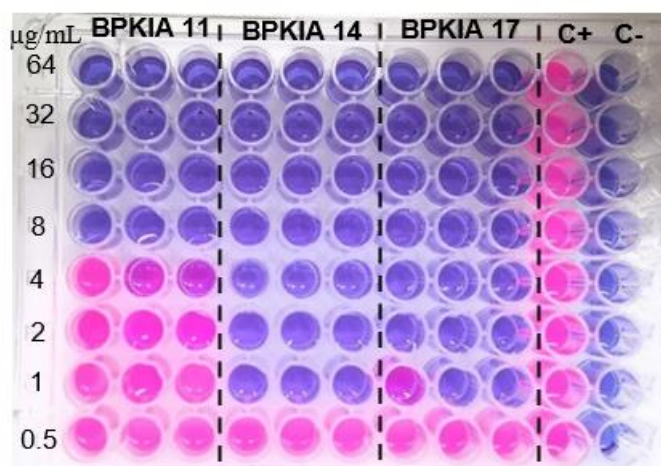
**Figure 90:** Helical wheel projections of BP100 and the newly designed BPKIA11. Positively charged Lys residues are marked in blue, hydrophobic residues in yellow. Image created using the Protein Origami software.<sup>286</sup>

## 2.4. Synthesis, purification, and characterization of BPKIA analogues

Peptides of the BPKIA series had been previously synthesized in group of Dr. Ulrich at Karlsruhe Institute of Technology, on an automated peptide synthesizer Syro II (from Multisynthtech GmbH), with and without  $^{15}\text{N}$  label, using standard solid phase Fmoc protocols. They were purified by high-pressure liquid chromatography on a Vydac C-18 column using an acetonitrile/water gradient. The characterization was done by analytical HPLC combined with ESI-MS, and all peptides were shown to be over 95 % pure.

## 2.5. Antimicrobial activity

A standard broth dilution assay was used,<sup>222</sup> which consists of serial dilutions of the peptide ( $256 - 2 \mu\text{g}\cdot\text{mL}^{-1}$  or  $64 - 0.5 \mu\text{g}\cdot\text{mL}^{-1}$ ) in a liquid microbial growth medium which was inoculated with a standardized number of organisms ( $10^6 \text{CFU}\cdot\text{mL}^{-1}$ ) and incubated at  $37^\circ\text{C}$  for a prescribed time. The plates were examined for visible bacterial growth evidenced by a redox indicator, resazurin, as it is shown in the Figure 91. Resazurin is a blue fluorogenic dye which is irreversibly reduced by enzymes in viable cells to generate a highly pink-fluorescent product, resorufin, therefore indicating the presence of still living bacteria. The lowest concentration of antibiotic that inhibited bacterial growth was considered to be the minimum inhibitory concentration.



**Figure 91:** Example of microtiter 96-well plate used in the MIC tests, where BPKIA11, BPKIA14 and BPKIA17 were tested in *Acinetobacter sp* DSM 586. As it can be observed, the activity was measured by triplicate directly in the plate. Columns 10 and 11 correspond to the positive (no peptide) and negative (no microorganism) controls. Therefore, BPKIA11 presented a MIC of  $8 \mu\text{g}\cdot\text{mL}^{-1}$  (lowest concentration which presents blue color) and BPKIA14 and BPKIA17,  $1 \mu\text{g}\cdot\text{mL}^{-1}$ .

The antimicrobial activity of BPKIA peptides were determined by triplicate and repeated two times in order to avoid environmental errors. Obtained values are shown in Table 29. BP100 and MSI-103 were used as control in each experiment.

**Table 29:** Antimicrobial activity of the peptides.

Peptide	MIC [ $\mu\text{g}\cdot\text{mL}^{-1}$ ]			
	<i>Escherichia coli</i> DSM 1116	<i>Acinetobacter sp.</i> DSM 586	<i>Bacillus subtilis</i> DSM 347	<i>Staphylococcus xylosus</i> DSM 20267
<b>BP100</b>	4	4	2	4
<b>KIA21</b>	8	4	4	2
<b>BPKIA4</b>	>256	>256	>256	>256
<b>BPKIA7</b>	>256	>256	>256	>256
<b>BPKIA10</b>	128	>256	64	32
<b>BPKIA11</b>	4	8	2	2
<b>BPKIA14</b>	2	1	2	1
<b>BPKIA17</b>	2	2	2	2
<b>BPKIA18</b>	8	4	4	4
<b>BPKIA21</b>	16	8	16	16
<b>BPKIA24</b>	16	16	16	16

Observing the MIC values, there is not a clear correlation between peptide length and activity. Overall, BPKIA14 appeared to be the most active peptide, followed by BPKIA17 and BPKIA11. The shortest peptides (BPKIA4 and BPKIA7) were inactive, while BPKIA10 presents some activity against *Bacillus subtilis* and *Staphylococcus xylosus*. Peptides longer than 18 amino acids showed a clear decrease in antimicrobial activity, apparently related with the excessive peptide length.

These results ruled out the possibility of a transmembrane pore formation mechanism, since BPKIA17 and longer versions should span the membrane easily, and therefore present improved antimicrobial activity, as it was observed for KIA peptides. Furthermore, BPKIA peptides presented similar activity against the different strains tested, whereas in KIA peptides the minimum threshold length to present activity differed for the different bacterial strains, depending on their membrane thickness.<sup>290</sup>

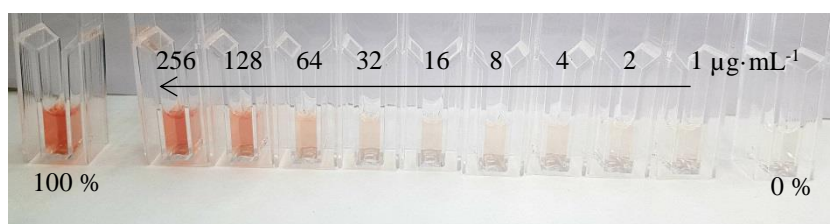
## 2.6. Hemolysis

The hemolytic activity of BPKIA peptides was examined with a serial 2-fold dilution assay, using citrate phosphate dextrose-stabilized blood bags with erythrocyte

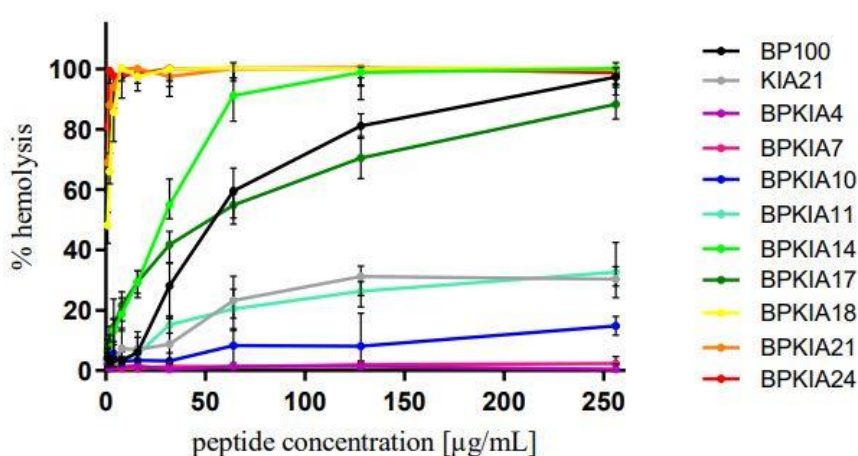
suspensions from healthy human donors. For each peptide concentration, the percentage hemolysis was measured and calculated according to the following equation:

$$\% \text{ hemolysis} = [(A_{\text{obs}} - A_{0\%}) / (A_{100\%} - A_{0\%})] \cdot 100$$

The 0 % hemolysis was determined by a test without any peptide, and 100 % was induced by adding the detergent Triton-X to the erythrocytes, as shown in Figure 92. Hemolysis curves for the peptides are shown in Figure 93.



**Figure 92:** Image of the obtained supernatant after 30 min incubation of the human erythrocytes with the BPKIA11, the concentration dependence can be visually detected.



**Figure 93:** Hemolytic activity of the BPKIA peptides. The error bars correspond to  $\pm$  the standard deviation for each data point.

The obtained results showed a clear correlation between peptide length and hemolysis. The shortest peptides presented low hemolytic values even at very high concentrations, while the longest ones presented nearly 100 % of red blood cell lysis already at  $2 \mu\text{g}\cdot\text{mL}^{-1}$ . Interestingly, the longer BPKIA17 presented lower hemolytic activity than BPKIA14.

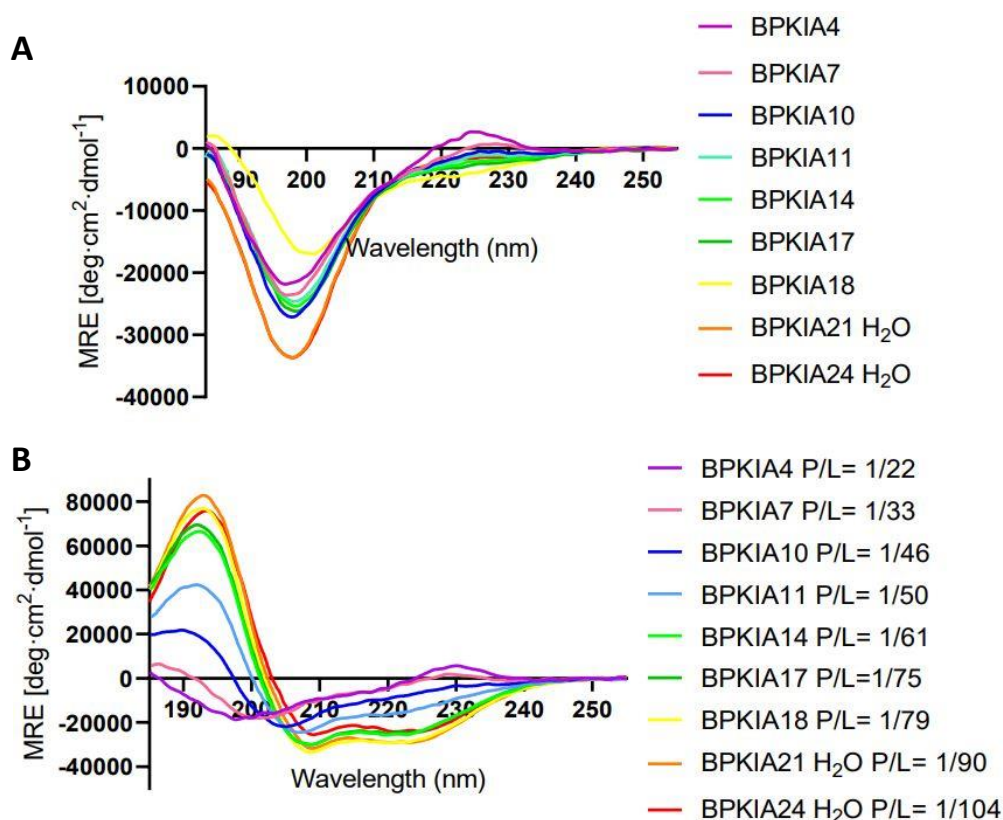
It could also be observed that BPKIA11, which had the same length that BP100 showed remarkably reduced hemolysis, probably due to the replacement of 6-Lys residue with an alanine, as it was previously reported by Zamora-Carreras et al.<sup>305</sup> However, BPKIA

peptides longer than 14 residues presented higher hemolytic activity compared with KIA peptides, where the long KIA21 showed a maximal hemolysis of around 20 % at  $256 \mu\text{g}\cdot\text{mL}^{-1}$ , whereas BPKIA21 gave 100 % hemolysis already at  $4 \mu\text{g}\cdot\text{mL}^{-1}$ .

## 2.7. Biophysical evaluation of the mechanism of action

### 2.7.1. Circular dichroism spectroscopy

In order to determine the secondary structure of the BPKIA peptides, CD spectra were recorded in buffer and in DMPC/DMPG (3:1) SUVs, chosen as a representative model of microbial membranes. Considering the different length of the peptides, the concentration was varied such that the number of amino acid residues per lipid was kept constant, with a peptide-to-lipid molar ratio of 1:50 for BPKIA11 (same length of BP100) as a starting point. The results are shown in Figure 94.



**Figure 94:** CD spectra of BPKIA peptides A) in phosphate buffer, B) in presence of DMPC/DMPG (3:1) vesicles at constant mass ratio of  $14 \mu\text{g}$  peptide and  $3 \text{mg}$  lipid.

Furthermore, in order to convert the spectral data to mean residue ellipticities, an accurate determination of peptide concentration was performed using the absorbance of ultraviolet

(UV) radiation by the intrinsic tryptophan chromophore at 280 nm. Finally, deconvolution of CD data was used to determine quantitative amounts of different secondary structure elements and the results are shown in Table 30.

**Table 30:** Secondary structure fractions (%) of BPKIA peptides in DMPC/DMPG (3:1) at a constant mass ratio of 14  $\mu$ g peptide and 3 mg lipid, evaluated from the CD spectra using CONTINLL-SP175, CDSSRR-SP175 and SELCON3-SP175 algorithms.<sup>316</sup>

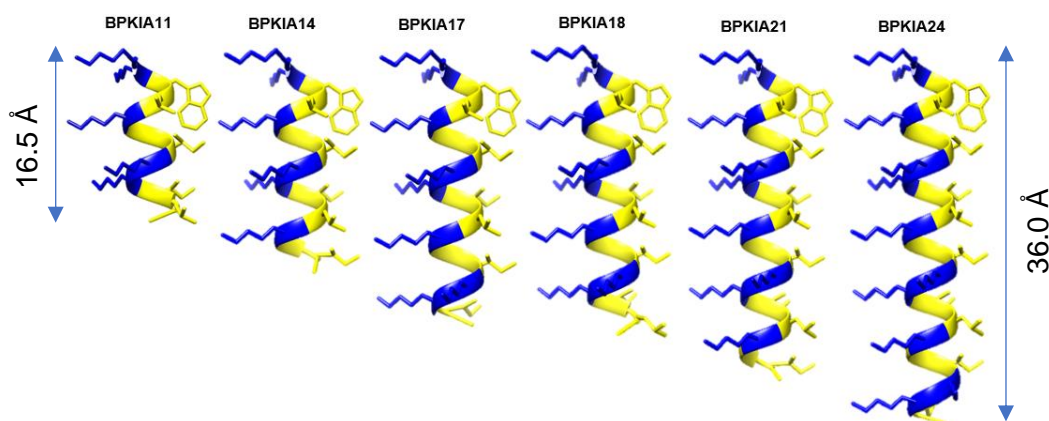
Peptide	$\alpha$ -Helix	B-sheet	Turn	Random Coil	Total
<b>BPKIA4*</b>	3	43	14	39	99
<b>BPKIA7*</b>	5	37	13	44	99
<b>BPKIA10*</b>	40	13	14	31	98
<b>BPKIA11</b>	57	9	11	22	99
<b>BPKIA14</b>	78	10	9	13	100
<b>BPKIA17</b>	79	1	8	11	100
<b>BPKIA18</b>	82	0	8	10	100
<b>BPKIA21</b>	86	0	7	7	100
<b>BPKIA24</b>	79	4	8	9	100

\*CD data deconvolution using only the CDSSRR-SP175 algorithm.

All BPKIA peptides showed spectra corresponding to random coil structure in phosphate buffer. It should be noted that CD spectra of BPKIA 21 and 24 were performed in water to avoid the scattering artefacts produced by their low solubility in phosphate buffer. This fact could be explained by a strong pH dependence of the longest and highly charged peptides which were more soluble in soft acidic conditions (pH in phosphate buffer 6.5, pH in water 5).

When measurements were performed in the presence of DMPC/DMPG (3:1) vesicles, peptides showed a clear length dependent  $\alpha$ -helical structure. This means that the peptides that were unstructured in solution formed helices when bound to the membrane. As it is shown in Figure 94B, BPKIA4, BPKIA7 and BPKIA10 were too short to form  $\alpha$ -helices, whereas the  $\alpha$ -helical fraction of the other peptides increased with length. BPKIA21 and BPKIA24 spectra were also measured in water to avoid the scattering artefacts produced by the low solubility buffer; it could be observed that peptides dissolved in water showed a shifted maximum. Furthermore, even in water, BPKIA24 was not completely dissolved, and it presented lower  $\alpha$ -helix fraction than BPKIA21. Figure 95 shows the model  $\alpha$ -helical structures of BPKIA peptides.





**Figure 95:** Models of the  $\alpha$ -helical structure of BPKIA peptides when bound to lipid membranes. Length was calculated assuming 1.5 Å per residue for an ideal  $\alpha$ -helix. Positively charged Lys residues are marked in blue, hydrophobic residues in yellow.

### 2.7.2. Peptide binding study

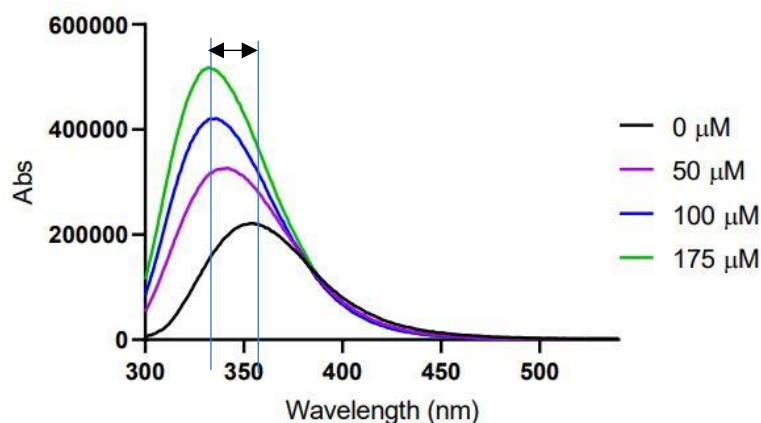
Tryptophan fluorescence is a powerful tool for the study of membrane-active proteins and peptides in model membranes. As mentioned above, this was one of the reasons why the Leu<sup>3</sup> of BP100 was replaced by a Trp residue in the BPKIA peptides design.

The fluorescence emission spectra of BPKIA peptides in buffer was recorded with excitation at 280 nm, and a maximum around 350 nm was observed for all peptides, indicating that the Trp residue was highly exposed to the solvent. After a series of peptide titration with increasing amounts of POPG/POPC (1:1) LUVs, the emission maximum showed a blueshift, indicating peptide binding to the lipid membrane. Figure 96 shows the changes of Trp fluorescence in presence of different BPKIA10 concentrations.

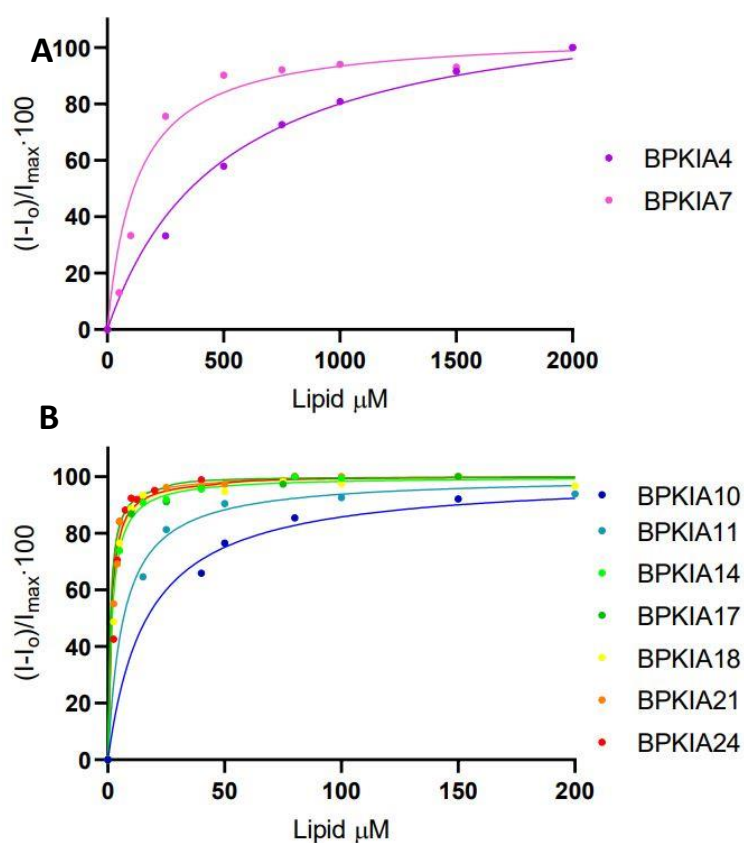
Changes in emission intensity yield conventional binding curves (Figure 97). Furthermore, the binding constant  $K$  (Table 31) was extracted following a non-linear hyperbolic curve fitting based on the following equation:

$$I = I_{max} \frac{K[L]}{1 + K[L]}$$

where  $I$  is the measured fluorescence intensity,  $I_{max}$  denotes asymptotic maximum intensity value,  $[L]$  is the molar lipid concentration and  $K$  is the calculated binding constant.



**Figure 96:** Tryptophan emission spectra of BPKIA10 in presence of increasing amounts of POPC/POPG (1:1) liposomes. The peptide binding to anionic vesicles results in a blue shift of 25 nm of the emission maximum.



**Figure 97:** Binding curves obtained from tryptophan fluorescence and titration with POPC/POPG (1:1) LUVs. A) binding curves of peptides BPKIA4 and BPKIA7, which are presented separately because they were performed in a larger scale of lipid concentrations due to their small binding to membranes; B) binding curves of the rest BPKIA peptides.

The shortest peptides BPKIA4 and BPKIA7 had very low binding constants and therefore they were weakly bound to membranes, a fact that is consistent with their lack of

antimicrobial and hemolytic activity, as well as their random coil structure in the presence of lipid. The rest of  $\alpha$ -helical BPKIA peptides showed higher binding constants, thus reflecting effective binding to POPC/POPG membranes. There was no clear correlation between length and binding constant values.

**Table 31:** Calculated binding constant (K) of BPKIA peptides to POPC/POPG (1:1) vesicles.

Peptide	K (M <sup>-1</sup> )
<b>BPKIA4</b>	2000
<b>BPKIA7</b>	8000
<b>BPKIA10</b>	60000
<b>BPKIA11</b>	150000
<b>BPKIA14</b>	570000
<b>BPKIA17</b>	485000
<b>BPKIA18</b>	690000
<b>BPKIA21</b>	950000
<b>BPKIA24</b>	750000

### 2.7.3. Leakage of aqueous contents

Peptide-induced lipid vesicle leakage was determined using the fluorescent-based assay previously described in chapter 1. Two different compositions of LUVs with well-defined membrane thickness were chosen (Table 32). In both cases, a 1:1 mixture of zwitterionic phosphatidylcholine (PC) and anionic phosphatidylglycerol (PG) head groups were used, since anionic lipids are known to be the main components of bacterial membranes, which contain in many cases well over 50 % PG.<sup>223</sup>

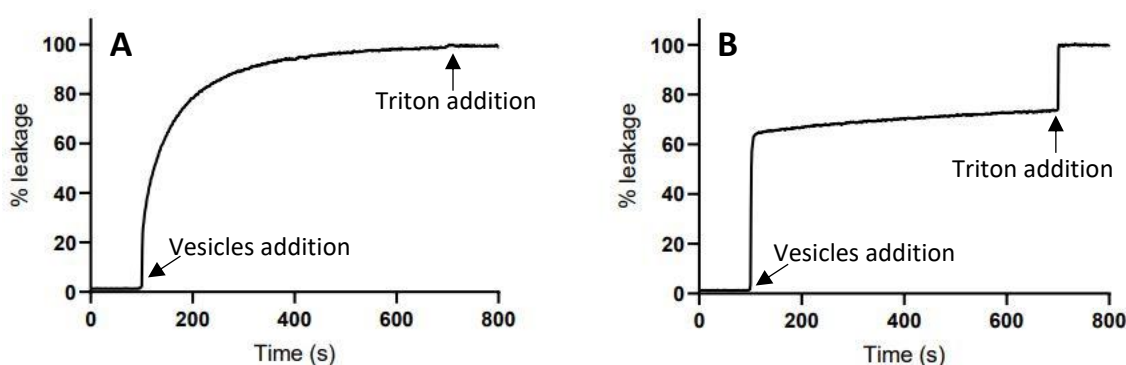
**Table 32:** Lipid mixtures used in the leakage experiments. The lipid numbers (number of carbons: number of insaturations) and hydrophobic thickness of lipid bilayers are also given.<sup>317</sup>

Lipid system	Acyl chain	Length (Å)	Membrane thickness
<b>POPC</b>	16:0/18:1	28.3	Medium
<b>POPG</b>	16:0/18:1	28.3	
<b>DErPC</b>	22:1	34.4	Long
<b>DErPG</b>	22:1	34.4	

The idea behind this experiment was to study the effect of membrane thickness, so that if transmembrane pores were formed, there would be a threshold minimum length needed to span the membrane and produce leakage, as reported for KIA peptides.<sup>290</sup> Therefore,

BPKIA peptides longer than 17 amino acids, which correspond to 25.5 Å, should produce leakage in POPC:POPG vesicles, whereas DErPC/DErPG membranes should only be spanned by BPKIA24 which has an approximate length of 36 Å.

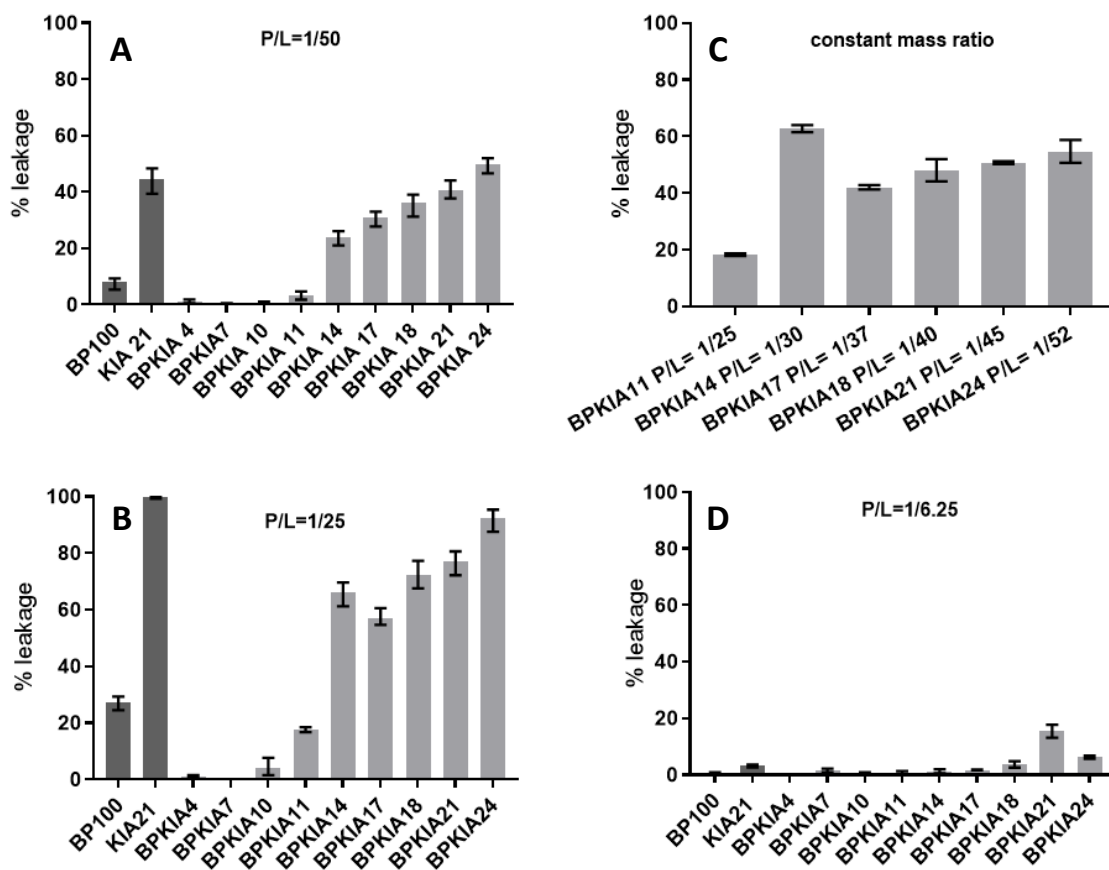
Interestingly, time dependent leakage produced by BPKIA peptides was notably different to that produced by KIA peptides, indicating a different mechanism of action of the two peptide series. As observed in Figure 98, KIA peptides produced an exponential time-dependent leakage increase, whereas BPKIA peptides produced a fast leakage upon vesicles addition, followed by a slower and time-dependent leakage increase.



**Figure 98:** Time dependent leakage of A) KIA21 and B) BPKIA21 in POPC/POPG (1:1) vesicles at P/L= 1/25. Vesicles were added after 100 s to the cuvette containing the peptide solution. After 700 s Triton-X was added to obtain the complete leakage of the vesicles (100 %).

Leakage of ANTS/DPX were measured at different P/L ratios, over 10 minutes after addition of the vesicle suspension to the peptide solution. In POPC/POPG vesicles, at low peptide concentration only partial leakage was observed (Figure 99A), whereas at a higher P/L of 1/25, peptides longer than 14 amino acids caused a leakage higher than 60 % (Figure 99B). At P/L 1/25, there was an apparent correlation between leakage and peptide length, but when the number of amino acid residues per lipid was kept constant, with a P/L of 1/25 for BPKIA11, very similar leakage results were obtained among peptides longer than 14 amino acids (Figure 99C). Even though BPKIA14 is nominally too short (21 Å), it produced similar leakage as other longer BPKIA peptides. Thus, the possibility of transmembrane pore forming mechanism was ruled out.

In DErPC/DErPG, no threshold length was observed; in fact, even at a very high peptide concentration (P/L= 1/6.5), only BPKIA21 showed a significant level of leakage, corresponding to 15 % (Figure 99D).



**Figure 99:** Leakage vesicles at different peptide-to-lipid molar ratio. A) POPC:POPG (1:1) at P/L= 1/50; B) POPC:POPG (1:1) at P/L= 1/25; C) POPC:POPG (1:1) at constant mass ratio, with a P/L of 1/25 for BPKIA11 as the starting point; D) DErPC/DErPG (1:1) at P/L=1/6.25.

#### 2.7.4. Solid state NMR

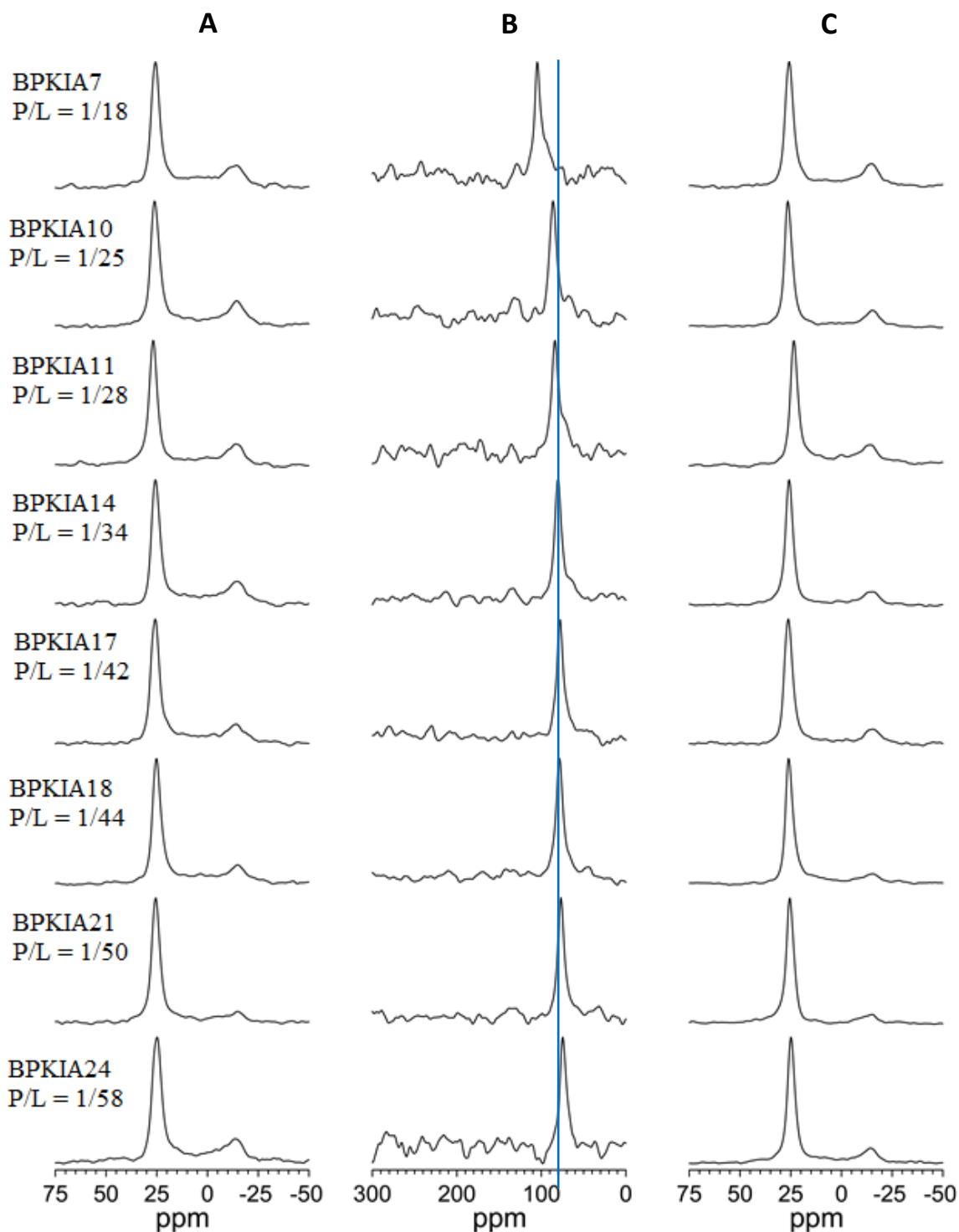
$\alpha$ -Helical BPKIA peptides were synthesized with  $^{15}\text{N}$ -label located in the 6-Ala residue. Peptides were then reconstituted into oriented bilayers of different compositions and investigated by proton-decoupled  $^{31}\text{P}$  and  $^{15}\text{N}$  solid-state NMR spectroscopy. Considering the different length of the peptides, the concentration was varied such that the number of amino acid residues per lipid was kept constant. In order to compare our results with the previously obtained to KIA peptides<sup>290</sup> a P/L of 1/50 for BPKIA21 was chosen as the starting point.

In POPC/POPG (1:1) bilayers, all BPKIA peptides exhibited chemical shifts close to 80 ppm (Figure 100).  $^{15}\text{N}$  chemical shifts values below 100 ppm are indicative of so-called “S-state”, with peptide alignments parallel to the membrane surface.<sup>313</sup> These results were expected, since it has been previously reported for other AMPs and KIA peptides that

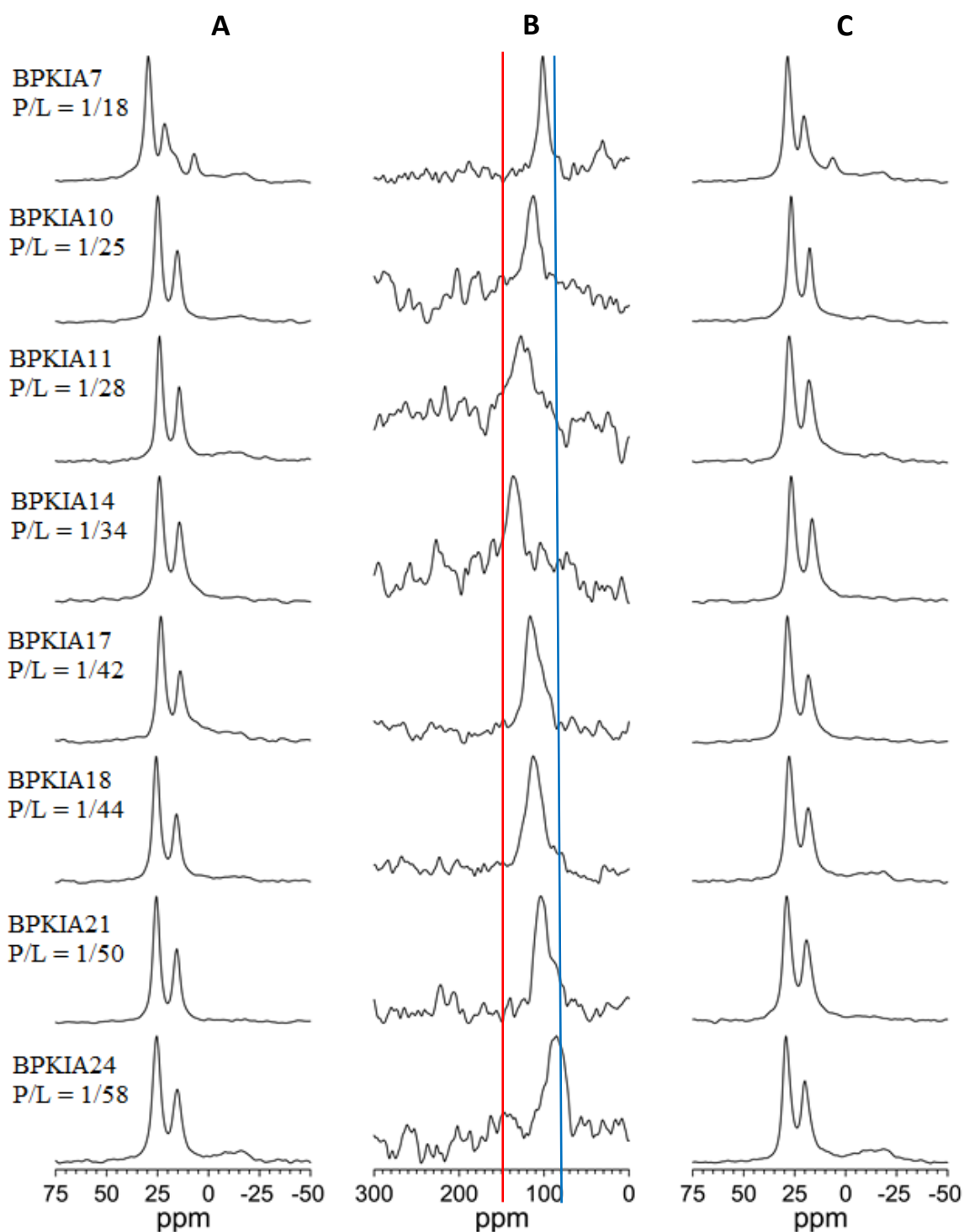
amphipathic helices always prefer this orientation in lipids with unsaturated chains, that induce a negative spontaneous curvature.<sup>318,319</sup>

On the other hand, in DMPC/lyso-MPC (2:1), with positive spontaneous curvature,<sup>320</sup> the obtained signal for all analogues was found between 140 and 80 ppm, indicating a more inserted state (Figure 101). BPKIA14 showed the largest chemical shift at 137 ppm, as it was previously reported for the native BP100 peptide,<sup>290</sup> whereas longer and shorter analogues presented a gradual displacement down to 80 ppm for BPKIA28 and 100 ppm for BPKIA7. It should be noted that the short peptides BPKIA4 and BPKIA7 were not helical, and BPKIA10 was only partly helical, according to CD, therefore <sup>15</sup>N chemical shifts cannot be used to indicate peptide orientation for these peptides

Figure 102 shows a comparison with previously reported data for KIA peptides in DMPC/lyso-MPC (2:1) membranes.<sup>290,291</sup> In this case, KIA14 gave a signal at 167 ppm, and longer peptides gradually had smaller shifts down to 134 ppm for KIA28, which means that shorter KIA peptides matching the hydrophobic thickness of the membrane had a straight upright orientation, while longer peptides were adapted to the membrane thickness by tilting. This is not the case of BPKIA peptides, where BPKIA14 and shorter peptides were only partially inserted with signals ranging from 137 and 100 ppm, and the longer BPKIA24 was oriented on the surface of the membrane.

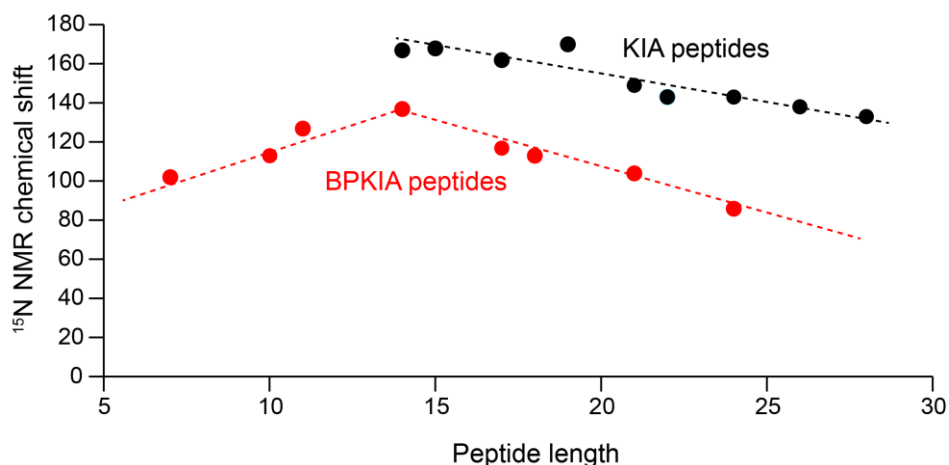


**Figure 100:** Solid state spectra of BP KIA peptides in POPC/POPG (1:1) at peptide-to-lipid constant mass ratio of approximately 1.2 mg peptide and 20 mg lipid. A)  $^{31}\text{P}$ -NMR spectra before  $^{15}\text{N}$ -NMR; B)  $^{15}\text{N}$ -NMR spectra; C)  $^{31}\text{P}$ -NMR spectra after  $^{15}\text{N}$ -NMR. All peptides showed a  $^{15}\text{N}$ -NMR signal close to 80 ppm (blue line), indicating that the peptides were orientated on the surface membrane.



**Figure 101:** Solid state spectra of BPKIA peptides in DMPC/lyso-MPC (2:1) at peptide-to-lipid constant mass ratio of approximately 1.2 mg peptide and 17 mg lipid. A)  $^{31}\text{P}$ -NMR spectra before  $^{15}\text{N}$ -NMR; B)  $^{15}\text{N}$ -NMR spectra; C)  $^{31}\text{P}$ -NMR spectra after  $^{15}\text{N}$ -NMR. The  $^{15}\text{N}$ -NMR signal at 80 ppm (blue line) is typical of the surface-bound state. Chemical shifts displaced to 140 ppm (red line) indicate partial insertion in DMPC/lysoMPC membranes.





**Figure 102:**  $^{15}\text{N}$  NMR chemical shifts presented by BPKIA and KIA peptides in DMPC/lysoMPC (1:1) membranes. KIA14 and BPKIA14 presented signals at 167 ppm and 137 ppm respectively, which means that they were more inserted in the bilayer than the other peptides. KIA data extracted from ref.<sup>290</sup>

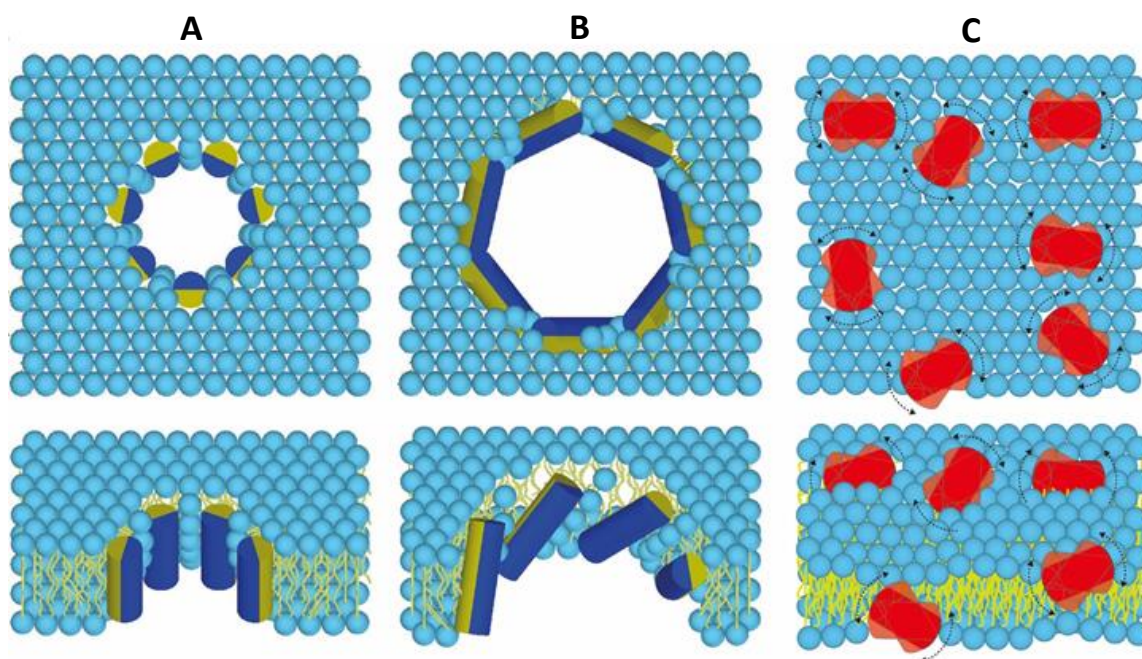
### 2.7.5. Proposed mechanism of action

The interaction of BP100 with the lipid membranes was studied by using model peptides with repeats of the basic heptamer KKILKAI. It was found that BPKIA4, BPKIA7 and BPKIA10 were not helical, and they did not bind into lipid membranes, as a consequence they did not show antimicrobial or hemolytic activity and they did not produce vesicle leakage. Longer peptides showed length dependent  $\alpha$ -helical structure when bound to membranes, but no apparent length dependent antimicrobial activity was observed, because the best results were obtained by the medium length peptides BPKIA11, BPKIA14, and BPKIA17. In the hemolysis assay, a stepwise increase with peptide length was detected, but no clear threshold length was found. Threshold length was found in the binding and leakage assays, where peptides longer than 14 residues yielded approximately the same results.

Regarding the solid-state NMR results, BPKIA peptides orient parallel into POPC/POPG (1:1) membrane surfaces, as observed previously also for BP100 and KIA peptides. In DMPC/lyso-MPC (2:1), BPKIA peptides are partially inserted, BPKIA14 was the most tilted peptide. The  $^{15}\text{N}$  NMR results were in good agreement with the weak length dependence observed in the previous assays and already give a rough idea on the helix re-alignment.

In conclusion, all these results are consistent with the hypothesis that BP100 is too short to span the membrane and form transmembrane toroidal peptide pores like KIA peptides.

BPKIA showed that no threshold length was necessary for activity ruling out the possibility of toroidal pore mechanism. However, they seem to get inserted into the hydrophobic core of the bilayer. Therefore, we conclude that BPKIA peptides and BP100 disturb the membrane via a “dynamic carpet” mechanism (Figure 103), from where they are able to insert dynamically into the bilayer core, inducing substantial disorder that leads to an increased membrane permeability and ultimately bacterial cell death.



**Figure 103:** Proposed mechanism of action of the studied peptides. A) transmembrane toroidal pore formed by short KIA peptides matching the hydrophobic thickness of the membrane; B) transmembrane toroidal pore formed by longer KIA peptides; C) dynamic carpet model proposed for BP100 and BPKIA peptides.

## 2.8. Conclusions

- By studying with a battery of biophysical techniques, the interaction with lipid model membranes of a series of peptides based on the  $\alpha$ -helical BP100, which ranged from 4 to 24 amino acid residues, it was possible to determine that the activity of BP100 is not influenced by its length. Peptides shorter than ten amino acids showed low binding to model membranes, random-coil structure, and therefore, low antimicrobial and hemolytic activity. However, longer peptides showed  $\alpha$ -helical structure, and comparable antimicrobial activity, with elevated binding affinity to model membranes, and peptide-induced leakage of aqueous contents. The penetration into model membranes was studied

by solid-state NMR, and it was determined that BP100 and its analogues got inserted dynamically into lipid membranes following a dynamic carpet mechanism, which consists of the bilayer perturbation, a membrane permeability increase and ultimately the bacterial cell death.

## **GENERAL CONCLUSIONS**



The conclusions reached during this thesis are:

- A novel cleavage reagent has been proposed and optimized, it allowed the deprotection of Bn-type protected peptides and the cleavage of C-terminal amidated peptides directly attached to MBHA resins. This methodology consists of a treatment with *in-situ* generated HBr from a solution of molecular bromine, triethyl silane and trifluoroacetic acid. Using this novel reagent, the model peptides polymyxin B<sub>3</sub>, dusquetide and RR4 were satisfactorily obtained.

- A set of 31 novel lipopeptides were designed by adding potential scissile bonds into the polymyxin B backbone in order to reduce the nephrotoxicity associated with polymyxins due to their accumulation in kidneys. The analogues were synthesized by solid phase peptide synthesis and widely studied through different microbiological and biophysical techniques. Finally, two thiothreonine compounds were selected as the most promising candidates according to their comparable potency to the natural polymyxin in *in vitro* and *in vivo* assays, their high exposure in plasma, and the low nephrotoxicity observed in *in vivo* assays. Moreover, the molecule metabolization *in vivo* was studied using mass spectrometry, both compounds showed a wider number of metabolites than natural polymyxin due to the easily degradation of ester and disulfide bonds upon accumulation in kidneys.

- The mechanism of action of the new lipopeptides has been studied. Their interaction with monolayers and bilayers of relevant lipid composition that mimic the different bacterial membranes was consistent with a membrane-based mechanism of action based on the alteration of the outer and inner bacterial membranes, but ruling out a detergent effect, similar to the vesicle-vesicle contact mechanism proposed for natural polymyxin.<sup>165</sup>

- By studying a series of peptides based on BP100 with different lengths ranging from 4 to 24 amino acids, it has been possible to determine the possible mechanism of action of BP100, which consists in a dynamic carpet mechanism, where peptides get inserted dynamically into the membrane, perturbing the bilayer, increasing the membrane permeability and ultimately producing the cell death.



## **EXPERIMENTAL SECTION**





### 3.1. Experimental section of chapter 1

#### 3.1.1. Materials

##### 3.1.1.1. Solvents

Solvent	Brand	Quality
ACN	Labkem	GC/HPLC GGR
CHCl <sub>3</sub>	Panreac	>99.5 %
DCM <sup>a</sup>	Scharlau	99.9 %
DMSO	Fisher	>99.8 %
DMSO-d <sub>6</sub>	Eurisotop	>99.8 %
DMF	Fisher	>99.5 %
EtOAc	Fisher	99 %
Et <sub>2</sub> O <sup>b</sup>	Scharlau	≥98 %
EtOH	Panreac	99.5%
H <sub>2</sub> O (Milli-Q) <sup>c</sup>	-	-
MeOH	Fisher	For HPLC analysis

<sup>a</sup>DCM was obtained by filtration through activated alumina. <sup>b</sup>The Et<sub>2</sub>O was dried and conserved over Na. <sup>c</sup>Milli-Q water was obtained by filtrating purified water using a Milli-Q Plus system (Millipore) to obtain water with a resistivity superior to 18 MΩ/cm.

##### 3.1.1.2. Reagents

Reagent	Brand
2-CTC resin	Iris Biotech
Trt-Cl resin	Alfa Aesar
MBHA resin	Novabiochem
Rink linker	Iris Biotech
Amino acid residues	Fluorochem, Iris Biotech, Polypeptide, LeapChem and Bachem
Boc <sub>2</sub> O	Acros Organics
Br <sub>2</sub>	Sigma-Aldrich
DIC	Iris Biotech
DIPEA	Sigma-Aldrich
Fatty acids	Fluka and Sigma-Aldrich

Fmoc-Cl	Bachem
HATU	Fluorochem
HCl 37%	Scharlau
HFIP	Acros Organics
HOAt	Sigma-Aldrich
HOBt	Fluorochem
KCN	Alfa Aesar
K-Oxyma	Fisher
Ninhydrin	Alfa Aesar
Na <sub>2</sub> SO <sub>4</sub>	Alfa Aesar
Pyridine	Fisher
Piperidine	Acros Organics
Polymyxin B sulfate salt	Sigma
Phenol	Alfa Aesar
TIS	
TES	Fluorochem
TFA	
TFE	Fisher
Bacterial strains	American Type Culture Collection
MHB	
TSA	Oxoid
Sephadex G-50	Sigma-Aldrich
ANTS	
DPX	Molecular probes
py-PG	
disC <sub>3</sub> (5)	Invitrogen
HEPES	Sigma
LPS	Sigma
NaCl	Panreac
TRIS	Acros Organics

Rh-PE	Avanti Polar Lipids
NBD-PE	
DOTAP	
POPC	
POPE	
POPG	

### 3.1.1.3. Other material

Material	Brand
Syringes	Teknokroma and Fisher
Filters	Teknokroma
96-well microtiter plates	Thermo Scientific
Fluorescence cuvettes	Hellma Analytics
Microsyringes	Hamilton
100 nm Nuclepore polycarbonate membrane	Whatman

### 3.1.1.4. Instrumentation

Instrument	Brand and model
Balances	Mettler Toledo <i>AG245</i>
	Mettler Toledo <i>ME204</i>
Centrifuges	Hettich <i>Rotofix 32A</i>
	Beckman Coulter <i>Allegra 25R</i>
HPLC	1) Analytical: Shimadzu <i>Series 20 Prominence</i> , with two <i>LC-20AD</i> pumps, automatic <i>SIL-20A</i> injector, controller <i>CBM-20A</i> and detector <i>SPD-M20A</i> .
	2) Semi-preparative: Waters <i>Delta Prep 3000</i> , with a Waters <i>600E</i> pump and controller, manual Waters <i>712</i> injector and a detector Waters <i>484</i> .

HPLC-MS	Waters 2795 Separation module, with automatic injector, Waters 2996 photodiode array detector, a Waters ESI-MS Micromass ZQ 4000 spectrometer, and Masslynx v4.1 system controller.
Lyophilizer	Christ <i>Alpha 2-4 LD plus</i>
Milli-Q water	Millipore <i>Milli-Q Plus</i>
NMR Spectrometer	Varian <i>Mercury 400</i> Bruker 400 MHz <i>Avance III</i>
Rotatory evaporator	Heidolph <i>Labrota 4003 Control</i>
Spectrophotometer	Segonam <i>Uvikon XS</i>
Microplate reader	BioTeK <i>Sinergy HT</i>
Extruder	Avestin <i>Liposofast-Basic Extruder</i>
Sonicator	Elma <i>Transsonic Digital S</i>
Spectrofluorimeter	AMINCO Bowman <i>Series 2</i>
Zetasizer	Malvern <i>II-C</i>
Langmuir balance	NIMA Technology 2

### 3.1.2. Methods

#### 3.1.2.1 Analytical methods

##### 3.1.2.1.1. Fmoc quantification and loading determination

The real loading level of the resin can be evaluated by quantifying the dibenzofulvene-piperidine adduct generated during the Fmoc removal of the first amino acid. To carry out the quantification, the resin was previously washed with DMF (5 x 30 s), and it was then treated twice with 20 % piperidine in DMF (approximately 1 mL per 200 mg of resin) during 10 minutes. Washings with DMF (5 x 30 s) were carried out after the deprotection treatment, collected in a volumetric flask, and further diluted in DMF. The UV absorbance at 301 nm of the resulting mixture was measured, and the loading capacity was calculated using the Lambert Beer law:

$$A = \varepsilon \cdot c \cdot l$$

where A is the observed absorbance,  $\varepsilon$  is the molar absorbance coefficient (7800 M<sup>-1</sup>·cm<sup>-1</sup> at 301 nm) and l cm is the optical path length.

### 3.1.2.1.2. Kaiser test

Kaiser test is a very sensitive technique that allows the qualitative evaluation of the efficiency of the amino acid couplings in SPPS. It is a colorimetric test based on the reaction of ninhydrin with primary amino groups of the *N*-terminal side of the growing peptidyl-resin, which gives a characteristic dark blue color indicating that the coupling reaction was not complete (positive result). If the reaction did not occur, the solution would present yellow coloration, which ensures 99 % of coupling rate (negative result).

In the assay, few beads of the dried peptide resin, which had been previously washed with DCM, were placed on a glass tube, 2 drops of solutions A, B and C were added, and the mixture was heated at 110 °C for 3 minutes.

The three solutions were prepared as follows:

- Solution A: 16.5 mg of KCN were dissolved in 25 mL of Milli-Q water. Finally, solution A was obtained by diluting 1 mL of the obtained solution in 49 mL pyridine (freshly distilled from ninhydrin).
- Solution B: 1.0 g of ninhydrin were dissolved in 20 mL of EtOH. The ninhydrin reagent is light sensitive; thus, solution B was kept in a flask protected from the light.
- Solution C: It consisted of 40 g of phenol dissolved in 20 mL of EtOH.

### 3.1.2.1.3. Thin-layer chromatography

Thin-layer chromatography (TLC) was performed on an aluminium sheet, which was coated with a thin layer of silica gel (stationary phase). The sample was applied on the plate and an appropriate solvent mixture (mobile phase) was eluted. Separation was achieved due to the different polarities of the analytes present in the sample. In order to visualize the results ultraviolet light at 254 nm was projected onto the sheet. TLC staining was also used to visualize compounds that did not absorb UV light. In our case, the staining solution consisted of a ninhydrin solution which forms colored adducts with many free amino acids. This ninhydrin stain solution was prepared by dissolving 3 g of ninhydrin in 100 mL of absolute EtOH. The obtained ninhydrin solution was kept protected from the light. The TLC sheets were exposed to the solution and analyzed visually, primary amines produce blue spots at room temperature and Boc-protected amines produce spots on heating.

#### 3.1.2.1.4. High performance liquid chromatography

##### 3.1.2.1.4.1. Analytical HPLC

Analytical RP-HPLC was performed on a Shimadzu Series 20 Prominence instrument comprising two solvent delivery pumps LC-20AD, a SIL-10A automatic injector, a CBM-20A controller, and a dual wavelength detector SPD-M20A. The column used was a Kinetex® reversed-phase column (4.6 x 250 mm) of 5 µm particle diameter. The samples were eluted at a flow rate of 1 mL·min<sup>-1</sup> using the lineal gradients of 0.045 % TFA/H<sub>2</sub>O (A) and 0.036 % TFA/ACN (B) and UV detection at 220 nm.

##### 3.1.2.1.4.2. Mass spectrometry

HPLC-MS was performed on a Waters instrument comprising a Waters 2695 separation module, an automatic injector, a Waters 2996 photodiode array detector, a Waters ESI-MS Micromass ZQ 4000 spectrometer, and a Masslynx v4.1 system controller. The column used was a Kinetex® C18 reversed-phase column (4.6 x 250 mm) of 5 µm particle diameter. The samples were eluted at a flow rate of 1 mL·min<sup>-1</sup> using the lineal gradients of 0.045 % TFA/H<sub>2</sub>O (A) and 0.036 % TFA/ACN (B) and UV detection at 220 nm.

Direct injection mass spectrometry was also performed in the same instrument. In this case the samples were analyzed using a isocratic elution of ACN at a flow rate of 0.5 mL·min<sup>-1</sup>.

#### 3.1.2.2. Solid phase peptide synthesis

Solid-phase peptide synthesis was carried out manually, using polypropylene syringes provided with a porous polyethylene filter disc. The reagent mixture was manually stirred using a Teflon® wand. After each coupling, the excess of reagents, solvents and other byproducts were eliminated by vacuum filtration. Washings between deprotection and coupling were performed using approximately 10 mL solvent/g resin for each wash. When not specified all reactions were carried out at room temperature.

##### 3.1.2.2.1. Resin conditioning and first amino acid coupling

The peptide synthesis was carried out using different solid supports depending on the characteristics of the synthesized peptides. Conditioning of the resin, prior to the first amino acid coupling, was required to favor the removal of impurities and to obtain

optimum swelling of the resin. This treatment is specific for each polymeric support as well as the conditions required for the first coupling.

#### 3.1.2.2.1.1. Trt-Cl and 2-CTC resins

Conditioning of trityl-based resins consisted of washes with DMF (5 x 30 s) to eliminate hydrochloric acid traces, and with DCM (5 x 1 min) to obtain an optimal swelling.

The loading of commercial trityl-based resins ranges from 0.5 to 2.5 mmol·g<sup>-1</sup>. High loading levels can cause aggregation, for that reason 1 - 1.2 eq of the first Fmoc-protected amino acid and 4 eq of DIEA were added onto the resin in order to obtain lower loadings (0.50 - 0.95 mmol·g<sup>-1</sup>). The reaction was left to react overnight in the minimum amount of DCM with occasional manual stirring. At the end of this time, the resin was washed with small volumes of DCM (5 x 30 s), DMF (5 x 30 s) and DCM (5 x 30 s). Then, an excess of MeOH (0.8 mL·g<sup>-1</sup> of resin) was added, and the reaction was left for 30 additional minutes. Finally, the solvents and the excess of reagents were filtered, and the resin was then washed again.

#### 3.1.2.2.1.2. MBHA resin

The MBHA resin was previously conditioned as summarized in Table 33.

The loading of commercially available MBHA resin was 0.69 mmol·g<sup>-1</sup>, and the first amino acid was incorporated using 3-fold molar excess of AA-DIC-HOBt coupling system in the minimum amount of DMF. The reaction was left to proceed during 1 hour with occasional manual agitation.

**Table 33:** Protocol used for the conditioning of the MBHA resin.

Reagent	Function	Repeats	Time
DCM	Wash	5	30 s
40 % TFA/DCM	Solvate	1	1 min
40 % TFA/DCM	Solvate	1	10 min
DCM	Wash	5	30 s
5 % DIEA/DCM	Neutralization	3	2 min
DCM	Wash	5	30 s
DMF	Wash	5	30 s



### 3.1.2.2.2. Elongation of the peptide chain

After the first amino acid coupling, successive cycles of Fmoc-deprotection with 20 % piperidine in DMF and Fmoc-protected amino acid coupling gave place to the protected peptides on resin. After each coupling step, the reaction completion was ascertained through the Kaiser test. The process was performed as summarized in Table 34.

**Table 34:** General elongation protocol of the peptide chain in a standard Fmoc-protection methodology.

Reagent	Operation	Repetitions	Time
DMF	Wash	5	30 s
20 % piperidine in DMF	Deprotection	1	1 min
20 % piperidine in DMF	Deprotection	2	10 min
DMF	Wash	5	30 s
Fmoc-AA + Coupling agents and additives	Coupling	1	1 h
DMF	Wash	5	30 s
DCM	Wash	5	30 s
Kaiser test	Control	1	3 min

### 3.1.2.2.3. Cleavage from the solid support and deprotection protocols

Once the sequence was assembled, cleavage of the peptides from the resin and lateral chain deprotection was carried out. According to the protection strategy used, a different cleavage reagent was considered to be the most suitable. Table 35 summarizes the cleavage conditions used in the present thesis.

The cleavage mixtures were added to the peptidyl resin placed in the syringe and were left to react for the desired time with occasional manual stirring. The resins were then filtered off and washed three times with a small volume of the cleavage solution and the peptides were precipitated and washed three times with cold Et<sub>2</sub>O or water. The solid peptides were isolated by centrifugation at 6000 rpm for 10 min, dissolved in H<sub>2</sub>O/ACN (1:1, v/v), lyophilized and analyzed by analytical HPLC and by ESI mass spectrometry.

**Table 35:** Acidolytic cleavage mixtures according with the protection strategy employed in the different synthesis used in this thesis.

Peptide	Resin	Side chain PG <sup>a</sup>		Cleavage reagents	Time	Repetitions
		removed during cleavage				
<b>PxB<sub>3</sub></b>	2-CTC	Boc		DCM/TFA/TES/H <sub>2</sub> O (55:40:3:2, v/v/v/v)	30 min	1
<b>Depsipeptide analogues</b>	2-CTC	Mtt		DCM/HFIP/TFE/TES (65:20:10:5, v/v/v/v)	60 min	1
<b>Hydroxamic acid analogues</b>	2-CTC	Boc, <sup>t</sup> Bu and Trt		TFA/TES/H <sub>2</sub> O (95:3:2, v/v/v)	30 min	1
<b>Thiothreonine analogues</b>	2-CTC	Boc, <sup>t</sup> Bu and Trt		TFA/TES/H <sub>2</sub> O (95:3:2, v/v/v)	30 min	1
<b>Thiothreonine analogues<sup>b</sup></b>	Trt-Cl	Boc, <sup>t</sup> Bu and Trt		TFA/TES (82:18, v/v)	45 min	1
<b>Dusquetide and RR4</b>	MBHA	Boc and Pbf		TFA/TES <sup>c</sup> /Br <sub>2</sub> (82.5:15:2.5 v/v/v)	90 min	1
<b>Cysteine analogues</b>	MHBA	Boc, <sup>t</sup> Bu and Trt		TFA/TES/H <sub>2</sub> O (95:3:2, v/v/v)	90 min	2

<sup>a</sup>PG: protecting group; <sup>b</sup>Optimized conditions; <sup>c</sup>TIS was used in the synthesis of RR4.

The lateral chain deprotection of polymyxin analogues which contained the amide ring closure (PxB<sub>3</sub> and depsipeptide analogues) was performed in two steps. Firstly, the 4-Dab was deprotected as explained in Table 35. Afterward, the peptides were cyclized, lyophilized and the remaining protecting groups were removed by an extra acidolytic treatment. <sup>t</sup>Bu and Boc groups employed in the synthesis of depsipeptide polymyxin analogues, were removed by a 30-minute treatment with DMC/TFA/TES/H<sub>2</sub>O (50:45:3:2, v/v/v/v) using 1 mL of acidic solution per 10 mg of semi-protected peptide. The crude peptide was precipitated and washed three times with cold Et<sub>2</sub>O. On the other hand, *in-situ* generated HBr were used to remove the Bn-type protecting groups of the PxB<sub>3</sub>. This acid solution was prepared by adding 8.25 mL (108 mmol) of TFA and 250 μL of Br<sub>2</sub> (4.9 mmol, 1 eq), in a glass vial placed in an ice bath and provided with mild stirring. Then, 1.5 mL of TES (9.4 mmol, 1.9 eq) were added dropwise. The solution was used immediately after its preparation. The acidic solution (1 mL of acidic solution per 2.5 mg of semi-protected peptide) was left to react for 30 minutes, and the crude peptide was precipitated and washed three times with cold Et<sub>2</sub>O.

#### 3.1.2.2.3. Peptide “mini-cleavage” to monitor reaction conversion

To evaluate conversion when performing a coupling reaction, a small aliquot of the peptidyl resin was treated with the appropriate cleavage conditions. The resulting solution was evaporated under a nitrogen steam. The growing peptide was isolated by precipitation with Et<sub>2</sub>O and centrifugation. Finally, the peptide was dissolved in a H<sub>2</sub>O:ACN (1:1, v/v) mixture and then analyzed by HPLC. This process was especially used to monitor the ester formation, since, in absence of free amines, it was not possible to use the Kaiser test.

#### 3.1.2.2.4. Cyclization

Cyclization of peptides by amide bond formation was performed using HATU-HOAt-DIPEA (2:2:4 eq) coupling system. The reaction was carried out in the minimum amount of DMF, and its progress was monitored by TLC stained by a ninhydrin reagent. The cyclized protected peptide was precipitated and washed by the addition of cold water, and the product was dried by lyophilization.

Cyclization of crude peptides by disulfide formation was carried out using a solution of 5 % DMSO in water using 1 mL of the oxidant solution per 1 mg of peptide. The reaction was left to react for 24-48 h and was monitored by HPLC. The resulting solutions were lyophilized, obtaining the cyclized lipopeptide as a yellowish oil.

#### 3.1.2.2.5. Peptide purification

Peptides were purified by semi-preparative RP-HPLC on a Waters Delta Prep 3000 instrument comprising a Waters 600E separation module, a Waters 712 manual injector, and a tunable absorbance detector Waters 484. Two different columns were used depending on the scale of the synthesis. For synthesis of 20 - 200 mg of crude peptide, the column used was a Kinetex® C18 (4.6 x 250 mm) of 5 µm particle diameter. For larger synthesis, the column used was a Kinetex® C18 (21.2 x 250 mm) of 5 µm particle diameter. The samples were eluted at a flow rate of 4 mL·min<sup>-1</sup> using the lineal gradients of 0.1 % TFA/H<sub>2</sub>O (A) and 0.1 % TFA/ACN (B) and UV detection at 220 nm.

Samples were prepared by dissolving the crude peptide in H<sub>2</sub>O/ACN solution containing 0.1 % TFA, in which the ACN percentage was varied depending on the nature of each peptide. These solutions had a final concentration of 10 or 50 mg·mL<sup>-1</sup> depending on the scale of the synthesis and the column used. The resulting solution was filtered through a

0.45 mm nylon filter and 2 mL were manually injected and purified using the optimal HPLC gradient. The collected fractions were analyzed by HPLC and all fractions with purity over 95 % were combined and lyophilized.

#### 3.1.2.2.6. Counter ion exchange

Pure lipopeptides obtained as TFA salts after purification, were subjected to three cycles of dilution and lyophilization with HCl 8 mM. Solutions of 1 mg·mL<sup>-1</sup> were prepared, thoroughly vortexed and immediately frozen and lyophilized. The completion of the counter ion exchange was assessed by <sup>19</sup>F quantitative NMR spectroscopy.

The sulfate counter ions of commercial polymyxin B were also exchanged through the obtention of the free-based peptide. Polymyxin B was neutralized using equimolar amounts of KOH 0.1 M. The resulting peptide, completely insoluble in neutral aqueous conditions, was isolated by centrifugation (6000 rpm, 10 min, 4 °C), and washed 3 times with cold water. The product was dried by lyophilization. Free-base polymyxin was treated with equimolar amounts of HCl 8 mM or HBr 0.25 mM until its complete dissolution and it was finally lyophilized.

#### 3.1.2.3. Antimicrobial activity

##### 3.1.2.3.1. Preparation of bacterial cells

All material used in the microbiological assays had been previously sterilized using an autoclave with the following conditions: 1 atm, 120 °C for 20 minutes.

Three Gram-negative strains, *Escherichia coli* (ATCC 25922), *Pseudomonas aeruginosa* (ATCC 27853), and *Acinetobacter baumannii* (ATCC 19606) were used, as well as one Gram-positive strain, *Staphylococcus aureus* (ATCC 25923). An isolated bacterial colony of each strain was used to inoculate 10 mL of MHB, and the bacterial pre-cultures were allowed to grow overnight at 37 °C. These overnight pre-cultures were then used to freshly inoculate 5 mL of MHB to a final OD<sub>540</sub> of 0.2, and the resulting bacterial suspension was incubated for 3 - 4 hours at 37 °C to reach the earlier exponential growth phase (OD<sub>540</sub> = 1 - 2). Test cultures were finally diluted to OD<sub>540</sub> = 0.2, which according to McFarland standard contains 1 - 2·10<sup>8</sup> CFU·mL<sup>-1</sup>.

#### 3.1.2.3.2. MIC assay

Microtiter plates (96 wells of 100  $\mu\text{L}$ ) were filled with 50  $\mu\text{L}$  of MHB, and serial 2-fold dilutions of peptides were arranged in rows from 32 to 0.06  $\mu\text{g}\cdot\text{mL}^{-1}$ . The two final columns served as positive (no peptide) and negative controls (no peptide and not inoculated with bacteria). The previously prepared bacterial suspensions with a  $\text{OD}_{540}$  of 0.2 were 100-fold diluted, and 50  $\mu\text{L}$  of the subsequent suspension were added to the wells (except for the final column), giving a final concentration of approximately  $10^6$   $\text{CFU}\cdot\text{mL}^{-1}$ . The plates were incubated at 37 °C for 18 - 20 hours. The MIC was determined visually as the lowest peptide concentration inhibiting bacterial growth. Each determination was carried out in triplicate.

#### 3.1.2.4. Hemolysis

The hemolytic effect of the peptides was evaluated by a serial 2-fold dilution assay, as previously described by Zaragoza et al.<sup>321</sup> The fresh rabbit blood used in this assay was supplied by the Animal Experimentation Unit of the Faculty of Pharmacy and Food Sciences of the University of Barcelona.

Red blood cells were washed three times with buffer (150 mN NaCl / 10 mM TRIS, pH 7.4) by centrifugation at 3000 rpm 10 min, and finally resuspended in the same initial volume of buffer. This erythrocyte concentrate was further diluted with buffer to obtain a suspension with  $\text{OD}_{540} = 1$ . Aliquots of 200  $\mu\text{L}$  were incubated for 1 h at 37 °C with the different lipopeptide concentrations in 96-well polypropylene microtiter plates. Plates were then centrifuged for 15 min at 5000 rpm, and hemoglobin release was determined by measuring the absorbance at 540 nm of released hemoglobin in the supernatant. As negative and positive controls, erythrocytes in buffer (0 % hemolysis) and in Titron X-100 (100 % hemolysis) were employed, respectively. Each determination was performed in triplicate and the hemolysis percentage was calculated according to the following equation:

$$\% \text{ hemolysis} = 100 \cdot (A_{\text{sample}} - A_{0\%} / A_{100\%} - A_{0\%})$$

#### 3.1.2.5. Transmission electron microscopy

To prepare bacterial cells for TEM, overnight cultures (12 - 16 hours) of *Pseudomonas aeruginosa* (ATCC 27853) and *Staphylococcus aureus* (ATCC 25923) were grown at

37 °C in LB. The pre-inoculums were then adjusted to  $OD_{540} = 0.2$  for a concentration of  $\sim 10^8$  CFU·mL<sup>-1</sup>. Aliquots of 10 mL were incubated with the desired lipopeptide at the MIC for 2 h at room temperature, and bacterial cells were collected by centrifugation (5000 rpm, 15 min). Samples were fixed with 2.5 % glutaraldehyde in phosphate buffer for 2 hours at 4 °C, washed with the same buffer and post fixed with 1 % osmium tetroxide in buffer containing 0.8 % potassium ferricyanide at 4 °C. The samples were then dehydrated for 1 hour in acetone, infiltrated in a graded series of Epon resin (Ted pella, Inc., USA) for 2 days, and finally embedded in fresh Epon resin and polymerized at 60 °C for 48 hours. Ultrathin sections were obtained using a Leica Ultracut UCT ultramicrotome (Leica, Vienna) and mounted on Formvar-coated copper grids. Sections were stained with 2 % aqueous uranyl acetate and lead citrate and examined in a JEM-1010 electron microscope (Jeol, Japan).

### 3.1.2.6. Biophysical experiments

#### *3.1.2.6.1. Insertion in monolayers*

Kinetics of insertion into monolayers were conducted at room temperature (25 °C) on a monolayer system (NIMA Technology, Coventry, England) by using a cylindrical PTFE plate (Teflon®) trough (internal dimensions: 5 cm diameter or 19.6 cm<sup>2</sup> area) containing a continuously stirred aqueous phase (30 mL, 10 mM Tris pH 7.4), and a Wilhelmy platinum plate connected to an electrobalance. The system was enclosed in a Plexiglas box to reduce surface contamination, and before each run the plate and the trough were thoroughly cleaned with hot water at >75 °C to avoid carryover of lipid and peptides. Monolayers of POPG, POPE/POPG (6:4), POPC or LPS from lipid stock solutions in chloroform were delivered slowly to the aqueous subphase using a microsyringe to achieve a surface pressure of 32 mN·m<sup>-1</sup>. After solvent evaporation, a known aliquot of peptide was added without disturbance of the monolayer via an inlet port, and the surface pressure was continuously recorded. Each determination was performed in triplicate.

#### *3.1.2.6.2. Liposome preparation*

LUVs of POPG, POPE/POPG (6:4), POPG/DOTAP (8:2) and POPC, alone or with the fluorescently labeled phospholipids NBD-PE, Rh-PE or pyPG, were prepared by co-dissolving the appropriate lipids and probes in chloroform. The lipid mixture was dried

under nitrogen steam and left to dry under vacuum overnight. The resulting thin films were resuspended in TRIS buffer (10 mM, pH 7.4) to the desired final lipid concentration and then sonicated until a clear dispersion was obtained (typically 3 - 5 minutes). LUVs were obtained by 41-fold extrusion of the liposomes through 2 stacked polycarbonate filters (100 nm pore-size) using a Liposofast-Basic Extruder. For the ANTS/DPX leakage assay, the dried films were hydrated in a buffer containing the fluorescent ANTS (12.5 mM), the quencher DPX (45 mM), NaCl (80 mM), and TRIS (10mM, pH 7.5). Moreover, they contained 0.2 mol% Rh-PE for monitoring the fluorescence before and after the separation of the unencapsulated material, which was carried out by gel-filtration on a Sephadex G-50 column. In this way, the exact lipid concentration was determined, accounting both for the dilution of the sample and any losses on the process of preparation of the liposomes. Generally, the concentration was 50 % of the initial.

The average diameter was determined by dynamic light scattering with a Malvern II-C Autosizer, typically obtaining a mean diameter between 90 to 117 nm, and a polydispersity below 0.1.

#### *3.1.2.6.3. Light scattering*

Vesicle aggregation induced by different peptide concentrations was measured as the change in the 90° scattered intensity at 360 nm with 1 nm slit-widths on a SLM-Aminco AB-2 spectrofluorimeter. An aliquot of vesicles of the desired composition was added to the cuvette containing 1.5 mL of Tris buffer (10 mM, pH 7.4) with constant stirring, and increasing aliquots of peptide stock solution were added successively. The relative change in the intensity of the scattered light,  $\delta I$ , was defined as  $(I - I_0)/I_0$ , where  $I_0$  is the scattering without peptide, and  $I$  is the scattering in the presence of peptide.

#### *3.1.2.6.4. Fluorescence resonance energy transfer*

Peptide-induced lipid mixing of vesicles of different composition was studied by measuring the increase in fluorescence resonance energy transfer (FRET) from NBD-PE as donor to an Rh-PE acceptor. Measurements were carried out on a SLM-Aminco AB-2 spectrofluorimeter at 25 °C. Two different FRET experiments were performed.

In one case, an equimolar mixture of vesicles of the desired composition containing 0.6 mol% of NBD-PE and vesicles containing 0.6 mol% Rh-PE (lipid concentration

107  $\mu\text{M}$ ) were mixed in 1.5 mL of Tris buffer (10 mM, pH 7.4) with constant stirring, followed by titration with peptide from a stock solution.

In the second experimental design, vesicles containing 0.3 mol% of each fluorophore (NBD and Rh) (13  $\mu\text{M}$ ) were mixed with a 25-fold excess of unlabeled vesicles of the same composition (320  $\mu\text{M}$ ). Then, the peptide was added from a stock solution in small aliquots.

The excitation wavelength was set at 460 nm, and the emission of fluorescence was monitored at 592 nm, which corresponds to rhodamine emission, with slit widths at 4 nm. The relative change in fluorescence was represented as  $\delta F$  for the first experiment, which was defined as  $(F - F_0)/F_0$ . For the second experimental design, the fusogenic agent  $\text{CaCl}_2$  was used, and FRET was expressed as  $(F - F_0)/(F_{\text{max}} - F_0)$ , where  $F_0$  is the fluorescence without peptide,  $F_{\text{max}}$  is the maximal FRET produced by the addition of 50  $\mu\text{L}$  of  $\text{CaCl}_2$  0.5 M, and  $F$  is the fluorescence emission intensity in the presence of peptide.

#### 3.1.2.6.5. Energy transfer from pyrene excimers

The transfer of 30 mol% pyrene-labelled phospholipids (0.83  $\mu\text{M}$ ) to an excess of unlabeled phospholipid vesicles (106  $\mu\text{M}$ ) was measured. Experiments were carried out on a SLM-Aminco AB-2 spectrofluorimeter at 25  $^\circ\text{C}$  in 1.5 mL of Tris buffer (10 mM, pH 7.4) with constant stirring. Increasing peptide aliquots were added to the cuvette containing vesicles of the desired composition. The pyrene monomer fluorescence emission was monitored at 395 nm, with excitation at 346 nm, and slit widths kept at 4 nm. The relative change in fluorescence,  $\delta F$  was defined as  $(F - F_0)/F_0$ , where  $F_0$  represents the initial monomer fluorescence without peptide and  $F$  is the fluorescence in the presence of peptide.

#### 3.1.2.6.6. Leakage of aqueous contents

Peptide-induced leakage of vesicles encapsulating both ANTS and DPX was investigated. The experiment was performed at 25  $^\circ\text{C}$  in 1.5 mL of TRIS buffer (10 mM, pH 7.4) on a SLM-Aminco AB-2 spectrofluorimeter with constant stirring. Lipid vesicles (107  $\mu\text{M}$ ) were titrated with increasing peptide volumes from a stock solution. ANTS emission was monitored at 530 nm, with excitation at 350 nm and slit widths at 4 nm. The maximum fluorescence value was obtained by adding 10  $\mu\text{L}$  of Triton X-100 to the lipid vesicles,



and represented the 100 % leakage, while the 0 % leakage corresponded to the fluorescence of the vesicles at time zero.

#### 3.1.2.6.7. Depolarization of the bacterial membrane

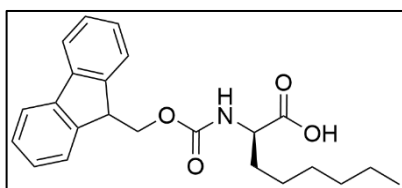
The peptide induced-cytoplasmic membrane depolarization in *Pseudomonas aeruginosa* (ATCC 27853) was investigated by using the membrane potential sensitive fluorescent dye diSC<sub>3</sub>(5). Cultures of *Pseudomonas aeruginosa* were grown to exponential phase and washed three times with buffer containing 5 mM HEPES and 20 mM glucose (pH 7.4). After final wash and centrifugation (5000 rpm, 10 min) the pellets were resuspended in buffer to an OD<sub>600</sub> of 0.05. The cell suspension was then treated with 0.2 mM EDTA and incubated with 0.4 mM diSC<sub>3</sub>(5) until a stable reduction of fluorescence was achieved (1 - 2 hours). Then KCl was added to a final concentration of 0.1 M to equilibrate the cytoplasmic and external K<sup>+</sup> concentrations. A volume of 1.5 mL of the cell suspension was then placed in a 1 cm quartz cuvette, and the peptides were added at their MIC 50 seconds after addition of the cell suspension. Changes in fluorescence were recorded using an a SLM-Aminco AB-2 spectrofluorimeter with an excitation wavelength of 622 nm and an emission wavelength of 670 nm and slit widths at 4 nm. Water addition was used as a negative control, while 10 μL of Triton X-100 were added to obtain the maximum depolarization value.

### 3.1.3. Synthetic procedures

#### 3.1.3.1. Amino acids protection

Most amino acids used in this thesis were commercially available in their protected form, but D-Adec and D-Aoc were purchased unprotected and therefore, they required a previous protection using the appropriate protecting group depending on the applied synthetic strategy.

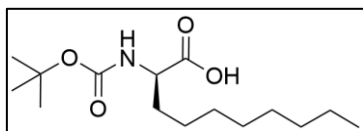
##### 3.1.2.1.1. Fmoc-DAoc-OH



415 mg (2.61 mmol, 1 eq) of H-D-Aoc-OH were dissolved in 15 mL of H<sub>2</sub>O/ACN (1:1, v/v), and 10 % NaHCO<sub>3</sub> solution was added to reach pH 9 - 10. The resulting solution was let to stir in an ice bath, and a solution of 810 g Fmoc-Cl (1.2 eq) in 15 mL of ACN was added. The reaction mixture

was stirred in the ice bath for 2 hours and 135 mg of Fmoc-Cl (0.52 mmols, 0.2eq) were added. The reaction was left to react overnight at room temperature. 20 mL of Milli-Q water were added, and the aqueous layer was washed with Et<sub>2</sub>O (3 x 50 mL) and acidified to pH 3 by addition of a 1.0 M HCl solution. The aqueous layer was extracted with EtOAc (3 x 50 mL). The extracts were dried with Na<sub>2</sub>SO<sub>4</sub>, filtered, and evaporated. The resulting crude product (785 mg) was obtained as a white powder, with a global yield of 79 % and a final purity of 82 %. It was reacted without further purification. **HPLC**: t<sub>R</sub> = 27.925 min G0595t30. **ESI MS**: m/z calculated for C<sub>23</sub>H<sub>27</sub>NO<sub>4</sub> 381.19, found 382.3 [M + H]<sup>+</sup>. **<sup>1</sup>H NMR (400MHz, DMSO)**: δ = 7.87 (d, J = 7.6 Hz, 2H, ArH), 7.70 (dd, J = 7.6, 2.2 Hz, 2H, ArH), 7.60 (d, J = 8.1 Hz, 1H, NH), 7.40 (t, J = 7.6 Hz, 2H, ArH), 7.30 (m, 2H, ArH), 4.28 - 4.17 (m, 3H, COOCH<sub>2</sub>CH and COOCH<sub>2</sub>CH), 3.90 (td, J = 8.9, 4.8 Hz, 1H, COCH) 1H. 1.67-1.55 (m, 2H, COCHCH<sub>2</sub>), 1.29 - 1.19 (m, 8H, CH<sub>2</sub>(CH<sub>2</sub>)<sub>4</sub>CH<sub>3</sub>), 0.83 (t, 6.7 Hz, 3H, CH<sub>3</sub>). **<sup>13</sup>C NMR (400MHz, DMSO)**: δ = 174.47 (C), 156.61 (C), 142.29 (2 x C), 141.14 (2 x C), 128.09 (2 x CH), 127.49 (2 x CH), 125.72 (2 x CH), 120.54 (2 x CH), 66.02 (CH<sub>2</sub>), 54.17 (CH), 47.10 (CH), 31.51 (CH<sub>2</sub>), 31.17 (CH<sub>2</sub>), 25.58 (CH<sub>2</sub>), 25.89 (CH<sub>2</sub>), 22.43 (CH<sub>2</sub>), 14.36 (CH<sub>3</sub>).

### 3.1.2.1.2. Boc-DAdec-OH



509 mg (2.72 mmol, 1 eq) of H-D-Adec-OH were dissolved in 20 mL of H<sub>2</sub>O/ACN (1:1, v/v), and 10 % NaHCO<sub>3</sub> solution was added to reach pH 9 - 10. The resulting solution was let to stir in an ice bath, and 712 mg of di-*tert*-butyl-dicarbamate (Boc<sub>2</sub>O) (3.26 mmol, 1.2 eq) dissolved in 20 mL of H<sub>2</sub>O/ACN (1:1, v/v) were added dropwise. The reaction mixture was stirred in the ice bath for 2 hours and 119 mg of Boc<sub>2</sub>O (0.54 mmols, 0.2eq) were added. The reaction was left to react overnight at room temperature. The turbid resulting solution was extracted with Et<sub>2</sub>O (3 x 50 mL) and carefully acidified to pH 4 - 5 by addition of a 1.0 M HCl solution at 0°C. The resulting solution was extracted with EtOAc (3 x 50 mL). The extracts were dried with Na<sub>2</sub>SO<sub>4</sub>, filtered, and evaporated. The resulting crude product (679 mg) was obtained as a yellow oil, with a global yield of 87 % and a final purity of 93 %. It was reacted without further purification. **HPLC**: t<sub>R</sub> = 26.8 min G0595t30. **ESI MS**: m/z calculated for C<sub>15</sub>H<sub>29</sub>NO<sub>4</sub> 287.21, found 288.2 [M + H]<sup>+</sup>, 310.2 [M + Na]<sup>+</sup>, 323.2. [M + K]<sup>+</sup>, and 286.3 [M - H]<sup>-</sup>. **<sup>1</sup>H NMR (400MHz, DMSO)**: δ = 6.99 (d, J = 8 Hz, 1H, NH), 3.82 (td, J = 8.8, 4.9 Hz, 1H,

COCH), 1.55 (ddt,  $J = 29.8, 9.5, 5.9$  Hz, 2H, COCHCH<sub>2</sub>), 1.35 (s, 9H, CH<sub>3</sub>), 1.21 (s, 12H, CH<sub>2</sub>), 0.85 - 0.81 (m,  $J =$  Hz, 3H, CH<sub>3</sub>). <sup>13</sup>C NMR (400MHz, DMSO):  $\delta = 174.73$  (C), 156.03 (C), 78.34 (C), 53.79 (CH), 31.68 (CH<sub>2</sub>), 31.21 (CH<sub>2</sub>), 29.24 (CH<sub>2</sub>), 29.02 (CH<sub>2</sub>), 28.94 (CH<sub>2</sub>), 28.64 (3 x CH<sub>3</sub>), 25.92 (CH<sub>2</sub>), 22.52 (CH<sub>2</sub>), 14.38 (CH<sub>3</sub>).

### 3.1.3.2. Synthesis of PxB<sub>3</sub>

A manual solid phase peptide synthesis was performed following a Fmoc/Bn protection strategy in a polypropylene syringe of 10 mL fitted with a polyethylene disc. Polymyxin B<sub>3</sub> was synthesized starting from 254 mg of 2-CTC resin (commercial functionalization: 1.6 mmol·g<sup>-1</sup> resin). The amino acids used were Fmoc-Thr(Bn)-OH, Fmoc-Dab(Z)-OH, Fmoc-Dab(Boc)-OH, Fmoc-Leu-OH, and Fmoc-DPhe-OH, as well octanoic acid. All coupling reactions reached yields  $\geq 99$  % as assessed by the Kaiser test.

After resin conditioning, the first amino acid of the sequence, Fmoc-Thr(Bn)-OH (210 mg, 0.49 mmol, 1.2 eq) was added to the resin along with DIPEA (283  $\mu$ L, 1.63 mmol, 4 eq), both reagents were then dissolved in the minimum possible amount of DCM and left to react overnight. After which, the resin was washed with DMF and DCM, treated with 0.8 mg·mL<sup>-1</sup> of MeOH for 15 minutes, and washed again with DCM. The Fmoc group was removed with 3 mL of 20% piperidine in DMF (1 x 1 min, 2 x 10 min) and the loading was monitored by quantifying the amount of dibenzofulvene-piperidine adduct via spectrophotometry ( $f = 0.75$  mmol·g<sup>-1</sup> of resin). The following amino acids of the sequence were coupled using 3-fold molar excess of amino acid, HOBt and DIC for 1 hour with occasional manual stirring at room temperature. Afterward, the resin was drained and washed with DMF (5 x 30 s) and DCM (5 x 30 s). After each coupling step, the *N*-terminal Fmoc group was removed as described above.

On peptide completion, the partially protected peptide was obtained after cleavage with 5 mL of DCM/TFA/TES/H<sub>2</sub>O (55:40:3:2, v/v/v/v) for 30 min. The resin was then removed by filtration and washed twice with 2 mL of the cleavage mixture. The combined filtrates were transferred to 50 mL microcentrifuge tubes, and the volume was reduced by evaporation using a stream of nitrogen. Thereafter, the peptide was precipitated and washed three times with 40 mL of cold water and lyophilized to yield 339 mg of white powder ( $\eta_{\text{cleavage}} = 82$  %). The partially protected PxB<sub>3</sub> was cyclized using HATU (119 mg, 0.31 mmol, 2 eq), HOAt (43 mg, 0.31 mmol, 2 eq), and DIPEA (109  $\mu$ L,

0.62 mmol, 4 eq) in the minimum possible volume of DMF. The cyclization was left to react for 2 - 3 hours, and it was monitored by TLC, which was stained with ninhydrin. The cyclized protected peptide was then precipitated with 10-fold excess of cold water, isolated by centrifugation, and lyophilized. The crude peptide, which yielded 257 mg ( $\eta_{\text{cyclization}} = 81\%$ ), was finally treated for 45 minutes with 100 mL of an acidic mixture composed of HBr and TES, which had been previously prepared from TFA/TES/Br<sub>2</sub> (82.5:15:2.5, v/v/v). The peptide solution was evaporated to a reduced volume under a gentle stream of nitrogen gas, and the crude product was precipitated and washed 3 times with Et<sub>2</sub>O, yielding a total amount of 184 mg ( $\eta_{\text{acidolysis}} = 92\%$ ) of an orange/off-white solid. Purification by semi-preparative HPLC was performed, obtaining 69 mg of white pure peptide ( $\eta_{\text{purification}} = 34\%$ ). Global yield: 21%. Homogeneity by area integration of HPLC trace revealed that the peptide was >97% pure. **HPLC:**  $t_R = 20.9$  min G2035t30 **ESI MS:** m/z calculated for C<sub>55</sub>H<sub>96</sub>N<sub>16</sub>O<sub>13</sub> 1188.7, found 1189.6 [M + H]<sup>+</sup>; 595.5 [M + 2H]<sup>+</sup>; 397.3 [M + 3H]<sup>+</sup>; 1224.3 [M + Cl]<sup>-</sup>.

#### 3.1.3.3. Synthesis of dusquetide and RR4

Dusquetide and RR4 were synthesized following standard Fmoc/<sup>t</sup>Bu procedures in 5 mL polypropylene syringes fitted with a polyethylene disc. For that purpose, MBHA resin (commercial functionalization: 0.69 mmol·g<sup>-1</sup> resin) and the following amino acids were used: Fmoc-Ala-OH, Fmoc-Arg(Pbf)-OH, Fmoc-Ile-OH, Fmoc-Leu-OH, Fmoc-Lys(Boc)-OH, Fmoc-Pro-OH, Fmoc-Trp-OH, and Fmoc-Val-OH. All coupling reactions proceeded to greater than 99% completion as assessed by Kaiser tests.

MBHA resin (100 mg, 0.07 mmol) was conditioned, and the first amino acid of the sequence was incorporated to the resin using 3-fold molar excess of amino acid, HOBt and DIC. Therefore, Fmoc-Ala-OH (64 mg, 0.21 mmol, 3 eq), HOBt (28 mg, 0.21 mmol, 3 eq), and DIC (32  $\mu$ L, 0.21 mmol, 3 eq) were added to the resin and left to react for 1 hour in DMF with occasional manual stirring. The resin was then drained and washed with DMF (5 x 30 s) and DCM (5 x 30 s). After each coupling step, the *N*-terminal Fmoc group was removed with 2 mL of 20% piperidine in DMF (1 x 1 min, 2 x 10 min). All amino acids of the sequence were added following the same protocol.

On peptide completion, the peptidyl resins were treated with 2 mL of DCM/TFA (1:1, v/v) for 1 minute. Afterward, the peptidyl resins were cleaved with 10 mL of the HBr

solution previously prepared from TFA/TES/Br<sub>2</sub> (82.5:15:2.5, v/v/v) for 90 minutes. TIS was used in the synthesis of RR4. The peptide solution was evaporated to a reduced volume under a gentle stream of nitrogen gas, and the crude product was precipitated and washed 3 times with Et<sub>2</sub>O. The peptides were obtained with an orange/off-white coloration that disappeared after 3 lyophilization cycles with 5 mL H<sub>2</sub>O/ACN (1:1, v/v). 43 mg ( $\eta_{\text{cleavage}} = 87\%$ ) of dusquetide and 72 mg ( $\eta_{\text{cleavage}} = 82\%$ ) of RR4 were obtained. The crude peptides were characterized by HPLC and ESI-MS (Table 36), and the crude purity was 95 % and 92 % respectively (purity calculated by area integration of HPLC trace). No further purification was performed.

**Table 36:** Dusquetide and RR4 characterization.

Peptide	t <sub>R</sub> (HPLC gradient)	Chemical formula	Exact mass	ESI (+) m/z	ESI (-) m/z
Dusquetide	9.408 min (G0595t30)	C <sub>25</sub> H <sub>47</sub> N <sub>9</sub> O <sub>5</sub>	553.37	554.4 [M + H] <sup>+</sup> 278.1 [M + 2H] <sup>2+</sup>	634.6 [M + Br] <sup>-</sup> 666.7 [M + TFA] <sup>-</sup>
RR4 (fragment 8 - 14)	10.695 min (G0595t30)	C <sub>44</sub> H <sub>76</sub> N <sub>16</sub> O <sub>7</sub>	940.61	941.7 [M + H] <sup>+</sup> 471.5 [M + 2H] <sup>2+</sup> 314.4 [M + 3H] <sup>2+</sup>	1019.7 [M + Br] <sup>-</sup> 1101.8 [M + 2Br + H] <sup>-</sup> 1183.9 [M + 3Br + 2H] <sup>-</sup> 1263.9 [M + 4Br + 3H] <sup>-</sup>

#### 3.1.3.4. Synthesis of depsipeptide polymyxin analogues

Depsipeptide analogues were synthesized starting from 200 mg of 2-CTC resin (commercial functionalization: 1.6 mmol·g<sup>-1</sup> resin) by established manual solid phase synthesis protocols using Fmoc/<sup>t</sup>Bu protection strategy. The amino acids used were Fmoc-Thr(<sup>t</sup>Bu)-OH, Fmoc-Dab(Boc)-OH, Fmoc-Dab(Mtt)-OH, Fmoc-DPhe-OH and Boc-DAdec-OH, as well as the (S)-2-hydroxy-4-methylpentanoic acid, octanoic and nonanoic acids. All coupling reactions yielded  $\geq 99\%$  as assessed by Kaiser tests or HPLC analysis after “mini-cleavage”.

Firstly, the resin was conditioned in a polypropylene syringe of 10 mL fitted with a polyethylene disc. Then, the first amino acid of the sequence, Fmoc-Thr(<sup>t</sup>Bu)-OH (127 mg, 0.32 mmol, 1 eq) was added to the resin along with DIPEA (223  $\mu$ L, 1.28 mmol, 4 eq). Both reagents were dissolved in the minimum possible amount of DCM and left to react overnight. Afterward, the resin was washed with DMF and DCM, treated with 0.8 mg·mL<sup>-1</sup> of MeOH for 15 minutes, and washed again with DCM. The Fmoc group

was removed with 2 mL of 20 % piperidine in DMF (1 x 1 min, 2 x 10 min) and dibenzofulvene-piperidine adduct was quantified in order to estimate the level of first residue attachment. The loading values obtained ranged from 0.75 to 0.90 mmol·g<sup>-1</sup> resin. A total of 3 eq of the following Fmoc amino acid, HOBt and DIC were added to the resin dissolved in a minimal amount of DMF, and the reaction was carried out for 1 hour with occasional manual stirring at room temperature. After each coupling step, the *N*-terminal Fmoc group was removed as described above. Particularly, the (S)-2-hydroxy-4-methylpentanoic acid was coupled twice using amino acid/DIC/HOBt (2:2:4 eq) to prevent polymerization. The ester bond was then achieved by using the symmetric anhydride of Fmoc-DPhe-OH, which was prepared beforehand using 6 eq of the amino acid and 3 eq of DIC dissolved in the minimum amount of DCM for 30 minutes. The anhydride was coupled to the growing peptide sequence in a second step along with 0.3 eq of DMAP in DMF for 1 hour.

On peptide completion, a total of 4 mL of DCM/HFIP/TFE/TES (65:20:10:5, v/v/v/v) was added to the peptidyl resin. The mixture was allowed to react at room temperature for 1 h. The resin was then removed by filtration and washed twice with 2 mL of the cleavage mixture. The combined filtrates were transferred to 50 mL microcentrifuge tubes, and the volume was reduced by evaporation using a stream of nitrogen gas. Afterward, the peptide was precipitated and washed three times with 40 mL of cold water and lyophilized to yield a white powder. The total amount of partially protected peptide was then cyclized using HATU/HOAt/DIPEA (2:2:4 eq) in the minimum volume of DMF. The cyclization was left to react for 2 - 3 hours, and it was monitored by TLC stained with ninhydrin. The cyclized protected peptide was then precipitated with 10-fold excess of cold water and lyophilized. The protected cyclic peptide was treated for 30 minutes with a solution of DCM/TFA/TES/H<sub>2</sub>O (50:45:3:2, v/v/v/v) to reach a final concentration of 10 mg·mL<sup>-1</sup>. The volume of the acidic mixture was then reduced by evaporation and the final product was precipitated and washed 3 times with cold Et<sub>2</sub>O. The obtained white powder was dissolved in H<sub>2</sub>O/ACN (1:1, v/v) and lyophilized. Purification was performed by semi-preparative HPLC, overall yields for synthesis of the depsipeptide analogues ranged from 7 to 12 % (Table 37). Purity (>95 %) was confirmed by HPLC and ESI MS (Table 38).

**Table 37:** Obtained quantities and synthetic yields of depsipeptide analogues.

Peptide	Functionalization (mmol·g <sup>-1</sup> of resin)	Cleavage yield	Cyclization yield	Acidolysis yield	Purification yield	Global yield <sup>a</sup>
<b>1</b>	0.75	183 mg	141 mg	99 mg	19 mg	13 mg
		61 %	85 %	72 %	19 %	7 %
<b>2</b>	0.90	254 mg	201 mg	167 mg	40 mg	27 mg
		70 %	87 %	85 %	24 %	12 %
<b>3</b>	0.87	218 mg	177 mg	136 mg	30 mg	20 mg
		65 %	90 %	79 %	22 %	9 %

<sup>a</sup> Free base peptide**Table 38:** Depsipeptide analogues characterization.

Peptide	tr (HPLC gradient)	Chemical formula	Exact mass	ESI (+)	ESI (-)
<b>1</b>	19.128 min (G2035t30)	C <sub>55</sub> H <sub>95</sub> N <sub>15</sub> O <sub>14</sub>	1189.7	1190.9 [M + H] <sup>+</sup>	1225.0 [M + Cl] <sup>-</sup>
				596.1 [M + 2H] <sup>2+</sup>	629.9 [M + 2Cl] <sup>2-</sup>
				397.6 [M + 3H] <sup>3+</sup>	
<b>2</b>	14.508 min (G2540t30)	C <sub>56</sub> H <sub>97</sub> N <sub>15</sub> O <sub>14</sub>	1203.7	1204.7 [M + H] <sup>+</sup>	1238.6 [M + Cl] <sup>-</sup>
				603.1 [M + 2H] <sup>2+</sup>	637.9 [M + 2Cl] <sup>2-</sup>
				402.4 [M + 3H] <sup>3+</sup>	
<b>3</b>	22.767 min (G2035t30)	C <sub>53</sub> H <sub>92</sub> N <sub>14</sub> O <sub>13</sub>	1132.7	1133.8 [M + H] <sup>+</sup>	1167.9 [M + Cl] <sup>-</sup>
				568.2 [M + 2H] <sup>2+</sup>	601.6 [M + 2Cl] <sup>2-</sup>
				378.7 [M + 3H] <sup>3+</sup>	

### 3.1.3.5. Synthesis of cysteine analogues

Cysteine analogues were synthesized starting from 50 - 200 mg of MBHA resin (commercial functionalization: 0.69 mmol·g<sup>-1</sup> resin) following standard Fmoc/<sup>t</sup>Bu procedures. The protected amino acids used were: Fmoc-Cys(Trt)-OH, Fmoc-DCys(Trt)-OH, Fmoc-Dab(Boc)-OH, Fmoc-Leu-OH, Fmoc-Nle-OH, Fmoc-DPhe-OH, Fmoc-Thr(<sup>t</sup>Bu)-OH, Fmoc-DTrp-OH, and Fmoc-DAoc-OH as well as the (S)-2-hydroxy-4-methylpentanoic acid, hexanoic, octanoic, nonanoic, decanoic and dodecanoic acids. All coupling reactions yields reached ≥ 99 % as assessed by the Kaiser test.

The resin was weighed and conditioned in a polypropylene syringe of 10 mL fitted with a polyethylene disc. Firstly, the amino acid of reference (Fmoc-Ala-OH) and the Fmoc-Rink-Linker were added using DIC/HOBt activation (3 eq amino acid/DIC/HOBt). Then,

the different sequences were assembled onto the Rink amide linker following standard coupling/washing/deprotection cycles. All couplings were carried out using a 3-fold molar excess of each reagent in DMF for 1 hour, and the Fmoc removal was achieved by successive treatments with 20 % piperidine/DMF (1 x 1 min, 2 x 10 min). Some analogues contained an ester bond between the positions 6 and 7, which was created via symmetrical anhydride, as explained in the previous section.

Cleavage of the peptides from the resin was carried out by acidolysis with 4 mL of TFA/TES/H<sub>2</sub>O (95:3:2, v/v/v) for 90 min. The cleavage procedure was repeated two times. TFA was removed via nitrogen stream, and the oily residue was treated with cold Et<sub>2</sub>O to obtain the peptide precipitate. The solid peptide was isolated by centrifugation, dissolved in H<sub>2</sub>O/ACN (1:1, v/v) and lyophilized. Cyclization of peptides through disulfide bonds was carried out at high dilution (1 mg·mL<sup>-1</sup>) in DMSO/ H<sub>2</sub>O (5:95, v/v) for 24 - 48 hours and monitored by analytical HPLC. Finally, peptides were purified by semi-preparative HPLC and characterized by analytical HPLC and ESI mass spectrometry. Overall yields for synthesis of the cysteine analogues ranged from 15 to 28 %, with final purities greater than 95 % (Tables 39 and 40).

**Table 39:** Obtained quantities and synthetic yields of cysteine analogues.

Peptide	Resin amount	Functionalization (mmol·g <sup>-1</sup> of resin)	Cleavage yield	Cyclization yield <sup>a</sup>	Purification yield	Global yield <sup>b</sup>
<b>4</b>	156 mg	0.69	136 mg 72 %	100 %	45 mg 33 %	30 mg 24 %
<b>5</b>	168 mg	0.69	167 mg 81 %	100 %	48 mg 29 %	32 mg 23 %
<b>6</b>	175 mg	0.69	157 mg 72 %	100 %	55 mg 35 %	37 mg 25 %
<b>7</b>	173 mg	0.69	151 mg 69 %	100 %	39 mg 26 %	26 mg 18%
<b>8</b>	180 mg	0.69	181 mg 82 %	100 %	53 mg 29 %	36 mg 24 %
<b>9</b>	172 mg	0.69	145 mg 68 %	100 %	46 mg 32 %	32 mg 22 %
<b>10</b>	177 mg	0.69	161 mg 73 %	100 %	55 mg 34 %	37 mg 25 %



<b>11</b>	181 mg	0.69	151 mg 66 %	100 %	42 mg 28 %	28 mg 18 %
<b>12</b>	68 mg	0.69	57 mg 68 %	100 %	17 mg 30 %	11 mg 20 %
<b>13</b>	81 mg	0.69	70 mg 69 %	100 %	20 mg 29 %	13 mg 20 %
<b>14</b>	72 mg	0.69	58 mg 65 %	100 %	22 mg 38 %	15 mg 25 %
<b>15</b>	123 mg	0.69	61 mg 41 %	100 %	22 mg 37%	15 mg 15%
<b>16</b>	137 mg	0.69	98 mg 59 %	100 %	27 mg 28 %	18 mg 17 %
<b>17</b>	124 mg	0.69	87 mg 57 %	100 %	27 mg 31 %	18 mg 18 %
<b>18</b>	162 mg	0.69	100 mg 53 %	100 %	36 mg 36 %	24 mg 19 %
<b>19</b>	160 mg	0.69	159 mg 85 %	100 %	52 mg 33 %	34 mg 28 %

<sup>a</sup>Cyclic compounds were obtained as an oil due to the presence of DMSO, for that reason, they were not weighed, and the cyclization (followed by HPLC) was estimated to be quantitative (100 %). <sup>b</sup>Free base peptide.

**Table 40:** Cysteine analogues characterization.

Peptide	t <sub>R</sub> (HPLC gradient)	Chemical formula	Exact mass	ESI (+) m/z
<b>4</b>	10.529 min (G2035t30)	C <sub>51</sub> H <sub>88</sub> N <sub>16</sub> O <sub>12</sub> S <sub>2</sub>	1180.6	1181.7 [M + H] <sup>+</sup> 591.3 [M + 2H] <sup>2+</sup>
<b>5</b>	12.974 min (G2540t30)	C <sub>53</sub> H <sub>92</sub> N <sub>16</sub> O <sub>12</sub> S <sub>2</sub>	1208.7	1209.6 [M + H] <sup>+</sup> 605.4 [M + 2H] <sup>2+</sup>
<b>6</b>	15.873 min (G2035t30)	C <sub>55</sub> H <sub>96</sub> N <sub>16</sub> O <sub>12</sub> S <sub>2</sub>	1236.7	1237.7 [M + H] <sup>+</sup> 619.3 [M + 2H] <sup>2+</sup>
<b>7</b>	18.547 min (G2035t30)	C <sub>57</sub> H <sub>100</sub> N <sub>16</sub> O <sub>12</sub> S <sub>2</sub>	1264.7	1265.6 [M + H] <sup>+</sup> 633.4 [M + 2H] <sup>2+</sup>
<b>8</b>	14.321 min (G2540t30)	C <sub>53</sub> H <sub>92</sub> N <sub>16</sub> O <sub>12</sub> S <sub>2</sub>	1208.7	1209.5 [M + H] <sup>+</sup> 605.4 [M + 2H] <sup>2+</sup>
<b>9</b>	15.463 min (G2540t30)	C <sub>54</sub> H <sub>94</sub> N <sub>16</sub> O <sub>12</sub> S <sub>2</sub>	1222.7	1223.6 [M + H] <sup>+</sup> 612.5 [M + 2H] <sup>2+</sup>
<b>10</b>	16.137 min (G2035t30)	C <sub>55</sub> H <sub>96</sub> N <sub>16</sub> O <sub>12</sub> S <sub>2</sub>	1236.7	1237.5 [M + H] <sup>+</sup> 619.5 [M + 2H] <sup>2+</sup>

<b>11</b>	19.282 min (G2035t30)	C <sub>57</sub> H <sub>100</sub> N <sub>16</sub> O <sub>12</sub> S <sub>2</sub>	1264.7	1265.7 [M + H] <sup>+</sup> 633.2 [M + 2H] <sup>2+</sup>
<b>12</b>	10.343 min (G2540t30)	C <sub>53</sub> H <sub>89</sub> N <sub>17</sub> O <sub>12</sub> S <sub>2</sub>	1219.6	1220.6 [M + H] <sup>+</sup> 611.0 [M + 2H] <sup>2+</sup>
<b>13</b>	13.426 min (G2540t30)	C <sub>54</sub> H <sub>91</sub> N <sub>17</sub> O <sub>12</sub> S <sub>2</sub>	1233.7	1234.8 [M + H] <sup>+</sup> 618.1 [M + 2H] <sup>2+</sup>
<b>14</b>	17.087 min (G2540t30)	C <sub>55</sub> H <sub>93</sub> N <sub>17</sub> O <sub>12</sub> S <sub>2</sub>	1247.7	1248.8 [M + H] <sup>+</sup> 625.2 [M + 2H] <sup>2+</sup>
<b>15</b>	9.166 min (G2540t30)	C <sub>50</sub> H <sub>93</sub> N <sub>15</sub> O <sub>13</sub> S <sub>2</sub>	1175.7	1176.7 [M + H] <sup>+</sup> 589.0 [M + 2H] <sup>2+</sup>
<b>16</b>	11.545 min (G2540t30)	C <sub>51</sub> H <sub>95</sub> N <sub>15</sub> O <sub>13</sub> S <sub>2</sub>	1189.7	1190.7 [M + H] <sup>+</sup> 596.0 [M + 2H] <sup>2+</sup>
<b>17</b>	15.330 min (G2540t30)	C <sub>52</sub> H <sub>97</sub> N <sub>15</sub> O <sub>13</sub> S <sub>2</sub>	1203.7	1204.8 [M + H] <sup>+</sup> 603.1 [M + 2H] <sup>2+</sup>
<b>18</b>	12.172 min (G2540t30)	C <sub>48</sub> H <sub>90</sub> N <sub>14</sub> O <sub>12</sub> S <sub>2</sub>	1118.6	1119.8 [M + H] <sup>+</sup> 560.5 [M + 2H] <sup>2+</sup>
<b>19</b>	10.916 (G2540t30)	C <sub>48</sub> H <sub>91</sub> N <sub>15</sub> O <sub>11</sub> S <sub>2</sub>	1117.7	1118.8 [M + H] <sup>+</sup> 560.0 [M + 2H] <sup>2+</sup>

### 3.1.3.6. Synthesis of hydroxamic acid analogues

Hydroxamic acid analogues were synthesized by SPPS following the method previously described by Mellor et al.<sup>258</sup> Firstly, a *N*-Fmoc-aminoxy-2-chlorotrityl resin was produced by the addition of Fmoc-NHOH (2 eq) and DIPEA (4 eq) to the pre-conditioned 2-CTC resin (commercial functionalization: 1.6 mmol·g<sup>-1</sup> resin). The reaction was left to react for 48 hours, and then the loading level was assessed by Fmoc quantification, the obtained values ranged from 0.50 to 0.60 mmol·g<sup>-1</sup> resin.

Afterward, peptide sequences were synthesized using 3 eq of amino acid/DIC/HOBt and successive Fmoc removal with 20 % piperidine/DMF treatments (1 x 1 min, 2 x 10 min). The amino acids used were: Fmoc-Cys(Trt)-OH, Fmoc-DCys(Trt)-OH, Fmoc-Dab(Boc)-OH, Fmoc-Leu-OH, Fmoc-DPhe-OH, Fmoc-Thr(<sup>t</sup>Bu)-OH, as well as the (*S*)-2-hydroxy-4-methylpentanoic acid and nonanoic acid. All coupling reactions yielded ≥99 % as assessed by Kaiser tests or HPLC analysis after “mini-cleavage”. For the depsipeptide hydroxamic acid analogues, ester bond was carried out via symmetrical anhydride, as explained in section 3.1.3.4.

Cleavage of the peptides from the resin was carried out by acidolysis with 4 mL of TFA/TES/H<sub>2</sub>O (95:3:2, v/v/v) for 30 min. The final volume of the acidic mixture was reduced under nitrogen stream, and the peptide was then precipitated and washed with cold Et<sub>2</sub>O. The solid peptide was isolated by centrifugation, dissolved in H<sub>2</sub>O/ACN (1:1, v/v) and lyophilized. Cyclization of peptides through disulfide bond formation was performed at high dilution (1 mg·mL<sup>-1</sup>) in DMSO/ H<sub>2</sub>O (5:95, v/v) for 24 - 48 hours and monitored by analytical HPLC. Finally, peptides were purified by semi-preparative HPLC and characterized by analytical HPLC and ESI mass spectrometry. Final purities greater than 95 % were obtained for all the synthesized analogues. Overall yields ranged from 5 to 9 % (Tables 41 and 42).

**Table 41:** Obtained quantities and synthetic yields of hydroxamic acid analogues.

Peptide	Resin amount	Functionalization (mmol·g <sup>-1</sup> of resin)	Cleavage yield	Cyclization yield <sup>a</sup>	Purification yield	Global yield <sup>b</sup>
<b>20</b>	102 mg	0.59	63 mg	100 %	11 mg	7 mg
			58 %			
<b>21</b>	100 mg	0.59	59 mg	100 %	10 mg	7 mg
			54 %			
<b>22</b>	152 mg	0.51	74 mg	100 %	8 mg	5 mg
			51 %			
<b>23</b>	156 mg	0.60	61 mg	100 %	9 mg	6 mg
			37 %			

<sup>a</sup>Cyclic compounds were obtained as an oil due to the presence of DMSO, for that reason, they were not weighed, and the cyclization (followed by HPLC) was estimated to be quantitative (100 %). <sup>b</sup>Free base peptide.

**Table 42:** Hydroxamic acid analogues characterization.

Peptide	t <sub>R</sub> (HPLC gradient)	Chemical formula	Exact mass	ESI (+) m/z	ESI (-) m/z
<b>20</b>	14.803 min (G2035t30)	C <sub>54</sub> H <sub>94</sub> N <sub>16</sub> O <sub>13</sub> S <sub>2</sub>	1238.7	1239.9 [M + H] <sup>+</sup>	1274.2 [M + Cl] <sup>-</sup>
				620.7 [M + 2H] <sup>2+</sup>	655.5 [M + 2Cl] <sup>2-</sup>
<b>21</b>	16.637 min (G2540t30)	C <sub>54</sub> H <sub>94</sub> N <sub>16</sub> O <sub>13</sub> S <sub>2</sub>	1238.7	1239.9 [M + H] <sup>+</sup>	1274.2 [M + Cl] <sup>-</sup>
				620.7 [M + 2H] <sup>2+</sup>	654.7 [M + 2Cl] <sup>2-</sup>
<b>22</b>	16.849 min (G2035t30)	C <sub>54</sub> H <sub>93</sub> N <sub>16</sub> O <sub>14</sub> S <sub>2</sub>	1239.7	1240.9 [M + H] <sup>+</sup>	1275.1 [M + Cl] <sup>-</sup>
				621.1 [M + 2H] <sup>2+</sup>	655.2 [M + 2Cl] <sup>2-</sup>
<b>23</b>	18.741 min (G2035t30)	C <sub>54</sub> H <sub>93</sub> N <sub>16</sub> O <sub>14</sub> S <sub>2</sub>	1239.7	1240.9 [M + H] <sup>+</sup>	1275.1 [M + Cl] <sup>-</sup>
				621.1 [M + 2H] <sup>2+</sup>	656.1 [M + 2Cl] <sup>2-</sup>

### 3.1.3.7. Synthesis of thiothreonine analogues

The thiothreonine analogues were initially synthesized starting from 100 - 200 mg of 2-CTC resin (commercial functionalization:  $1.6 \text{ mmol}\cdot\text{g}^{-1}$  resin) following standard Fmoc/<sup>t</sup>Bu protection strategy. 2 eq of the threonine derivative, Fmoc-Trt(<sup>t</sup>Bu)-OH, were added to the pre-conditioned resin along with 4 eq of DIPEA. Both reagents were dissolved in the minimum possible amount of DCM and left to react overnight. Then, the resin was washed with DMF and DCM, capped using  $0.8 \text{ mg}\cdot\text{mL}^{-1}$  of MeOH for 15 minutes, and washed again with DCM. The reaction conversion was estimated by Fmoc quantification, and the obtained loading levels ranged from 0.8 to  $0.95 \text{ mmol}\cdot\text{g}^{-1}$  resin. Then, the peptide sequence was assembled by addition of Fmoc-protected amino acid and HOBt/DIC activating agents (3 eq each, 1 hour in DMF). The protected amino acids used were: Fmoc-Abu-OH, Fmoc-Cys(Trt)-OH, Fmoc-Dab(Boc)-OH, Fmoc-Dap(Boc)-OH, Fmoc-Leu-OH, Fmoc-DPhe-OH, Fmoc-Nva-OH, Fmoc-Thr(<sup>t</sup>Bu)-OH, and Boc-DAdec-OH as well as the (S)-2-hydroxy-4-methylpentanoic acid, and octanoic acid. All coupling and reactions yielded  $\geq 99 \%$  as assessed by Kaiser tests and/or HPLC analysis after “mini-cleavage”. The Fmoc removal was achieved by successive treatments with 20 % piperidine/DMF (1 x 1 min, 2 x 10 min). Analogues with ester bonds in the structure were synthesized using the symmetrical anhydride method, as explained in section 3.1.3.4.

Cleavage of the peptides from the resin was carried out by acidolysis with 4 mL of TFA/TES/H<sub>2</sub>O (95:3:2, v/v) for 30 min. TFA was removed under nitrogen stream, and the residue was precipitated and washed with cold Et<sub>2</sub>O. The solid peptide was isolated by centrifugation, dissolved in H<sub>2</sub>O/ACN (1:1, v/v) and lyophilized. Cyclization of peptides through disulfide bonds was carried out at high dilution ( $1 \text{ mg}\cdot\text{mL}^{-1}$ ) in DMSO/H<sub>2</sub>O (5:95, v/v) for 24 - 48 hours and monitored by analytical HPLC. Finally, peptides were purified by semi-preparative HPLC and characterized by analytical HPLC and ESI mass spectrometry. Final purities  $\geq 95 \%$  were obtained for all the synthesized analogues. Overall yields for synthesis of the cysteine analogues ranged from 5 to 21 % (Tables 43 and 44).

**Table 43:** Obtained quantities and synthetic yields of thiothreonine analogues.

Peptide	Resin amount	Functionalization (mmol·g <sup>-1</sup> of resin)	Cleavage yield	Cyclization yield <sup>a</sup>	Purification yield	Global yield <sup>b</sup>
<b>24</b>	126 mg	0.80	65 mg	100 %	27 mg	18 mg
			36 %		42 %	15 %
<b>25</b>	126 mg	0.80	72 mg	100 %	29 mg	20 mg
			42 %		40 %	17 %
<b>26</b>	165 mg	0.90	89 mg	100 %	24 mg	16 mg
			34 %		27 %	9 %
<b>27</b>	165 mg	0.90	103 mg	100 %	30 mg	20 mg
			40 %		30 %	12 %
<b>28</b>	100 mg	0.92	72 mg	100 %	22 mg	14 mg
			45 %		31 %	13 %
<b>29</b>	100 mg	0.92	76 mg	100 %	32 mg	21 mg
			49 %		42 %	21 %
<b>30</b>	102 mg	0.95	80 mg	100 %	17 mg	11 mg
			47 %		21 %	10 %
<b>31</b>	102 mg	0.95	83 mg	100 %	27 mg	18 mg
			50 %		32 %	16 %

<sup>a</sup>Cyclic compounds were obtained as an oil due to the presence of DMSO, for that reason, they were not weighed, and the cyclization (followed by HPLC) was estimated to be quantitative (100 %). <sup>b</sup>Free base peptide.

**Table 44:** Thiothreonine analogues characterization.

Peptide	t <sub>R</sub> (HPLC gradient)	Chemical formula	Exact mass	ESI (+) m/z	ESI (-) m/z
<b>24</b>	16.093 min (G2035t30)	C <sub>54</sub> H <sub>95</sub> N <sub>15</sub> O <sub>12</sub> S <sub>2</sub>	1209.7	1210.6 [M + H] <sup>+</sup>	1244.4 [M + Cl] <sup>-</sup>
				606.1 [M + 2H] <sup>2+</sup>	640.3 [M + 2Cl] <sup>2-</sup>
				404.1 [M + 3H] <sup>3+</sup>	
<b>25</b>	22.681 min (G2035t30)	C <sub>52</sub> H <sub>92</sub> N <sub>14</sub> O <sub>11</sub> S <sub>2</sub>	1152.7	1152.7 [M + H] <sup>+</sup>	1187.9 [M + Cl] <sup>-</sup>
				577.7 [M + 2H] <sup>2+</sup>	611.6 [M + 2Cl] <sup>2-</sup>
				385.4 [M + 3H] <sup>3+</sup>	
<b>26</b>	13.222 min (G2540t30)	C <sub>54</sub> H <sub>94</sub> N <sub>14</sub> O <sub>13</sub> S <sub>2</sub>	1210.7	1211.3 [M + H] <sup>+</sup>	1245.4 [M + Cl] <sup>-</sup>
				606.4 [M + 2H] <sup>2+</sup>	640.5 [M + 2Cl] <sup>2-</sup>
				404.6 [M + 3H] <sup>3+</sup>	
<b>27</b>	17.864 min (G2540t30)	C <sub>52</sub> H <sub>91</sub> N <sub>13</sub> O <sub>12</sub> S <sub>2</sub>	1153.6	1154.3 [M + H] <sup>+</sup>	1188.4 [M + Cl] <sup>-</sup>
				577.9 [M + 2H] <sup>2+</sup>	612.6 [M + 2Cl] <sup>2-</sup>
				385.6 [M + 3H] <sup>3+</sup>	

<b>28</b>	11.209 min (G2035t30)	C <sub>51</sub> H <sub>89</sub> N <sub>15</sub> O <sub>12</sub> S <sub>2</sub>	1167.6	1168.6 [M + H] <sup>+</sup>	1202.6 [M + Cl] <sup>-</sup>
				585.0 [M + 2H] <sup>2+</sup>	619.0 [M + 2Cl] <sup>2-</sup>
				390.4 [M + 3H] <sup>3+</sup>	
<b>29</b>	16.570 min (G2035t30)	C <sub>49</sub> H <sub>86</sub> N <sub>14</sub> O <sub>11</sub> S <sub>2</sub>	1110.6	1111.4 [M + H] <sup>+</sup>	1145.6 [M + Cl] <sup>-</sup>
				556.5 [M + 2H] <sup>2+</sup>	591.0 [M + 2Cl] <sup>2-</sup>
				371.3 [M + 3H] <sup>3+</sup>	
<b>30</b>	14.387 min (G2035t30)	C <sub>53</sub> H <sub>93</sub> N <sub>15</sub> O <sub>12</sub> S <sub>2</sub>	1195.7	1196.6 [M + H] <sup>+</sup>	1230.7 [M + Cl] <sup>-</sup>
				599.0 [M + 2H] <sup>2+</sup>	633.8 [M + 2Cl] <sup>2-</sup>
				399.8 [M + 3H] <sup>3+</sup>	
<b>31</b>	19.499 min (G2035t30)	C <sub>51</sub> H <sub>90</sub> N <sub>14</sub> O <sub>11</sub> S <sub>2</sub>	1138.6	1139.6 [M + H] <sup>+</sup>	1173.6 [M + Cl] <sup>-</sup>
				570.5 [M + 2H] <sup>2+</sup>	604.5 [M + 2Cl] <sup>2-</sup>
				380.7 [M + 3H] <sup>3+</sup>	

### 3.1.3.8. Optimized synthesis of thiothreonine analogues

The previous synthesis was optimized and scaled up in order to obtain hundreds of milligrams by replacing the 2-CTC resin by the less electronegatively charged Trt-Cl resin. Near 2.5 g of Trt-Cl resin were weighed in polypropylene syringes of 60 mL fitted with a polyethylene disc. The conditions of the coupling/washing/deprotection cycles presented in the previous section were maintained. However, the cleavage was carried out by acidolysis with 25 mL of TFA/TES (82:18 v/v) for 45 min. The peptides were then precipitated directly in 250 mL of cold Et<sub>2</sub>O dried and conserved under sodium, washed 3 additional times, dissolved in ACN and lyophilized. Cyclization was carried out at 2.5 mg·mL<sup>-1</sup> in DMSO/H<sub>2</sub>O (5:95, v/v) for 24 - 48 hours and it was monitored by analytical HPLC. Finally, peptides were purified by semi-preparative HPLC and characterized by analytical HPLC and ESI mass spectrometry. Final purities greater than 95 % were obtained for all the synthesized analogues.

**Table 45:** Obtained quantities and synthetic yields analogues #25 and #27.

Peptide	Resin amount	Functionalization (mmol·g <sup>-1</sup> of resin)	Cleavage	Cyclization	Purification	Global
			yield	yield <sup>a</sup>	yield	yield <sup>b</sup>
<b>25</b>	2.455 g	0.72	2.378 g	100 %	1.197 g	802 mg
			78 %		50 %	39 %
<b>27</b>	2.486 g	0.70	2.102 g	100 %	543 mg	364 mg
			70 %		26 %	18 %

<sup>a</sup>Cyclic compounds were obtained as an oil due to the presence of DMSO, for that reason, they were not weighed, and the cyclization (followed by HPLC) was estimated to be quantitative (100 %). <sup>b</sup>Free base peptide.

## 3.2. Materials and methods of chapter 2

### 3.2.1. Materials

#### 3.2.1.1. Solvents

Solvent	Brand	Quality
CHCl <sub>3</sub>	VWR	UV-grade
H <sub>2</sub> O (Milli-Q) <sup>a</sup>	Millipore	-
MeOH	VWR	UV-grade

<sup>a</sup>Milli-Q water was obtained by filtrating purified water using a Milli-Q Plus system (Millipore) to obtain water with a resistivity superior to 18 MΩ·cm<sup>-1</sup>.

#### 3.2.1.2. Reagents

All material used in the microbiological assays was previously sterilized using an autoclave with the following conditions: 1 atm, 120 °C for 20 minutes. All reagents used were of the maximum quality possible.

Reagent	Brand
Bacterial strains	Deutsche Samm Mikroorganismen und Zellkulturen
Blood	Healthy donors from Ständtisches Klinikum, Karlsruhe, Germany
HEPES	Sigma
LB Agar	Roth
MHB	BD Biosciences
NaCl	Fluka
TRIS Hydrochloride	VWR
Rh-PE	
DErPC	
DErPG	
DMPC	Avanti Polar Lipids
Lyso-MPC	
POPC	
POPG	

Triton X-100	Sigma-Aldrich
Sephacryl 100-HR	
ANTS	Molecular Probes
DPX	

### 3.2.1.3. Other material

<b>Material</b>	<b>Brand</b>
96-well microtiter plates	Sarstedt
Fluorescence cuvettes	Hellma
100 nm Nuclepore polycarbonate membrane	Whatman
ss-NMR glass plates	Marienfeld Laboratory Glassware

### 3.2.1.4. Instruments

<b>Instrument</b>	<b>Brand and model</b>
Balance	Sartorius <i>GL623i-1CEU</i>
Centrifuge	Sigma <i>6K15</i>
Extruder	Avanti Polar Lipids <i>Mini Extruder</i>
Shaker	Heidolph Instruments <i>Unimax 1010</i>
Sonicator	Hielscher Ultrasonics <i>UTR200</i>
Spectrophotometer	BIORAD <i>SmartSpec Plus</i>
Spectrophotometer	HORIBA Jobin Yvon <i>FluoroMax2</i>
Spectropolarimeter	Jasco <i>J-815</i>
NMR Spectrometer	Bruker <i>Avance III 500 MHz</i>

## **3.2.2. Methods**

### 3.2.2.1. Antimicrobial activity

#### *3.2.2.1.1. Preparation of bacterial cells*

Two Gram-positive strains, *Staphylococcus xylosus* (DSM 20267) and *Bacillus subtilis* (DSM 347), and two Gram-negative, *Escherichia coli* (DSM 1103) and *Acinetobacter* sp. (DSM 586) were used. Firstly, 10 mL of MHB liquid medium were inoculated by a single



cryogenic culture, which had been stored at -80 °C. The four cultures were incubated overnight at 37 °C and 200 rpm, followed by overnight culture in LB agar plate. An isolated bacterial colony of each strain was then used to inoculate 10 mL of MHB, and the bacterial pre-cultures were allowed to grow overnight at 37 °C and 200 rpm. These overnight pre-cultures were used to freshly inoculate 5 mL of MHB to a final OD<sub>550</sub> of 0.2, and the resulting bacterial suspension was incubated for 3 - 4 hours at 37 °C and 200 rpm to reach the earlier exponential growth phase (OD<sub>550</sub> = 1 - 2). Test cultures were finally diluted to OD<sub>550</sub> = 0.2, which according to McFarland standard contains 1·10<sup>8</sup> CFU·mL<sup>-1</sup>.

#### 3.2.2.1.2. MIC assay

Microtiter plates (96 wells of 100 µL) were filled with 50 µL of MHB, and serial 2-fold dilution of peptides was arranged in columns from 256 to 2 µg·mL<sup>-1</sup> for BPKIA4, BPKIA7 and BPKIA10 and 64 to 0.5 µg·mL<sup>-1</sup> for the other peptides. The two final columns served as positive (no peptide) and negative controls (no peptide and not inoculated with bacteria). The previously prepared bacterial suspensions with a OD<sub>600</sub> of 0.2 were 100-fold diluted and 50 µL of the subsequent suspension were added to the wells (except for the final column), giving a final concentration of 10<sup>6</sup> CFU·mL<sup>-1</sup>. The plates were incubated at 37 °C for 18 - 20 hours. After incubation, 20 µL of redox indicator Resazurin in concentration 0.2 mg·mL<sup>-1</sup> were added to each well. The plates were incubated for the next 2 hours at 37 °C and finally, the MIC was determined visually as the lowest peptide concentration inhibiting bacterial growth (pink wells). The experiments were carried out in triplicate and repeated two times in order to avoid environmental errors.

#### 3.2.2.2. Hemolysis

The hemolytic effect of the peptides was examined by a serial 2-fold dilution assay, as previously described by Strandberg et al.<sup>313</sup> Citrate phosphate dextrose-stabilized blood bags with erythrocyte suspensions from healthy donors obtained from the blood bank of the local municipal hospital (Städtisches Klinikum, Karlsruhe, Germany).

Erythrocytes were washed twice with 9-fold excess of TRIS buffer (172 mM, pH 7.6 at RT) followed by centrifugation at 1500 rpm for 10 minutes. 1 mL of the obtained

sediment was then transferred to a fresh tube containing 9 mL of the same buffer precooled at 37 °C. 500 µL of the stock cell suspension were further diluted with 9.5 mL of precooled buffer to obtain a suspension about 0.5 % (v/v) hematocrit. This suspension was freshly prepared and pre-incubated for 5 min at 37 °C for each tested peptide. During the incubation time, serial 2-fold dilutions of each peptide were prepared in TRIS buffer (pH 7.6 at 37 °C), ranging from 2 to 512 µg·mL<sup>-1</sup>. Afterward, 200 µl of the 0.5% erythrocyte suspension were transferred to each reaction tubes containing the same volume of the corresponding peptide to yield a final erythrocyte concentration of 0.25 %. The final peptide concentration was between 1 and 256 µg·mL<sup>-1</sup>. Samples were incubated at 37 °C for 30 minutes with gentle shaking, and subsequently centrifuged at 13000 rpm for 10 min to pellet the cells. The supernatant was transferred to cuvettes and the absorbance at 540 nm was measured against water. Furthermore, for each dilution series, 0 % hemolysis was obtained by erythrocytes in TRIS buffer and 100 % hemolysis was obtained by erythrocytes in 0.2 % of Triton X-100.

For each peptide the hemolysis assay was performed two times in different days to avoid environmental effects, and for each data point the absorbance was measured three times. The average of those measurements and the standard deviation SD was calculated.

### 3.2.2.3. Circular dichroism spectroscopy

#### *3.2.2.3.1. Vesicle preparation*

The lipid powders (DMPC and DMPG) were dissolved in chloroform/methanol (1:1) (v/v) to obtain stock solutions with concentration of 5 mg·mL<sup>-1</sup> (7.4 mM for DMPC and 7.3 mM for DMPG). The liposomes were prepared by co-solubilizing aliquots of the stock solutions and which were thoroughly vortexed to obtain a DMPC/DMPG (3:1) (mol/mol) mixture. Subsequently, the organic solvents were evaporated under a stream of nitrogen gas and dried under vacuum for 3 hours. After drying, the lipid film was dispersed in phosphate buffer (10 mM, pH 7), and homogenized by 10 freeze-thaw cycles followed by vigorous vortexing for 1 minute after each cycle. Finally, SUVs were generated by sonication of the obtained MLVs for 16 minutes in a strong ultrasonic bath at 35 °C.

### 3.2.2.3.2. Peptide solutions preparation

Peptide stock solutions in water were prepared with a concentration from weighed material of  $1 \text{ mg}\cdot\text{mL}^{-1}$ , this value was corrected by measuring the exact concentration of each peptide stock solution based on the 280 nm UV absorbance of the Trp residue contained in the sequence. The absorption spectrum in the range of aromatic bands was recorded from 360 to 200 nm in a quartz glass half-micro-cuvette with 1 cm optical path length, using milliQ-water as a blank. The corrected peptide concentration was calculated using a molar extinction coefficient of  $5500 \text{ L}\cdot\text{mol}^{-1}\cdot\text{cm}^{-1}$ . Corrected concentrations of the peptide stock solutions were in the range  $0.628$  and  $0.752 \text{ mg}\cdot\text{mL}^{-1}$ .

### 3.2.2.3.3. CD measurements and analysis

CD spectra were recorded on J-815 spectropolarimeter between 260 and 180 nm at 0.1 nm intervals using 1 mm quartz-glass cells. Three repeated scans at a scan-rate of  $10 \text{ nm min}^{-1}$ , 8 seconds response time and 1 nm bandwidth were averaged for each sample and for the baseline of the corresponding peptide-free sample. An aliquot of  $30 \mu\text{L}$  of the respective peptide stock solution was added to  $270 \mu\text{L}$  of pure PB (10 mM, pH = 6.5) at  $25 \text{ }^\circ\text{C}$ . In samples containing DMPC/DMPG (3:1) vesicles, the temperature was kept at  $30 \text{ }^\circ\text{C}$  (above the phase transition temperature of the lipids) and the peptide concentration was varied such that the number of amino acid residues per lipid was kept constant. An initial peptide-to-lipid molar ratio of 1:50 for BPKIA11 was chosen as the starting point, which corresponded to a constant mass ratio of  $14 \mu\text{g}$  of peptide per  $3 \text{ mg}$  of lipid ( $1.47 \text{ mM}$ ). After subtracting the baseline from the sample spectra, CD data were processed with the adaptive smoothing method, which is part of the Jasco Spectra Analysis software. Finally, the spectral data were converted to mean residue ellipticities.

Secondary structure estimation from CD data was performed using CDSSTR-175, CONTIN-LL, and SELCON-3 programs.<sup>322</sup> The three algorithms were provided by the DICHROWEB on-line server.<sup>316</sup> The quality of the fit between experimental and back-calculated spectra corresponding to the estimated secondary structure fractions was assessed from the normalized root mean square deviation (NRMSD), with a value  $<0.1$  (for CONTIN-LL and CDSSTR) and  $<0.25$  (for SELCON-3) considered as a good fit. Finally, the secondary structure element fractions of each sample were calculated as the average value of the individual data obtained with the three algorithms. Individual results

of the different analyses were not considered when the sum of all structural element fractions was <0.98 or >1.02, or when the NRMSD (normalized root mean square deviation) between the experimental and back-calculated CD spectrum was above the threshold value (0.1 for CONTINLL-SP175 and CDSSTR-SP175, and 0.25 for SELCON3-SP175).

#### 3.2.2.4. Peptide binding study

##### *3.2.2.4.1. Vesicle preparation*

Liposomes were prepared by co-dissolving POPC/POPG (1:1) (mol/mol) mixtures of lipids in chloroform/methanol (1:1) (v/v), together with 0.1 mol% Rh-PE by which the lipid concentration could be accurately quantified. The lipid mixture was thoroughly vortexed, evaporated under a nitrogen stream and dried under vacuum for 3 hours. After drying, the lipid film was dispersed in phosphate buffer (10 mM, pH 7), and homogenized by 10 freeze-thaw cycles followed by vigorous vortexing for 1 minute after each cycle. Finally, LUVs were generated by 41-fold extrusion of the liposomes through a Nuclepore polycarbonate membrane with a pore size of 100 nm.

##### *3.2.2.4.2. Binding measurements*

Fluorescence measurements were made with a FluoroMax2 spectrofluorimeter with an excitation wavelength of 280 nm. Excitation and emission slits were not wider than 7 nm. Photomultiplier voltage was 800 V. Spectra were measured using 2 mm cuvettes in the emission region of 295 - 500 nm with an increment of 1 nm. A final concentration of 0.5  $\mu\text{M}$  peptide (2.5  $\mu\text{M}$  in the case of BPKIA4 and BPKIA7) was titrated with increasing portions of LUVs suspension up to 1 mM in 5 - 10 steps. Titration was performed with mild stirring at 22 °C. From each spectrum, background was subtracted (by measuring a lipid sample with no peptide). The titration curves were constructed as normalized intensity values versus the wavelength. The obtained spectra described non-linear hyperbolic curves that were fitted according to the equation:

$$I = I_{\max} \frac{K[L]}{1 + K[L]}$$

where  $I$  is the measured fluorescence intensity,  $I_{\max}$  denotes asymptotic maximum intensity value,  $[L]$  is the molar lipid concentration and  $K$  is the calculated binding constant.

### 3.2.2.5. Vesicle leakage assay

#### *3.2.2.5.1. Vesicle preparation*

Liposomes of POPC/POPG and DErPC/DErPG (1:1) (mol/mol) were prepared by co-dissolving the PC/PG lipids in chloroform/methanol (1:1) (v/v), together with 0.1 mol% Rh-PE, which was employed to monitor the lipid loss during vesicle preparation (extrusion and gel filtration, see below). The lipid mixture was dried under nitrogen gas and left to dry under vacuum for 3 hours. The obtained thin film was then resuspended in the buffer which contained the fluorophore ANTS (12.5 mM), the quencher DPX (45 mM), NaCl (150 mM), and HEPES (10 mM, pH 7.5). After 10 freeze-thaw cycles followed by thoroughly vortexing for 1 minute after each cycle, LUVs were obtained by 41-fold extrusion of the liposomes through a Nuclepore polycarbonate membrane (pore size 100 nm). Unencapsulated dye was removed by gel filtration using spin columns filled with Sephacryl 100-HR and equilibrated with the elution buffer (150 mM NaCl, 10 mM HEPES, pH 7.5) which balances the internal vesicle osmolarity.

#### *3.2.2.5.2. Leakage*

Leakage of encapsulated contents was monitored by fluorescence dequenching of ANTS by DPX. Fluorescence measurements were performed in NaCl and HEPES buffer (150 mM and 10 mM respectively, pH 7.5) with constant stirring at 30 °C on a FluoroMax2 spectrofluorimeter. ANTS emission was set to 510 nm (5 nm slit) and the excitation to 422 nm (5 nm slit). An appropriate volume of a peptide stock solution was added to the cuvette to obtain the desired peptide-to-lipid ratio, and 100  $\mu$ M vesicle were added 100 seconds after peptide addition. The 0 % leakage corresponded to the fluorescence immediately after vesicle addition, while 100 % leakage was the fluorescence value obtained after addition of a 0.25 vol% Triton X-100 after 700 seconds.

### 3.2.2.6. Solid-state NMR

#### *3.2.2.6.1. NMR sample preparation*

Macroscopically oriented NMR samples were prepared by co-dissolving appropriate amounts of lipids and peptides in a mixture of methanol, chloroform and Milli-Q water, spreading onto 16 thin glass plates of dimensions 9 mm x 7.5 mm x 0,08 mm. The plates were dried in air for 1 h, followed by drying under vacuum overnight. Then, the plates

were stacked and placed into a hydration chamber at 48 °C and 96 % relative humidity for 18 - 24 hours. 0.7 mg of  $^{15}\text{N}$ -labeled peptide and appropriate amounts of lipids were used to obtain the desired P/L ratio.

#### 3.2.2.6.2. Solid state NMR

All measurements were performed on an Avance III Bruker wide bore 500 MHz spectrometer at 308 K.  $^{31}\text{P}$  NMR measurements to assess the sample quality and the degree of lipid alignment were performed using a Hahn echo sequence with  $90^\circ$  pulse of 5  $\mu\text{s}$  and 30  $\mu\text{s}$  echo time,<sup>323</sup> with  $^1\text{H}$  SPINAL64 decoupling during acquisition.<sup>324</sup> 256 scans were accumulated using an acquisition time of 10 ms and a relaxation delay of 1s.  $^1\text{H}$ - $^{15}\text{N}$  cross polarization experiments were done using a CP-MOIST pulse sequence<sup>325</sup> using a home-built double-tuned probe with a low-E flat-coil resonator, employing a  $^1\text{H}$  and  $^{15}\text{N}$  radiofrequency field strength of 65 kHz during cross-polarization, and 36 kHz  $^1\text{H}$  SPINAL16 decoupling<sup>324</sup> during acquisition. A mixing time of 500  $\mu\text{s}$  was used, and up to 20.000 scans were accumulated. The acquisition time was 10 ms and the recycle time 4 s. The  $^{15}\text{N}$  chemical shift was referenced using the signal of a dry powder of ammonium sulfate, of which the chemical shift was set to 26.8 ppm. The oriented samples were placed in the flat-coil probe such that the lipid bilayer normal was aligned parallel to the external magnetic field.



## **REFERENCES**





- (1) Pećanac, M.; Janjić, Z.; Komarcević, A.; Pajić, M.; Dobanovacki, D.; Misković, S. Burns Treatment in Ancient Times. *Med. Pregl.* **2013**, *66* (5–6), 263–267.
- (2) Ebbell, B. *The Papyrus Ebers: The Greatest Egyptian Medical Document*; Levin & Munksgaard: Copenhagen, 1937.
- (3) Bassett, E. J.; Keith, M. S.; Armelagos, G. J.; Martin, D. L.; Villanueva, A. R. Tetracycline-Labeled Human Bone from Ancient Sudanese Nubia (A.D. 350). *Science* **1980**, *209* (4464), 1532–1534.
- (4) Nelson, M. L.; Dinardo, A.; Hochberg, J.; Armelagos, G. J. Brief Communication: Mass Spectroscopic Characterization of Tetracycline in the Skeletal Remains of an Ancient Population from Sudanese Nubia 350–550 CE. *Am. J. Phys. Anthropol.* **2010**, *143* (1), 151–154.
- (5) Ehrlich, P.; Hata, S. *Die Experimentelle Chemotherapie Der Spiriloszen*; Springer-Verlag: Berlin, 1910.
- (6) Schwartz, R. S. Paul Ehrlich's Magic Bullets. *N. Engl. J. Med.* **2004**, *350* (11), 1079–1080.
- (7) Ehrlich, P. Über Laboratoriumsversuche Und Klinische Erprobung von Heilstoffen. *Chemiker-Zeitung* **1912**, *36*, 637–638.
- (8) Domagk, G. Ein Beitrag Zur Chemotherapie Der Bakteriellen Infektionen. *Dtsch. Med. Wochenschr.* **1913**, *7*, 250–253.
- (9) Gelmo, P. Über Sulfamide Der p -Amidobenzolsulfonsäure. *J. für Prakt. Chemie* **1908**, *77*, 369–382.
- (10) Chain, E.; Florey, H. W.; Gardner, A. D.; Heatley, N. G.; Jennings, M. A.; Orr-Ewing, J.; Sanders, A. G. THE CLASSIC: Penicillin as a Chemotherapeutic Agent. 1940. *Clin. Orthop. Relat. Res.* **2005**, *439*, 23–26.
- (11) Hodgkin, D. C. The X-Ray Analysis of the Structure of Penicillin. *Adv. Sci.* **1949**, *6* (22), 85–89.
- (12) Waksman, S. A. What Is an Antibiotic or an Antibiotic Substance? *Mycologia* **1947**, *39* (5), 565–569.
- (13) Schatz, A.; Bugle, E.; Waksman, S. A. Streptomycin, a Substance Exhibiting Antibiotic Activity against Gram-Positive and Gram-Negative Bacteria. *Proc. Soc. Exp. Biol. Med.* **1944**, *55* (1), 66–69.
- (14) Leach, K. L.; Brickner, S. J.; Noe, M. C.; Miller, P. F. Linezolid, the First Oxazolidinone Antibacterial Agent. *Ann. N. Y. Acad. Sci.* **2011**, *1222* (1), 49–54.
- (15) Burdette, S. D.; Trotman, R. Tedizolid: The First Once-Daily Oxazolidinone Class Antibiotic. *Clin. Infect. Dis.* **2015**, *61* (8), 1315–1321.
- (16) Tally, F. P.; DeBruin, M. F. Development of Daptomycin for Gram-Positive Infections. *J. Antimicrob. Chemother.* **2000**, *46* (4), 523–526.
- (17) Abraham, E. P.; Chain, E. An Enzyme from Bacteria Able to Destroy Penicillin. *Nature* **1940**, *146*, 837.
- (18) Chang, Y.; Chusri, S.; Sangthong, R.; McNeil, E.; Hu, J.; Du, W.; Li, D.; Fan, X.; Zhou, H.; Chongsuvivatwong, V.; Tang, L. Clinical Pattern of Antibiotic Overuse and Misuse in Primary Healthcare Hospitals in the Southwest of China. *PLoS One* **2019**, *14* (6), e0214779.
- (19) Manyi-Loh, C.; Mamphweli, S.; Meyer, E.; Okoh, A. Antibiotic Use in Agriculture and Its Consequential Resistance in Environmental Sources: Potential Public Health Implications. *Molecules* **2018**, *23*, 795.
- (20) Hao, H.; Cheng, G.; Iqbal, Z.; Ai, X.; Hussain, H. I.; Huang, L.; Dai, M.; Wang, Y.; Liu, Z.; Yuan, Z. Benefits and Risks of Antimicrobial Use in Food-Producing Animals. *Front. Microbiol.* **2014**, *5*, 288.
- (21) Interagency Coordination Group on Antimicrobial Resistance. No Time to Wait: Securing the Future from Drug-Resistant Infections Report to the Secretary-General of the United Nations. April 2019. Available online: <https://www.who.int/publications/i/item/no-time-to-wait-securing-the-future-from-drug-resistant-infections> (accessed Aug 22, 2021).
- (22) Boucher, H. W.; Talbot, G. H.; Bradley, J. S.; Edwards, J. E.; Gilbert, D.; Rice, L. R.; Scheld, M.; Spellberg, B.; Bartlett, J. Bad Bugs, No Drugs: No ESKAPE! An Update from the Infectious Diseases Society of America. *Clin. Infect. Dis.* **2009**, *48* (1), 1–12.

- (23) Beovic, B.; Dousak, M.; Ferreira-Coimbra, J.; Nadrah, K.; Rubulotta, F.; Belliato, M.; Berger-Estilita, J.; Ayoade, F.; Rello, J.; Erdem, H. Antibiotic Use in Patients with COVID-19: A “snapshot” Infectious Diseases International Research Initiative (ID-IRI) Survey. *J. Antimicrob. Chemother.* **2020**, *75* (11), 3386–3390.
- (24) Vaughn, V. M.; Gandhi, T. N.; Petty, L. A.; Patel, P. K.; Prescott, H. C.; Malani, A. N.; Ratz, D.; McLaughlin, E.; Chopra, V.; Flanders, S. A. Empiric Antibacterial Therapy and Community-Onset Bacterial Coinfection in Patients Hospitalized With Coronavirus Disease 2019 (COVID-19): A Multi-Hospital Cohort Study. *Clin. Infect. Dis.* **2021**, *72* (10), e533–e541.
- (25) Lucien, M. A. B.; Canarie, M. F.; Kilgore, P. E.; Jean-Denis, G.; Fénélon, N.; Pierre, M.; Cerpa, M.; Joseph, G. A.; Maki, G.; Zervos, M. J.; Dely, P.; Bony, J.; Sati, H.; Rio, A. del; Ramon-Pardo, P. Antibiotics and Antimicrobial Resistance in the COVID-19 Era: Perspective from Resource-Limited Settings. *Int. J. Infect. Dis.* **2021**, *104*, 250–254.
- (26) Silver, L. L. Challenges of Antibacterial Discovery. *Clin. Microbiol. Rev.* **2011**, *24* (1), 71–109.
- (27) World Health Organization. Global Priority List of Antibiotic-Resistant Bacteria to Guide Research, Discovery, and Development of New Antibiotics. February 2017. Available online: [https://www.who.int/medicines/publications/WHO-PPL-Short\\_Summary\\_25Feb-ET\\_NM\\_WHO.pdf](https://www.who.int/medicines/publications/WHO-PPL-Short_Summary_25Feb-ET_NM_WHO.pdf) (accessed Aug 22, 2021).
- (28) World Health Organization. Global Action Plan on Antimicrobial Resistance. 2015, Available online: <https://www.who.int/publications/i/item/9789241509763> (accessed Aug 23, 2021).
- (29) Gilbert, D. N.; Guidos, R. J.; Boucher, H. W.; Talbot, G. H.; Spellberg, B.; Edwards, J. E.; Michael Scheld, W.; Bradley, J. S.; Bartlett As, J. G. The 10 x '20 Initiative: Pursuing a Global Commitment to Develop 10 New Antibacterial Drugs by 2020. *Clin. Infect. Dis.* **2010**, *50* (8), 1081–1083.
- (30) European Centre for Disease Prevention and Control. Surveillance of Antimicrobial Resistance in Europe 2018, 2019. Available online: <https://www.ecdc.europa.eu/sites/default/files/documents/surveillance-antimicrobial-resistance-Europe-2018.pdf> (accessed Aug 23, 2021).
- (31) Rex, J. H. ND4BB: Addressing the Antimicrobial Resistance Crisis. *Nat. Rev. Microbiol.* **2014**, *12* (4), 231–232. <https://doi.org/10.1038/nrmicro3245>.
- (32) World Health Organization. 2020 Antibacterial Agents in Clinical and Preclinical Development an overview and analysis, 2020. Available online: <https://www.who.int/publications/i/item/9789240021303> (accessed Sept 03 2021).
- (33) Galdiero, S.; Falanga, A.; Berisio, R.; Grieco, P.; Morelli, G.; Galdiero, M. Antimicrobial Peptides as an Opportunity Against Bacterial Diseases. *Curr. Med. Chem.* **2015**, *22* (14), 1665–1677.
- (34) De Lucca, A. J. Antifungal Peptides: Potential Candidates for the Treatment of Fungal Infections. *Expert Opin. Investig. Drugs* **2000**, *9* (2), 273–299.
- (35) Ahmed, A.; Siman-Tov, G.; Hall, G.; Bhalla, N.; Narayanan, A. Human Antimicrobial Peptides as Therapeutics for Viral Infections. *Viruses* **2019**, *11* (8), 1–26.
- (36) Torrent, M.; Pulido, D.; Rivas, L.; Andreu, D. Antimicrobial Peptide Action on Parasites. *Curr. Drug Targets* **2012**, *13* (9), 1138–1147.
- (37) Hoskin, D. W.; Ramamoorthy, A. Studies on Anticancer Activities of Antimicrobial Peptides. *Biochim. Biophys. Acta - Biomembr.* **2008**, *1778* (2), 357–375.
- (38) Otvos, L. Immunomodulatory Effects of Anti-Microbial Peptides. *Acta Microbiol. Immunol. Hung.* **2016**, *63* (3), 257–277.
- (39) Chopra, L.; Singh, G.; Taggar, R.; Dwivedi, A.; Nandal, J.; Kumar, P.; Sahoo, D. K. Antimicrobial Peptides from Bacterial Origin: Potential Alternative to Conventional Antibiotics. In *High Value Fermentation Products*; Saran, S., Babu, V., Chuabey, A., Eds.; Wiley, 2019; pp 193–204.
- (40) Petranka, Z.; Maya, Y.; Kaloyan, K.; Ivanka, P. Antimicrobial Peptides with Plant Origin. *Int. J. Nutr. Food Sci.* **2016**, *5* (6), 5–9.
- (41) Bhat, Z. F.; Kumar, S.; Bhat, H. F. Bioactive Peptides of Animal Origin: A Review. *J. Food Sci. Technol.* **2015**, *52* (9), 5377–5392.

- (42) Fleming, A. On a Remarkable Bacteriolytic Element Found in Tissues and Secretions. *Proc. R. Soc. B Biol. Sci.* **1922**, *93*, 306–317.
- (43) Rogers, L. A.; Whittier, E. O. Limiting Factors in the Lactic Fermentation. *J. Bacteriol.* **1928**, *16* (4), 211–229.
- (44) Hotchkiss, R. D.; Dubos, R. J. Bactericidal Fractions From an Aerobic Sporulating Bacillus. *J. Biol. Chem.* **1940**, *136* (3), 803–804.
- (45) Glukhov, E.; Stark, M.; Burrows, L. L.; Deber, C. M. Basis for Selectivity of Cationic Antimicrobial Peptides for Bacterial versus Mammalian Membranes. *J. Biol. Chem.* **2005**, *280* (40), 33960–33967.
- (46) Hancock, R. E. W. Peptide Antibiotics. *Lancet* **1997**, *349* (9049), 418–422.
- (47) Jenssen, H.; Hamill, P.; Hancock, R. E. W. Peptide Antimicrobial Agents. *Clin. Microbiol. Rev.* **2006**, *19* (3), 491–511.
- (48) Ong, Z. Y.; Wiradharma, N.; Yang, Y. Y. Strategies Employed in the Design and Optimization of Synthetic Antimicrobial Peptide Amphiphiles with Enhanced Therapeutic Potentials. *Adv. Drug Deliv. Rev.* **2014**, *78*, 28–45.
- (49) Li, J.; Koh, J. J.; Liu, S.; Lakshminarayanan, R.; Verma, C. S.; Beuerman, R. W. Membrane Active Antimicrobial Peptides: Translating Mechanistic Insights to Design. *Front. Neurosci.* **2017**, *11*, 73.
- (50) Nguyen, L. T.; Haney, E. F.; Vogel, H. J. The Expanding Scope of Antimicrobial Peptide Structures and Their Modes of Action. *Trends Biotechnol.* **2011**, *29* (9), 464–472.
- (51) Brogden, K. A. Antimicrobial Peptides: Pore Formers or Metabolic Inhibitors in Bacteria? *Nat. Rev. Microbiol.* **2005**, *3* (3), 238–250.
- (52) Le, C. F. Intracellular Targeting Mechanisms by Antimicrobial Peptides. *Antimicrob. Agents Chemother.* **2017**, *61* (4), 1–16.
- (53) Hancock, R. E. W. Alterations in Structure of the Cell Envelope. *Ann. Rev. Microbiol.* **1984**, *38*, 237–264.
- (54) Hancock, R. E. W.; Chapple, D. S. Peptide Antibiotics. *Antimicrob. Agents Chemother.* **1999**, *43* (6), 1317–1323.
- (55) Hancock, R. E. Cationic Peptides: Effectors in Innate Immunity and Novel Antimicrobials. *Lancet Infect. Dis.* **2001**, *1* (3), 156–164.
- (56) Shai, Y. Mechanism of the Binding, Insertion and Destabilization of Phospholipid Bilayer Membranes by  $\alpha$ -Helical Antimicrobial and Cell Non-Selective Membrane-Lytic Peptides. *Biochim. Biophys. Acta - Biomembr.* **1999**, *1462* (1–2), 55–70.
- (57) Pouny, Y.; Rapaport, D.; Shai, Y.; Mor, A.; Nicolas, P. Interaction of Antimicrobial Dermaseptin and Its Fluorescently Labeled Analogs with Phospholipid Membranes. *Biochemistry* **1992**, *31* (49), 12416–12423.
- (58) Yamaguchi, S.; Huster, D.; Waring, A.; Lehrer, R. I.; Kearney, W.; Tack, B. F.; Hong, M. Orientation and Dynamics of an Antimicrobial Peptide in the Lipid Bilayer by Solid-State NMR Spectroscopy. *Biophys. J.* **2001**, *81* (4), 2203–2214.
- (59) Efimova, S. S.; Schagina, L. V.; Ostroumova, O. S. Channel-Forming Activity of Cecropins in Lipid Bilayers: Effect of Agents Modifying the Membrane Dipole Potential. *Langmuir* **2014**, *30* (26), 7884–7892.
- (60) Boheim, G. Statistical Analysis of Alamethicin Channels in Black Lipid Membranes. *J. Membr. Biol.* **1974**, *19* (1), 277–303.
- (61) Vogel, H.; Jähnig, F. The Structure of Melittin in Membranes. *Biophys. J.* **1986**, *50* (4), 573–582.
- (62) Sansom, M. S. The Biophysics of Peptide Models of Ion Channels. *Prog. Biophys. Mol. Biol.* **1991**, *55* (3), 139–235.
- (63) He, K.; Ludtke, S. J.; Huang, H. W.; Worcester, D. L. Antimicrobial Peptide Pores in Membranes Detected by Neutron In-Plane Scattering. *Biochemistry* **1995**, *34* (48), 15614–15618.
- (64) Yang, L.; Harroun, T. A.; Weiss, T. M.; Ding, L.; Huang, H. W. Barrel-Stave Model or Toroidal Model? A Case Study on Melittin Pores. *Biophys. J.* **2001**, *81* (3), 1475–1485.

- (65) Zeth, K.; Sancho-Vaello, E. The Human Antimicrobial Peptides Dermcidin and LL-37 Show Novel Distinct Pathways in Membrane Interactions. *Front. Chem.* **2017**, *5*, 86.
- (66) Ramamoorthy, A.; Lee, D.-K.; Narasimhaswamy, T.; Nanga, R. P. R. Cholesterol Reduces Pardaxin's Dynamics – A Barrel-Stave Mechanism of Membrane Disruption Investigated by Solid-State NMR. *Biochim. Biophys. Acta.* **2010**, *1798* (2), 223–227.
- (67) Ludtke, S. J.; He, K.; Heller, W. T.; Harroun, T. A.; Yang, L.; Huang, H. W. Membrane Pores Induced by Magainin. *Biochemistry* **1996**, *35* (43), 13723–13728.
- (68) Matsuzaki, K.; Murase, O.; Fujii, N.; Miyajima, K. An Antimicrobial Peptide, Magainin 2, Induced Rapid Flip-Flop of Phospholipids Coupled with Pore Formation and Peptide Translocation. *Biochemistry* **1996**, *35* (35), 11361–11368.
- (69) Henzler-Wildman, K. A.; Martinez, G. V.; Brown, M. F.; Ramamoorthy, A. Perturbation of the Hydrophobic Core of Lipid Bilayers by the Human Antimicrobial Peptide LL-37. *Biochemistry* **2004**, *43* (26), 8459–8469.
- (70) Sengupta, D.; Leontiadou, H.; Mark, A. E.; Marrink, S. J. Toroidal Pores Formed by Antimicrobial Peptides Show Significant Disorder. *Biochim. Biophys. Acta - Biomembr.* **2008**, *1778* (10), 2308–2317.
- (71) Kobayashi, S.; Chikushi, A.; Tougu, S.; Imura, Y.; Nishida, M.; Yano, Y.; Matsuzaki, K. Membrane Translocation Mechanism of the Antimicrobial Peptide Buforin 2. *Biochemistry* **2004**, *43* (49), 15610–15616.
- (72) Subbalakshmi, C.; Sitaram, N. Mechanism of Antimicrobial Action of Indolicidin. *FEMS Microbiol. Lett.* **1998**, *160* (1), 91–96.
- (73) Kragol, G.; Lovas, S.; Varadi, G.; Condie, B. A.; Hoffmann, R.; Otvos, L. The Antibacterial Peptide Pyrrolicin Inhibits the ATPase Actions of DnaK and Prevents Chaperone-Assisted Protein Folding. *Biochemistry* **2001**, *40* (10), 3016–3026.
- (74) Prince, A.; Sandhu, P.; Kumar, P.; Dash, E.; Sharma, S.; Arakha, M.; Jha, S.; Akhter, Y.; Saleem, M. Lipid-II Independent Antimicrobial Mechanism of Nisin Depends on Its Crowding and Degree of Oligomerization. *Sci. Rep.* **2016**, *6*, 37908.
- (75) Sieprawska-Lupa, M.; Mydel, P.; Krawczyk, K.; Wójcik, K.; Puklo, M.; Lupa, B.; Suder, P.; Silberring, J.; Reed, M.; Pohl, J.; Shafer, W.; McAleese, F.; Foster, T.; Travis, J.; Potempa, J. Degradation of Human Antimicrobial Peptide LL-37 by Staphylococcus Aureus-Derived Proteinases. *Antimicrob. Agents Chemother.* **2004**, *48* (12), 4673–4679.
- (76) Hritonenko, V.; Stathopoulos, C. OmpTn Proteins: An Expanding Family of Outer Membrane Proteases in Gram-Negative Enterobacteriaceae (Review). *Mol. Membr. Biol.* **2007**, *24* (5–6), 395–406.
- (77) Frick, I. M.; Åkesson, P.; Rasmussen, M.; Schmidtchen, A.; Björck, L. SIC, a Secreted Protein of Streptococcus Pyogenes That Inactivates Antibacterial Peptides. *J. Biol. Chem.* **2003**, *278* (19), 16561–16566.
- (78) Branda, S. S.; Chu, F.; Kearns, D. B.; Losick, R.; Kolter, R. A Major Protein Component of the Bacillus Subtilis Biofilm Matrix. *Mol. Microbiol.* **2006**, *59* (4), 1229–1238.
- (79) Abbas, H.; Serry, F. M. E.; EL-Masry, E. M. Combating Pseudomonas Aeruginosa Biofilms by Potential Biofilm Inhibitors. *Asian J. Res. Pharm. Sci.* **2012**, *2* (2), 66–72.
- (80) Ceri, H.; Olson, M. E.; Stremick, C.; Read, R. R.; Morck, D. The Calgary Biofilm Device. *J. Clin. Microbiol.* **1999**, *37* (6), 1771–1776.
- (81) Nickel, J. C.; Ruseska, I.; Wright, J. B.; Costerton, J. W. Tobramycin Resistance of Pseudomonas Aeruginosa Cells Growing as a Biofilm on Urinary Catheter Material. *Antimicrob. Agents Chemother.* **1985**, *27* (4), 619–624.
- (82) Singh, R.; Sahore, S.; Kaur, P.; Rani, A.; Ray, P. Penetration Barrier Contributes to Bacterial Biofilm-Associated Resistance against Only Select Antibiotics, and Exhibits Genus-, Strain- and Antibiotic-Specific Differences. *Pathog. Dis.* **2016**, *74* (6), 1–6.
- (83) Conibear, T. C. R.; Collins, S. L.; Webb, J. S. Role of Mutation in Pseudomonas Aeruginosa Biofilm Development. *PLoS One* **2009**, *4* (7), e6289.

- (84) Chan, C.; Burrows, L. L.; Deber, C. M. Helix Induction in Antimicrobial Peptides by Alginate in Biofilms. *J. Biol. Chem.* **2004**, *279* (37), 38749–38754.
- (85) Vuong, C.; Voyich, J. M.; Fischer, E. R.; Braughton, K. R.; Whitney, A. R.; DeLeo, F. R.; Otto, M. Polysaccharide Intercellular Adhesin (PIA) Protects Staphylococcus Epidermidis against Major Components of the Human Innate Immune System. *Cell. Microbiol.* **2004**, *6* (3), 269–275.
- (86) Overhage, J.; Campisano, A.; Bains, M.; Torfs, E. C. W.; Rehm, B. H. A.; Hancock, R. E. W. Human Host Defense Peptide LL-37 Prevents Bacterial Biofilm Formation. *Infect. Immun.* **2008**, *76* (9), 4176–4182.
- (87) Okuda, K. I.; Zendo, T.; Sugimoto, S.; Iwase, T.; Tajima, A.; Yamada, S.; Sonomoto, K.; Mizunoe, Y. Effects of Bacteriocins on Methicillin-Resistant Staphylococcus Aureus Biofilm. *Antimicrob. Agents Chemother.* **2013**, *57* (11), 5572–5579.
- (88) Peschel, A.; Otto, M.; Jack, R. W.; Kalbacher, H.; Jung, G.; Götz, F. Inactivation of the Dlt Operon in Staphylococcus Aureus Confers Sensitivity to Defensins, Protegrins, and Other Antimicrobial Peptides. *J. Biol. Chem.* **1999**, *274* (13), 8405–8410.
- (89) Tran, A. X.; Lester, M. E.; Stead, C. M.; Raetz, C. R. H.; Maskell, D. J.; McGrath, S. C.; Cotter, R. J.; Trent, M. S. Resistance to the Antimicrobial Peptide Polymyxin Requires Myristoylation of Escherichia Coli and Salmonella Typhimurium Lipid A. *J. Biol. Chem.* **2005**, *280* (31), 28186–28194.
- (90) Campos, M. A.; Vargas, M. A.; Regueiro, V.; Llompart, C. M.; Albertí, S.; Bengoechea, J. A. Capsule Polysaccharide Mediates Bacterial Resistance to Antimicrobial Peptides. *Infect. Immun.* **2004**, *72* (12), 7107–7114.
- (91) Houtsmuller, U. M. T.; Van Deenen, L. L. M. On the Amino Acid Esters of Phosphatidyl Glycerol from Bacteria. *Biochim. Biophys. Acta* **1965**, *106* (3), 564–576.
- (92) Macfarlane, M. Characterization of Lipoamino-Acids as O-Amino-Acid Esters of Phosphatidyl-Glycerol. *Nature* **1962**, *196*, 136–138.
- (93) Fischer, W.; Leopold, K. Polar Lipids of Four Listeria Species Containing L-Lysylcardiolipin, a Novel Lipid Structure, and Other Unique Phospholipids. *Int. J. Syst. Bacteriol.* **1999**, *49* (2), 653–662.
- (94) Ernst, C. M.; Staubitz, P.; Mishra, N. N.; Yang, S. J.; Hornig, G.; Kalbacher, H.; Bayer, A. S.; Kraus, D.; Peschel, A. The Bacterial Defensin Resistance Protein MprF Consists of Separable Domains for Lipid Lysinylation and Antimicrobial Peptide Repulsion. *PLoS Pathog.* **2009**, *5* (11), e1000660.
- (95) Klein, S.; Lorenzo, C.; Hoffmann, S.; Walther, J. M.; Storbeck, S.; Piekarski, T.; Tindall, B. J.; Wray, V.; Nimt, M.; Moser, J. Adaptation of Pseudomonas Aeruginosa to Various Conditions Includes TRNA-Dependent Formation of Alanyl-Phosphatidylglycerol. *Mol. Microbiol.* **2009**, *71* (3), 551–565.
- (96) Tzeng, Y. L.; Ambrose, K. D.; Zughair, S.; Zhou, X.; Miller, Y. K.; Shafer, W. M.; Stephens, D. S. Cationic Antimicrobial Peptide Resistance in Neisseria Meningitidis. *J. Bacteriol.* **2005**, *187* (15), 5387–5396.
- (97) Shafer, W. M.; Qu, X. D.; Waring, A. J.; Lehrer, R. I. Modulation of Neisseria Gonorrhoeae Susceptibility to Vertebrate Antibacterial Peptides Due to a Member of the Resistance/Nodulation/Division Efflux Pump Family. *Proc. Natl. Acad. Sci. U. S. A.* **1998**, *95* (4), 1829–1833.
- (98) Li, M.; Cha, D. J.; Lai, Y.; Villaruz, A. E.; Sturdevant, D. E.; Otto, M. The Antimicrobial Peptide-Sensing System Aps of Staphylococcus Aureus. *Mol. Microbiol.* **2007**, *66* (5), 1136–1147.
- (99) Islam, D.; Bandholtz, L.; Nilsson, J.; Wigzell, H.; Christensson, B.; Agerberth, B.; Gudmundsson, G. H. Downregulation of Bactericidal Peptides in Enteric Infections: A Novel Immune Escape Mechanism with Bacterial DNA as a Potential Regulator. *Nat. Med.* **2001**, *7* (2), 180–185.
- (100) Jia, F.; Wang, J.; Peng, J.; Zhao, P.; Kong, Z.; Wang, K.; Yan, W.; Wang, R. D-Amino Acid Substitution Enhances the Stability of Antimicrobial Peptide Polybia-CP. *Acta Biochim. Biophys. Sin. (Shanghai)*. **2017**, *49* (10), 916–925.

- (101) Hong, S. Y.; Oh, J. E.; Lee, K. H. Effect of D-Amino Acid Substitution on the Stability, the Secondary Structure, and the Activity of Membrane-Active Peptide. *Biochem. Pharmacol.* **1999**, *58* (11), 1775–1780.
- (102) Wallace, R. J. Acetylation of Peptides Inhibits Their Degradation by Rumen Micro-Organisms. *Br. J. Nutr.* **1992**, *68* (2), 365–372.
- (103) Arnesen, T. Towards a Functional Understanding of Protein N-Terminal Acetylation. *PLoS Biol.* **2011**, *9* (5), e1001074.
- (104) Makowski, M.; Silva, Í. C.; Do Amaral, C. P.; Gonçalves, S.; Santos, N. C. Advances in Lipid and Metal Nanoparticles for Antimicrobial Peptide Delivery. *Pharmaceutics* **2019**, *11* (11), 588.
- (105) Gaglione, R.; Pane, K.; Dell’Olmo, E.; Cafaro, V.; Pizzo, E.; Olivieri, G.; Notomista, E.; Arciello, A. Cost-Effective Production of Recombinant Peptides in Escherichia Coli. *N. Biotechnol.* **2019**, *51*, 39–48.
- (106) Law V, Knox C, Djoumbou Y, Jewison T, Guo AC, Liu Y, Maciejewski A, Arndt D, Wilson M, Neveu V, Tang A, Gabriel G, Ly C, Adamjee S, Dame ZT, Han B, Zhou Y, W. D. DrugBank 4.0: Shedding New Light on Drug Metabolism. *Nucleic Acids Res.* **2014**, *42* (Database issue), D1091-D1097.
- (107) Gan, B. H.; Gaynord, J.; Rowe, S. M.; Deingruber, T.; Spring, D. R. The Multifaceted Nature of Antimicrobial Peptides: Current Synthetic Chemistry Approaches and Future Directions. *Chem. Soc. Rev.* **2021**, 7820–7880.
- (108) Dijksteel, G. S.; Ulrich, M. M. W.; Middelkoop, E.; Boekema, B. K. H. L. Review: Lessons Learned From Clinical Trials Using Antimicrobial Peptides (AMPs). *Front. Microbiol.* **2021**, *12*, 616979.
- (109) Stawikowski, M.; Fields, G. B. Introduction to Peptide Synthesis. *Curr. Protoc. Protein Sci.* **2012**, *69*, 18.1.1-18.1.13.
- (110) Wang, Q.; Zhu, F.; Xin, Y.; Liu, J.; Luo, L.; Yin, Z. Expression and Purification of Antimicrobial Peptide Buforin IIb in Escherichia Coli. *Biotechnol. Lett.* **2011**, *33* (11), 2121–2126.
- (111) Ingham, A. B.; Moore, R. J. Recombinant Production of Antimicrobial Peptides in Heterologous Microbial Systems. *Biotechnol. Appl. Biochem.* **2007**, *47* (1), 1–9.
- (112) Chen, F.; Zhang, F.; Wang, A.; Li, H.; Wang, Q.; Zeng, Z.; Wang, S.; Xie, T. Recent Progress in the Chemo-Enzymatic Peptide Synthesis. *African J. Pharm. Pharmacol.* **2010**, *4* (10), 721–730.
- (113) Hou, R. Z.; Zhang, N.; Li, G.; Huang, Y. B.; Wang, H.; Xiao, Y. P.; Liu, Y. J.; Yang, Y.; Zhao, L.; Zhang, X. Z. Synthesis of Tripeptide RGD Amide by a Combination of Chemical and Enzymatic Methods. *J. Mol. Catal. B Enzym.* **2005**, *37* (1–6), 9–15.
- (114) Walsh, G. Therapeutic Insulins and Their Large-Scale Manufacture. *Appl. Microbiol. Biotechnol.* **2005**, *67* (2), 151–159.
- (115) Curtius, T. Ueber Einige Neue Der Hippursäure Analog Constituierte, Synthetisch Dargestellte Amidosäure. *J. für Prakt. Chem.* **1882**, *26*, 145–208.
- (116) Fourneau, E.; Fisher, E. Ueber Einige Derivate Des Glykocolls. *Ber. Dtsch. Chem. Ges.* **1901**, *34*, 2868–2877.
- (117) Curtius, T.; Gumlich, O. Verkettung von Amidosäuren. VII. Abhandlung. Kettenbildung Zwischen Hippurazid Und  $\beta$ -Amino- $\alpha$ -Oxypropionsäure Und  $\beta$ -Aminobuttersäure. *J. für Prakt. Chemie* **1904**, *70* (1), 195–223. <https://doi.org/10.1002/prac.19040700110>.
- (118) Curtius, T.; Müller, E. Neue Untersuchungen Über Diazofettsäureester. *Ber. Dtsch. Chem. Ges.* **1904**, *37*, 1261–1279.
- (119) Fischer, E. Synthese von Polypeptiden. XVII. *Ber. Dtsch. Chem. Ges.* **1907**, *40* (2), 1754–1767..
- (120) Bergmann, M.; Zervas, L. Über Ein Allgemeines Verfahren Der Peptid-Synthese. *Ber. dtsch. Chem. Ges.* **1932**, *65*, 1192–1201.
- (121) McKay, F. C.; Albertson, N. F. New Amine-Masking Groups for Peptide Synthesis. *J. Am. Chem. Soc.* **1957**, *79* (17), 4686–4690.
- (122) Carpino, L. A. Oxidative Reactions of Hydrazines. IV. Elimination of Nitrogen from 1,1-Disubstituted-2-Arenesulfonylhydrazides. *J. Am. Chem. Soc.* **1957**, *79* (16), 4427–4431.

- (123) Sheehan, J. C.; Hess, G. P. A New Method of Forming Peptide Bonds. *J. Am. Chem. Soc.* **1955**, *77* (4), 1067–1068.
- (124) König, W.; Geiger, R. Eine Neue Methode Zur Synthese von Peptiden: Aktivierung Der Carboxylgruppe Mit Dicyclohexylcarbodiimid Unter Zusatz von 1-Hydroxy-benzotriazolen. *Chem. Ber.* **1970**, *103* (3), 788–798.
- (125) Vigneaud, V. du; Ressler, C.; Swan, C. J. M.; Roberts, C. W.; Katsoyannis, P. G.; Gordon, S. The Synthesis of an Octapeptide Amide with the Hormonal Activity of Oxytocin. *J. Am. Chem. Soc.* **1953**, *75* (19), 4879–4880.
- (126) Merrifield, R. B. Solid Phase Peptide Synthesis. *Excerpta Med., I.C.S.* **1963**, *374*, 29–39.
- (127) Carpino, L. A.; Han, G. Y. 9-Fluorenylmethoxycarbonyl Function, a New Base-Sensitive Amino-Protecting Group. *J. Am. Chem. Soc.* **1970**, *92* (19), 5748–5749.
- (128) Sherrington, D. C. Preparation, Structure and Morphology of Polymer Supports. *Chem. Commun.* **1998**, *21*, 2275–2286.
- (129) Benoiton, N. L.; Chen, F. M. F. Not the Alkoxy-carbonylamino -Acid O -Acyloisourea. *J. Chem. Soc. Chem. Commun.* **1981**, *11*, 543–545.
- (130) Bates, H. S.; Jones, J. H.; Witty, M. J. Direct Observation of an Alkoxy-carbonylamino Acid O -Acyloisourea. *J. Chem. Soc. Chem. Commun.* **1980**, *773* (16), 773–774.
- (131) Subirós-Funosas, R.; Prohens, R.; Barbas, R.; El-Faham, A.; Albericio, F. Oxyma: An Efficient Additive for Peptide Synthesis to Replace the Benzotriazole-Based HOBt and HOAt with a Lower Risk of Explosion. *Chem. Eur. J.* **2009**, *15*, 9394–9403.
- (132) Castro, B.; Dormoy, J. R.; Evin, G.; Selve, C. Reactifs de Couplage Peptidique I (1) - l'hexafluorophosphate de Benzotriazolyl N-Oxytrisdiméthylamino Phosphonium (B.O.P.). *Tetrahedron Lett.* **1975**, *16*, 1219–1222.
- (133) Albericio, F.; Cases, M.; Alsina, J.; Triolo, S. A.; Carpino, L. A.; Kates, S. A. On the Use of PyAOP, a Phosphonium Salt Derived from HOAt, in Solid-Phase Peptide Synthesis. *Tetrahedron Lett.* **1997**, *38* (27), 4853–4856.
- (134) Subirós-Funosas, R.; Moreno, J. A.; Bayó-Puxan, N.; Abu-Rabeah, K.; Ewenson, A.; Atias, D.; Marks, R. S.; Albericio, F. PyCloCk, the Phosphonium Salt Derived from 6-Cl-HOBt. *Chim. Oggi* **2008**, *26* (4 SUPPL.), 10–12.
- (135) Carpino, L. A.; El-Faham, A.; Minor, C. A.; Albericio, F. Advantageous Applications of Azabenzotriazole (Triazolopyridine)-Based Coupling Reagents to Solid-Phase Peptide Synthesis. *J. Chem. Soc. Chem. Commun.* **1994**, *2*, 201–203.
- (136) Dourtoglou, V.; Ziegler, J. C.; Gross, B. L'hexafluorophosphate de O-Benzotriazolyl-N,N-Tetraméthyluronium: Un Réactif de Couplage Peptidique Nouveau et Efficace. *Tetrahedron Lett.* **1978**, *19* (15), 1269–1272.
- (137) Knorr, R.; Trzeciak, A.; Bannwarth, W.; Gillissen, D. New Coupling Reagents in Peptide Chemistry. *Tetrahedron Lett.* **1989**, *30* (15), 1927–1930.
- (138) Carpino, L. A. 1-Hydroxy-7-Azabenzotriazole. An Efficient Peptide Coupling Additive. *J. Am. Chem. Soc.* **1993**, *115* (10), 4397–4398.
- (139) Marder, O.; Shvo, Y.; Albericio, F. HCTU and TCTU. New Coupling Reagents: Development and Industrial Aspects. *Chim. Oggi* **2002**, *20* (7–8), 37–41.
- (140) Valeur, E.; Bradley, M. Amide Bond Formation: Beyond the Myth of Coupling Reagents. *Chem. Soc. Rev.* **2009**, *38* (2), 606–631.
- (141) El-Faham, A.; Albericio, F. Peptide Coupling Reagents, More than a Letter Soup. *Chem. Rev.* **2011**, *111* (11), 6557–6602.
- (142) Al-Warhi, T. I.; Al-Hazimi, H. M. A.; El-Faham, A. Recent Development in Peptide Coupling Reagents. *J. Saudi Chem. Soc.* **2012**, *16* (2), 97–116.
- (143) Albericio, F.; El-Faham, A. Choosing the Right Coupling Reagent for Peptides: A Twenty-Five-Year Journey. *Org. Process Res. Dev.* **2018**, *22* (7), 760–772.
- (144) Mant, C. T.; Chen, Y.; Yan, Z.; Popa, T. V.; Kovacs, J. M.; Mills, J. B.; Triplet, B. P.; Hodges, R. S. HPLC Analysis and Purification of Peptides. *Methods Mol. Biol.* **2007**, *386*, 3–55.



- (145) Wouters, O. J.; McKee, M.; Luyten, J. Estimated Research and Development Investment Needed to Bring a New Medicine to Market, 2009-2018. *JAMA - J. Am. Med. Assoc.* **2020**, *323* (9), 844–853.
- (146) American Association for Cancer Research. Cancer Progress Report 2011. Available online: <http://www.cancerprogressreport-digital.org/cancerprogressreport/2011?pg=1#pg1> (accessed Sep 07, 2021).
- (147) Food and Drug Administration. The Drug Development Process. Available online: <https://www.fda.gov/patients/learn-about-drug-and-device-approvals/drug-development-process> (accessed Sep 07, 2021).
- (148) Rabanal, F.; Cajal, Y. Recent Advances and Perspectives in the Design and Development of Polymyxins. *Nat. Prod. Rep.* **2017**, *34* (7), 886–908.
- (149) Falagas, M. E.; Kasiakou, S. K. Colistin: The Revival of Polymyxins for the Management of Multidrug-Resistant Gram-Negative Bacterial Infections. *Clin. Infect. Dis.* **2005**, *40* (9), 1333–1341.
- (150) Benedict, R. G.; Langlykke, A. F. Antibiotic Activity of Bacillus Polymyxa. *J. Bacteriol.* **1947**, *54* (1), 24.
- (151) Stansly, P. G.; Shepherd, R. G.; White, H. J. Polymyxin: A New Chemotherapeutic Agent. *Bull. Johns Hopkins Hosp.* **1947**, *81* (1), 43–54.
- (152) Ainsworth, G. C.; Brown, A. M.; Brownlee, G. Aerosporin, an Antibiotic Produced by Bacillus Aerosporus Greer. *Nature* **1947**, *159* (4060), 263.
- (153) Brownlee, G.; Bushby, S. R. M.; Short, E. I. The Pharmacology of Polymyxin A, B, and D. *Ann. N. Y. Acad. Sci.* **1949**, *51* (5), 952–967.
- (154) Falagas, M. E.; Kasiakou, S. K. Toxicity of Polymyxins: A Systematic Review of the Evidence from Old and Recent Studies. *Crit. Care* **2006**, *10* (1).
- (155) Bergen, P. J.; Li, J.; Rayner, C. R.; Nation, R. L. Colistin Methanesulfonate Is an Inactive Prodrug of Colistin against Pseudomonas Aeruginosa. *Antimicrob. Agents Chemother.* **2006**, *50* (6), 1953–1958.
- (156) Olaitan, A. O.; Iumuyiw.; Thongmalayvong, B.; Akkhavong, K.; Somphavong, S.; Paboriboune, P.; Khounsy, S.; Morand, S.; Rolain, J. M. Clonal Transmission of a Colistin-Resistant Escherichia Coli from a Domesticated Pig to a Human in Laos. *J. Antimicrob. Chemother.* **2015**, *70* (12), 3402–3404.
- (157) Zhang, R.; Shen, Y.; Walsh, T. R.; Wang, Y.; Hu, F. Use of Polymyxins in Chinese Hospitals. *Lancet Infect. Dis.* **2020**, *20* (10), 1125–1126.
- (158) European Medicines Agency. Use of Glycylcyclines in Animals in the European Union: Development of Resistance and Possible Impact on Human and Animal Health. 2013, Available online: [https://www.ema.europa.eu/en/documents/report/use-glycylcyclines-animals-european-union-development-resistance-possible-impact-human-animal-health\\_en.pdf](https://www.ema.europa.eu/en/documents/report/use-glycylcyclines-animals-european-union-development-resistance-possible-impact-human-animal-health_en.pdf) (accessed Sep 14, 2021).
- (159) Walsh, T. R.; Wu, Y. China Bans Colistin as a Feed Additive for Animals. *Lancet Infect. Dis.* **2016**, *16* (10), 1102–1103. [https://doi.org/10.1016/S1473-3099\(16\)30329-2](https://doi.org/10.1016/S1473-3099(16)30329-2).
- (160) Moubareck, C. A. Polymyxins and Bacterial Membranes: A Review of Antibacterial Activity and Mechanisms of Resistance. *Membranes (Basel)*. **2020**, *10* (8), 1–30.
- (161) Raetz, C. R. H.; Whitfield, C. Lipopolysaccharide Endotoxins as Activators of Innate Immunity. *Annu. Rev. Biochem.* **2008**, *71*, 635–700.
- (162) Velkov, T.; Thompson, P. E.; Nation, R. L.; Li, J. Structure-Activity Relationships of Polymyxin Antibiotics, 2010.
- (163) Landman, D.; Georgescu, C.; Martin, D. A.; Quale, J. Polymyxins Revisited. *Clin. Microbiol. Rev.* **2008**, *21* (3), 449–465.
- (164) Dixon, R. A.; Chopra, I. Polymyxin b and Polymyxin b Nonapeptide Alter Cytoplasmic Membrane Permeability in Escherichia Coli. *J. Antimicrob. Chemother.* **1986**, *18* (5), 557–563.

- (165) Cajal, Y.; Rogers, J.; Berg, O. G.; Jain, M. K. Intermembrane Molecular Contacts by Polymyxin B Mediate Exchange of Phospholipids. *Biochemistry* **1996**, *35* (1), 299–308.
- (166) Cajal, Y.; Berg, O. G.; Kumar-Jain, M. Direct Vesicle-Cesicle Exchange of Phospholipids Mediated by Polymyxin B. *Biochem. Biophys. Res. Commun.* **1995**, *210* (3), 746–752.
- (167) Ramos, P. I. P.; Custódio, M. G. F.; Quispe Saji, G. del R.; Cardoso, T.; da Silva, G. L.; Braun, G.; Martins, W. M. B. S.; Girardello, R.; de Vasconcelos, A. T. R.; Fernández, E.; Gales, A. C.; Nicolás, M. F. The Polymyxin B-Induced Transcriptomic Response of a Clinical, Multidrug-Resistant *Klebsiella Pneumoniae* Involves Multiple Regulatory Elements and Intracellular Targets. *BMC Genomics* **2016**, *17* (Suppl 8), 737.
- (168) Sampson, T. R.; Liu, X.; Schroeder, M. R.; Kraft, C. S.; Burd, E. M.; Weiss, D. S. Rapid Killing of *Acinetobacter Baumannii* by Polymyxins Is Mediated by a Hydroxyl Radical Death Pathway. *Antimicrob. Agents Chemother.* **2012**, *56* (11), 5642–5649.
- (169) Imlay, J. A. The Oxidative Stress : Lessons from a Model Bacterium. *Nat. Rev. Microbiol.* **2013**, *11* (7), 443–454.
- (170) Hill, C.; Jain, A.; Takemoto, H.; Silver, M. D.; Nagesh, S. V. S.; Ionita, C. N.; Bednarek, D. R.; Rudin, S. A Secondary Mode of Action of Polymyxins against Gram- Negative Bacteria Involves the Inhibition of NADH-Quinone Oxidoreductase Activity. *J. Antibiot. (Tokyo)*. **2014**, *67* (2), 147–151.
- (171) Mortensen, N. P.; Fowlkes, J. D.; Sullivan, C. J.; Allison, D. P.; Larsen, N. B.; Molin, S.; Doktycz, M. J. Effects of Colistin on Surface Ultrastructure and Nanomechanics of *Pseudomonas Aeruginosa* Cells. *Langmuir* **2009**, *25* (6), 3728–3733.
- (172) Koch-Weser, J.; Sidel, V. W.; Federman, E. B.; Kanarek, P.; Finer, D. C.; Eaton, A. E. Adverse Effects of Sodium Colistimethate. Manifestations and Specific Reaction Rates during 317 Courses of Therapy. *Ann. Intern. Med.* **1970**, *72* (6), 857–868.
- (173) Brown, J. M.; Dorman, D. C.; Roy, L. P. Acute Renal Failure Due to Overdosage of Colistin. *Med. J. Aust.* **1970**, *2* (20), 923–924.
- (174) Wagenlehner, F.; Lucenteforte, E.; Pea, F.; Soriano, A.; Tavoschi, L.; Steele, V. R.; Henriksen, A. S.; Longshaw, C.; Manissero, D.; Pecini, R.; Pogue, J. M. Systematic Review on Estimated Rates of Nephrotoxicity and Neurotoxicity in Patients Treated with Polymyxins. *Clin. Microbiol. Infect.* **2021**, *27* (5), 671–686.
- (175) Nilsson, A.; Goodwin, R. J. A.; Swales, J. G.; Gallagher, R.; Shankaran, H.; Sathe, A.; Pradeepan, S.; Xue, A.; Keirstead, N.; Sasaki, J. C.; Andren, P. E.; Gupta, A. Investigating Nephrotoxicity of Polymyxin Derivatives by Mapping Renal Distribution Using Mass Spectrometry Imaging. *Chem. Res. Toxicol.* **2015**, *28* (9), 1823–1830.
- (176) Grill, M. F.; Maganti, R. K. Neurotoxic Effects Associated with Antibiotic Use: Management Considerations. *Br. J. Clin. Pharmacol.* **2011**, *72* (3), 381–393.
- (177) Hamad, M. A.; Di Lorenzo, F.; Molinaro, A.; Valvano, M. A. Aminoarabinose Is Essential for Lipopolysaccharide Export and Intrinsic Antimicrobial Peptide Resistance in *Burkholderia Cenocepacia*. *Mol. Microbiol.* **2012**, *85* (5), 962–974.
- (178) Yang, Q.; Pogue, J. M.; Li, Z.; Nation, R. L.; Kaye, K. S.; Li, J. Agents of Last Resort: An Update on Polymyxin Resistance. *Infect. Dis. Clin. North Am.* **2020**, *34* (4), 723–750.
- (179) Li, Z.; Cao, Y.; Yi, L.; Liu, J. H.; Yang, Q. Emergent Polymyxin Resistance: End of an Era? *Open Forum Infect. Dis.* **2019**, *6* (10), 1–10.
- (180) Moffatt, J. H.; Harper, M.; Boyce, J. D. Mechanisms of Polymyxin Resistance. *Adv. Exp. Med. Biol.* **2019**, *1145*, 55–71.
- (181) Liu, Y. Y.; Wang, Y.; Walsh, T. R.; Yi, L. X.; Zhang, R.; Spencer, J.; Doi, Y.; Tian, G.; Dong, B.; Huang, X.; Yu, L. F.; Gu, D.; Ren, H.; Chen, X.; Lv, L.; He, D.; Zhou, H.; Liang, Z.; Liu, J. H.; Shen, J. Emergence of Plasmid-Mediated Colistin Resistance Mechanism MCR-1 in Animals and Human Beings in China: A Microbiological and Molecular Biological Study. *Lancet Infect. Dis.* **2016**, *16* (2), 161–168.
- (182) Vogler, K.; Studer, R. O.; Lanz, P.; Lergier, W.; Böhni, E. Total Synthesis of the Antibiotic Polymyxin B1. *Experientia* **1964**, *20* (7), 365–366.

- (183) Sharma, S. K.; Wu, A. D.; Chandramouli, N.; Fotsch, C.; Kardash, G.; Bair, K. W. Solid-Phase Total Synthesis of Polymyxin B1. *J. Pept. Res.* **1999**, *53* (5), 501–506.
- (184) Tsubery, H.; Ofek, I.; Cohen, S.; Fridkin, M. Structure - Function Studies of Polymyxin B Nonapeptide: Implications to Sensitization of Gram-Negative Bacteria. *J. Med. Chem.* **2000**, *43* (16), 3085–3092.
- (185) Hindo, M. S.; Akura, N. S. Contribution of Each Amino Acid Residue in Polymyxin B 3 to Antimicrobial and Lipopolysaccharide Binding Activity. **2009**, *57* (3), 240–244.
- (186) Vaara, M.; Fox, J.; Loidl, G.; Siikanen, O.; Apajalahti, J.; Hansen, F.; Frimodt-Møller, N.; Nagai, J.; Takano, M.; Vaara, T. Novel Polymyxin Derivatives Carrying Only Three Positive Charges Are Effective Antibacterial Agents. *Antimicrob. Agents Chemother.* **2008**, *52* (9), 3229–3236. <https://doi.org/10.1128/AAC.00405-08>.
- (187) Vaara, M.; Vaara, T. Sensitization of Gram-Negative Bacteria to Antibiotics and Complement by a Nontoxic Oligopeptide. *Nature* **1983**, *303* (5917), 526–528.
- (188) Tsubery, H.; Ofek, I.; Cohen, S.; Fridkin, M. N-Terminal Modifications of Polymyxin B Nonapeptide and Their Effect on Antibacterial Activity. *Peptides* **2001**, *22* (10), 1675–1681.
- (189) Sakura, N.; Itoh, T.; Uchida, Y.; Ohki, K.; Okimura, K.; Chiba, K.; Sato, Y.; Sawanishi, H. The Contribution of the N-Terminal Structure of Polymyxin B Peptides to Antimicrobial and Lipopolysaccharide Binding Activity. *Bull. Chem. Soc. Jpn.* **2004**, *77* (10), 1915–1924.
- (190) Chihara, S.; Ito, A.; Yahata, M.; Tobita, T.; Koyama, Y. Chemical Synthesis, Isolation and Characterization of  $\alpha$ -n-Fattyacyl Colistin Nonapeptide with Special Reference to the Correlation between Antimicrobial Activity and Carbon Number of Fattyacyl Moiety. *Agric. Biol. Chem.* **1974**, *38* (3), 521–529.
- (191) Tsubery, H.; Ofek, I.; Cohen, S.; Eisenstein, M.; Fridkin, M. Modulation of the Hydrophobic Domain of Polymyxin B Nonapeptide: Effect on Outer-Membrane Permeabilization and Lipopolysaccharide Neutralization. **2002**, *62* (5), 1036–1042.
- (192) Barnett, M.; Bushby, S. R. M.; Wilkinson, S. Sodium Sulphomethyl Derivatives of Polymyxins. *Br. J. Pharmacol. Chemother.* **1964**, *23* (3), 552–574.
- (193) Grau-Campistany, A.; Manresa, Á.; Pujol, M.; Rabanal, F.; Cajal, Y. Tryptophan-Containing Lipopeptide Antibiotics Derived from Polymyxin B with Activity against Gram Positive and Gram Negative Bacteria. *Biochim. Biophys. Acta - Biomembr.* **2016**, *1858* (2), 333–343.
- (194) Grau-Campistany, A.; Pujol, M.; Marqués, A. M.; Manresa, Á.; Rabanal, F.; Cajal, Y. Membrane Interaction of a New Synthetic Antimicrobial Lipopeptide Sp-85 with Broad Spectrum Activity. *Colloids Surfaces A Physicochem. Eng. Asp.* **2015**, *480*, 307–317.
- (195) Kwon, Y. U.; Kodadek, T. Quantitative Comparison of the Relative Cell Permeability of Cyclic and Linear Peptides. *Chem. Biol.* **2007**, *14* (6), 671–677.
- (196) Horton, D. A.; Bourne, G. T.; Smythe, M. L. Exploring Privileged Structures: The Combinatorial Synthesis of Cyclic Peptides. *Mol. Divers.* **2000**, *5* (4), 289–304.
- (197) Tsubery, H.; Ofek, I.; Cohen, S.; Fridkin, M. Structure Activity Relationship Study of Polymyxin b Nonapeptide. *Adv. Exp. Med. Biol.* **2000**, *479*, 219–222.
- (198) Leese, R. A. Antibiotic Compositions for the Treatment of Gram Negative Infections. Patent Application WO2020075416, 2010.
- (199) Magee, T. V.; Brown, M. F.; Starr, J. T.; Ackley, D. C.; Abramite, J. A.; Aubrecht, J.; Butler, A.; Crandon, J. L.; Dib-Hajj, F.; Flanagan, M. E.; Granskog, K.; Hardink, J. R.; Huband, M. D.; Irvine, R.; Kuhn, M.; Leach, K. L.; Li, B.; Lin, J.; Luke, D. R.; Macvane, S. H.; Miller, A. A.; McCurdy, S.; McKim, J. M.; Nicolau, D. P.; Nguyen, T. T.; Noe, M. C.; O'Donnell, J. P.; Seibel, S. B.; Shen, Y.; Stepan, A. F.; Tomaras, A. P.; Wilga, P. C.; Zhang, L.; Xu, J.; Chen, J. M. Discovery of Dap-3 Polymyxin Analogues for the Treatment of Multidrug-Resistant Gram-Negative Nosocomial Infections. *J. Med. Chem.* **2013**, *56* (12), 5079–5093.
- (200) Vaara, M.; Siikanen, O.; Apajalahti, J.; Frimodt-Møller, N.; Vaara, T. Susceptibility of Carbapenemase-Producing Strains of *Klebsiella pneumoniae* and *Escherichia coli* to the Direct Antibacterial Activity of NAB739 and to the Synergistic Activity of NAB7061 with Rifampicin and Clarithromycin. *J. Antimicrob. Chemother.* **2010**, *65* (5), 942–945.

- (201) Coleman, S., Bleavins, M., Lister, T., Vaara, M. & Parr, T. J. The Assessment of SPR741 for Nephrotoxicity in Cynomolgus Monkeys and Sprague-Dawley Rats. In *ASM Microbe*; Boston, MA, USA, 2016.
- (202) U.S. National Library of Medicine <https://clinicaltrials.gov/ct2/show/NCT04865393> (accessed Oct 5, 2021).
- (203) Brown, P.; Abbott, E.; Abdulle, O.; Boakes, S.; Coleman, S.; Divall, N.; Duperchy, E.; Moss, S.; Rivers, D.; Simonovic, M.; Stanway, S.; Wilson, A.; Dawson, M. J. Design of next Generation Polymyxins with Lower Toxicity: The Discovery of SPR206. **2021**, *5* (10), 1645–1656.
- (204) Boakes, S., Duperchy, E., Brown, P., Simonovic, M., Abdulle, O., Divall, N., et al. Novel Polymyxin Derivative CA824: Efficacy in Neutropenic Mouse Infection and Lung Infection Models. Poster. In *Proceedings of the 55th Interscience Conference on Antimicrobial Agents and Chemotherapy*; San Diego, CA, USA, 2015.
- (205) Velkov, T.; Roberts, K. D.; Nation, R. L.; Wang, J.; Thompson, P. E.; Li, J. Teaching “old” Polymyxins New Tricks: New-Generation Lipopeptides Targeting Gram-Negative “Superbugs.” *ACS Chem. Biol.* **2014**, *9* (5), 1172–1177.
- (206) Castanheira, M.; Lindley, J.; Huynh, H.; Mendes, R. E.; Olga Lomovskaya. Activity of a Novel Polymyxin Analog, QPX9003, Tested Against Resistant Gram-Negative Pathogens, Including Carbapenem-Resistant Acinetobacter, Enterobacterales, and Pseudomonas. *Open Forum Infect. Dis.* **2019**, *6* (Suppl 2), S313.
- (207) Sack, D.; Deschacht, C.; Erin, G.; Aaron, K.; Barreto, E.; Rompaey, S. Van. 707. QPX9003: Pharmacology of a Novel Polymyxin in Mice and Rats. *Open Forum Infect. Dis.* **2019**, *6* (Suppl 2), S319.
- (208) U. S. National Library of Medicine <https://clinicaltrials.gov/ct2/show/NCT04808414> (accessed Oct 5, 2021).
- (209) Gordeev, M. F.; Liu, J.; Wang, X.; Yuan, Z. Antimicrobial Polymyxins for Treatment of Bacterial Infections. Patent Application WO2016100578, 2017.
- (210) Lepak, A. J.; Wang, W.; Andes, D. R. Pharmacodynamic Evaluation of MRX-8, a Novel Polymyxin, in the Neutropenic Mouse Thigh and Lung Infection Models against Gram-Negative Pathogens. *Antimicrob. Agents Chemother.* **2020**, *64* (11), 1–11.
- (211) U. S. National Library of Medicine <https://clinicaltrials.gov/ct2/show/NCT04649541?term=MRX-8&draw=2&rank=1> (accessed Oct 5, 2021).
- (212) Gallardo-Godoy, A.; Muldoon, C.; Becker, B.; Elliott, A. G.; Lash, L. H.; Huang, J. X.; Butler, M. S.; Pelingon, R.; Kavanagh, A. M.; Ramu, S.; Phetsang, W.; Blaskovich, M. A. T.; Cooper, M. A. Activity and Predicted Nephrotoxicity of Synthetic Antibiotics Based on Polymyxin B. *J. Med. Chem.* **2016**, *59* (3), 1068–1077.
- (213) Rabanal, F.; Grau-Campistany, A.; Vila-Farrés, X.; Gonzalez-Linares, J.; Borràs, M.; Vila, J.; Manresa, A.; Cajal, Y. A Bioinspired Peptide Scaffold with High Antibiotic Activity and Low in Vivo Toxicity. *Sci. Rep.* **2015**, *5*, 1–11.
- (214) Clark, D. P.; Durell, S.; Maloy, W. L.; Zasloff, M. Renalexin. A Novel Antimicrobial Peptide from Bullfrog (*Rana Catesbeiana*) Skin, Structurally Related to the Bacterial Antibiotic, Polymyxin. *J. Biol. Chem.* **1994**, *269* (14), 10849–10855.
- (215) Rustici, A.; Velucchi, M.; Faggioni, R.; Sironi, M.; Ghezzi, P.; Quataert, S.; Green, B.; Porro, M. Molecular Mapping and Detoxification of the Lipid A Binding Site by Synthetic Peptides. *Science* **1993**, *259* (5093), 361–365.
- (216) Bernhard, N.; Wolfgang, S. Simple Method for the Esterification of Carboxylic Acids. *Angew. Chemie Int. Ed. English* **1978**, *17* (7), 522–524.
- (217) Cornish, J.; Callon, K. E.; Lin, C. Q. X.; Xiao, C. L.; Mulvey, T. B.; Cooper, G. J. S.; Reid, I. R. Trifluoroacetate, a Contaminant in Purified Proteins, Inhibits Proliferation of Osteoblasts and Chondrocytes. *Am. J. Physiol. - Endocrinol. Metab.* **1999**, *277* (5 40-5), 1–6.
- (218) Boullerne, A. I.; Polak, P. E.; Braun, D.; Sharp, A.; Pelligrino, D.; Feinstein, D. L. Effects of Peptide Fraction and Counter Ion on the Development of Clinical Signs in Experimental Autoimmune Encephalomyelitis. *J. Neurochem.* **2014**, *129* (4), 696–703.

- (219) Blondelle, S. E.; Ostresh, J. M.; Houghten, R. A.; Pérez-Payá, E. Induced Conformational States of Amphipathic Peptides in Aqueous/Lipid Environments. *Biophys. J.* **1995**, *68* (1), 351–359.
- (220) Johansson, J.; Gudmundsson, G. H.; Rottenberg, M. E.; Berndt, K. D.; Agerberth, B. Conformation-Dependent Antibacterial Activity of the Naturally Occurring Human Peptide LL-37. *J. Biol. Chem.* **1998**, *273* (6), 3718–3724.
- (221) Pini, A.; Lozzi, L.; Bernini, A.; Brunetti, J.; Falciani, C.; Scali, S.; Bindi, S.; Di Maggio, T.; Rossolini, G. M.; Niccolai, N.; Bracci, L. Efficacy and Toxicity of the Antimicrobial Peptide M33 Produced with Different Counter-Ions. *Amino Acids* **2012**, *43* (1), 467–473.
- (222) Wiegand, I.; Hilpert, K.; Hancock, R. E. W. Agar and Broth Dilution Methods to Determine the Minimal Inhibitory Concentration (MIC) of Antimicrobial Substances. *Nat. Protoc.* **2008**, *3* (2), 163–175.
- (223) Epand, R. M.; Rotem, S.; Mor, A.; Berno, B.; Epand, R. F. Bacterial Membranes as Predictors of Antimicrobial Potency. *J. Am. Chem. Soc.* **2008**, *130* (43), 14346–14352.
- (224) Malanovic, N.; Lohner, K. Gram-Positive Bacterial Cell Envelopes: The Impact on the Activity of Antimicrobial Peptides. *Biochim. Biophys. Acta - Biomembr.* **2016**, *1858* (5), 936–946.
- (225) Li, X.; Smith, A. W. Quantifying Lipid Mobility and Peptide Binding for Gram-Negative and Gram-Positive Model Supported Lipid Bilayers. *J. Phys. Chem. B* **2019**, *123* (49), 10433–10440.
- (226) Dupuy, F. G.; Pagano, I.; Andenoro, K.; Peralta, M. F.; Elhady, Y.; Heinrich, F.; Tristram-Nagle, S. Selective Interaction of Colistin with Lipid Model Membranes. *Biophys. J.* **2018**, *114* (4), 919–928.
- (227) Giner-Casares, J. J.; Brezesinski, G.; Möhwald, H. Langmuir Monolayers as Unique Physical Models. *Curr. Opin. Colloid Interface Sci.* **2014**, *19* (3), 176–182.
- (228) Wilhelmy, L. Ueber Die Abhängigkeit Des Capillaritäts-Constanten Des Alkohols von Substanz Und Gestalt Des Benetzten Festen Körpers. *Ann. der Phys. und Chemie* **1863**, *6*, 178–217.
- (229) Marsh, D. Lateral Pressure in Membranes. *Biochim. Biophys. Acta - Rev. Biomembr.* **1996**, *1286* (3), 183–223.
- (230) Bangham, A. D.; Horne, R. W. Negative Staining of Phospholipids and Their Structural Modification by Surface-Active Agents as Observed in the Electron Microscope. *J. Mol. Biol.* **1964**, *8* (5), 660–668.
- (231) Andrade, S.; Ramalho, M. J.; Loureiro, J. A.; Pereira, M. C. Liposomes as Biomembrane Models: Biophysical Techniques for Drug-Membrane Interaction Studies. *J. Mol. Liq.* **2021**, *334*.
- (232) Zhang, Y.; Huang, L. Liposomal Delivery System. In *Nanoparticles for Biomedical Applications*; Chung, E. J., Leon, L., Rinaldi, C., Eds.; Elsevier Inc., 2020; pp 145–152.
- (233) Sforzi, J.; Palagi, L.; Aime, S. Liposome-based Bioassays. *Biology (Basel)*. **2020**, *9* (8), 1–28.
- (234) Akbarzadeh, A.; Rezaei-Sadabady, R.; Davaran, S.; Joo, S. W.; Zarghami, N.; Hanifehpour, Y.; Samiei, M.; Kouhi, M.; Nejati-Koshki, K. Liposome: Classification, Preparation, and Applications. *Nanoscale Res. Lett.* **2013**, *8* (1), 1.
- (235) Clegg, R. M. Fluorescence Resonance Energy Transfer. *Chem. Anal.* **1996**, *137*, 179–252.
- (236) Šachl, R.; Humpolíčková, J.; Štefl, M.; Johansson, L. B.; Hof, M. Limitations of Electronic Energy Transfer in the Determination of Lipid Nanodomain Sizes. *Biophys. J.* **2011**, *101* (11), 60–62.
- (237) Baptista, A. L. F.; Coutinho, P. J. G.; Real Oliveira, M. E. C. D.; Rocha Gomes, J. I. N. Effect of Surfactants in Soybean Lecithin Liposomes Studied by Energy Transfer between NBD-PE and N-Rh-PE. *J. Liposome Res.* **2000**, *10* (4), 419–429.
- (238) Sims, P. J.; Waggoner, A. S.; Wang, C. H.; Hoffman, J. F. Mechanism by Which Cyanine Dyes Measure Membrane Potential in Red Blood Cells and Phosphatidylcholine Vesicles. *Biochemistry* **1974**, *13* (16), 3315–3330.
- (239) Bashford, C. L. The Measurement of Membrane Potential Using Optical Indicators. *Biosci. Rep.* **1981**, *1* (3), 183–196.
- (240) Ehrenberg, B.; Montana, V.; Wei, M.-D.; P. Wuskell, J.; Loew, L. M. Membrane Potential Can Be Determined in Individual Cells From the Nernstian. *Biophys. J.* **1988**, *53*, 785–794.

- (241) Jain, R.; Chen, D.; White, R.; Patel, D.; Yuan, Z. Bacterial Peptide Deformylase Inhibitors: A New Class of Antibacterial Agents. *Curr. Med. Chem.* **2005**, *12* (14), 1607–1621.
- (242) Guay, D. R. P. Drug Forecast - The Peptide Deformylase Inhibitors as Antibacterial Agents. *Ther. Clin. Risk Manag.* **2007**, *3* (4), 513–525.
- (243) Chen, D. Z.; Patel, D. V.; Hackbarth, C. J.; Wang, W.; Dreyer, G.; Young, D. C.; Margolis, P. S.; Wu, C.; Ni, Z. J.; Trias, J.; White, R. J.; Yuan, Z. Actinonin, a Naturally Occurring Antibacterial Agent, Is a Potent Deformylase Inhibitor. *Biochemistry* **2000**, *39* (6), 1256–1262.
- (244) Ben-Ishai, D.; Berger, A. Cleavage of N-Carbobenzyloxy Groups by Dry Hydrogen Bromide and Hydrogen Chloride. *J. Org. Chem.* **1952**, *17* (12), 1564–1570.
- (245) Sakakibara, S.; Shimonishi, Y.; Kishida, Y.; Okada, M.; Sugihara, H. Use of Anhydrous Hydrogen Fluoride in Peptide Synthesis. I. Behavior of Various Protective Groups in Anhydrous Hydrogen Fluoride. *Bull. Chem. Soc. Jpn.* **1967**, *40* (9), 2164–2167.
- (246) Tam, J. P.; Heath, W. F.; Merrifield, R. B. SN<sub>2</sub> Deprotection of Synthetic Peptides with a Low Concentration of HF in Dimethyl Sulfide: Evidence and Application in Peptide Synthesis. *J. Am. Chem. Soc.* **1983**, *105* (21), 6442–6455.
- (247) Applied Biosystems Inc. Introduction to Cleavage Techniques. Available online: [http://tools.thermofisher.com/content/sfs/manuals/cms\\_040797.pdf](http://tools.thermofisher.com/content/sfs/manuals/cms_040797.pdf) (accessed 20 Sep 2021).
- (248) Entwistle, I. D.; Wood, W. W. *Hydrogenolysis of Allyl and Benzyl Halides and Related Compounds*; Sittingbourne, UK, 1991.
- (249) Rodríguez-Núñez, M. Disseny, Síntesi i Estudi de l'activitat Biològica i Biofísica d'antibiòtics Lipopeptídics Cíclics, University of Barcelona, Department of Organic Chemistry, 2011.
- (250) Rabanal, F.; Rodríguez-Núñez, M.; Cajal, Y. Method for the Deblocking/Deprotection of Compounds Obtained by Solid Phase Synthesis. Patent Application WO2009000950A1, 2007.
- (251) Deans, D. R.; Eaborn, C. The Reaction between Iodine and Trisubstituted Silanes. *J. Chem. Soc.* **1954**, 3169–3173.
- (252) Rink, H. Solid-Phase Synthesis of Protected Peptide Fragments Using a Trialkoxy-Diphenyl-Methylester Resin. *Tetrahedron Lett.* **1987**, *28* (33), 3787–3790.
- (253) Kudrimoti, M.; Curtis, A.; Azawi, S.; Worden, F.; Katz, S.; Adkins, D.; Bonomi, M.; Elder, J.; Sonis, S. T.; Straube, R.; Donini, O. Dusquetide: A Novel Innate Defense Regulator Demonstrating a Significant and Consistent Reduction in the Duration of Oral Mucositis in Preclinical Data and a Randomized, Placebo-Controlled Phase 2a Clinical Study. *J. Biotechnol.* **2016**, *239*, 115–125.
- (254) U.S. National Library of Medicine <https://clinicaltrials.gov/ct2/show/NCT03237325> (accessed Sep 28, 2021).
- (255) Mohamed, M. F.; Brezden, A.; Mohammad, H.; Chmielewski, J.; Seleem, M. N. A Short D-Enantiomeric Antimicrobial Peptide with Potent Immunomodulatory and Antibiofilm Activity against Multidrug-Resistant *Pseudomonas Aeruginosa* and *Acinetobacter Baumannii*. *Sci. Rep.* **2017**, *7* (1), 1–13.
- (256) Wang, S. S.; Wang, B. S. H.; Hughes, J. L.; Leopold E. J.; Wu, C. R.; Tam, J. P. Cleavage and Deprotection of Peptides on MBHA-Resin with Hydrogen Bromide. *Inr. J. Pept. Protein Res* **1992**, *40*, 344–349.
- (257) Hughes, J. L.; Leopold, E. J. Cleavage and Deprotection of Peptides from MBHA-Resin with Bromotrimethylsilane. *Tetrahedron Lett.* **1993**, *34* (48), 7713–7716.
- (258) Mellor, S. L.; McGuire, C.; Chan, W. C. N-Fmoc-Aminoxy-2-Chlorotriptyl Polystyrene Resin: A Facile Solid-Phase Methodology for the Synthesis of Hydroxamic Acids. *Tetrahedron Lett.* **1997**, *38* (18), 3311–3314.
- (259) Spengler, J.; Fernandez-Llamazares, A. I.; Albericio, F. Use of an Internal Reference for the Quantitative HPLC-UV Analysis of Solid-Phase Reactions: A Case Study of 2-Chlorotriptyl Chloride Resin. *ACS Comb. Sci.* **2013**, *15* (5), 229–234.
- (260) Cherkupally, P.; Acosta, G. A.; Nieto-Rodríguez, L.; Spengler, J.; Rodríguez, H.; Khattab, S. N.; El-Faham, A.; Shamis, M.; Luxembourg, Y.; Prohens, R.; Subiros-Funosas, R.; Albericio, F. K-Oxyma: A Strong Acylation-Promoting, 2-Ctc Resin-Friendly Coupling Additive. *European J.*

- Org. Chem.* **2013**, No. 28, 6372–6378.
- (261) Diaz-Rodriguez, V.; Mullen, D. G.; Ganusova, E.; Becker, J. M.; Distefano, M. D. Synthesis of Peptides Containing C -Terminal Methyl Esters Using Trityl Side-Chain Anchoring: Application to the Synthesis of a-Factor and a-Factor Analogs. *Org. Lett.* **2012**, *14* (22), 5648–5651.
- (262) Rocheleau, M.-J. Analytical Methods for Determination of Counter-Ions in Pharmaceutical Salts. *Curr. Pharm. Anal.* **2008**, *4* (1), 25–32.
- (263) Lentz, N. B.; Houk, R. S. Counter Ion Clusters. *Am. Soc. Mass Spectrom.* **2007**, *18*, 285–293.
- (264) Koike, M.; Iida, K.; Matsuo, T. Electron Microscopic Studies on Mode of Action of Polymyxin. *J. Bacteriol.* **1969**, *97* (1), 448–452.
- (265) Liou, J. W.; Hung, Y. J.; Yang, C. H.; Chen, Y. C. The Antimicrobial Activity of Gramicidin a Is Associated with Hydroxyl Radical Formation. *PLoS One* **2015**, *10* (1), 5–7.
- (266) Friedrich, C. L.; Moyles, D.; Beveridge, T. J.; Hancock, R. E. W. Antibacterial Action of Structurally Diverse Cationic Peptides on Gram- Positive Bacteria. *Antimicrob. Agents Chemother.* **2000**, *44* (8), 2086–2092.
- (267) Santhana Raj, L.; Hing, H. L.; Baharudin, O.; Teh Hamidah, Z.; Aida Suhana, R.; Nor Asih, C. P.; Vimala, B.; Paramasvaran, S.; Sumarni, G.; Hanjeet, K. Mesosomes Are a Definite Event in Antibiotic-Treated Staphylococcus Aureus ATCC 25923. *Trop. Biomed.* **2007**, *24* (1), 105–109.
- (268) Cajal, Y.; Ghanta, J.; Easwaran, K.; Surolia, A.; Kumar, M. Specificity for the Exchange of Phospholipids through Polymyxin B Mediated Intermembrane Molecular Contacts. *Biochemistry* **1996**, *35* (18), 5684–5695.
- (269) Grau-Campistany, A. Design, Synthesis and Study of the Biological and Biophysical Activity of Antimicrobial Peptides, University of Barcelona, Department of Organic Chemistry, 2014.
- (270) Clausell, A.; Garcia-Subirats, M.; Pujol, M.; Busquets, M. A.; Rabanal, F.; Cajal, Y. Gram-Negative Outer and Inner Membrane Models: Insertion of Cyclic Cationic Lipopeptides. *J. Phys. Chem. B* **2007**, *111* (3), 551–563.
- (271) Struck, D. K.; Hoekstra, D.; Pagano, R. E. Use of Resonance Energy Transfer To Monitor Membrane Fusion. *Biochemistry* **1981**, *20* (14), 4093–4099.
- (272) Zhao, H.; Sood, R.; Jutila, A.; Bose, S.; Fimland, G.; Nissen-Meyer, J.; Kinnunen, P. K. J. Interaction of the Antimicrobial Peptide Pheromone Plantaricin A with Model Membranes: Implications for a Novel Mechanism of Action. *Biochim. Biophys. Acta.* **2006**, *1758* (9), 1461–1474.
- (273) Murzyn, K.; Róg, T.; Pasenkiewicz-Gierula, M. Phosphatidylethanolamine-Phosphatidylglycerol Bilayer as a Model of the Inner Bacterial Membrane. *Biophys. J.* **2005**, *88* (2), 1091–1103.
- (274) Gil-Marqués, M. L.; Pachón-Ibáñez, M. E.; Pachón, J.; Smani, Y. Effect of Hypoxia on the Pathogenesis of Acinetobacter Baumannii and Pseudomonas Aeruginosa in Vitro and in Murine Experimental Models of Infection. *Infect. Immun.* **2018**, *86* (10), 1–12.
- (275) Ramesh, S.; Govender, T.; Kruger, H. G.; Albericio, F.; De La Torre, B. G. An Improved and Efficient Strategy for the Total Synthesis of a Colistin-like Peptide. *Tetrahedron Lett.* **2016**, *57* (17), 1885–1888.
- (276) Yeaman, M. R.; Yount, N. Y. Mechanisms of Antimicrobial Peptide Action and Resistance. *Pharmacol. Reviews* **2003**, *55* (1), 27–55.
- (277) Pasupuleti, M.; Schmidtchen, A.; Malmsten, M. Antimicrobial Peptides: Key Components of the Innate Immune System. *Crit. Rev. Biotechnol.* **2012**, *32* (2), 143–171.
- (278) Hoffmann, W.; Richter, K.; Kreil, G. A Novel Peptide Designated PYLa and Its Precursor as Predicted from Cloned MRNA of Xenopus Laevis Skin. *EMBO J.* **1983**, *2* (5), 711–714.
- (279) Gibson, B. W.; Poulter, L.; Williams, D. H.; Maggio, J. E. Novel Peptide Fragments Originating from PGLa and the Caerulein and Xenopsin Precursors from Xenopus Laevis. *J. Biol. Chem.* **1986**, *261* (12), 5341–5349.
- (280) Zasloff, M. Magainins, a Class of Antimicrobial Peptides from Xenopus Skin: Isolation, Characterization of Two Active Forms, and Partial CDNA Sequence of a Precursor. *Proc. Natl. Acad. Sci. U. S. A.* **1987**, *84* (15), 5449–5453.

- (281) Zasloff, M. Antimicrobial Peptides of Multicellularorganisms. *Nature* **2002**, *415*, 389–395.
- (282) Bevins, C. L.; Zasloff, M. Peptides from Frog Skin. *Annu. Rev. Biochem.* **1990**, *59* (1), 395–414.
- (283) Maloy, W. L.; Kari, U. P. Structure–Activity Studies on Magainins and Other Host Defense Peptides. *Biopolymers* **1995**, *37* (2), 105–122.
- (284) Strandberg, E.; Tiltak, D.; Ieronimo, M.; Kanithasen, N.; Wadhvani, P.; Ulrich, A. S. Influence of C-Terminal Amidation on the Antimicrobial and Hemolytic Activities of Cationic  $\alpha$ -Helical Peptides. *Pure Appl. Chem.* **2007**, *79* (4), 717–728.
- (285) Soravia, E.; Martini, G.; Zasloff, M. Antimicrobial Properties of Peptides from *Xenopus* Granular Gland Secretions. *FEBS Lett.* **1988**, *228* (2), 337–340.
- (286) Reißer, S.; Prock, S.; Heinzmann, H.; Ulrich, A. S. Protein ORIGAMI: A Program for the Creation of 3D Paper Models of Folded Peptides. *Biochem. Mol. Biol. Educ.* **2018**, *46* (4), 403–409.
- (287) Qian, S.; Wang, C.; Yang, L.; Huang, H. W. Structure of the Alamethicin Pore Reconstructed by X-Ray Diffraction Analysis. *Biophys. J.* **2008**, *94* (9), 3512–3522.
- (288) Lee, M. T.; Sun, T. L.; Hung, W. C.; Huang, H. W. Process of Inducing Pores in Membranes by Melittin. *Proc. Natl. Acad. Sci. U. S. A.* **2013**, *110* (35), 14243–14248.
- (289) Matsuzaki, K.; Mitani, Y.; Akada, K. Y.; Murase, O.; Yoneyama, S.; Zasloff, M.; Miyajima, K. Mechanism of Synergism between Antimicrobial Peptides Magainin 2 and PGLa. *Biochemistry* **1998**, *37* (43), 15144–15153.
- (290) Grau-Campistany, A.; Strandberg, E.; Wadhvani, P.; Reichert, J.; Bürck, J.; Rabanal, F.; Ulrich, A. S. Hydrophobic Mismatch Demonstrated for Membranolytic Peptides, and Their Use as Molecular Rulers to Measure Bilayer Thickness in Native Cells. *Sci. Rep.* **2015**, *5*, 20–24.
- (291) Grau-Campistany, A.; Strandberg, E.; Wadhvani, P.; Rabanal, F.; Ulrich, A. S. Extending the Hydrophobic Mismatch Concept to Amphiphilic Membranolytic Peptides. *J. Phys. Chem. Lett.* **2016**, *7* (7), 1116–1120.
- (292) Gagnon, M. C.; Strandberg, E.; Grau-Campistany, A.; Wadhvani, P.; Reichert, J.; Bürck, J.; Rabanal, F.; Auger, M.; Paquin, J. F.; Ulrich, A. S. Influence of the Length and Charge on the Activity of  $\alpha$ -Helical Amphipathic Antimicrobial Peptides. *Biochemistry* **2017**, *56* (11), 1680–1695.
- (293) Strandberg, E.; Bentz, D.; Wadhvani, P.; Bürck, J.; Ulrich, A. S. Terminal Charges Modulate the Pore Forming Activity of Cationic Amphipathic Helices. *Biochim. Biophys. Acta - Biomembr.* **2020**, *1862* (4), 183243.
- (294) Habermann, E.; Zeuner, G. Comparative Studies of Native and Synthetic Melittins. *Naunyn. Schmiedebergs. Arch. Pharmacol.* **1971**, *270* (1), 1–9.
- (295) H. Steiner, D. Hultmark, A. Engstom, H. Bennich, H. G. B. Sequence and Specificity of Two Antibacterial Proteins Involved in Insect Immunity. *Nature* **1981**, *292*, 246–248.
- (296) Silvestro, L.; Weiser, J. N.; Axelsen, P. H.; Gupta, K.; Weiser, J. H.; Axelsen, P. H. Antibacterial and Antimembrane Activities of Cecropin A in *Escherichia Coli*. *Antimicrob Agents Chemother.* **2000**, *44* (3), 602–607.
- (297) Boman, H. G.; Wade, D.; Boman, I. A.; Wählin, B.; Merrifield, R. B. Antibacterial and Antimalarial Properties of Peptides That Are Cecropin-Melittin Hybrids. *FEBS Lett.* **1989**, *259* (1), 103–106.
- (298) Saugar, J. M.; Rodríguez-Hernández, M. J.; De La Torre, B. G.; Pachón-Ibañez, M. E.; Fernández-Reyes, M.; Andreu, D.; Pachón, J.; Rivas, L. Activity of Cecropin A-Melittin Hybrid Peptides against Colistin-Resistant Clinical Strains of *Acinetobacter Baumannii*: Molecular Basis for the Differential Mechanisms of Action. *Antimicrob. Agents Chemother.* **2006**, *50* (4), 1251–1256.
- (299) Ferre, R.; Badosa, E.; Feliu, L.; Planas, M.; Montesinos, E.; Bardají, E. Inhibition of Plant-Pathogenic Bacteria by Short Synthetic Cecropin A-Melittin Hybrid Peptides. *Appl. Environ. Microbiol.* **2006**, *72* (5), 3302–3308.
- (300) Andreu, D.; Ubach, J.; Boman, A.; Wählin, B.; Wade, D.; Merrifield, R. B.; Boman, H. G. Shortened Cecropin A-Melittin Hybrids: Significant Size Reduction Retains Potent Antibiotic Activity. *FEBS Lett.* **1992**, *296* (2), 190–194.



- (301) Badosa, E.; Ferre, R.; Planas, M.; Feliu, L.; Besalú, E.; Cabrefiga, J.; Bardají, E.; Montesinos, E. A Library of Linear Undecapeptides with Bactericidal Activity against Phytopathogenic Bacteria. *Peptides* **2007**, *28* (12), 2276–2285.
- (302) Alves, C. S.; Melo, M. N.; Franquelim, H. G.; Ferre, R.; Planas, M.; Feliu, L.; Bardají, E.; Kowalczyk, W.; Andreu, D.; Santos, N. C.; Fernandes, M. X.; Castanho, M. A. R. B. Escherichia Coli Cell Surface Perturbation and Disruption Induced by Antimicrobial Peptides BP100 and PepR. *J. Biol. Chem.* **2010**, *285* (36), 27536–27544.
- (303) Eggenberger, K.; Mink, C.; Wadhvani, P.; Ulrich, A. S.; Nick, P. Using the Peptide BP100 as a Cell-Penetrating Tool for the Chemical Engineering of Actin Filaments within Living Plant Cells. *ChemBioChem* **2011**, *12* (1), 132–137.
- (304) Wadhvani, P.; Strandberg, E.; Van Den Berg, J.; Mink, C.; Bürck, J.; Ciriello, R. A. M.; Ulrich, A. S. Dynamical Structure of the Short Multifunctional Peptide BP100 in Membranes. *Biochim. Biophys. Acta* **2014**, *1838* (3), 940–949.
- (305) Zamora-Carreras, H.; Strandberg, E.; Mühlhäuser, P.; Bürck, J.; Wadhvani, P.; Jiménez, M. Á.; Bruix, M.; Ulrich, A. S. Alanine Scan and <sup>2</sup>H NMR Analysis of the Membrane-Active Peptide BP100 Point to a Distinct Carpet Mechanism of Action. *Biochim. Biophys. Acta* **2016**, *1858* (6), 1328–1338.
- (306) Velluz, L.; Legrand, M.; Grosjean, M. *Optical Circular Dichroism: Principles, Measurements, and Applications.*, Verlag Che.; New York and London, 1965.
- (307) Johnson, W. C. Proteins Through Circular Dichroism. *Ann. Rev. Biophys. Biophys. Chem* **1988**, *17* (Cd), 145–166.
- (308) Brahms, S.; Brahms, J. Determination of Protein Secondary Structure in Solution by Vacuum Ultraviolet Circular Dichroism. *J. Mol. Biol.* **1980**, *138* (2), 149–178.
- (309) Mason, J. Conventions for the Reporting of Nuclear Magnetic Shielding (or Shift) Tensors Suggested by Participants in the NATO ARW on NMR Shielding Constants at the University of Maryland, College Park, July 1992. *Solid State Nucl. Magn. Reson.* **1993**, *2* (5), 285–288.
- (310) Filippov, A. V.; Khakimov, A. M.; Munavirov, B. V. <sup>31</sup>P NMR Studies of Phospholipids. *Annu. Reports NMR Spectrosc.* **2015**, *85*, 27–92.
- (311) Lee, J. H.; Komoroski, R. A.; Chu, W. J.; Dudley, J. A. Methods and Applications of Phosphorus NMR Spectroscopy in Vivo. In *Annual Reports on NMR Spectroscopy*; 2012; Vol. 75, pp 115–160.
- (312) Bechinger, B.; Kinder, R.; Helmle, M.; Vogt, T. C. B.; Harzer, U.; Schinzel, S. Peptide Structural Analysis by Solid-State NMR Spectroscopy. *Biopolym. - Pept. Sci. Sect.* **1999**, *51* (3), 174–190.
- (313) Bechinger, B.; Sizun, C. Alignment and Structural Analysis of Membrane Polypeptides by <sup>15</sup>N and <sup>31</sup>P Solid-State NMR Spectroscopy. *Concepts Magn. Reson.* **2003**, *18A*, 130–145.
- (314) Blondelle, S. E.; Houghten, R. A. Design of Model Amphipathic Peptides Having Potent Antimicrobial Activities. *Biochemistry* **1992**, *31* (50), 12688–12694.
- (315) Béven, L.; Castano, S.; Dufourcq, J.; Wieslander, Å.; Wróblewski, H. The Antibiotic Activity of Cationic Linear Amphipathic Peptides: Lessons from the Action of Leucine/Lysine Copolymers on Bacteria of the Class Mollicutes. *Eur. J. Biochem.* **2003**, *270* (10), 2207–2217.
- (316) Whitmore, L.; Wallace, B. A. DICHROWEB, an Online Server for Protein Secondary Structure Analyses from Circular Dichroism Spectroscopic Data. *Nucleic Acids Res.* **2004**, *32* (WEB SERVER ISS.), 668–673.
- (317) Kučerka, N.; Tristram-Nagle, S.; Nagle, J. F. Structure of Fully Hydrated Fluid Phase Lipid Bilayers with Monounsaturated Chains. *J. Membr. Biol.* **2006**, *208* (3), 193–202.
- (318) Strandberg, E.; Zerweck, J.; Wadhvani, P.; Ulrich, A. S. Synergistic Insertion of Antimicrobial Magainin-Family Peptides in Membranes Depends on the Lipid Spontaneous Curvature. *Biophys. J.* **2013**, *104* (6), L9.
- (319) Strandberg, E.; Tiltak, D.; Ehni, S.; Wadhvani, P.; Ulrich, A. S. Lipid Shape Is a Key Factor for Membrane Interactions of Amphipathic Helical Peptides. *Biochim. Biophys. Acta* **2012**, *1818* (7), 1764–1776.

- 
- (320) Strandberg, E.; Bentz, D.; Wadhvani, P.; Ulrich, A. S. Chiral Supramolecular Architecture of Stable Transmembrane Pores Formed by an  $\alpha$ -Helical Antibiotic Peptide in the Presence of Lyso-Lipids. *Sci. Rep.* **2020**, *10* (1), 1–17.
- (321) Zaragoza, A.; Aranda, F. J.; Espuny, M. J.; Teruel, J. A.; Marqués, A.; Manresa, Á.; Ortiz, A. Hemolytic Activity of a Bacterial Trehalose Lipid Biosurfactant Produced by *Rhodococcus* Sp.: Evidence for a Colloid-Osmotic Mechanism. *Langmuir* **2010**, *26* (11), 8567–8572.
- (322) Sreerama, N.; Woody, R. W. Estimation of Protein Secondary Structure from Circular Dichroism Spectra: Comparison of CONTIN, SELCON, and CDSSTR Methods with an Expanded Reference Set. *Anal. Biochem.* **2000**, *287* (2), 252–260.
- (323) Rance, M.; Byrd, R. A. Obtaining High-Fidelity Spin-1/2 Powder Spectra in Anisotropic Media: Phase-Cycled Hahn Echo Spectroscopy. *J. Magn. Reson.* **1983**, *52* (2), 221–240.
- (324) Fung, B. M.; Khitrin, A. K.; Ermolaev, K. An Improved Broadband Decoupling Sequence for Liquid Crystals and Solids. *J. Magn. Reson.* **2000**, *142* (1), 97–101.
- (325) Levitt, M. H.; Suter, D.; Ernst, R. R. Spin Dynamics and Thermodynamics in Solid-State NMR Cross Polarization. *J. Chem. Phys.* **1986**, *84* (8), 4243–4255.



## **APPENDIX**



## Appendix I: Abbreviations and acronyms

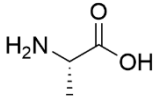
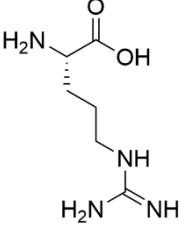
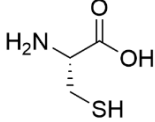
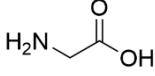
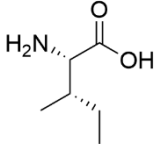
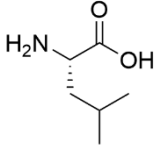
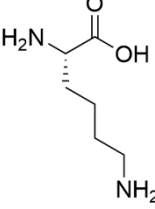
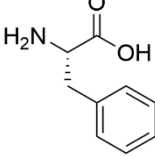
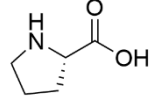
A	Absorbance
AA	Amino acid
Ac	Acetyl
ACN	Acetonitrile
AcOH	Acetic acid
AMP	Antimicrobial peptide
ANTS	1-aminonaphthalene-3,6,8-trisulfonic acid
ATCC	American Type Culture Collection
ABSSSI	Acute bacterial skin and skin structure infections
B <sub>0</sub>	Magnetic field
Boc	<i>tert</i> -Butoxycarbonyl
Boc <sub>2</sub> O	Di- <i>tert</i> -butyl dicarbonate
CD	Circular dichroism
CFU	Colony-forming unit
CSA	Chemical shift anisotropy
CMS	Colistimethate sodium
2-CTC	2-Chlorotrityl chloride resin
DCC	<i>N-N'</i> -Dicyclohexylcarbodiimide
DCM	Dichloromethane
DErPC	1,2-Dierucoyl- <i>sn</i> -glycero-3- phosphocholine
DErPG	1,2-Dierucoyl- <i>sn</i> -glycero-3-phospho-(1'- <i>rac</i> -glycerol)
DIC	<i>N-N'</i> -Diisopropylcarbodiimide
DisC <sub>3</sub> (5)	3,3-Dipropylthiadicyanide iodide
DIPEA	<i>N-N'</i> -Diisopropylethylamine
DMAP	4-Dimethylaminopyridine
DMF	Dimethyl formamide
DMPC	1,2-Dimyristoyl- <i>sn</i> -glycero-3-phosphocholine
DMPG	1,2-Dimyristoyl- <i>sn</i> -glycero-3-phospho-(1'- <i>rac</i> -glycerol)
DMSO	Dimethyl sulfoxide
DOTAP	1,2-Dioleoyl-3-trimethylammonium-propane
DPX	<i>p</i> -Xylene-bis( <i>N</i> -pyridinium bromide)
DSM	Deutsche Samm Mikroorganismen und Zellkulturen
EMA	European Medicines Agency
eq	Equivalent

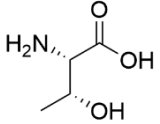
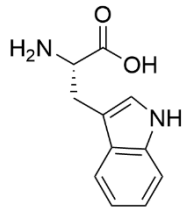
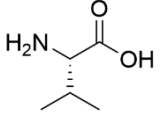
ESI MS	Electrospray ionization mass spectrometry
ESI-HR MS	Electrospray ionization high resolution mass spectrometry
EtOAc	Ethyl acetate
EtOH	Ethanol
Et <sub>2</sub> O	Diethyl ether
f	Functionalization
F	Fluorescence
FA	Fatty acid
FDA	Food and Drug Administration
FID	Free induction decay
Fmoc	9-Fluorenylmethoxycarbonyl
Fmoc-Cl	9-Fluorenylmethoxycarbonyl chloride
FRET	Fluorescence resonance energy transfer
G0595t30	Linear HPLC gradient from 5 % to 95 % of B over 30 minutes, using as elution system A: 0.045 % TFA in H <sub>2</sub> O and B: 0.036 % TFA in ACN
HAP	Hospital-acquired bacterial pneumonia
HATU	<i>N</i> -[(Dimethylamino)-1 <i>H</i> -1,2,3-triazolo-[4,5- <i>b</i> ]pyridin-1-ylmethylene]- <i>N</i> -methylmethanaminium hexafluorophosphate <i>N</i> -oxide
HFIP	1,1,1,3,3,3-Hexafluoro-2-propanol
HEPES	4-(2-Hydroxyethyl)piperazine-1-ethanesulfonic acid
HOAt	1-Hydroxy-7-azabenzotriazole
HOBt	1-Hydroxybenzotriazole
HPLC	High-performance liquid chromatography
HPLC-MS	High-performance liquid chromatography-mass spectrometry
IDSA	Infectious Disease Society of America
LB	Luria broth
LPS	Lipopolysaccharide
Lyso-MPC	1-Myristoyl-2-hydroxy- <i>sn</i> -glycero-3-phosphocholine
MBHA	4-Methylbenzhydramine
MDR	Multidrug-resistant
MeOH	Methanol
MHB	Mueller-Hinton Broth
MIC	Minimum inhibitory concentration
MRSA	Multidrug-resistant <i>Staphylococcus aureus</i>
MS	Mass spectrometry
Mtt	4-Methyltrityl

MW	Molecular weight
NBD	7-Nitrobenz-2-oxa-1,3-diazol-4-yl
NMR	Nuclear magnetic resonance
OD	Optical density
Pbf	2,2,4,6,7-Pentamethyldihydrobenzofuran-5-sulfonyl
PDF	Peptide deformylase
PG	Protecting group
POPC	1-Palmitoyl-2-oleoyl- <i>sn</i> -glycero-3-phosphocholine
POPE	1-Palmitoyl-2-oleoyl- <i>sn</i> -glycero-3-phosphoethanolamine
POPG	1-Palmitoyl-2-oleoyl- <i>sn</i> -glycero-3-phospho-(1'- <i>rac</i> -glycerol)
ppm	Parts per million
PxB	Polymyxin B
PxBN	Polymyxin B nonapeptide
PxE	Polymyxin E / colistin
py	Pyrene
Rh	Rhodamine
SAR	Structure-activity relationship
ssNMR	Solid-state nuclear magnetic resonance
SPPS	Solid phase peptide synthesis
<sup>t</sup> Bu	<i>tert</i> -Butyl
TES	Triethylsilane
TESBr	Triethylsilyl bromide
TEM	Transmission electron microscopy
TFA	Trifluoroacetic acid
TFE	Trifluoroethanol
TIS	Triisopropylsilane
TLC	Thin layer chromatography
TMSCl	Trimethylsilyl chloride
t <sub>R</sub>	Retention time
Trt	Trityl
Trt-Cl	Trityl chloride
TSA	Tryptone soya agar
UV	Ultraviolet
VAP	Ventilator associated pneumonia
WHO	World Health Organization

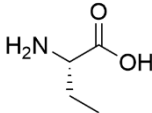
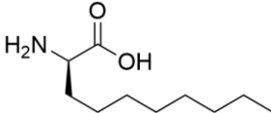
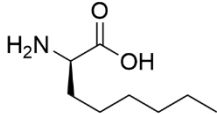
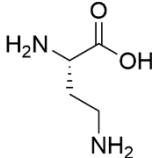
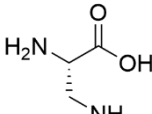
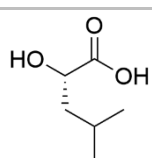
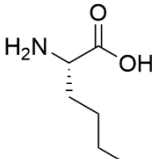
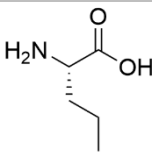


## Appendix II: Amino acids used in this thesis

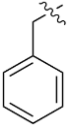
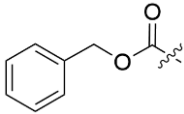
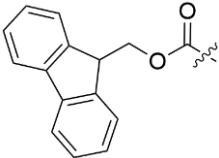
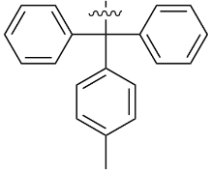

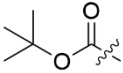
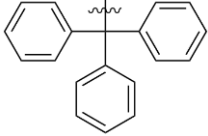
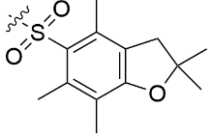
Amino acid	Code	Structure
<b>L-Alanine</b>	Ala, A	
<b>L-Arginine</b>	Arg, R	
<b>L-Cysteine</b>	Cys, C	
<b>Glycine</b>	Gly, G	
<b>L-Isoleucine</b>	Ile, I	
<b>L-Leucine</b>	Leu, L	
<b>L-Lysine</b>	Lys, K	
<b>L-Phenylalanine</b>	Phe, F	
<b>L-Proline</b>	Pro, P	

<b>L-Threonine</b>	Thr, T	
<b>L-Tryptophan</b>	Trp, W	
<b>L-Valine</b>	Val, V	

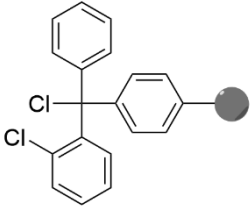
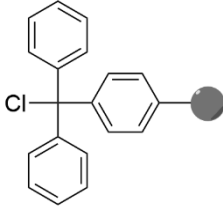
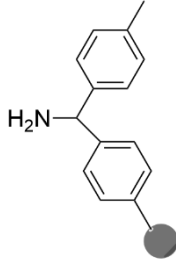
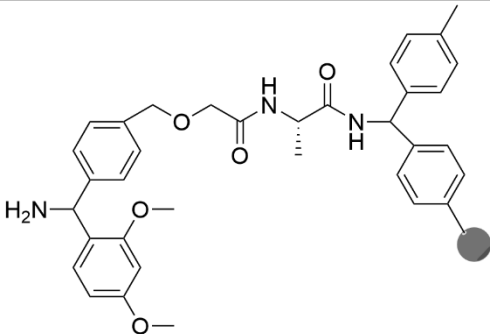
## Appendix III: Special amino acids used in this thesis

Amino acid	Code	Structure
L-2-Aminobutanoic acid	Abu	
D-2-Aminodecanoic acid	D-Adec	
D-2-Amino-octanoic acid	D-Aoc	
L-2,4-Diaminobutiric acid	Dab	
L-2,3-Diaminopropanoic acid	Dap	
L-Leucic acid	ALeu	
L-Norleucine	Nle	
L-Norvaline	Nva	

## Appendix IV: Protecting groups

Protecting group	Symbol	Structure
Benzyl	Bn	
Benzyloxycarbonyl	Z	
9-Fluorenylmethoxycarbonyl	Fmoc	
4-Methyltrityl	Mtt	
<i>tert</i> -Butyl	<sup>t</sup> Bu	
<i>tert</i> -Butoxycarbonyl	Boc	
Trityl	Trt	
2,2,4,6,7-Pentamethyldihydrobenzofuran-5-sulfonyl	Pbf	

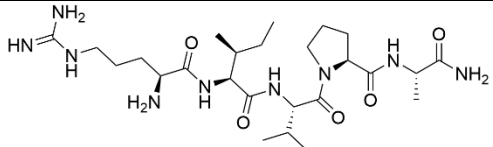
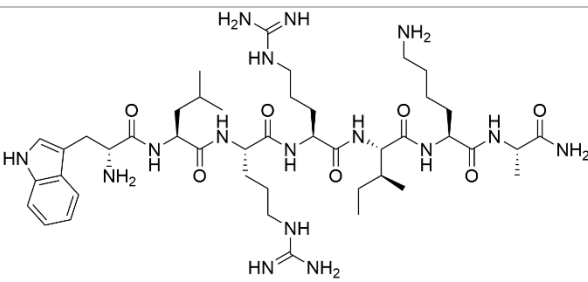
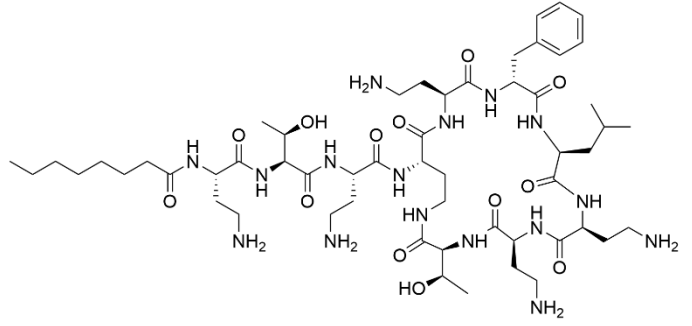
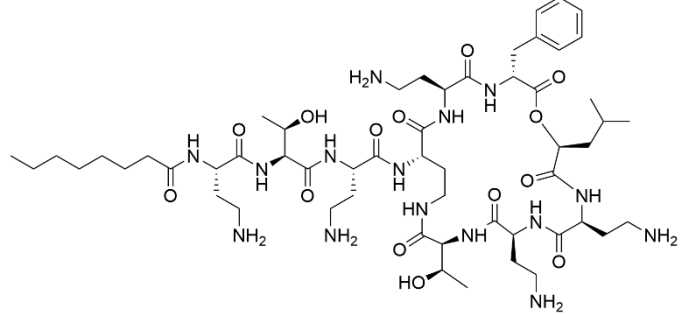
## Appendix V: Solid supports

Resin	Structure
2-CTC	
Trt-Cl	
MBHA	
RL-Ala-MBHA	

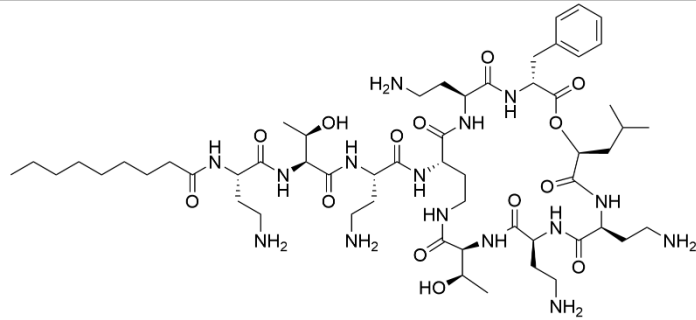
## Appendix VI: Coupling reagents and additives

Coupling agent	Structure
DIC	The structure shows a central carbon atom double-bonded to two nitrogen atoms. Each nitrogen atom is further bonded to a tert-butyl group, represented by a central carbon atom bonded to three methyl groups.
DMAP	The structure shows a pyridine ring with a nitrogen atom at the bottom position. A dimethylamino group, consisting of a nitrogen atom bonded to two methyl groups, is attached to the 4-position of the ring.
HATU	The structure shows a benzotriazole ring system. The central nitrogen atom is bonded to a dimethyliminium group (N(CH3)2+). The two terminal nitrogen atoms are also bonded to methyl groups. The central nitrogen is also bonded to a uronium group (C(=O)N(CH3)2). The entire cation is associated with a hexafluorophosphate anion (PF6-).
HOAt	The structure shows a benzotriazole ring system with a hydroxyl group (-OH) attached to the 4-position of the ring.
HOBt	The structure shows a benzotriazole ring system with a hydroxyl group (-OH) attached to the 4-position of the ring.
K-Oxyma	The structure shows a central carbon atom double-bonded to a nitrogen atom which is bonded to a hydroxyl group (-OH). The central carbon is also single-bonded to a cyano group (-C≡N) and a carbonyl group (-C(=O)-). The carbonyl group is further bonded to an ethoxy group (-OCH2CH3).

**Appendix VII: Synthesized peptides**

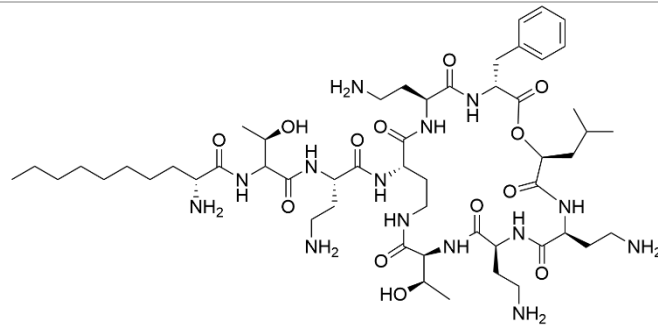
Peptide	Structure and sequence
<b>Dusquetide</b>	 <p data-bbox="790 548 1061 582">Arg-Ile-Val-Pro-Ala</p>
<b>RR4 (Fragment 8-14)</b>	 <p data-bbox="726 896 1125 929">Trp-Leu- Arg-Arg-Ile-Lys-Ala</p>
<b>PxB3</b>	 <p data-bbox="566 1288 1276 1332">C8-Dab-Thr-Dab-[Dab-Dab-DPhe-Leu-Dab-Dab-Thr]</p>
<b>1</b>	 <p data-bbox="566 1680 1276 1724">C8-Dab-Thr-Dab-[Dab-Dab-DPhe-ALeu-Dab-Dab-Thr]</p>

2



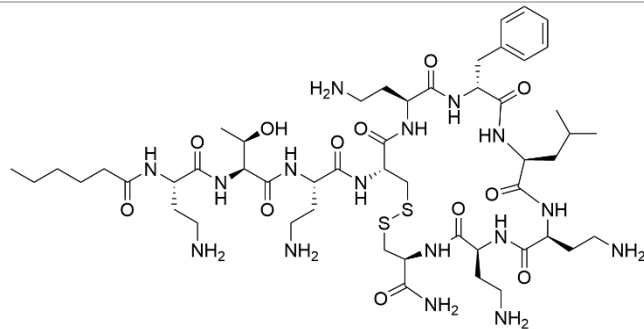
C9-Dab-Thr-Dab-[Dab-Dab-DPhe-ALeu-Dab-Dab-Thr]

3



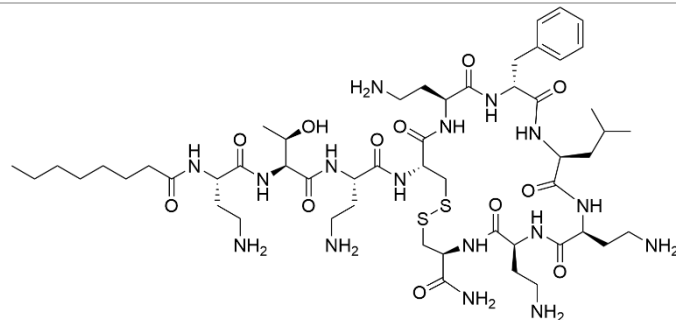
DAdec-Thr-Dab-[Dab-Dab-DPhe-ALeu-Dab-Dab-Thr]

4



C6-Dab-Thr-Dab-[Cys-Dab-DPhe-Leu-Dab-Dab-DCys]

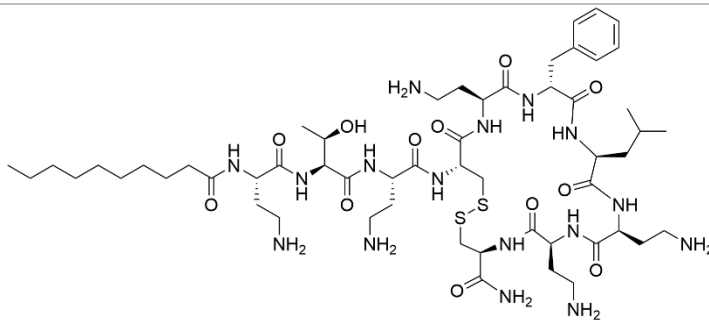
5



C8-Dab-Thr-Dab-[Cys-Dab-DPhe-Leu-Dab-Dab-DCys]

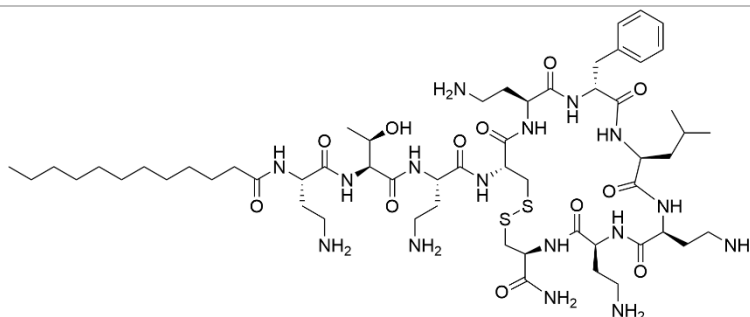


6



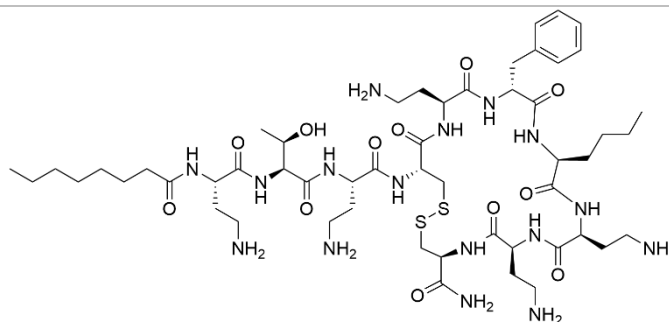
C10-Dab-Thr-Dab-[Cys-Dab-DPhe-Leu-Dab-Dab-DCys]

7



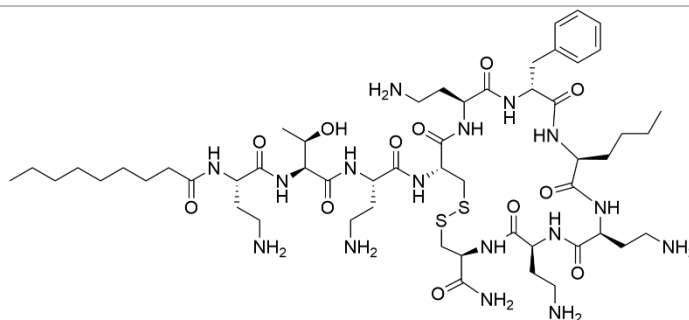
C12-Dab-Thr-Dab-[Cys-Dab-DPhe-Leu-Dab-Dab-DCys]

8



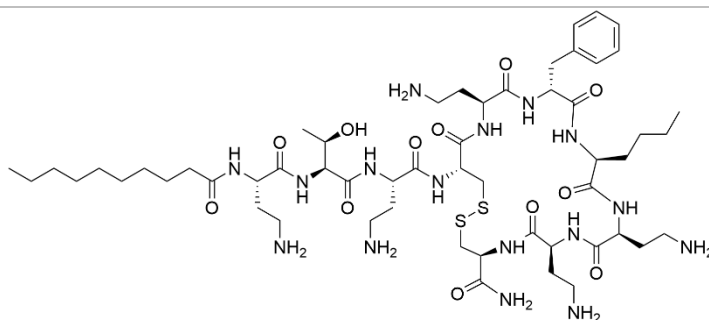
C8-Dab-Thr-Dab-[Cys-Dab-DPhe-Nle-Dab-Dab-DCys]

9



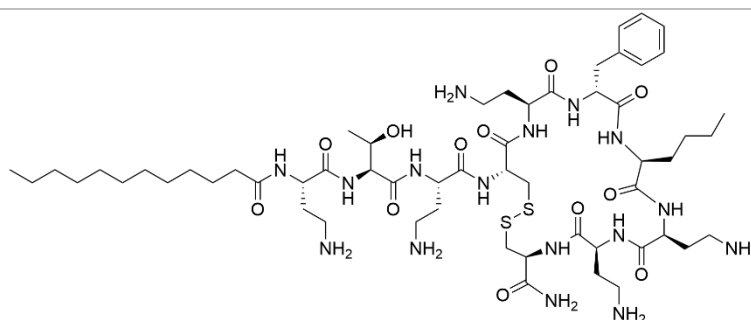
C9-Dab-Thr-Dab-[Cys-Dab-DPhe-Nle-Dab-Dab-DCys]

10



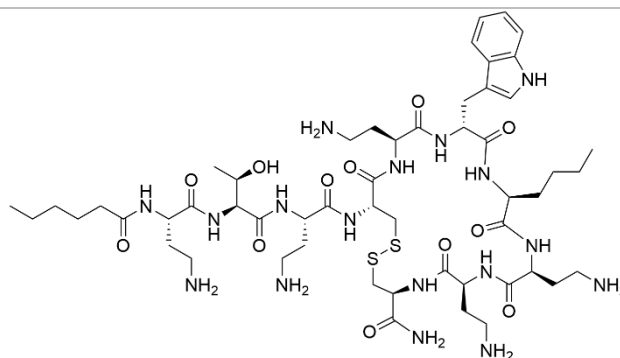
C10-Dab-Thr-Dab-[Cys-Dab-DPhe-Nle-Dab-Dab-DCys]

11



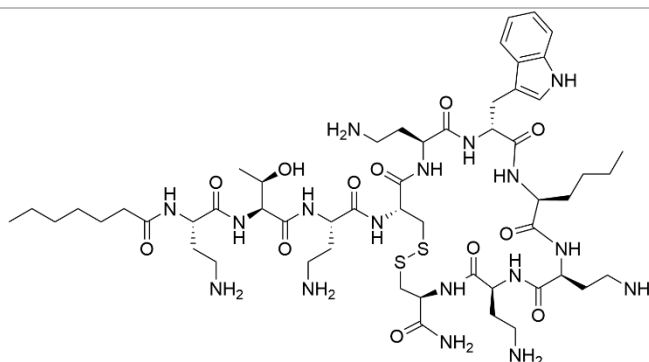
C12-Dab-Thr-Dab-[Cys-Dab-DPhe-Nle-Dab-Dab-DCys]

12



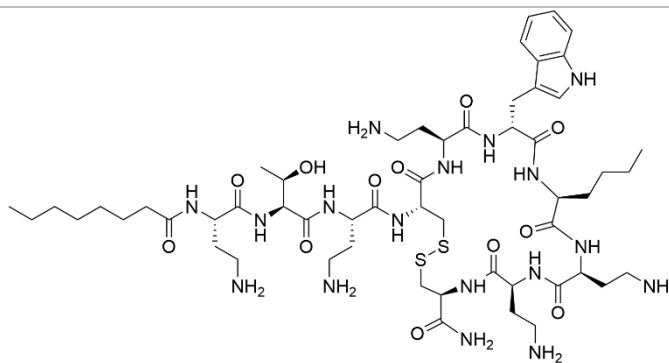
C6-Dab-Thr-Dab-[Cys-Dab-DTrp-Nle-Dab-Dab-DCys]

13



C7-Dab-Thr-Dab-[Cys-Dab-DTrp-Nle-Dab-Dab-DCys]

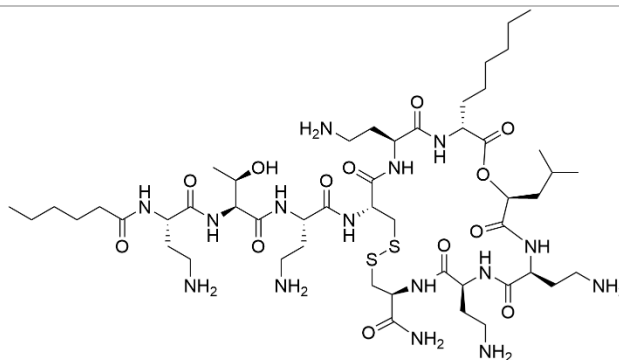
14



C8-Dab-Thr-Dab-[Cys-Dab-DTrp-Nle-Dab-Dab-DCys]

---

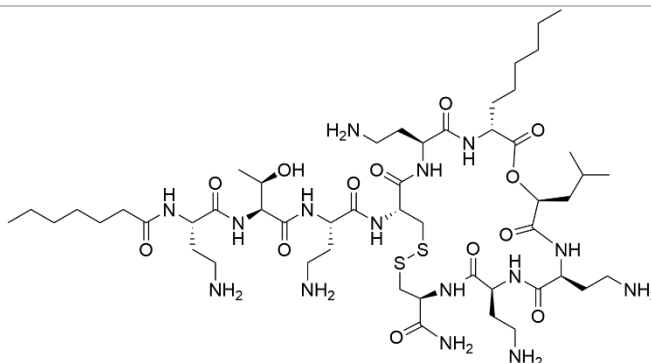
15



C6-Dab-Thr-Dab-[Cys-Dab-DAoc-ALeu-Dab-Dab-DCys]

---

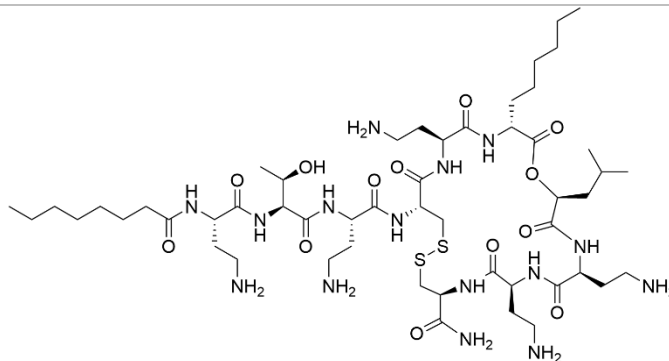
16



C7-Dab-Thr-Dab-[Cys-Dab-DAoc-ALeu-Dab-Dab-DCys]

---

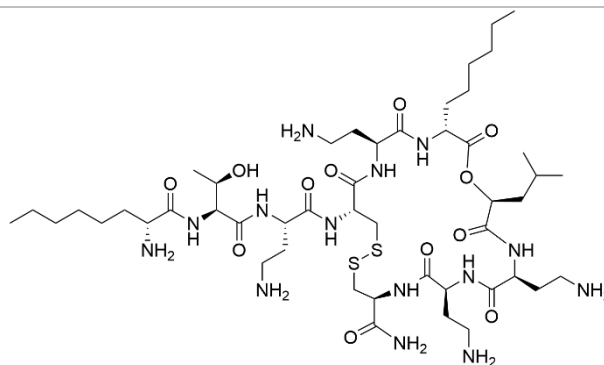
17



C8-Dab-Thr-Dab-[Cys-Dab-DAoc-ALeu-Dab-Dab-DCys]

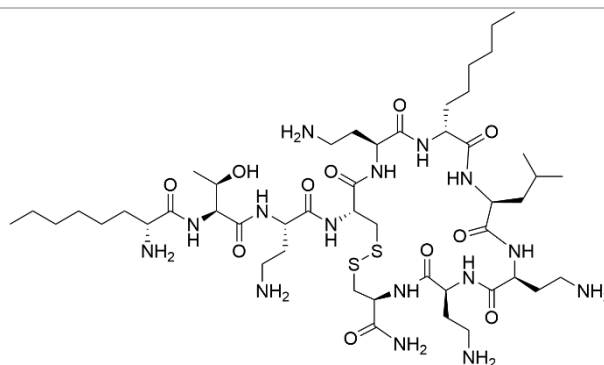
---

18



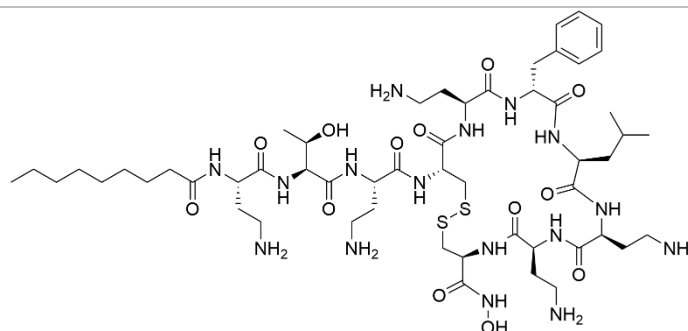
DAoc-Thr-Dab-[Cys-Dab-DAoc-ALeu-Dab-Dab-DCys]

19



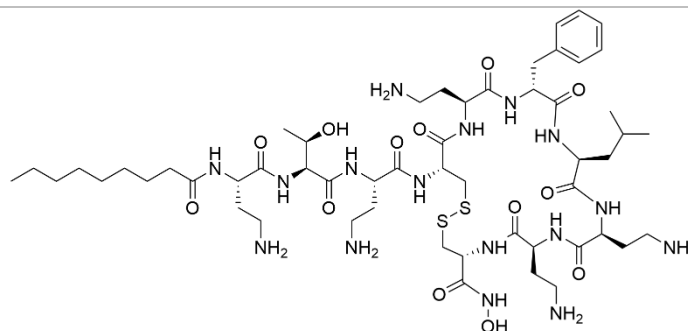
DAoc-Thr-Dab-[Cys-Dab-DAoc-Leu-Dab-Dab-DCys]

20



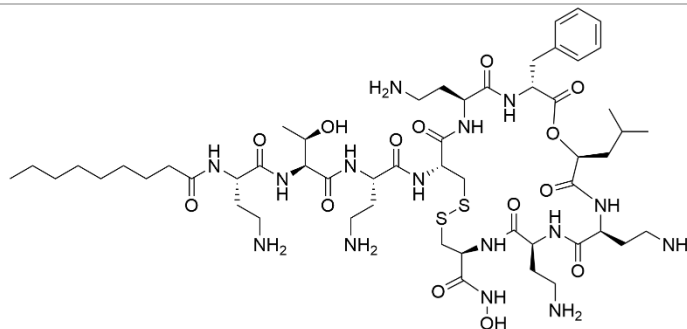
C9-Dab-Thr-Dab-[Cys-Dab-DPhe-Leu-Dab-Dab-DCys-NHOH]

21



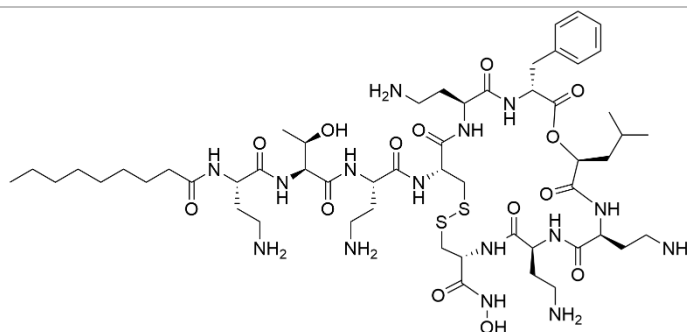
C9-Dab-Thr-Dab-[Cys-Dab-DPhe-Leu-Dab-Dab-Cys-NHOH]

22



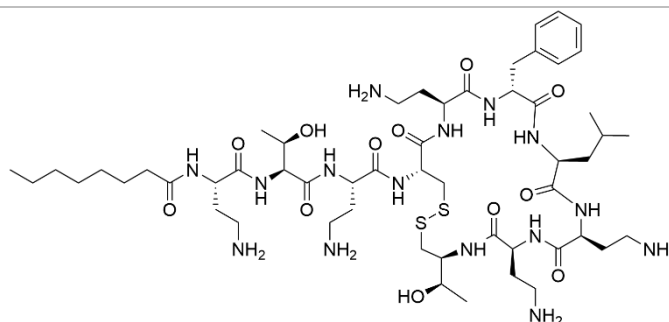
C9-Dab-Thr-Dab-[Cys-Dab-DPhe-ALeu-Dab-Dab-DCys-NHOH]

23



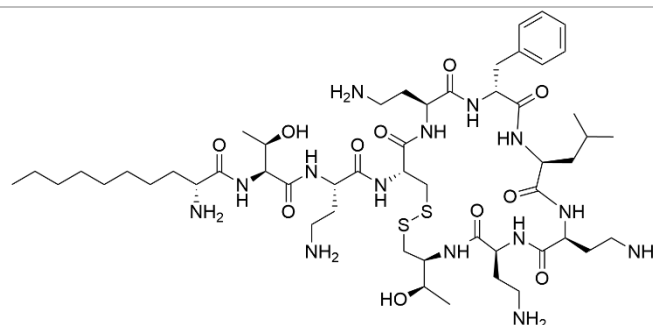
C9-Dab-Thr-Dab-[Cys-Dab-DPhe-ALeu-Dab-Dab-Cys-NHOH]

24



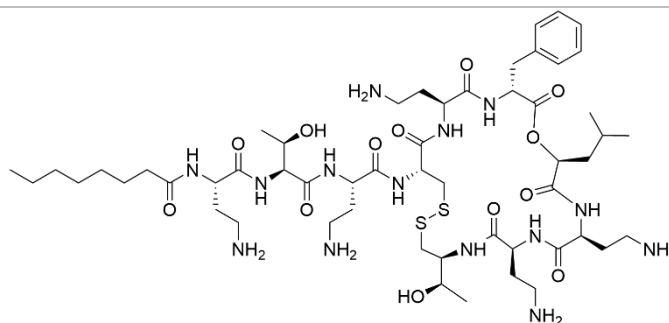
C8-Dab-Thr-Dab-[Cys-Dab-DPhe-Leu-Dab-Dab-Ttr]

25



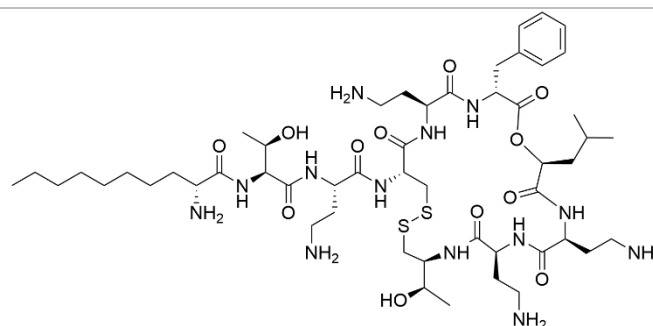
DAdec-Thr-Dab-[Cys-Dab-DPhe-Leu-Dab-Dab-Ttr]

26



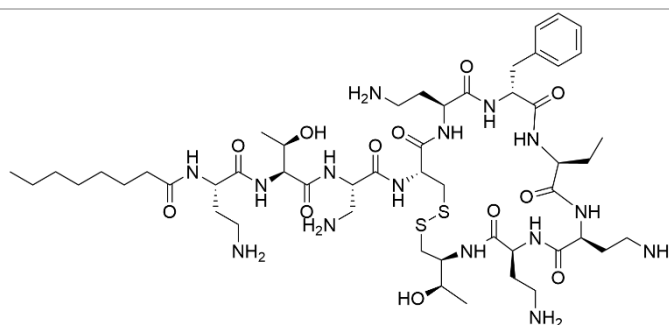
C8-Dab-Thr-Dab-[Cys-Dab-DPhe-ALeu-Dab-Dab-Ttr]

27



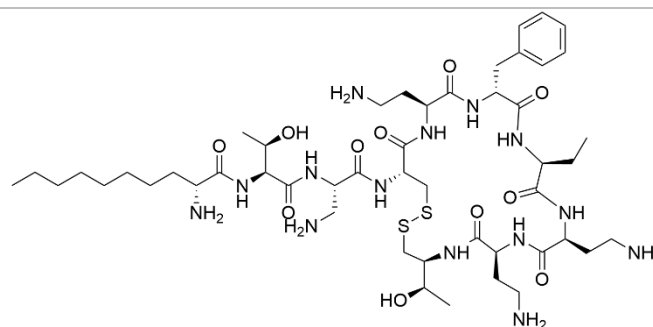
DAdec-Thr-Dab-[Cys-Dab-DPhe-ALeu-Dab-Dab-Ttr]

28



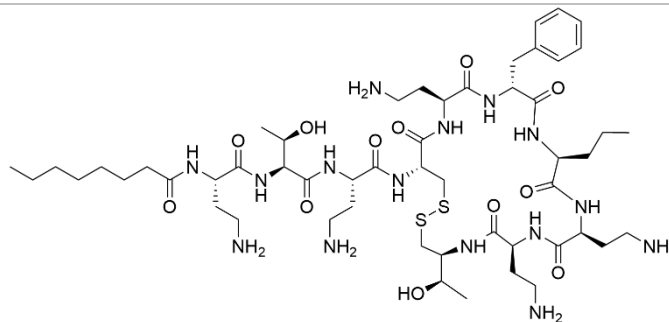
C8-Dab-Thr-Dap-[Cys-Dab-DPhe-Abu-Dab-Dab-Ttr]

29



DAdec-Thr-Dap-[Cys-Dab-DPhe-Abu-Dab-Dab-Ttr]

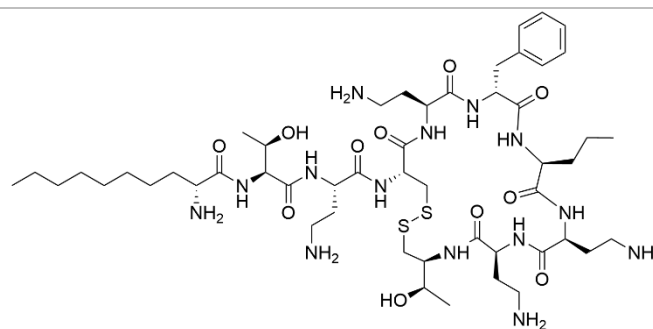
30



C8-Dab-Thr-Dab-[Cys-Dab-DPhe-Nva-Dab-Dab-Ttr]

---

31



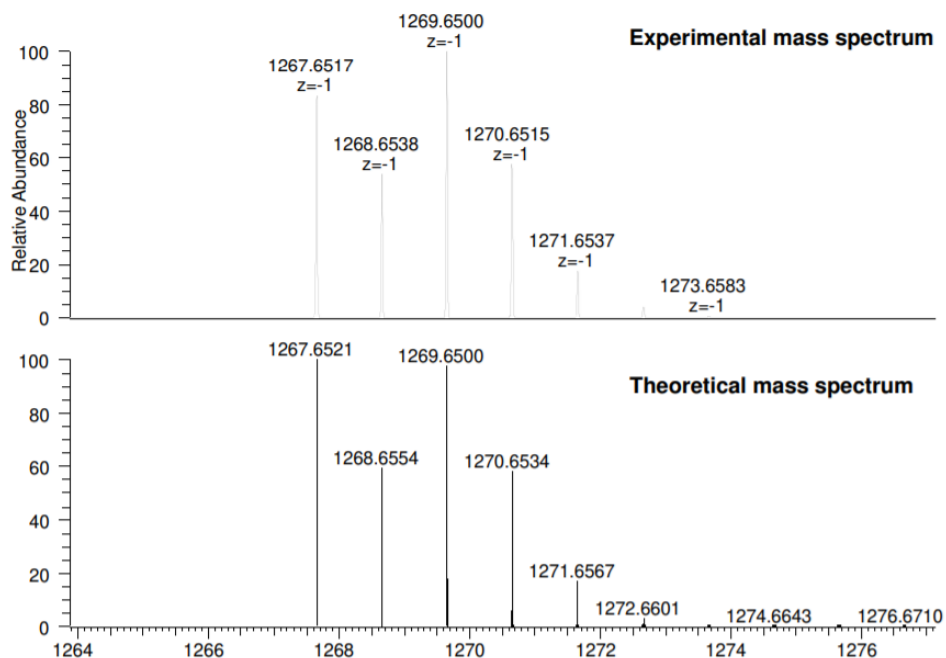
DAdec-Thr-Dab-[Cys-Dab-DPhe-Nva-Dab-Dab-Ttr]

---

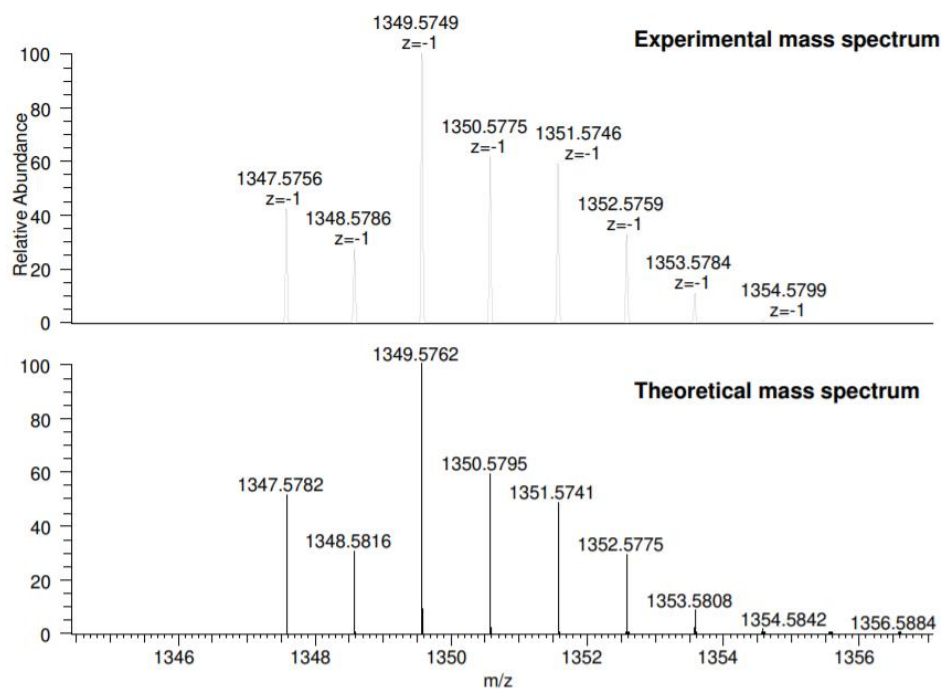
## Appendix VIII: Phospholipids

Lipid	Structure
<b>DErPC</b> (21:1)	
<b>DErPG</b> (21:1)	
<b>DMPC</b> (14:0)	
<b>Lyso-MPC</b> (14:0)	
<b>DMPG</b> (14:0)	
<b>DOTAP</b> (18:1)	
<b>POPC</b> (16:0-18:1)	
<b>POPE</b> (16:0-18:1)	
<b>POPG</b> (16:0-18:1)	

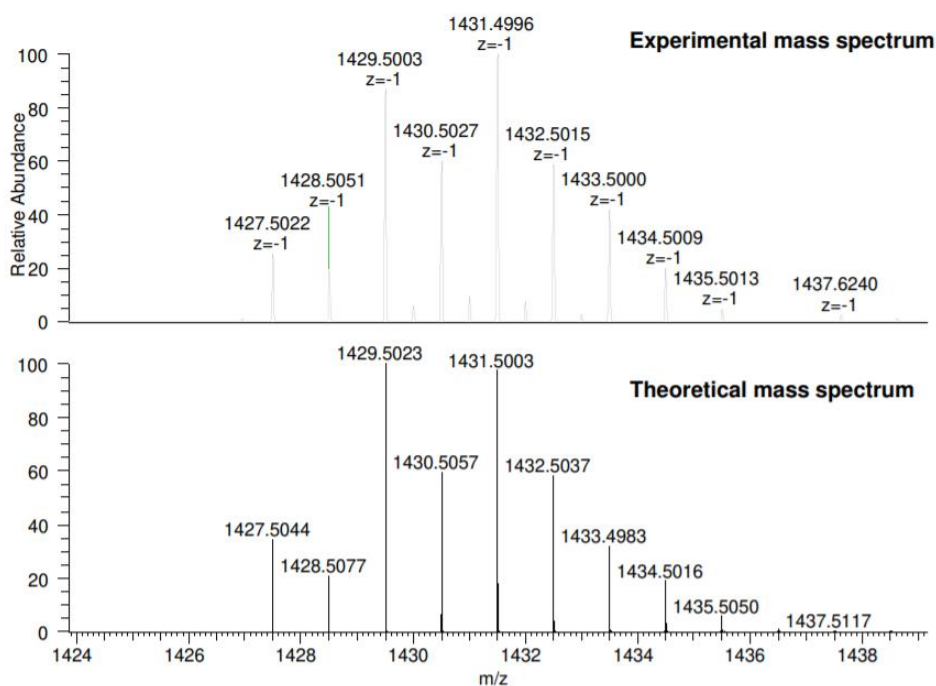


Appendix IX: ESI-HR MS study of the ionic composition of  $PxB_3$  $PxB_3$  after cleavage with HBr

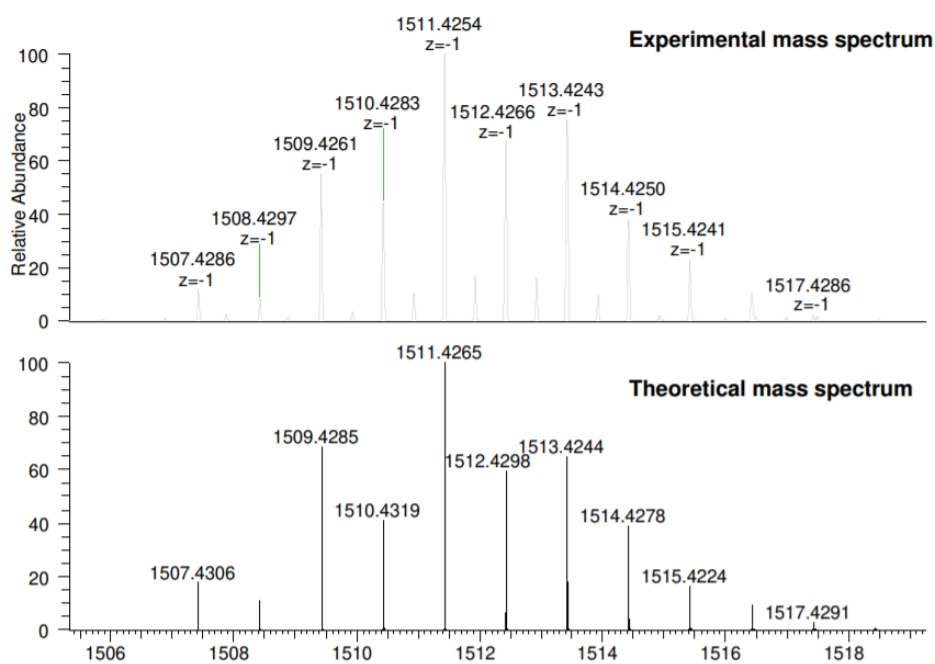
**Figure A1:** Experimental and theoretical distribution of the peak corresponding to  $[M + Br]^-$ ,  $C_{55}H_{96}O_{13}N_{16}Br$ .



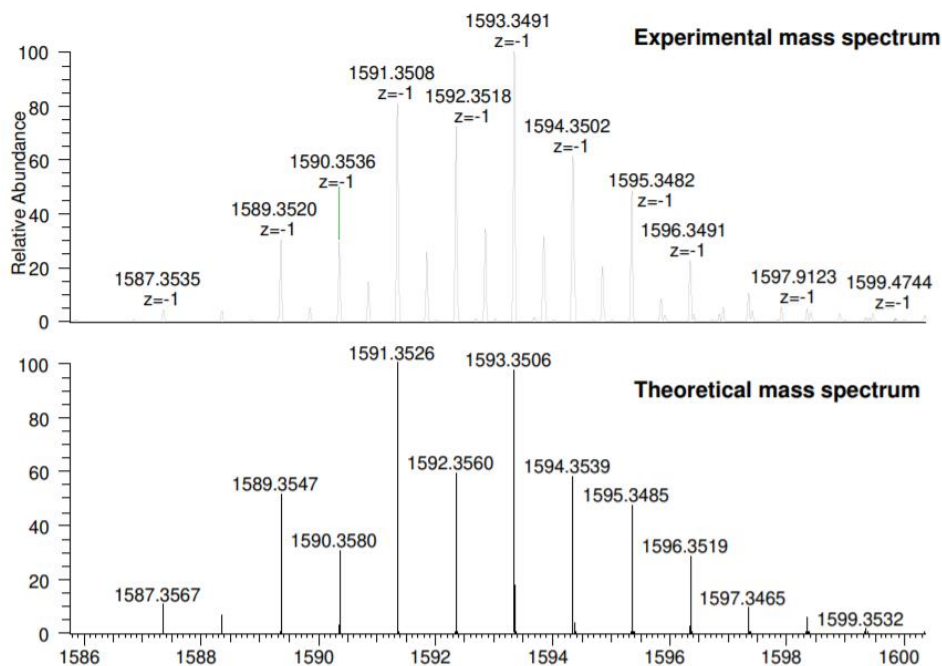
**Figure A2:** Experimental and theoretical distribution of the peak corresponding to  $[M + 2Br + H]^-$ ,  $C_{55}H_{97}O_{13}N_{16}Br_2$ .



**Figure A3:** Experimental and theoretical distribution of the peak corresponding to  $[\text{M} + 3\text{Br} + 2\text{H}]^-$ ,  $\text{C}_{55}\text{H}_{98}\text{O}_{13}\text{N}_{16}\text{Br}_3$ .

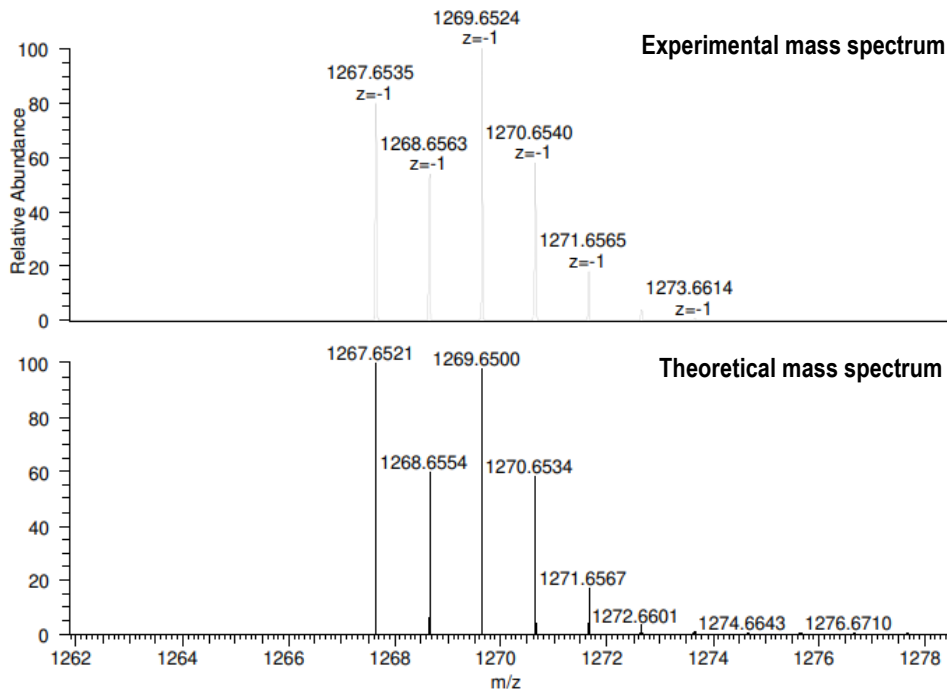


**Figure A4:** Experimental and theoretical distribution of the peak corresponding to  $[\text{M} + 4\text{Br} + 3\text{H}]^-$ ,  $\text{C}_{55}\text{H}_{99}\text{O}_{13}\text{N}_{16}\text{Br}_4$ .

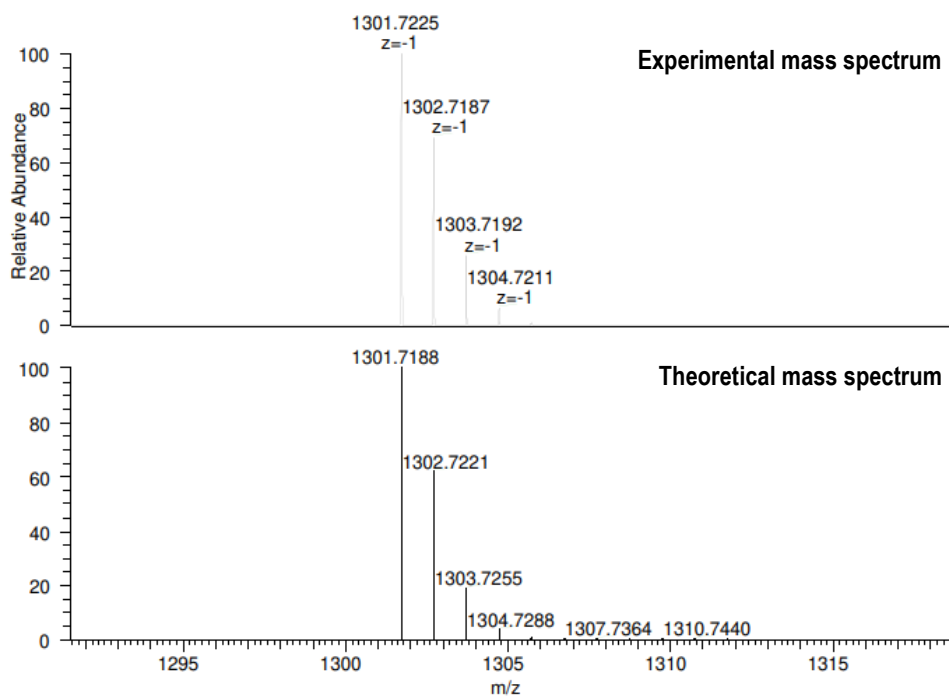


**Figure A5:** Experimental and theoretical distribution of the peak corresponding to  $[M + 5Br + 4H]^-$ ,  $C_{55}H_{100}O_{13}N_{16}Br_5$ .

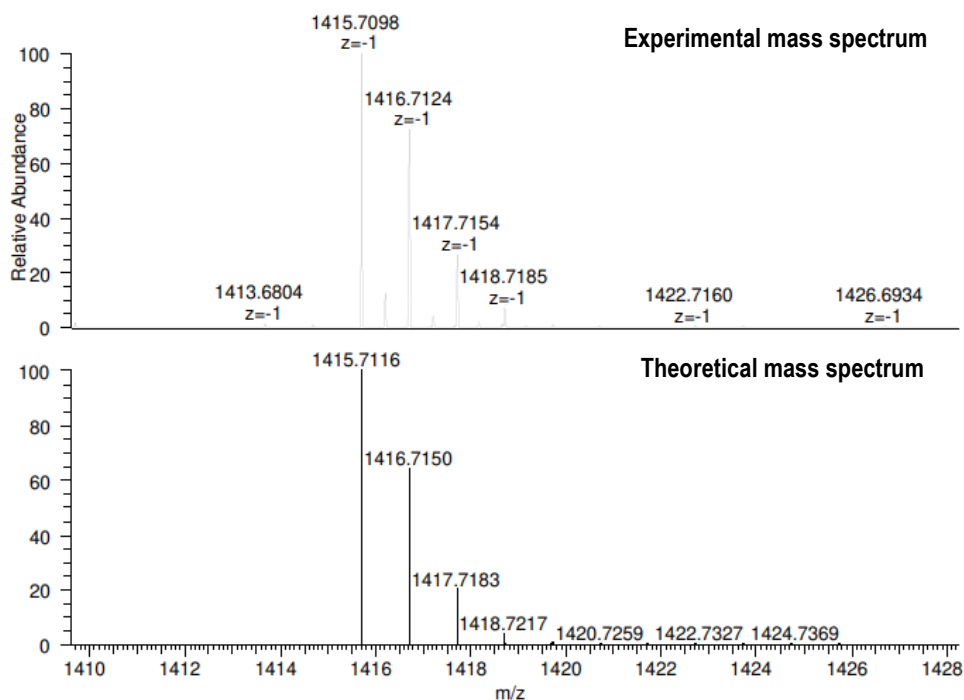
**$PxB_3$  after purification in presence of 0.1 % TFA**



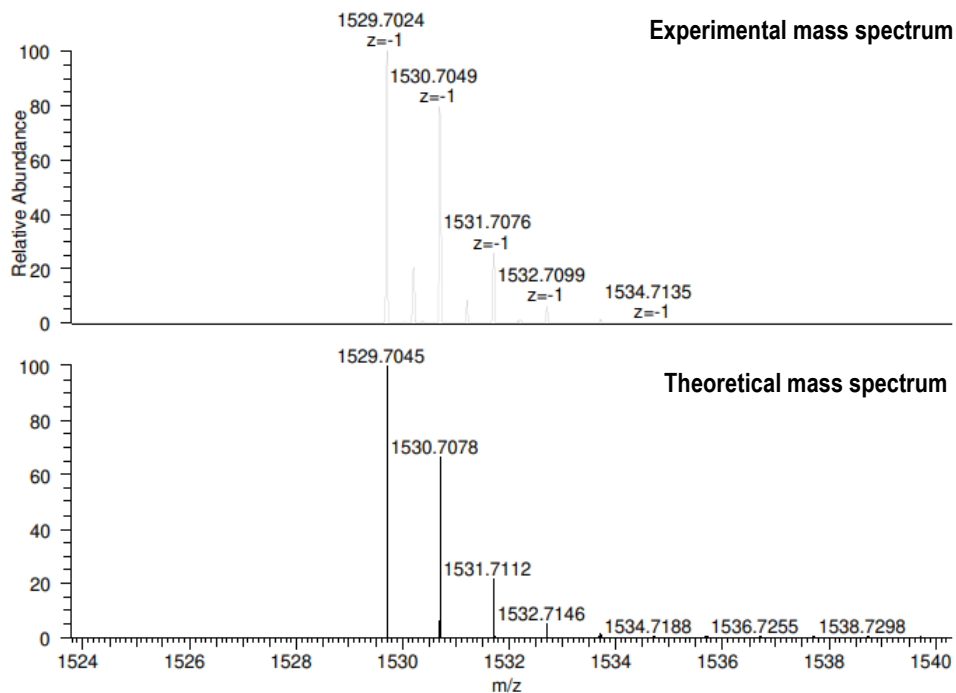
**Figure A6:** Experimental and theoretical distribution of the peak corresponding to  $[M + Br]^-$ ,  $C_{55}H_{96}O_{13}N_{16}Br$ .



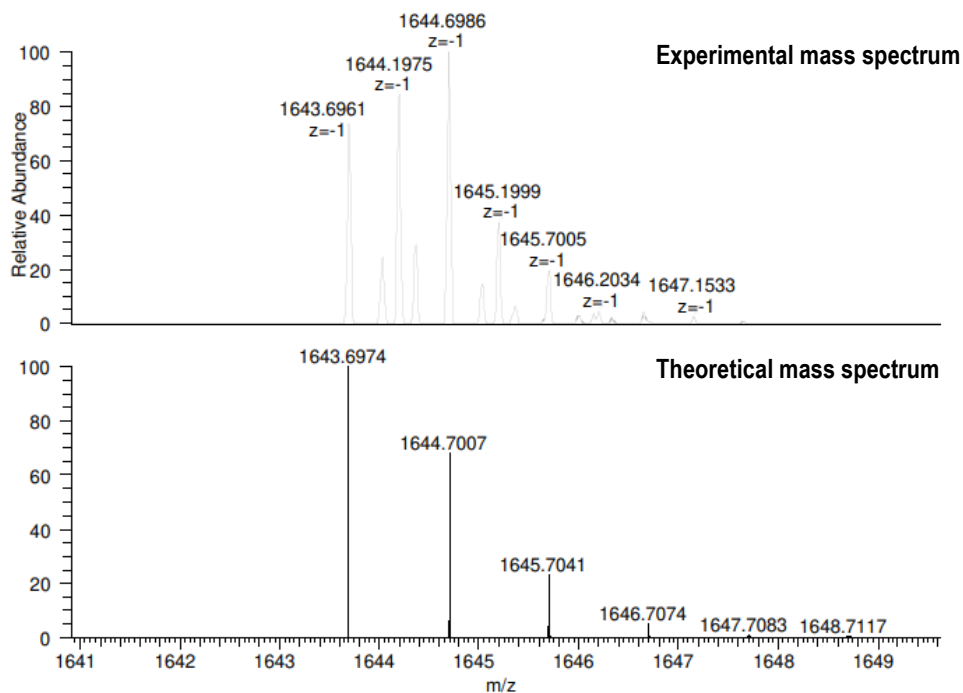
**Figure A7:** Experimental and theoretical distribution of the peak corresponding to  $[M + TFA]^-$ ,  $C_{57}H_{96}O_{15}N_{16}F_3$ .



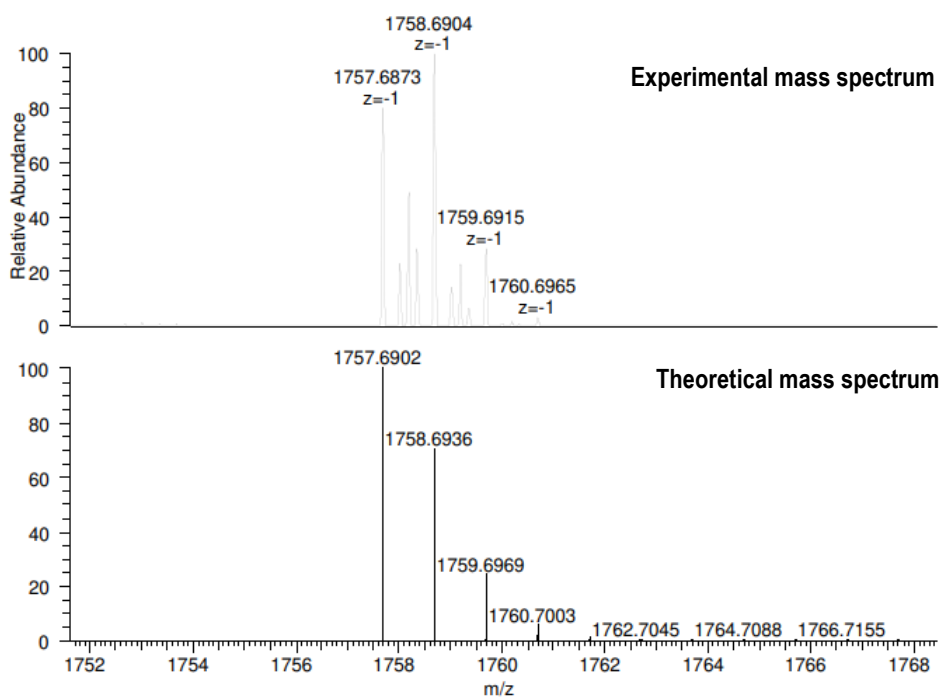
**Figure A8:** Experimental and theoretical distribution of the peak corresponding to  $[M + 2TFA + H]^-$ ,  $C_{59}H_{97}O_{17}N_{16}F_6$ .



**Figure A9:** Experimental and theoretical distribution of the peak corresponding to  $[M + 3TFA + 2H]^+$ ,  $C_{61}H_{98}O_{19}N_{16}F_9$ .

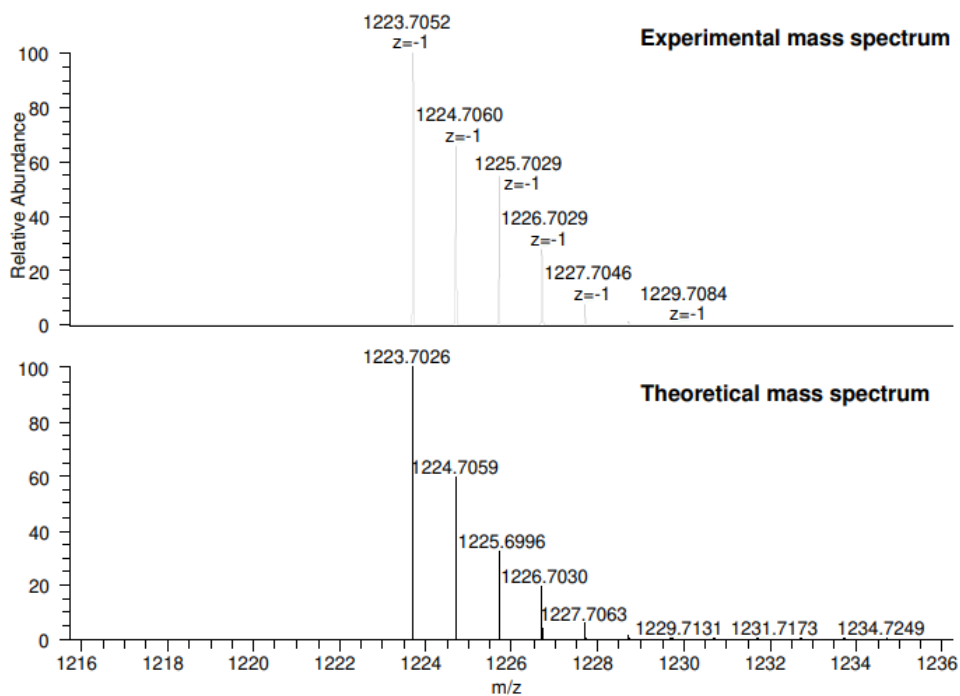


**Figure A10:** Experimental and theoretical distribution of the peak corresponding to  $[M + 4TFA + 3H]^+$ ,  $C_{61}H_{99}O_{21}N_{16}F_{12}$ .

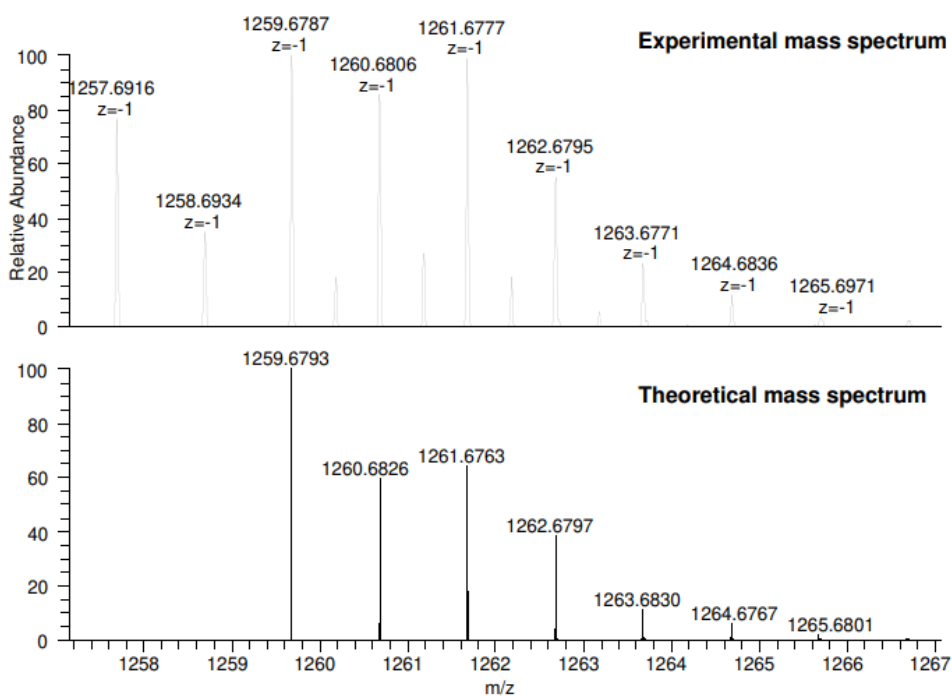


**Figure A11:** Experimental and theoretical distribution of the peak corresponding to  $[M + 5TFA + 4H]^+$ ,  $C_{65}H_{100}O_{23}N_{16}F_{15}$ .

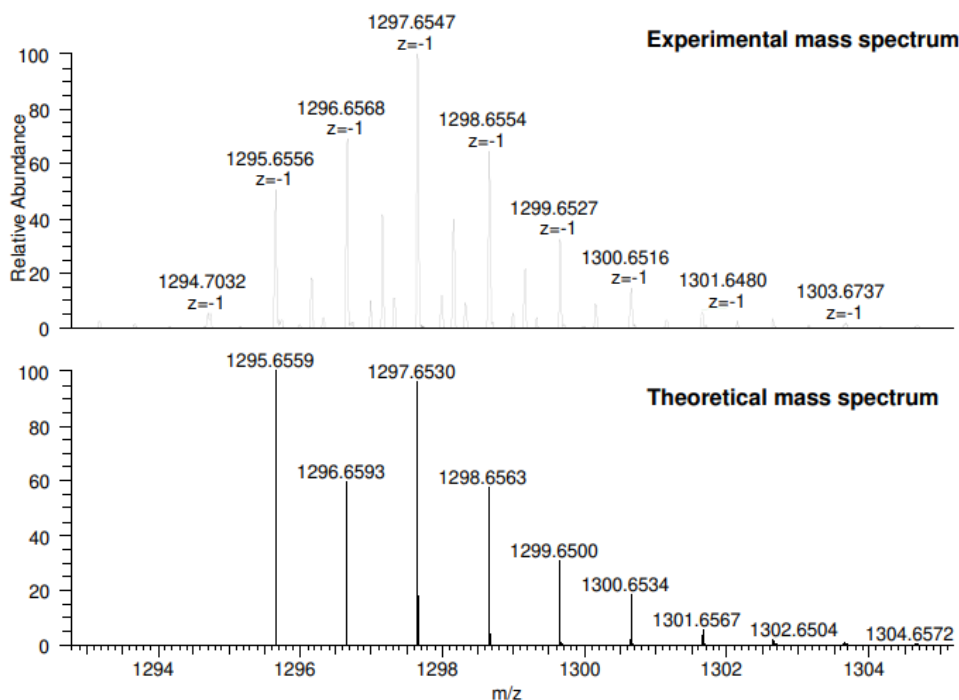
### $PxB_3$ after lyophilization with HCl 8mM



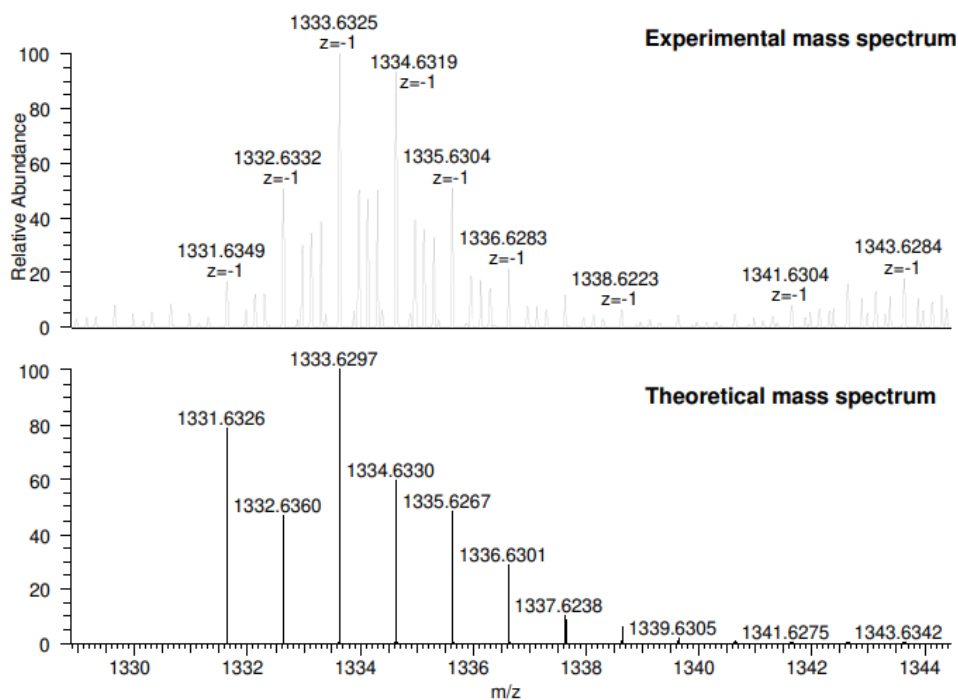
**Figure A12:** Experimental and theoretical distribution of the peak corresponding to  $[M + Cl]^+$ ,  $C_{55}H_{96}O_{13}N_{16}Cl$ .



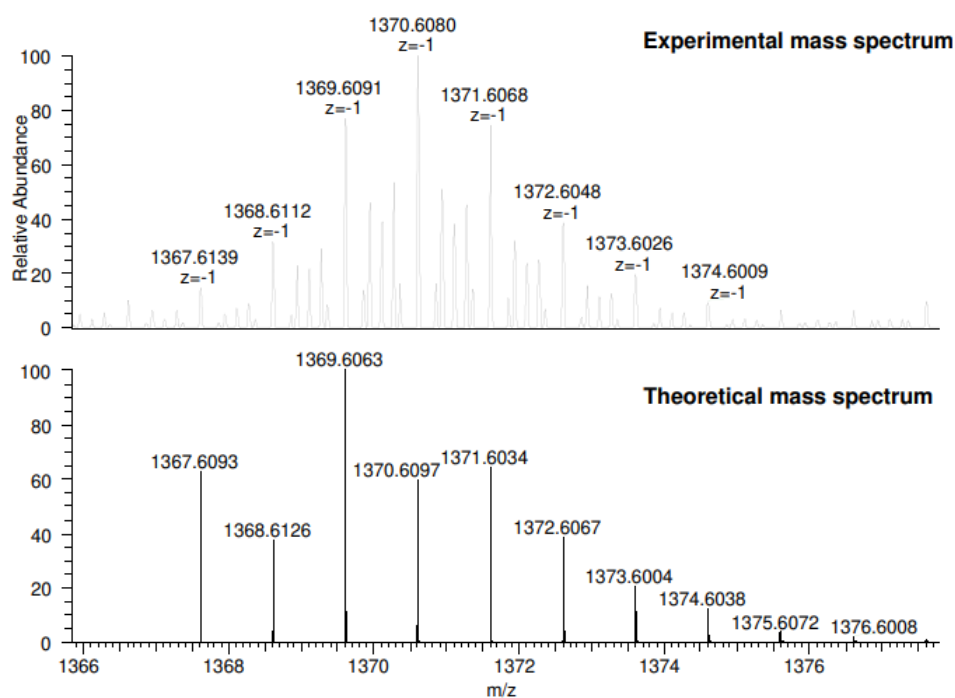
**Figure A13:** Experimental and theoretical distribution of the peak corresponding to  $[M + 2Cl + H]^-$ ,  $C_{55}H_{97}O_{13}N_{16}Cl_2$ .



**Figure A14:** Experimental and theoretical distribution of the peak corresponding to  $[M + 3Cl + 2H]^-$ ,  $C_{55}H_{98}O_{13}N_{16}Cl_3$ .



**Figure A15:** Experimental and theoretical distribution of the peak corresponding to  $[\text{M} + 4\text{Cl} + 3\text{H}]^-$ ,  $\text{C}_{55}\text{H}_{99}\text{O}_{13}\text{N}_{16}\text{Cl}_4$ .



**Figure A16:** Experimental and theoretical distribution of the peak corresponding to  $[\text{M} + 5\text{Cl} + 4\text{H}]^-$ ,  $\text{C}_{55}\text{H}_{100}\text{O}_{13}\text{N}_{16}\text{Cl}_5$ .



## Appendix X: Antibiotic susceptibility profiles of all tested microorganisms

**Table A1:** Antibiotic susceptibility profiles of all microorganisms tested in section 1.8.1. Resistant (R, Red); Susceptible (S, Green).

Bacterial strain		IP	MP	CAZ	FEP	CTX	Gm	Ak	Col	TG	Cip	Lev
<i>Escherichia coli</i>	ATCC 25922	S	S	S	S	S	S	S	S	S	S	S
	MB799	R	S	R	R	R	R	R	S	R	R	R
	C22	S	S	R	R	R	R	S	R	S	R	R
	MB1410	S	S	R	R	R	R	S	S	R	R	R
<i>Klebsiella pneumoniae</i>	ATCC 13883	S	S	S	S	S	S	S	R	S	S	S
	MB674	R	R	R	R	R	S	R	S	S	R	R
	MB1052	R	R	R	R	R	S	R	R	R	R	R
<i>Acinetobacter baumannii</i>	ATCC 19606	S	S	R	R	R	R	S	S	S	S	S
	ATCC 17978	S	S	S	S	S	S	S	S	S	S	S
	CR17	R	R	R	R	R	S	S	R	S	R	R
<i>Pseudomonas aeruginosa</i>	ATCC 27853	S	S	S	S	R	S	S	S	S	S	S
	36A	R	R	R	S	R	R	S	S	S	R	R

IP: Imipenem; MP: Meropenem; CAZ: Ceftazidime; FEP: Cefepime; CTX: Cefotaxime; Gm: Gentamicin; Ak: Amikacin; Col: Colistin; TG: Tigecycline; Cip: Ciprofloxacin; Lev: Levofloxacin.